Université Victor Segalen Bordeaux 2

Année 2010 Thèse N°1712

THESE

Pour le

DOCTORAT DE L'UNIVERSITE BORDEAUX 2

Mention : Sciences, Technologie, Santé

Option : Biologie Végétale

Présentée et soutenue publiquement

Le 18 Juin 2010

Par Mehdi NAFATI

Né le 12 Juillet 1982 à Talence

Caractérisation fonctionnelle des inhibiteurs de Cyclin-Dependent Kinase (CDK) dans le fruit de tomate (*Solanum lycopersicum*)

Membres du Jury :

M. G. Beemster	Rapporteur
Mme. M. Causse	Examinateur
M. C. Chevalier	Directeur de thèse
M. A. Schnittger	Rapporteur
M. M. Teichmann	Examinateur

Remerciements

Tout d'abord, je tiens à remercier Christian Chevalier, non seulement pour m'avoir accepté au sein du laboratoire, mais aussi pour nos discussions enrichissantes et pour sa forte implication durant la préparation et la rédaction des articles joints dans la présente thèse. Sa capacité à diriger nos recherches tout en nous laissant une grande liberté de choix, et le caractère profondément humain qu'il aura su donner au laboratoire resteront parmi mes très bon souvenirs.

Je voudrais aussi remercier Mr Gerrit Beemster, Mme Mathilde Causse, Mr Arp Schnittger et Mr Martin Teichmann pour avoir accepté d'évaluer mes travaux de recherche. Disposer d'un jury de thèse comprenant des spécialistes du développement des plantes, de la physiologie du fruit de tomate, du cycle cellulaire et de ma protéine favorite fut une chance et un plaisir.

Je ne pourrais pas écrire ces remerciements et omettre Frédéric Gévaudant. Connu de tous dans les locaux pour sa jovialité, sa bonne humeur, et sa tendance aux coups de gueule qui démarrent au quart de tour (toujours très divertissants), il s'est montré d'une patience que je n'ai jamais réussi à briser, malgré mes très nombreuses tentatives. Son aide, aussi bien scientifique, technique, que matérielle s'est montrée si déterminante que je me dois d'admettre que les travaux présentés sont autant siens que miens. Bien qu'il fut un véritable « associé » dans ce travail de thèse, il m'a néanmoins permis d'explorer toutes les pistes, parfois loufoques, qui me venaient en tête, sans jamais me décourager et en étant toujours prêt à s'investir.

Une des forces de notre équipe, et dans une certaine mesure, de toute l'UMR, est l'esprit solidaire de ses membres. Ainsi, je voudrais remercier Michel Hernould, une mine d'or de connaissance au sein du laboratoire. D'un caractère tranquille, amical et sincère, d'une capacité de travail digne de Stakhanov, il a été un professeur d'exception. Mes pensées vont aussi vers Nathalie Frangne, toujours souriante et prête à discuter de tel ou tel aspect de mes travaux. Je n'oublierai pas qu'elle s'est lancé d'elle-même pour m'aider plus d'une fois, malgré l'éloignement relatif de nos sujets d'intérêt au sein du laboratoire. Mes remerciements vont aussi à Catherine Cheniclet, qui s'est montrée indispensable pour l'étude de mes plantes. Là

encore, Catherine a toujours été prête à m'aider, que ce soit pour me donner de précieux conseils, m'apprendre différentes techniques, ou pour mettre directement la main à la pâte. Mes pensées vont aussi vers Frédéric Delmas, à qui je souhaite la meilleure carrière possible au sein de l'équipe, et Armand Mouras, qui nous a abandonné pour partir en retraite (quelle idée !!) mais qui trouvait tout de même le moyen lors de ses brefs passages au laboratoire d'apporter des idées auxquelles nous n'avions pas pensé. Mes remerciements vont aussi à Patricia Ballias et Aurélie Honoré. Chacune leur tour elles se sont montrées plus que patientes et arrangeantes pour ce qui est de mon travail en serre, et elles ont sauvé la vie de mes plantes à plus d'une reprise !

Mes pensées vont bien sûr aussi vers mes camarades stagiaires, thésards et post-docs, bien sûr pour les instants de détente mais aussi parfois pour des discussions scientifiques sérieuses (si si !!). Ainsi, je me souviendrai de points scientifiques importants, tel que le caractère fondamental et indémodable de la loi de Beer-Lambert, l'utopie qu'est le RNA-fish, l'implication évidente de la théorie du chaos dans la PCR ou encore que le calcul du nombre de répétitions nécessaires à l'obtention d'un Western Blot propre fait appel à la loi des grands nombres. Je saurai aussi me souvenir que quelle que soit la thématique étudiée, on peut la lier au potassium.

Bien entendu, je ne vais pas faire des remerciements exhaustifs, tant il y a eu de gens prêts à m'aider durant ma thèse. Je vous adresse simplement à tous un grand merci.

La réussite de ma thèse, je la dois aussi à celle qui fait partie de ma vie. Nos caractères sont opposés sur de nombreux domaines, et tu m'as offert un certain équilibre qui est pour beaucoup dans l'avancée de mes travaux. Ton soutien a été indéfectible, et j'espère seulement que j'arrive à te rendre ne serait ce qu'une fraction de tout ce que tu m'apportes.

Enfin, je pense à mes parents, qui ont toujours été là pour moi. Vous n'avez hésité devant aucun sacrifice pour m'aider à m'accomplir, et je ne saurai jamais vous en remercier assez.

TABLE OF CONTENTS

ABBREVIATIONS

Specific terminology

APC	Anaphase Promoting Complex
CAK	CDK Activating Kinase
Ccs52	cell cycle switch 52 kDa
Cdc	Cell-Division-Cycle
CDK	Cyclin-Dependent Kinase
CKI	Cyclin-dependent Kinase Inhibitor
CKS	Cyclin-dependent Kinase Subunit
CTD	C-Terminal Domain of RNA polymerase 2
Cyc	Cyclin
DEL	DP-E2F-Like
E2F	Elongation Factor
ICK	Interactor of Cdc2 kinase
KRP	Kip-related-protein
ORC	Origin of Recognition Complex
PCNA	Proliferating Cell Nuclear Antigen
RB	Retinoblastoma
RBR	Retinoblastoma Related

Nucleic acids and nucleotides

DNA	desoxyribonucleic acid
cDNA	complementary desoxyribonucleic acid
tDNA	transfer desoxyribonucleic acid
ATP	Adenosine 5' triphosphate
ARN	ribonucleic acid
ARNt	transfer ribonucleic acid
C, G, T, UTP	Cytosine, guanosine, thymidine, uridine 5' triphosphate
dNTP	Desoxynucleotide 5' triphosphate (dATP, dCTP, dGTP, dTTP)

Units

°C	Celsius degree
g	acceleration
kDa	kiloDalton
bp, kb, kbp,	base pairs, kilobases, kilobase pairs,
rpm	revolutions per minute
s, min, h	seconde, minute, hour

Miscellaneous

BAP	Benzyl-aminopurine
BSA	Bovine Serum Albumin
CaMV	Cauliflower mosaic virus
cv	Cultivar
2-4 D	Dichloro-2,4 phenoxyacetic Acid
DAPI	4',6-diamino-2-phenylindole
DEPC	Diethylpyrocarbonate
DNAse I	Desoxyribonuclease I
OD	Optic density
DTT	Dithiothreitol
EDTA	Ethylene diamine tetraacetic
EGTA	Ethylene glycol-bis-(β-aminoethyl ether) N,N,N',N'- tetraacetate
FAA	Formaldehyde/Alcohol /Acetic acid
GUS	β-glucuronidase
IPTG	Isopropyl-β-thiogalactopyranoside

DPA	days post-anthesis
LB, RB	Left border, right border
mQ	milliQ
NBT	Nitroblue tetrazolium
ORF	Open reading frame
w/w, w/v, v/v	weight/weight, weight/volume, volume/volume
PBS	Phosphate buffered salin
PCR	Polymerase chain reaction
PEG	Polyethylene glycol
Rif^R, Chl^R	rifampicine resistant, chloramphenicol resistant
RNAse	Ribonuclease
RNasin	Ribonuclease inhibitor
RT-PCR	Reverse transcription-Polymerase chain reaction
SDS	Sodium dodecyl sulfate
TAE	Tris/Acetic Acid/EDTA
TE	Tris/EDTA
TEMED	N,N,N',N'-tetramethyl-ethylenediamine
Tris	Tris(hydroxyméthyl)-aminomethane
UV	Ultraviolet
X-Gal	5-bromo-4-chloro-3-indolyl β-Dgalactoside

CHAPTER 1 : INTRODUCTION

1 The Cell Cycle

1.1 Cell Cycle and Plant Development

1.1.1 Overview of Development in Higher Plants

Plants have the specificity to grow and to develop new organs throughout their life. This post-embryonic growth is controlled in localized regions of cell division called meristems. In young plants, the most active meristems are the apical meristems, located at the tips of the stem and the root (Figure 1).

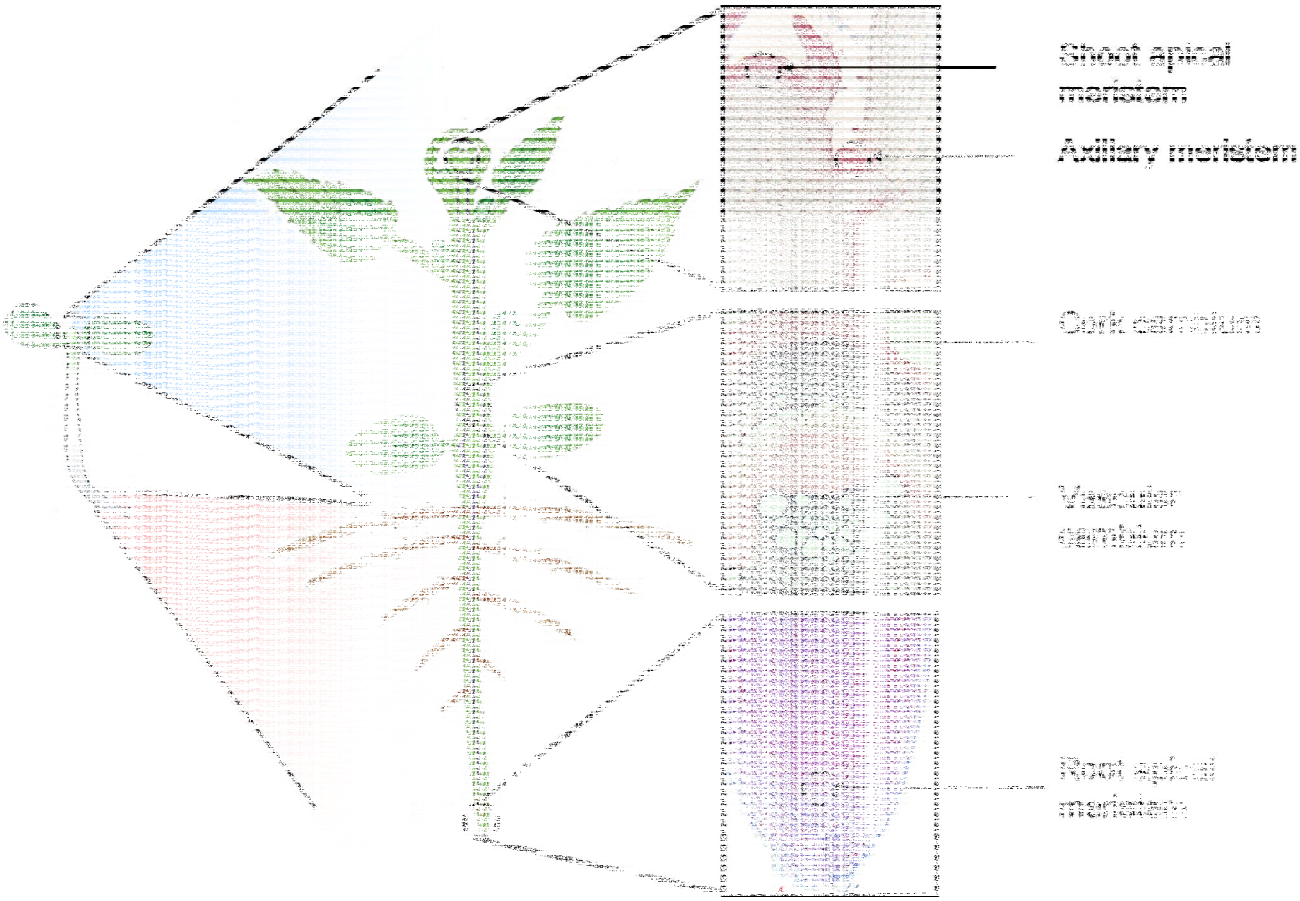

Figure 1 : The plant development

The vegetative shoot meristem generates the stem, as well as the lateral organs attached to the stem (stems and axillary buds). At the nodes, axillary buds contain

the apical meristems for shoot branching. Lateral roots arise from the pericycle, an internal meristematic tissue.

Root and shoot apical meristems, formed during embryogenesis, are called primary meristems. After germination, their activity generates the primary tissues and organs. Most plants also develop a variety of secondary meristems during post-embryonic development. These include axillary meristems, inflorescence meristems, floral meristems, intercalary meristems, and lateral meristems: the vascular cambium for the complementation of the conducting vessels and the cork cambium (for phelloderm and suber).

1.1.2 Role of the Cell Cycle in the Establishment and Development of tissues

A fundamental difference between plants and animals is that each cell is surrounded by a rigid cell wall. In plants, cell migration from one location to another is prevented because cell walls are binded together by a middle lamella. As a consequence, plant development, unlike animal development, depends solely on patterns of cell division and cell enlargement.

1.2 The mitotic Cell Cycle

The classical cell cycle, also called mitotic cycle, is the sequence of events occurring within a cell leading to cell division into two identical daughter cells. The mitotic cycle is composed of four main phases (Figure 2), sequentially G1 for Gap phase 1, the S phase for DNA Synthesis phase, G2 for gap phase 2, and finally M phase for Mitosis phase. G1 and G2 are preparation phases for respectively S and M phases. The duration of a full mitotic cycle is extremely variable, because the start up of both S and M phases is determined by both endogenous and exogenous factors.

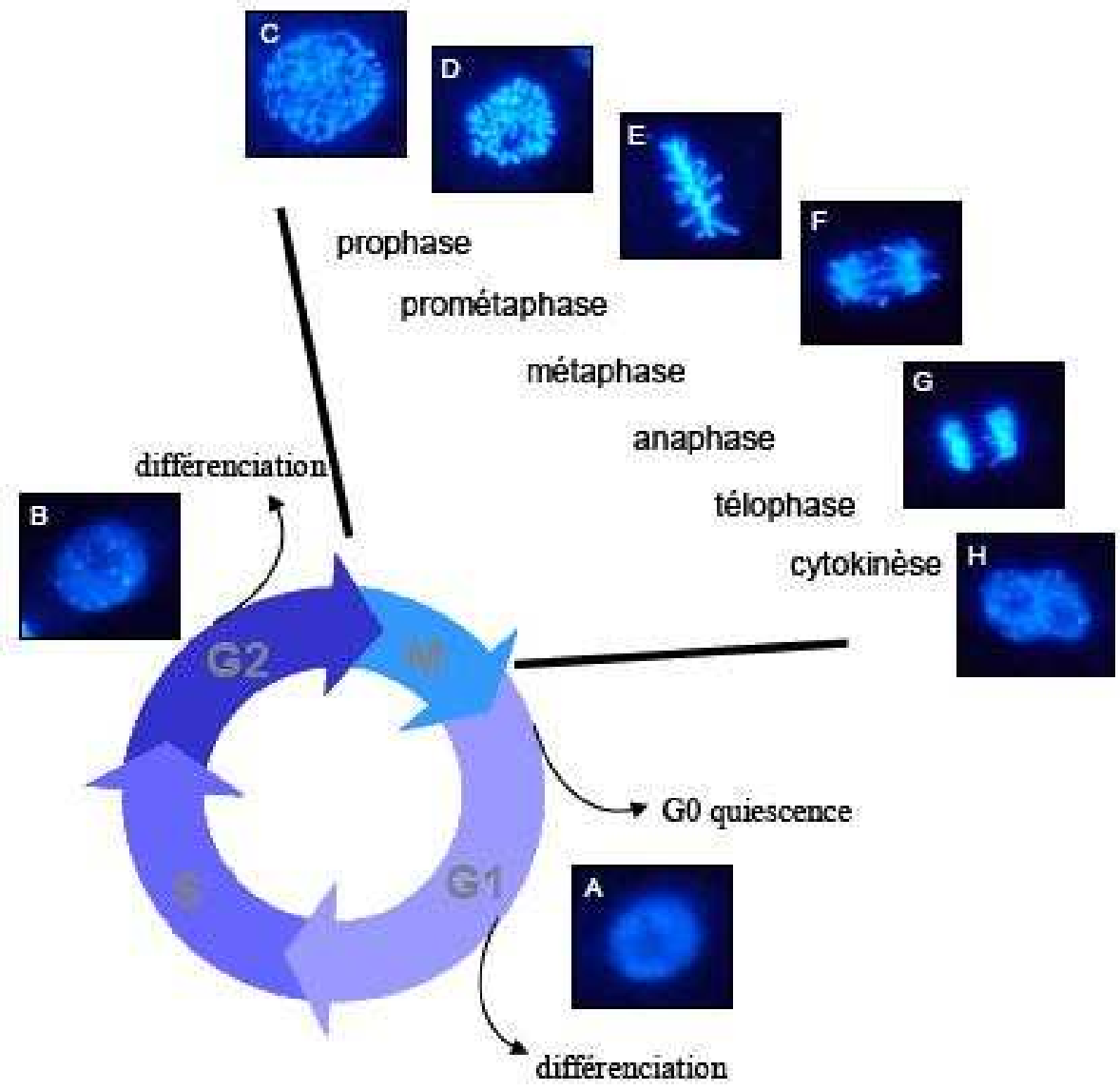

Figure 2 : The mitotic cell cycle in tobacco BY-2 cultured cells observed with DAPI, from Frédéric Delmas (PhD thesis, 2004)

1.2.1 The S phase

The S phase is characterized by the doubling in ploidy of the cell, so that each daughter cell after mitosis has the same amount of genetic information as the parent cell. Thus, at the end of S phase, the cell passes from a 2C state to a 4C state. The synthesis of DNA begins at multiple points of the genome at specific DNA sequences called replication origins. Pre-replication complexes (pre-RC) are formed at these sequences. Once the pre-RC are activated, a particular enzyme called helicase separates the two strands of the DNA double helix, allowing the attachment of the DNA polymerase responsible for synthesizing the complementary strand to each original strand.

At the end of this phase, each chromosome is thus composed of two sister chromatids. DNA synthesis is said to be semi-conservative, as each new double-stranded DNA consists of an original strand and a newly synthesized strand.

1.2.2 The M phase

Mitosis is the phase where the cell in G2, which has doubled its amount of genomic DNA during the S phase, divides into two daughter cells. The formation of daughter cell nuclei is called karyokinesis, and is followed by division of membranes and organelles called cytokinesis.

The separation of chromosomal DNA between the two future daughter cells is achieved during several cytologically observable phases (Figure 2):

- In late G2 phase, the chromatid is decondensed, and the chromosomes are not individualized.

- Prophase, the first stage of mitosis, is characterized by the individualization of chromosomes, consisting in two chromatids joined by the centromere. At the same time, the nuclear envelope breaks down and the nucleolus disappears.

- In early metaphase (prometaphase), a microtubule spindle forms, within which individual chromosomes are regrouping.

- Metaphase continuing, the chromosomes move to the equator of the microtubules spindle.

- Anaphase begins with the simultaneous separation of the two chromatids of each replicated chromosomes which are held together at their kinetochore. The two sets of chromosomes then move to the poles of the mitotic spindle.

Finally, once the chromosomes are grouped in clusters (telophase), the new cell wall forms from the centre of the cell (phragmoplast); chromosomes loose their individuality; new nuclear membranes are formed and the new cell wall separates the two daughter cells completely.

The cell division plane is conditioned by the setting of actin filaments and cortical microtubules parallel to each other along the plasma membrane, blocking the cell that can only extend in one axis perpendicular to the vise formed.

1.2.3 Regulation of cell cycle

To ensure harmonious tissue development, plant cells are able to control the rate of progression in each stage of the cycle, and to verify that the previous step has been achieved correctly. This cycle regulation is achieved throughout various checkpoints. There are three major checkpoints (Inzé and De Veylder, 2006):

- The G1/S transition, where the cycle is stopped if environmental conditions are not favourable. This particular phase of the cycle is called G0 phase, and cells are said in quiescent state.

- The G2/M transition, where mitosis occurs only if DNA replication is completed and considered without error;

- The M/G1transition, where successful mitosis is controlled.

In addition, the cell cycle can be stopped if the cell enters into differentiation.

At the key regulatory point in early G1 of the cell cycle, the cell becomes committed to the initiation of DNA synthesis. In yeasts, this point is called START. Once the cell has passed START, it is irreversibly committed to intitiate DNA synthesis and

completes the cell cycle through mitosis and cytokinesis. After the cell has completed mitosis, it may leave the cell cycle and differentiate or reenter the cell cycle. This choice is made at the initial G1 point. DNA replication and mitosis are linked in mammalian cells. In contrast, plant cells can leave the cell cycle either before or after replicating their DNA. As a consequence, whereas most animal cells are diploid, plant cells are frequently tetraploid or even polyploid after going through additional cycles of nuclear DNA replication without mitosis. As an alternative of cell cycle arrest, the process of endoreduplication, widespread in plants, is defined by the iteration of DNA replications without successive cytokinesis, leading to an exponential increase of nuclear DNA content. This phenomenon will be discussed in more detail in part 4.1 of this chapter.

2 Molecular mechanisms governing the cell cycle

The molecular mechanisms controlling the cell cycle are highly conserved among Eukaryotes.The molecular machinery in the heart of this control is composed of proteins homologous in plants, animals and yeasts. At the centre of this machinery are protein complexes with serine/threonine kinase activity called CDK/cyclin complexes. These complexes are composed of a Cyclin-Dependent Kinase protein (CDK) owing the catalytic activity of the complex, and a protein called cyclin, which confers to the complex a regulatory activity. These complexes serve as integrators of both endogenous and exogenous stimuli to control the cycle checkpoints, through the fine tuning of their catalytic activity and their specificities of targets. Figure 3 is a simplified diagram of the cell cycle incorporating the key molecular players that will be addressed in this part.

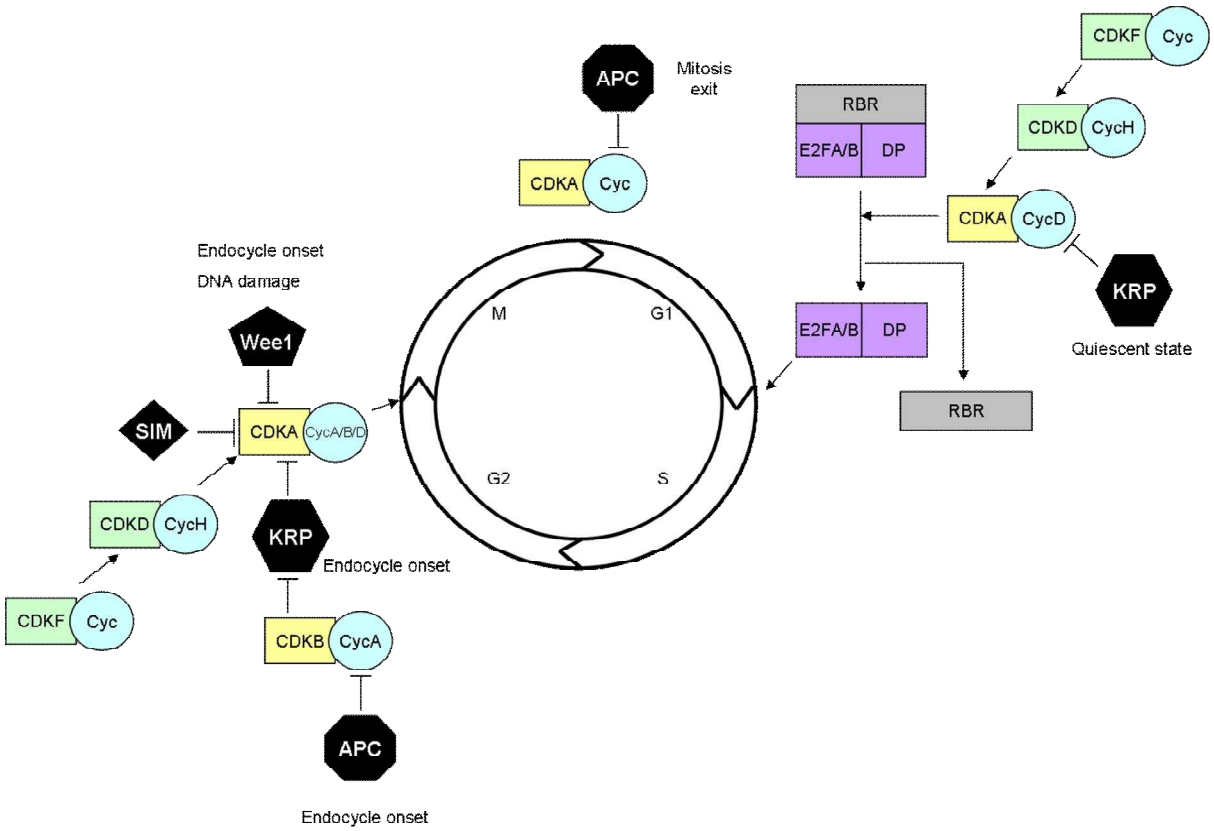

Figure 3 : Simplified diagram representing the different CDK/Cyc complexes involved in plant cell cycle and theirs various inhibitors. Indicated pathways are mostly putative.

2.1 Classification of Plant Cyclin-Dependent Kinases

From studies of the *Arabidopsis thaliana* genome, seven classes of CDKs, numbered from A to G, plus a class of CDK-like, or CKL, have been discovered (Vanderpoele *et al.,* 2002, Menges *et al.*, 2005, see also Figure 4).

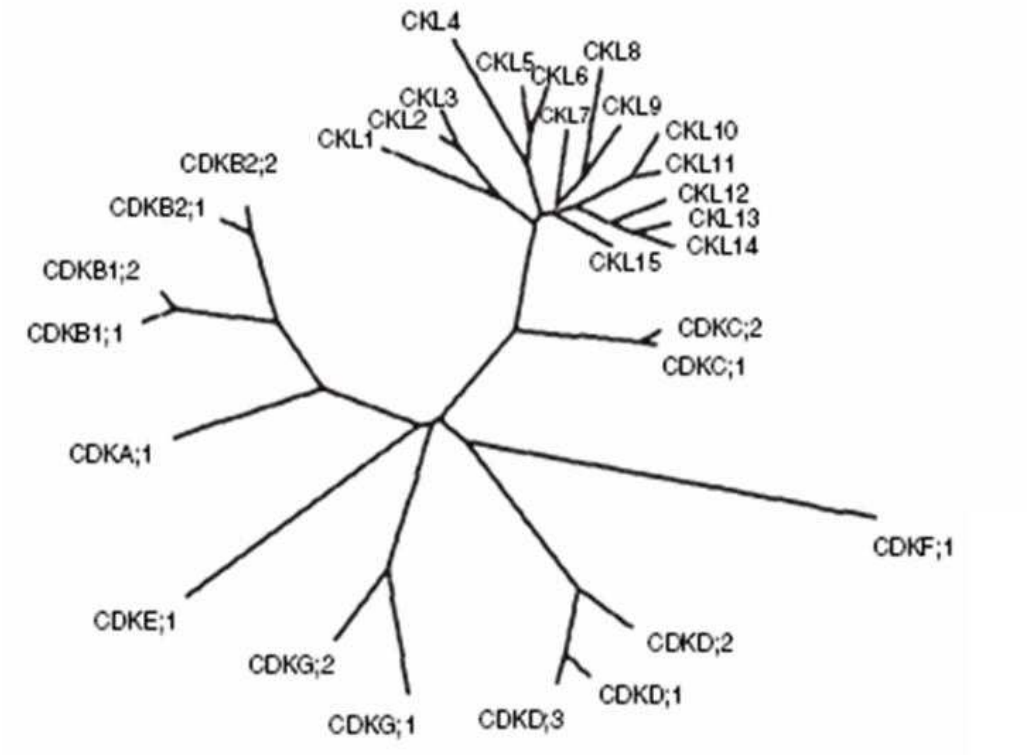

Figure 4 : Phylogenetic tree of the different CDKs from *Arabidopsis thaliana*, from Menges *et al.* (2005)

A-Type Cyclin-Dependent Kinases (CDKA) are the first CDKs to have been discovered in plants (Ferreira *et al.*, 1991). Homologous to yeast cdc2/CDC28 and animals CDK1/CDK2, they are characterized by the presence of a conserved motif PSTAIRE as a cyclin-binding site. A single CDKA sequence, CDKA1, has been found in *Arabidopsis thaliana*.

B-Type Cyclin-Dependent Kinases (CDKB) are unique to the plant kingdom. They comprise 2 subclasses, CDKB1 and CDKB2. Their sequences are characterized by the absence of PSTAIRE motif, replaced by a PPTALRE motif in the case of CDKB1, or a PPTTLRE motif in the case of CDKB2. In *Arabidopsis thaliana*, each CDKB sub-

class includes 2 genes. These are noted CDKB1;1, CDKB1;2, CDKB2;1 and CDKB2;2.

C-Type cyclin-dependent kinases (CDKC) are characterized by the presence of a PITAIRE motif. There are 2 CDKC in *Arabidopsis thaliana*, CDKC1 and CDKC2.

D-type Cyclin-dependent kinases (CDKD) have a N(F/I/V)TARLE type motif. Three genes encoding a CDKD have been identified in *Arabidopsis thaliana*, CDKD1, CDKD2 and CDKD3.

E-type Cyclin-dependent kinases (CDKE) have a SPTAIRE type motif. There is only one CDKE in *Arabidopsis thaliana*, called CDKE1.

F-type Cyclin-dependent kinases (CDKF) have the unique feature of carrying a ≈110 amino acid insertion between its kinase active site and its phosphoregulatory site, and its function *in vitro* does not require a cyclin partner. There is only one CDKF in *Arabidopsis thaliana*, called CDKF1.

G-Type Cyclin-dependent kinases (CDKG) have a PLTSLRE pattern, and show sequence homology with the protein kinase p58/GTA originately discovered as associated with the human galactosyltransferase. There are 2 CDKG *Arabidopsis thaliana* (CDKG1 and CDKG2). The function of these genes is unknown.

In addition to these 7 classes of CDKs, Menges *et al.* (2005) have identified a set of 15 genes close to CDKs, appointed CDK-LIKE 1 to 15.

Associated with CDKs, there are 49 cyclins grouped into 8 classes with 23 sub-groups: CYCA1-3, CYCB1-3, CYCC, CYCD1-7 CYCH, CYCL, CYCP1-4, CYCT, SOLODANCER, CYCJ18, CYL1 (Menges *et al.*, 2005; see also Figure 5).

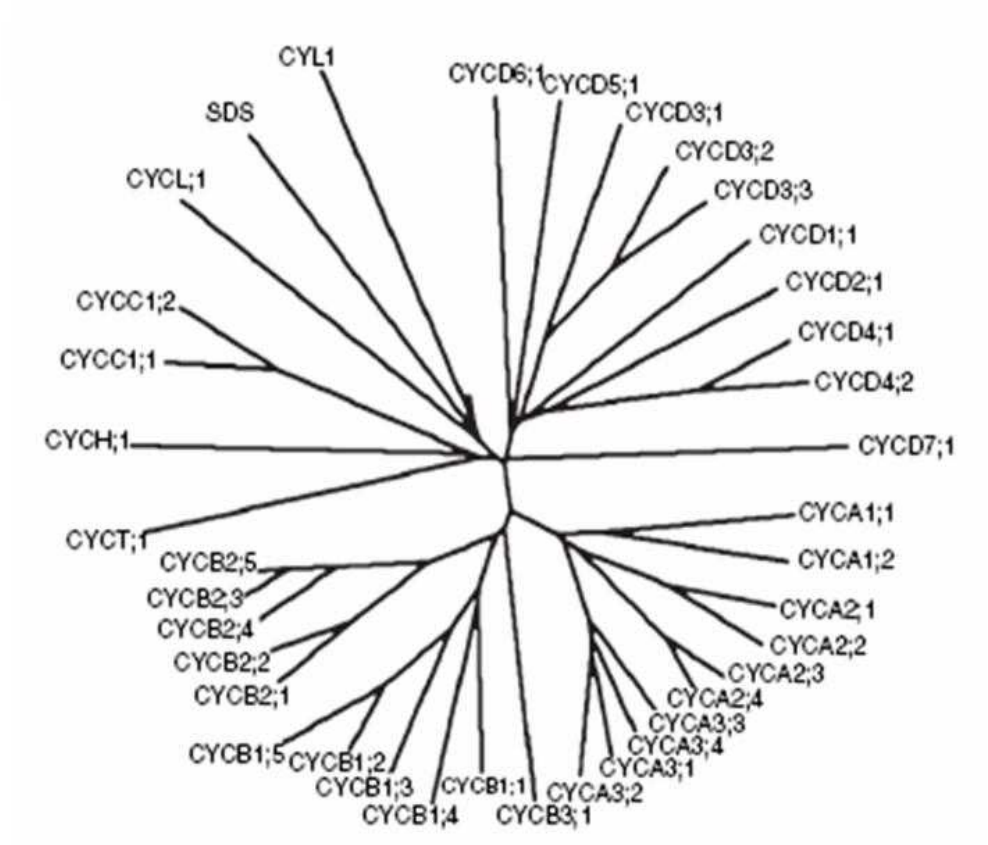

Figure 5 : Phylogenetic tree of the different cyclins from *Arabidopsis thaliana*, from Menges *et al.* (2005)

2.2 Functions of CDK/Cyclin Complexes

2.2.1 CDKA, central regulator of G1/S and G2/M transitions

The A-Type CDK shows the highest sequence homology with the single yeast CDK (cdc2). This homology is also functional, because AtCDKA1 can complement a cdc2 mutation in yeast (Ferreira *et al.*, 1991). The over-expression of *Arabidopsis thaliana* AtCDKA1 shows no phenotype, which suggests that the level of CDKA protein is not a limiting factor in the plant development process. Conversely, over-expression of a dominant negative form of CDKA blocks cell division and plant development. It is interesting to note that among the few plants that were regenerated, tissue differentiation was unaffected, and plants were composed of few cells which were much larger than those of control plants (Hemerly *et al.*, 1995).

Various studies have shown that cyclins D are CDKA partners (Healy *et al.*, 2001, Koroleva *et al.*, 2004). The over-expression of AtCycD3, 1 in *Arabidopsis* leads to cell hyperproliferation and incomplete differentiation (Dewitte *et al.*, 2003). The over-expression of *Antirrhinum majus* CycD1; 1 in a tobacco cell culture induces an increase of cell division rate, both in G0/G1/S and S/G2/M phases The over-expression of AtCycD3,1 in *Arabidopsis* cell culture lengthens the G2 phase in favour of a shortened G1/S transition (Menges *et al.*, 2006). The fact that the D type cyclins are expressed cyclically during cell cycle, unlike CDKA (Menges *et al.*, 2005), combined with the fact that unlike CDKA, cyclin D overexpression did induce a phenotype, show that D-Type cyclins are limiting partner of CDKA/CyclinD complexes.

During the G1/S transition, the complex CDKA/CyclinD phosphorylates the Retinoblastoma-Related Protein (RBR). Once phosphorylated, RBR detaches from E2F/DP transcription factor complex, which is then able to activate transcription of genes involved in DNA synthesis and replication, like CDC6, MCM, CDT1 and ORC1 of the pre-replication complex (Boniotti and Gutierrez., 2001, Vandepoele *et al.*, 2005).

A role of CDKA in G2/M transition is also proposed as the over-expression of AtKRP2, an inhibitor of CDKs, inhibits the activity of mitotic CDKA complexes *in vitro* and induces the blocking of cell division in favour of endoreduplication *in vivo* (Verkest *et al.*, 2005, Pettko-Szandtner *et al.*, 2006). In addition, the CDKA protein fused to GFP is localized in specific cytoskeletal structures during mitosis (Colasanti *et al.*, 1993; Stals *et al.*, 1997; Weingartner *et al.*, 2001). Finally, the A and B-type cyclins, which are considered as being mitotic cyclins because of their specificity of expression in G2/M, are potential partners of CDKA. However the *in vivo* role of such complexes has not been documented so far (Nakagami *et al.*, 1999; Roudier *et al.*, 2000; Healy *et al.*, 2001).

The involvement of CDKA proteins in the translation control is also suspected as CDKA is capable of complexing with eIF4A *in vivo* (Hutchins *et al.*, 2003).

Like their yeast and animal counterparts, CDKA proteins must be phosphorylated at their T-loop to be active, through the kinase activity of cyclin-dependent kinase

activating kinases or CAK (Dissmeyer *et al.*, 2007, Harashima *et al.,* 2007, see 2.2.4).

2.2.2 CDKB, and the G2/M transition

Unlike CDKA, the CDKB gene expression level varies during the cycle, and peaks between S and M phases. Transcripts encoding CDKB are logically found mainly in young tissues and dividing meristematic tissues and are associated with the G2/M transition (Porceddu *et al.*, 2001, Menges *et al.*, 2005).

Like CDKA, the over-expression of a CDKB1 induces no phenotype in *Arabidopsis thaliana* (Boudolf *et al.*, 2004). On the contrary, the over-expression of a dominant negative form of *Arabidopsis* CDKB1 led to an increase of cell endoreduplication at the expense of cell division, whereas in tobacco cell culture the same construction induces growth slowdown mainly by delaying the G2/M transition (Porceddu *et al.*, 2001).

In *Arabidopsis*, the over-expression of CDKB2 gene or CDKB2;1/CDKB2;2 double silencing induces the disruption of apical meristems, which tends to involve the role of this sub-class of CDK in coordinating meristematic divisions (Andersen *et al.*, 2008).

Little information is available about the mode of action of CDKB, but it has been suggested that CDKB1 associated with the mitotic cyclin A2 activates mitosis (Boudolf *et al.*, 2009). CDKB also seems to be able to associate with D type cyclins to form functional complexes (Nakai *et al.*, 2005, Kono *et al.*, 2003, Kawamura *et al.*, 2006). A hypothesis concerning the action of CDKB during the G2/M transition is that the complex CDKB/Cyclin phosphorylates a cyclin dependent kinase inhibitor (CKI) which would then be degraded. The drop in the amount of inhibitor would increase the kinase activity of CDKA, which would trigger mitosis establishment (Verkest *et al.*, 2005).

In animals and yeast, mitosis start is conditioned by the activation of a CDC25 phosphatase which regulates the activity of the CDKA counterparts. No protein of this type has been found in plants. Boudolf *et al.*, 2006 have suggested the replacement

in plants of CDC25 phosphatase function by the emergence of a new class of CDKs, the CDKBs, which in plants are responsible of mitosis establishment.

2.2.3 Cyclin-Dependent Kinases involved in basal transcription control: CDKC, CDKD and CDKE

The RNA Polymerase II (RNAP II) is responsible for the transcription of protein coding genes in eukaryotes (Sims *et al.*, 2004). Once bound to the promoter region of the target gene in a preinitiation complex, the RNAP II transcriptional activity is regulated through phosphorylation of C-terminal domain of the protein (CTD). In the animal kingdom, different cyclin-dependent kinases regulate RNAP II transcriptional activity, either positively, in the case of CDK7/CycH (Nigg, 1996), CDK9/CycT or CDK9/CycK complexes (Marshall and Price, 1995), or negatively, in the case of CDK8/CycC complex (Akoulitchev *et al.*, 2000).

Several genes encoding CTD kinase proteins have been found in *Arabidopsis thaliana*.

The C-Type CDKs are CDK9 functional counterparts: CDKC1 is capable of complexing with cyclin T1, has a CTD kinase activity, and restores the transcriptional activity of nuclear extracts from CDK9 complex depleted HeLa cells. So C-Type CDKs may be positive regulators of RNAP II in plants (Fulop *et al.*, 2005). In *Arabidopsis*, CDKC1/CDKC2 or CycT1;4/CycT1,5 loss of function leads to phenotypes of impaired growth of the leaf and flower and delayed flowering. It is interesting to note that these mutant plants are highly resistant to the CaMV virus (Cauliflower mosaic virus) (Cui *et al.*, 2007). It has also been shown that CDKC2 is co-localized with components of the spliseosome. Kitsio *et al.* (2008) hypothesized that this protein is found at the interface of transcription and splicing mechanisms.

D-Type CDKs, capable of complexing with cyclin H, have also a high CTD kinase activity. On the other hand, the kinase activity of OsCDKD1 rice is highest during S phase, which suggests its involvement in the process of DNA replication, especially as in cell culture overexpressing OsCDKD1, S phase is accelerated (Fabian-Marwedel *et al.*, 2002). However, in *Arabidopsis thaliana* CDKD1 and CDKD3 mutations induce no visible phenotype (Shimotohno *et al.*, 2003).

Conversely, CDKE1, the only member in *Arabidopsis* of a different class of CDK with CTD kinase activity, is necessary for the establishment of the identity of carpels and stamens, and the restriction of floral meristem cells. CDKE would be implicated in regulation of cell differentiation (Wang and Chen, 2004).

2.2.4 CDK activating kinase (CAK) and CDK activating kinase activating Kinases (CAKAK): CDKD and CDKF

In yeast and animals, several CDKs have been identified as CDK-activating kinase, called CAK, or CAKAK if their targets are themselves CAK (Saiz and Fisher, 2002, Fisher and Morgan., 1994, Hermand *et al.*, 2001).

In plants, it has been shown that CDKD and CDKF were active CAK (Chao *et al.*, 2007, Umeda *et al.*, 1998, Yamaguchi *et al.*, 1998). While CDKD are able to phosphorylate CDKA1 and activate its kinase activity, CDKF1 is able to phosphorylate CDKD2 and CDKD3 at the level of their T-loop and functions as a CAKAK. Interestingly, the authors found that this protein does not require a cyclin partner to activate its function (Shimotohno *et al.*, 2004). *In vivo*, mutation of *Arabidopsis* CDKF1 leads to growth retardation, due by both a drop in the number of cells and a lower cells size. In these plants, the protein level of CDKD2 is significantly decreased, while the level of CDKA1 remains unchanged. These results suggest that CDKF1 play a stabilizing role of CDKD2 at the protein level (Takatsuka *et al.*, 2009).

2.2.5 The E2F Transcription Factors

The transcription factor proteins E2F are the most studied CDK/cyclin targets. In *Arabidopsis thaliana*, 6 E2F genes have been found (E2FA to E2FF) (Mariconti *et al.*, 2002). E2F proteins can be classified into 2 subgroups:

The E2FA to C have a DNA binding domain, a transactivation domain, a RBR binding domain and a heterodimerization domain with DP proteins, of which there are two members in *Arabidopsis* (DPA and DPB). While E2FA and B induce cell division (De Veylder *et al.*, 2002), E2FC represses division at the benefit of endoreduplication (Del Poso *et al.*, 2006).

The E2FD, E and F (also called DEL2, DEL1 and DEL3) do not have these various motifs but have a double motif of DNA-binding allowing to recognize and bind to *cis*

sequences recognized by E2F, and this in the absence of DP protein (Vandepoele *et al.*, 2002). These proteins could compete with the complexes E2F/DP and thus prevent transcription of target genes (Mariconti *et al.*, 2002).

The overexpression of E2FD activates cell division at the expense of cell elongation. E2FD overexpression also seems to activate transcription of genes encoding E2FA, E2FB and E2FE, while its mutation causes overexpression of genes coding for the cyclin-dependent kinase inhibitors ICK1/KRP1 and SIM (Sozzani *et al.*, 2010).

E2FE overexpression leads to a decrease in the ploidy level of the target tissue, while its mutation leads to an opposite effect (Vlieghe *et al.*, 2005). Lammens *et al.* (2008) showed that E2FE represses the transition from mitotic cell cycle to endoreduplication cycle by repressing CCS52A2 gene transcription (see 2.3.2).

Finally, E2FF does not seem involved in cell cycle regulation, but cell elongation in the hypocotyls and root by repressing genes involved in cell wall biogenesis. It is interesting to note that the modulation of E2FF expression does not involve any change in ploidy of the cells (Ramirez-Parra *et al.*, 2004).

2.3 Regulation of CDK/Cyclin activity

2.3.1 Transcriptional regulation of cyclins

Previous studies have shown that CDKA or CDKB over-expression, contrary to the over-expression of cyclins, rarely leads to phenotypic changes (see 2.2.1 and 2.2.2). The concentration of cyclin in the cell is a limiting factor in the progression of different phases of the cycle. Cyclins initially derive their name from the fact that these proteins have their quantity oscillating during cell cycle (Evans *et al.*, 1983). The transcriptome analysis of *Arabidopsis* cultured cells has clarified the transcript levels of plant cyclins during the different phases of cell cycle (Menges *et al.*, 2005). Cyclins A and B are preferentially expressed between G2 and M phases, with the exception of cyclin A3. The study of gene promoters of tobacco mitotic cyclins allowed to identify specific motifs involved in mitosis, called mitosis-specific elements (MSE), which are targets of specific proteins of the Myb family of transcription factors (Ito *et al.*, 2001).

Meanwhile, D type cyclins, with the exception of cyclin D3;1, are expressed mainly around the S phase, which make them good candidates for G1/S transition control.

2.3.2 Cyclin degradation: role of the Anaphase Promoting Complex (APC)

As explained above, the limiting factor of CDK/cyclin activity is the availability of cyclins. The quantity of cyclins, in addition to being regulated at the transcriptional level, is the subject of post-translational regulation through ubiquitin-dependent degradation machinery, allowing regulating finely the concentration of cyclin for a short time. Thus, in animals and yeast, the mitotic cyclins are ubiquitinated by the anaphase promoting complex (APC), an ubiquitin ligase complex. Once ubiquitinated, the cyclin is recognized by the proteasomal machinery. The ubiquitin-dependent degradation is activated by the WD40 domain proteins CDC20/FZY and CDH1/HCT1, responsible for the binding of the APC to the target (Fang *et al.*, 1998, Lorca *et al.*, 1998, Zachariae *et al.*, 1998). The first plant homolog of CDH1, called CCS52, was discovered in *Medicago trunculata*. The over-expression of this protein in plant leads to degradation of mitotic cyclins, and early cessation of cell division in favour of endoreduplication and cell growth. Conversely, down-regulation of this gene causes cells division, and smaller and less endoreduplicated cells (Cebolla *et al.*,

1999). In *Arabidopsis*, there are 4 genes encoding CCS52, separated into two groups: CCS52A1/CCS52A2 and CCS52B1/CCS52B2. It has been shown that the misregulation of E2Fe/DEL1 transcription factor complex causes early transcription of AtCCS52A2 and therefore premature start of endoreduplication cycles, highlighting the transcriptional control of AtCCS52A2 by E2Fe/DEL1 (Lammens *et al.*, 2008). Boudolf *et al.* (2009) have shown that cyclinA2;3 is a target of CCS52A. The decrease in the amount of cyclinA2;3 leads to the inactivation of CDKB1;1, which explains the phenotypic effect of CCS52A overexpression. More recently, it has been shown in tomato that affecting the expression of SlCCS52A induces a decrease in fruit size: downregulation of CCS52A induces a decrease in fruit ploidy level and cell size, while upregulation of CCS52A induces a delay in the very early fruit growth and after 15 days post-anthesis an increase in fruit development to match normal fruit size. The *in planta* role of the second class of CCS52, CCS52B, has not yet been studied in detail.

2.3.3 CDKs Phosphorylation: WEE1

As previously shown, CDKs can be phosphorylated at their T-loop, which activates their cyclin interaction motif (see 2.2.4). In contrast, CDKs can also be phosphorylated negatively by WEE1 protein. WEE1 is a protein kinase conserved among plants, animals, and yeast. In plants, WEE1 coding genes have been identified in maize, *Arabidopsis*, and tomato (Sun *et al.* 1999, Sorrell *et al.*, 2002, Gonzalez *et al.*, 2004). Their function as CDK/cyclin inhibitory kinase has been demonstrated *in vitro* (Sun *et al.* 1999) and happens through phosphorylation of the amino acid Tyr-15 of SlCDKA1 (Shimotohno *et al.*, 2006). In tomato, the under-expression of SlWEE1 induces a phenotype of plant dwarfism, with smaller fruits, which have smaller and less endoreduplicated cells than control plants. These results suggest that WEE1 is involved in the onset of endoreduplication cycle (Gonzalez *et al.*, 2007). In *Arabidopsis*, AtWEE1 downregulation induced no phenotype detected when the plants are cultured in normal growth conditions. However, the transformed plants were hypersensitive to DNA-degrading agents, such as UV. Meanwhile, it has been shown that AtWEE1 is induced during such stress. Thus, AtWEE1 plays a role in blocking the cell cycle at G2/M transition in case of DNA damage (De Schutter *et al.*, 2007).

2.3.4 Steric hindrance and blocking of ATP binding sites: The CDK inhibitors (CKI)

The CDK/cyclin kinase activity can be inhibited by stable binding of cyclin-dependent kinase inhibitor proteins (CKI). The next part will deal in more detail with these proteins, the object of study of the present thesis.

3 Role of CDK/Cyc inhibitors in cell cycle control

CDK Inhibitors, or CKI, present in animals, plants and yeast, have been intensively studied in mammalian cells. Indeed, these proteins, which are responsible for inhibition of the CDK/cyclin kinase activity, are frequently found associated with the phenomena of oncogenesis when misregulated. In humans, there are two major families: the INK4 family and the Cip/Kip family. The first plant CKI was discovered in 1997 (Wang *et al.*, 1997). Since then, plants CKIs have been the subject of many studies which will be detailed on the following part.

3.1 Phylogeny and Structure

3.1.1 Two big families: ICK/KRP and SIM

The first plant CKI, discovered in *Arabidopsis thaliana* in 1997, has been named interactor of cyclin-dependent kinase 1 (ICK1) (Wang *et al.*, 1997). Since then, six other CKI counterparts have been found in *Arabidopsis thaliana* (De Veylder *et al.*, 2001). These seven proteins have a common motif at the C-terminus of protein. This motif, identified as a CDK/cyclin interaction domain, has a partial sequence homology with the Kip/Cip family proteins. Surprisingly, the proteins of the Kip/Cip family have this CDK/Cyclin interaction pattern not on their C-terminal side but on their N-terminal side. Apart from this motif, no homology was found between plant CKIs and animal or yeast CKIs.

One functional difference between animal Cip and Kip proteins is that proteins from Cip family, unlike Kip, are able to complex and inhibit PCNA, a protein that forms a homotrimer around DNA that tethers proteins such as polymerase for DNA replication or repair. The fact that the plant CKI are unable to bind PCNA (DeVeylder *et al.*, 2001) associated with a slightly higher homology with p27Kip1 than with p21Cip1, led the authors to rename these proteins Kip-related protein (KRP), name which is now the most widely used and will be used later.

So far, there are seven *Arabidopsis thaliana* KRPs, two in tomato (Bisbis *et al.*, 2006), two in tobacco (Jasinsky *et al.*, 2002), one in Chenopodium rubum (Fountain *et al.*, 1998), one in *Medicago* (Pettzo-Sandtzner *et al.*, 2006), seven in rice (Barocco

et al., 2006, Guo *et al.*, 2007), and four in maize (Coelho *et al.*, 2005, Rimen et al., 2007).

More recently, another family of inhibitors was discovered. The gene SIAMESE (SIM), initially studied because its mutation induced phenotypes in *Arabidopsis thaliana* trichomes, has been functionally identified as a CKI (Walker *et al.*, 2000; Churchman *et al.*, 2006). Other proteins of the same family were identified by sequence homology. There are currently six SIM genes in *Arabidopsis*, three in tomato, two in maize, one in potato, two in rice, one in poplar and one in glycine.

These proteins have very low sequence homology with KRPs, with only 6 conserved amino acids identified: E[ILM][ED][EDR][FL]F (Churchman *et al.*, 2006).

They have only in common with animal CKIs the presence of 4 conserved residues ZRXL (Z with a cysteine or basic amino acid, and X preferably basic) also found in proteins that interact with cyclins such as E2F1, p107 and p130 (Adams *et al.*, 1996; Chen *et al.*, 1996; Peres *et al.*, 2007).

3.1.2 Sequence Homology within the KRPs family

KRPs from *Arabidopsis thaliana* have a molecular mass predicted between 20 and 30 kDa. This size variation of KRPs also exists between distinct species.

As mentioned above, KRPs have homology with p27KIP1 counterparts in only a short amino acid sequence, which is located moreover in opposite positions in p27KIP1 and in KRPs (see Figure 6).

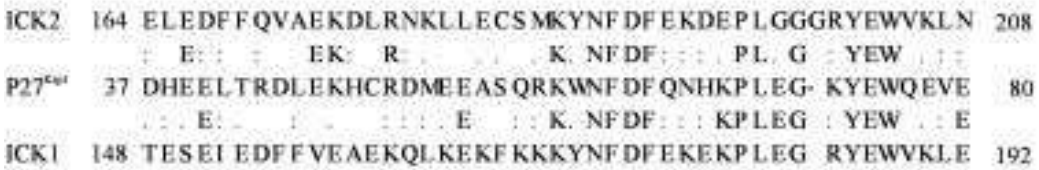

Figure 6 : Comparison of CDK/Cyclin binding motif sequences between p27Kip1, ICK1/KRP1 and ICK2/KRP2, from Lui *et al.*, 2000

Apart from this motif, little homology exists between KRPs of the same species or between different plant KRPs. Nevertheless, several bioinformatics studies have highlighted different conserved motifs in some KRPs (Wang *et al.*, 2007b; DeVeylder *et al.*, 2001; Barroco *et al.*, 2006).

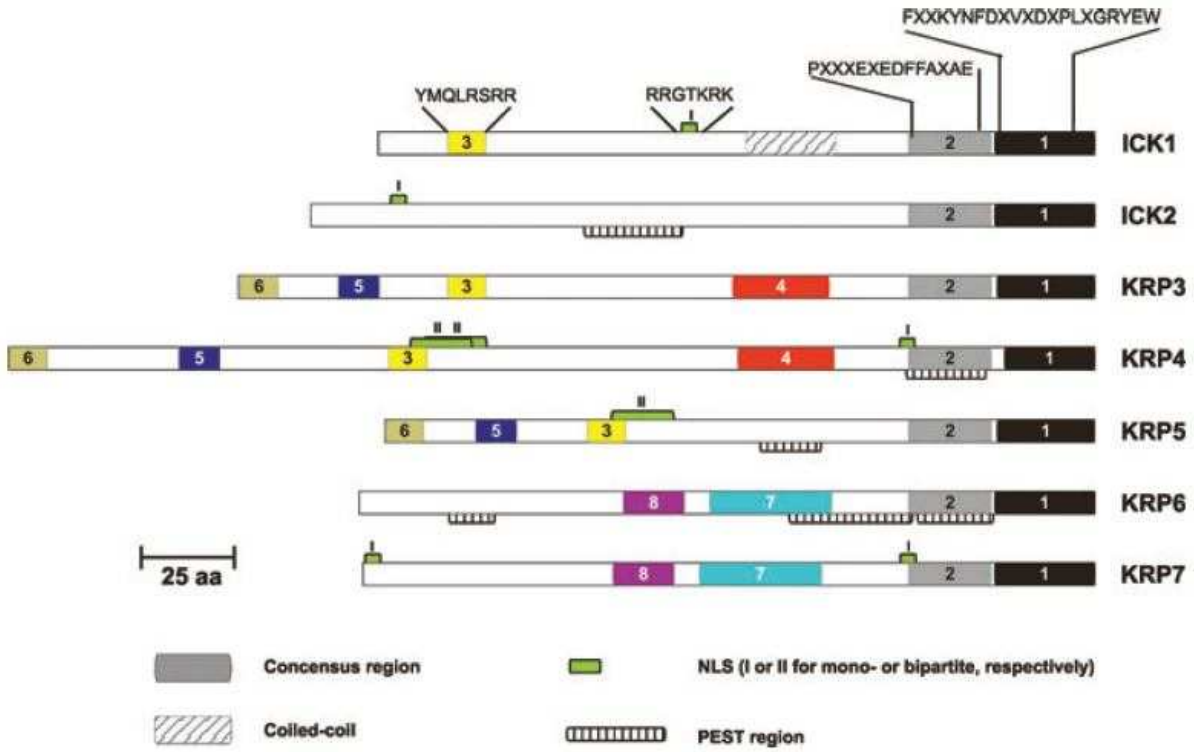

Figure 7 : Schematic representation of the sequences of seven *Arabidopsis thaliana* KRPs and their conserved motifs, from Wang *et al.*, 2007b.

The representation of Wang *et al.* 2007b (Figure 7) shows different boxes which are conserved in *Arabidopsis*, but also in other plants KRPs studied. Motif 1 is the CDK/cyclin binding motif common with p27Kip1.

Motif 2 is specific to all plants CKI. Although its exact function is unknown, it has been suggested that this is a cyclin binding motif, since the deletion of this motif in the SIM -like protein OsEL2 induced loss of interaction with cyclin D in two-hybrid and FRET (Peres *et al.*, 2007). Apart from motif 3, which seems to be a sub-cellular localization signal (see 3.2.3), the other motifs are of unknown function.

3.2 Expression and localization of KRPs

3.2.1 Expression of KRPs in tissues

KRPs form a multigenic family. The studies of gene expression patterns of *Arabidopsis thaliana* KRPs showed a distinct spatial pattern for each one of them (Ormenese *et al.*, 2004; Menges *et al.*, 2005; Engler *et al.*, 2009; Himanen *et al.*, 2002). However, some expression pattern redundancy does exist, and so far, no phenotype has been associated with a mutation in a KRP, probably due to a

compensatory function by other KRPs present. However, in some mutant contexts, the downregulation of KRP can have a physiological effect (Ren *et al.*, 2008; see 3.3.3).

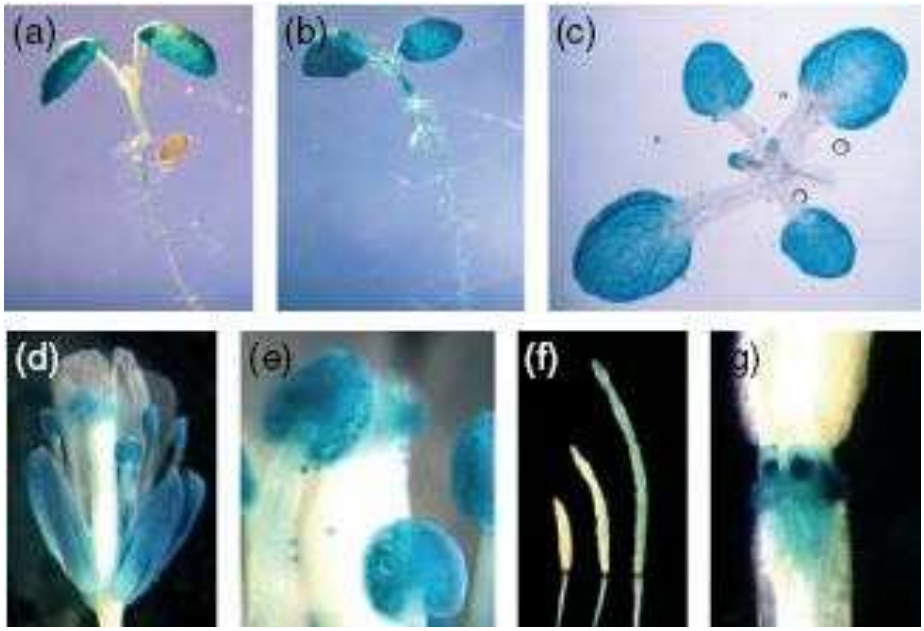

Figure 8 : GUS staining in *Arabidopsis* plants carrying the transgene KRP1::GUS

(A) / (b) Staining of seedlings for 4h/24h, (c) rosette leaves, (d) mature flowers, (e) anthers, (f) siliques, (g) Basis of the silique, from Ren *et al.* (2008)

As shown in the above figure (Figure 8), AtKRP1 is expressed in multiple tissues during plant development. It is mainly expressed in leaves, flowers in the sepals, anthers and stigma, and at the basis of the silique and in mature silique (Ren *et al.*, 2008). It has been shown that AtKRP1 is induced by absissic acid, low temperatures, and salt stress (Wang *et al.*, 1998; Ruggiero *et al.*, 2004). This suggests that AtKRP1 is induced under stress conditions to stop the cell cycle.

AtKRP2 seems to be specifically expressed in epidermal layers. AtKRP2 is negatively regulated by auxin. In the roots, the auxin could thus allow initiation of lateral roots by the removal of inhibition by AtKRP2 (Richard *et al.*, 2001; Himanen *et al.*, 2002; Engler *et al.*, 2009). Gibberellic acid could also downregulate AtKRP2, through the negative control of DELLA (Achard *et al.*, 2009).

According to the TAIR, AtKRP3 and AtKRP5 are highly expressed in meristems and AtKRP4 in seeds.

AtKRP6 and AtKRP7 profiles are less clear, AtKRP6 being absent from most DNA chips. These two genes are nevertheless important in gametogenesis (Kim *et al.*, 2008, Liu *et al.*, 2008, Gusti *et al.*, 2009).

In tomato, the expression profiles in different tissues of two KRPs, SlKRP1 and SlKRP2, have been described (Bisbis *et al.*, 2006). Each of these two genes has a specific expression pattern. While these two genes are expressed strongly in early fruit development, SlKRP2 is also expressed strongly during fruit ripening, and SlKRP1 is rather associated with the expansion phase in endoreduplicating cells.

3.2.2 KRPs Expression during cell cycle

Most genes involved in cell cycle control are differentially expressed during the different phases of the cycle (Menges *et al.*, 2005). It has been shown that *Arabidopsis thaliana* KRPs are differentially expressed, which suggests specific roles within the family during the cycle (see Figure 9).

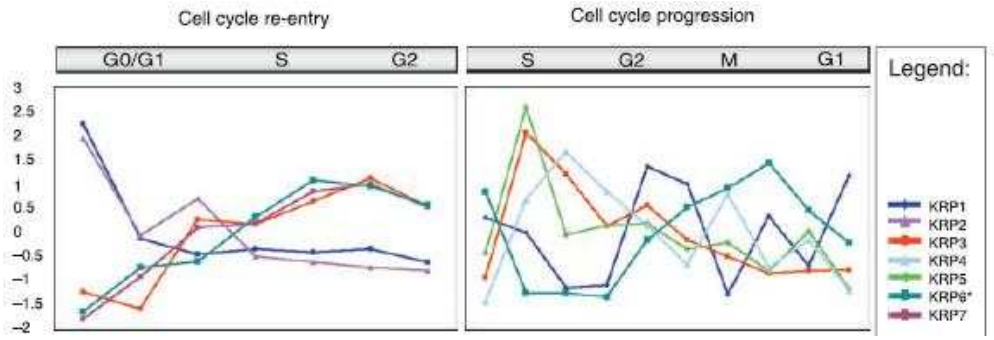

Figure 9 : Expression of the *Arabidopsis* KRPs in synchronized cells in culture, according to Menges *et al.* (2005). The left graph shows the evolution of different KRPs expression after latency by sugar starvation, and the graph at right shows the gene expression evolution after aphidicolin synchronization

Menges *et al.* (2005) have shown that, during the cell cycle, KRP3, -4 and -5 are preferentially expressed in S phase, while KRP1 shows a clear peak of expression in G2/M and KRP6 peaks from G2 to the end of M phase. Furthermore, upon entry into the cell cycle, KRP-3, -6 and -7 tend to increase while on the contrary to KRP1 and KRP2 tend to decrease. These results led logically to the hypothesis that KRP1 and -6 are involved in the mitotic mechanism and that KRP3, -4 and -5 are involved in the regulation of CDK/cyclin to control S phase. It is interesting to correlate these results

with the presence of conserved motifs within KRP3, -4 and -5 (see 3.1.2). Indeed, these three KRPs share several specific motifs.

3.2.3 Sub-Cellular localization of KRPs

Other motifs, in addition to those previously cited (see 3.1.2), are present in only some KRPs. Two of them have seen their function partially identified:

Thus, the AtKRP1 protein carries a functional NLS “RRGTKRK” at the centre of the protein sequence and a conserved sequence “YMQLRSRR”, noted motif 3 by Wang *et al.* (2007b), also present in AtKRP3, -4 and -5, which provides a spotted nuclear localization to these proteins, while other KRPs which do not have this motif are distributed homogenously in the nucleus.

Figure 10 shows the sub-nuclear localization of *Arabidopsis thaliana* AtKRP1 fused to GFP in *Arabidopsis* protoplasts.

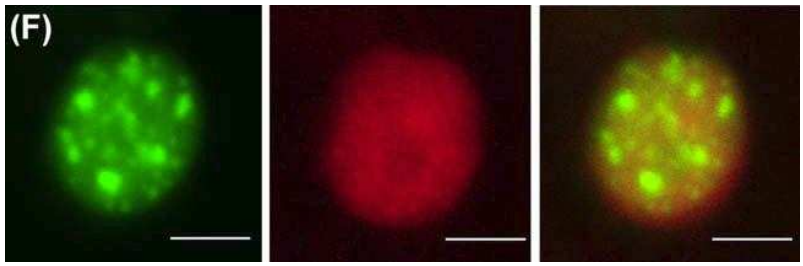

Figure 10 : Sub-nuclear localization AtKRP1 (left), compared with DAPI (centre), showing the punctuate nuclear localization of certain KRPs from Zhou *et al.* (2006)

The *Arabidopsis* KRPs, which are all nuclear, can be separated into two categories according to their sub-nuclear localization:

ICK2/KRP2, ICK4/KRP6 and ICK5/KRP7 are uniformly localized in the nucleus, while ICK1/KRP1, ICK6/KRP3, ICK7/KRP4 and ICK3/KRP5 are heterogeneously distributed in the nucleus.

The suppression of motif 3 “YMQLRSRR” in AtKRP1 leads to loss of any preference to protein localization (Zhou *et al.*, 2006). This suggests a role for this motif in locating KRPs heterogeneously in the nucleus. However, the same motif deleted in AtKRP3 has no effect on the localization of the protein (Bird *et al.*, 2007).

The particular location of this sub-category of KRPs seems dynamic, since in experiments of colocalization with DAPI, a marker of DNA, and MBD3, a marker specific zones of methylated DNA, AtKRP1 colocalizes intensively at the level of condensed chromatin or in turn with DNA, with MBD3, or neither. To date, despite various attempts, no function or any nuclear structure could be linked to these nuclear bodies (Bird *et al.*, 2007).

3.3 Biochemical function and Post-Translational regulation

3.3.1 KRP Biochemical activity

Originally, the first KRP was discovered during a two-hybrid experiment between AtCDKA1 as bait and an *Arabidopsis thaliana* cDNA library (Wang *et al.*, 1997). The interaction between CDKA and KRP was subsequently demonstrated by *in vitro* binding assay (Wang *et al.*, 1998), then *in vivo* (Verkest *et al.*, 2005; Bisbis *et al.*, 2006).

The ability of KRPs to inhibit purified CDK/cyclin complexes was proven by measuring the CDK/cyclin kinase activity on histone H1 or on RBR, in the presence or absence of KRP (Wang *et al.*, 1997; Jasinski *et al.*, 2002b; Verkest *et al.*, 2005; Bisbis *et al.*, 2006; Pettko-Szandtner *et al.*, 2006; see Figure 11).

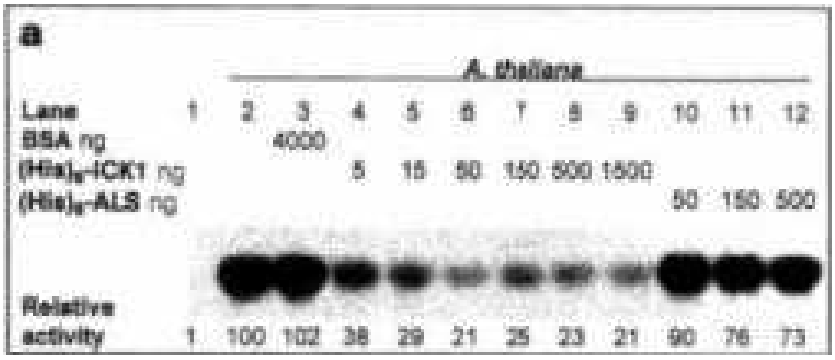

Figure 11 : ICK1/ KRP1 Inhibitory activity on Histone H1 kinase activity of CDKA complex, from Wang *et al.* (1997)

However, the KRPs have necessarily other targets than CDKA/cyclin complexes. Indeed, mutation in the *CDKA* gene does not lead to alteration of the cycle during female gametogenesis (Iwakawa *et al.*, 2006; Nowack *et al.*, 2006), while mutated *ICK4/KRP6* is able to block the development of the female gametophyte (Liu *et al.*, 2008).

Meanwhile, several studies have shown that KRPs could bind and inhibit CDKB complexes *in vitro* (Pettko-Szandtner *et al.*, 2006; Nakai *et al.*, 2005). However, there is no evidence that such a function exists *in planta*.

In addition to interacting with CDKA, it has been shown by two-hybrid that KRPs are capable of binding to cyclin D (Wang *et al.*, 1998). This ability seems to have a reality *in planta* as in tobacco and *Arabidopsis*, the over-expression of cyclin D partially compensates the phenotype induced by KRP overexpression (Jasinski *et al.*, 2002; Zhou *et al.*, 2003; Schnittger *et al.*, 2003).

The inhibition of purified CDK/CycA1 and -A2 complexes by KRPs has also been shown in *Medicago* and maize (Coelho et al, 2005; Pettko-Szandtner *et al.*, 2006). During these studies, no inhibition of complexes associated with cyclin B has been detected.

It is interesting to note that the CDK/cyclins found in G2 and M are more sensitive to inhibition by KRP than CDK/cyclin found in G1 and S (Pettko-Szandtner *et al.*, 2006).

3.3.2 KRP/CDK/Cyc interaction at the molecular scale

The study of the structure of CDK/Cyc/CKI was made by crystallography in humans (Russo *et al.*, 1996).

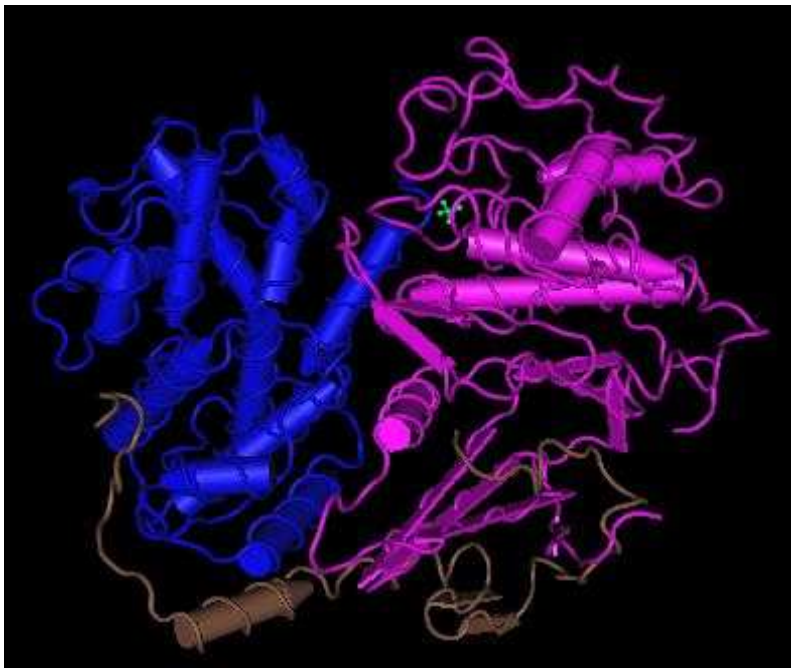

Figure 12 : Representation of a human complex Cdk2 (pink) / CycA (blue) / p27Kip1 (brown) observed by crystallography, from Russo *et al.*, 1996

As shown in Figure 12, p27Kip1 binds to CDK/Cyclin complexes both at the cyclin level, and at the CDK level. The association with the CDK modifies the conformation of the N-terminal lobe of the protein, and occupies the binding site for ATP (Russo *et al.*, 1996).

So far, no structural data exists in plant models. The presence of sequence homology between KRP and p27Kip1 at the binding site for CDK/cyclin complexes suggests that plants and animal CKI could have a similar structure. However, in p27Kip1 the binding motif CDK/cyclin is located in the N-terminus of the protein, whereas this motif is on the C-terminal part of KRPs, which suggests a complex at least partially different from the point of view of its structure, and maybe its functioning.

3.3.3 Degradation of KRPs

In humans, p27Kip1 can be phosphorylated by CDK1/CDK2. Once phosphorylated, p27Kip1 protein is recognized by CSN5 and is then transported for ubiquitination and degradation by the proteasome (Tomoda *et al.*, 1999).

Clues on the degradation of KRP proteins existed for several years.

The over-expression in *Arabidopsis* trichomes of a truncated version of KRP1 without its N-terminal part leads to a phenotype stronger than in the case of similar over-expression of the entire protein (Schnittger *et al.*, 2003). Indeed, it appears that a truncated protein fused to GFP gives a more intense signal than the entire protein, showing that the N-terminal KRP1 is responsible for the instability of the protein (Zhou *et al.*, 2003). In addition, it appears that a C-terminal located motif could be also responsible of KRP degradation (Jacoby *et al.*, 2006). The first evidence of the involvement of 26S proteasome in the degradation of KRPs were obtained in experiments blocking the proteasome by the chemical agent MG132: MG132 treatment of plants over-expressing a KRP leads to increased amounts of KRP protein (Verkest *et al.*, 2005; Jacoby *et al.*, 2006). Finally, KRPs can be phosphorylated *in vitro* by CDK/cyclin, and it has been shown *in vivo* that the amount of protein KRP2 increases in plants downregulating CDKB (Verkest *et al.*, 2005).

More recently, many studies suggest that KRPs are subject to regulatory pathways similar to those discovered in humans.

Thus, it was shown that NtKIS1a and NtKIS1b can interact with NtCSN5 in tobacco (Le Foll *et al.*, 2008).

In addition, the E3 ubiquitin ligases SCF^{Skp2b} and RKP could be responsible for KRPs degradation. Indeed, in *Arabidopsis*, the mutation of SKP2b or RKP leads to an increase in the amount of AtKRP1 (Ren *et al.*, 2008). More recently, it has been shown that RKP is induced by BSCTV infection, which lead to ICK/KRPs decrease, and hence cell proliferation and geminivirus propagation (Lai et al., 2009).

Finally, two studies showed that KRPs are finely regulated, and this in the particular context of gametophyte development:

- The mutation of two *Arabidopsis* RING class E3 ligases, RHF1 and RHF2, results in the stabilization of AtKRP6 protein and leads to arrest of gametophytic male and female development between the stages of meiosis and mitosis. The downregulation of AtKRP6 in the rhf1/rhf2 double mutant context restores gametophytic development, showing that KRP6 is an *in vivo* substrate of these E3 ligases (Liu *et al.*, 2008). As CDKA1 mutation does not induce defects at the female gametophyte (Iwakawa *et al.*, 2006; Nowack *et al.*, 2006), KRP6 must have necessarily another target to cause development failure in this context.

- AtFBL17, an F-box protein responsible for binding specificity between a target and the SCF complex is responsible of AtKRP6 and AtKRP7 degradation specifically to ensure mitosis of the male gametophyte (Nam *et al.*, 2008).

3.3.4 Activating Post-Translational Regulation

There is very little information about possible activating post-translational regulation of KRPs. The only conclusive study about this subject concerns MtKRP1 phosphorylation by a calmodulin-like kinase, MsCPK3, in *Medicago* (Pettko-Szandtner *et al.*, 2006). In this study, the authors have demonstrated the *in vitro* phosphorylation of serines located in the N-terminal part of MsKRP1 by MsCPK3. Once phosphorylated, the CDKA/cyclin inhibitory activity of KRP is increased.

3.4 Physiological role

3.4.1 Inventory of different studies concerning over-expression of KRPs

The *in planta* role of KRPs was studied by transgenesis repeatedly. While so far no phenotype has been associated with downregulation or mutation of a KRP, several series of plants from various species over-expressing a KRP were analyzed.

The studies mainly concern the constitutive over-expression (under control of the constitutive 35S promoter) of AtKRP1 (Wang *et al.*, 2000) and AtKRP2 (Verkest *et al.*, 2005) in *Arabidopsis thaliana*, of NtKIS1a NtKIS1b in tobacco (Jasinski *et al.*, 2002a, Jasinski *et al.*, 2002b), and of OsKRP1 in rice (Barroco *et al.*, 2006). These studies are summarized Table 1.

Meanwhile, KRP over-expression has been achieved by tissue specific promoters, with AtKRP1 controlled by Bgp1 or AP3 promoters in *Brassica* (Zhou *et al.*, 2002), AtKRP1 and AtKRP4 under the control of ML1 promoter in *Arabidopsis* (Bemis *et al.* 2007), AtKRP1under control of GL2 promoter in *Arabidopsis* (Schnittger *et al.*, 2003, Weinl *et al.*, 2005) and ZmKRP1 under the control of UBI1 promoter in maize calli (Coelho *et al.*, 2005). These studies are summarized Table 2.

Some of these studies also include co-expression of the protein with another candidate (Table 3).

Table 1 : Summary of studies involving constitutively over-overpressed KRPs

Species	Genes	Focused Tissue	Effect on			Particular Conclusions	References
			Cell divisions	Cell size	Endocycle		
Arabidopsis	AtKRP1	leaves	-	+	-	KRPs are in vivo cell cycle inhibitors	Wang et al., 2000/ Zhou et al., 2003
	AtKRP2	leaves (weak overexpression)	-	-	+	divisions require high CDKA activity	Verkest et al., 2005
		leaves (strong overexpression)	-	+	-	endoreduplications require low CDKA activity	
	AtKRP2	roots	ND	ND	ND	AtKRP2 prevents lateral root initiation	Himanen et al., 2002
	AtKRP2	cinetic of leaf growth	-	+	-	Inhibition induces cell size compensation during the mitotic cycle	De Veylder et al., 2001, Ferjani et al., 2007
Tobacco	NtKIS1a	leaves	-	+	-	KRP post-translational downregulation inside shoot meristem	Jasinsky et al., 2002a, Le Foll et al., 2008
	NtKIS1b (lacks motif 1)	leaves	=	=	=	motif1 necessary for inhibition	Jasinsky et al., 2002b
Rice	OsKRP1	cinetic of leaf growth	-	+	ND	cycle slow down/ cell size compensation	Barroco et al., 2006
		endosperm	ND	ND	-	inhibition blocks endoreduplication	

Table 2 : Summary of stuides involving over-expressed KRPs using tissue specific promoters

Species	Genes	Promoter : tissue affected	Focused Tissue	Effect on			Particular Conclusions	References
				Cell divisions	Cell size	Endocycle		
Brassica	AtKRP1	AP3	petals	-	=	ND	AP3 expresses only during divisions	Zhou et al., 2002
Arabidopsis	AtKRP1	GL2 : trichomes	trichomes	NA	-	-	KRPs are in vivo cell cycle inhibitors	Schnittger et al., 2003/Weinl et al., 2005
			cells neighbouring trichomes	-	+	+	KRPs can travel to and inhibit cell cycle of neighbouring cells	
	AtKRP1 del1-109	GL2 : trichomes	trichomes	NA	-	-	N-ter of KRP1 devoted to protein instabiility	
		TTM : young leaf stomatal lineage and neighborbing cells	leaves	-	+	+	Inhibition blocking mitosis promotes endoreduplication	
	AtKRP1 del1-152	GL2 : trichomes	trichomes	-	=	=	C-ter of KRP1 devoted to inhibition activity	
	AtKRP1 or AtKRP4	ML1 : meristematic layer L1	epidermis	-	+	ND	no epidermis to endoderm harmonization	Bemis et al., 2007
			meristems	=	=	ND	inhibition effect is context dependent	
	AtKRP2	STM : Apical meristem	leaves	-	+	+	premature endoreduplication onset	Verkest et al., 2005
Maize	ZmKRP1	UBI1	endosperm cells calli	-	ND	+	inhibition promotes endoreduplication	Coelho et al., 2005

Table 3 : Summary of studies involving in vivo complementation between KRPs and candidate proteins

Expression Type	Species	KRP	candidate	effect	References
co-expressions	Tobacco	35S::NtKIS1a	35S::NtCycD3;1	restoration	Jasinsky et al., 2002a
	Arabidopsis	35S::AtKRP1	35S::AtCycD2 or 35S::AtCycD3	restoration	Zhou et al., 2003
		35S::AtKRP6-RNAi	rhf1a/rhf2a double mutant	restoration	Liu et al., 2008
		pGL2::AtKRP1del1-109	pGL2::AtCycD4;1	no rescue	Schnittger et al., 2003
		pGL2::AtKRP1del1-109	pGL2::AtCycD3;1	restoration	
		pGL2::AtKRP1del1-109	pGL2::CycB1;2	no rescue	
		pGL2::AtKRP1del1-109	pGL2::CDKA1	restoration	
		pGL2::AtKRP1del1-109	pGL2::CDKB1;1	no rescue	
		pGL2::AtKRP1	sim mutant	restoration	

3.4.2 Effects of constitutive over-expression of a KRP on Plant Development

All plants subject to the constitutive over-expression of a KRP share the same phenotype of dwarfism more or less pronounced (see Figure 13).

Figure 13 : Size comparison between *Arabidopsis* over-expressing AtKRP1 (right) and a wild plant (left), from Wang *et al.* (2000)

The study of some of these plants by microscopy techniques nevertheless unravelled that the alteration of plant size may be due to different phenotypes at the cellular level depending on the level of transgene expression and the model studied:

The over-expression of the KRP NtKIS1a in tobacco leads to an increase in cell size with a drop of endoreduplication. This phenotype is gradual depending on the degree of over-expression (Jasinski *et al.*, 2002a; see Figure 14).

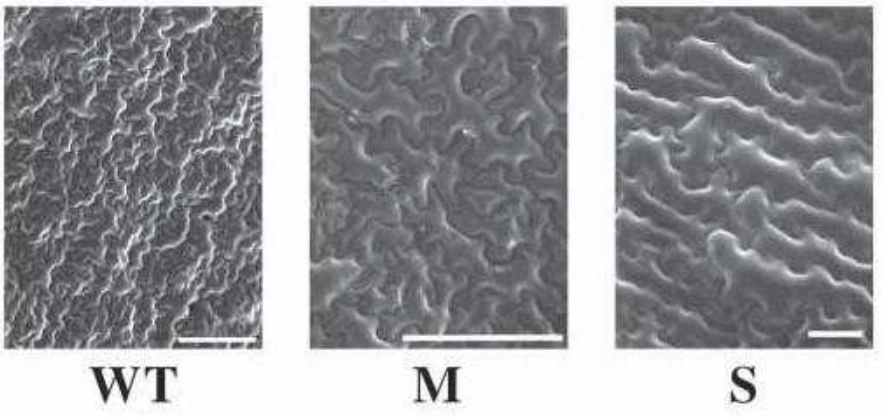

Figure 14 : Electron microscopy view of the underside of leaves of wild tobacco (WT) and transgenic tobacco overexpressing NtKIS1a at a moderate level (M) or at a strong level (S) from Jasinski *et al.* (2002a). Note the difference in scale (representing 100 µm) between each image

The over-expression of AtKRP2 in *Arabidopsis thaliana* leads (Verkest *et al.*, 2005) either to:

- Slightly smaller plants, which are composed of slightly fewer cells, which are themselves slightly smaller than WT cells, but more endoreduplicted (moderate over-expression).

- Much smaller plants composed of very few cells, which are much larger than in the wild type plants. These cells are much less endoreduplicated compared to WT cells (strong over-expression).

The over-expression of AtKRP1 in *Arabidopsis thaliana* leads to plants with fewer cells, which were slightly larger than the cells of the wild type but less endoreduplicated (Zhou *et al.*, 2003)

It should be noted in this study that astonishingly, the F1 homozygous plant 35S::AtKRP1 expressed the transgene less strongly than F2 heterozygous plants WT X F1 crosses.

Finally, the over-expression of OsKRP1 in rice led to a slowdown in the rate of cell division in developing leaves, partially offset by larger cells. The endosperm of affected plants is less endoreduplicated than in WT.

Although in all these cases the cell cycle is affected, some results may seem contradictory. However, it is possible to explain these results by correlating them with the fact that the CDK/cyclin complexes found in G2 and M are more sensitive to inhibition by KRPs than CDK/cyclin found in G1 and S (see 3.3.1).

Thus, CDK/cyclin complexes responsible for mitosis are more strongly affected than CDK/cyclin complexes responsible for S phase. It follows that at low over-expression levels, only the M phase is significantly affected, reducing the divisions in favour of endoreduplication. At a higher level of over-expression, DNA replication is also inhibited, resulting in very few cells with low levels of ploidy.

In almost all cases, the cells of transformed plants are larger than the corresponding control plants. As the size of an organ is the result of multiplying the number of cells

by their size, these studies would suggest the existence of a size control of the organ, including both cell division and cell expansion. In this case, slowdown in cell division would be compensated by increasing cell expansion. This effect is well illustrated in the case of the growth dynamics of rice leaf explained above, but appears to be only active during the growth phase of plants. Indeed, when compared to the control, the plants stopped growing when they became mature without having catched their delay. The timing of development is therefore independent of this control in cell division/cell size. It is interesting to note that in *Arabidopsis* plants overexpressing constitutively AtKRP2, the compensation of lower division by cell growth in leaves occurs during the mitotic phase of development (De Veylder *et al*., 2001; Ferjani *et al.*, 2007).

Finally, there is in almost all cases a decoupling, or even an inverse relationship between cell size and endoreduplication. Thus, whether endoreduplication and cell size have no causal relationship, but result from parallel development contexts or signalling pathway, both phenomena occur upstream of KRPs targets or the control carried out at the scale of the organ only affects cell expansion, masking the coupling endoreduplication/expansion existing at the cellular level.

3.4.3 Effects of tissue-specific over-expression

Studies of transgenic plants over-expressing constitutively a KRP have the advantage of showing the effect of the gene throughout the whole plant, but have the disadvantage of being unable to discern in a given tissue the transgene effects from the effects due to abnormal development of the rest of the organ and of the plant.

Thus, several more detailed studies were conducted where the over-expression of KRP was directed to specific tissues.

Verkest *et al.*, 2005 have shown that KRP overexpression specifically in shoot meristem and subsequent dividing tissues by the STM promoter can lead mitotic cells to enter prematurely into endoreduplication. Indeed, ploidy level of leaflets began to increase sooner in transgenic lines than in control plants, effect which could be clearly detected at 12 days after sowing.

Meanwhile, Bemis *et al.* (2007) have over-expressed alternatively AtKRP1 and AtKRP4 specifically in the L1 layer of the apical meristem. This layer of the meristem is responsible of the formation of the epidermis of aerial surfaces.

Resulting plants suffer from the phenotype of dwarfism, mainly due to the restriction of cell divisions in the epidermis. However, epidermal cells are larger, with nuclei larger than WT nuclei.

The fact that the reduction of the surface of the epidermis leads to a reduction in organ size is consistent with physical constraints of the epidermis on development (Green *et al.*, 1996). At the same time, the cells of inner layers of organs continue to divide in a reduced space, leading to their disorganization (see **Figure 15**).

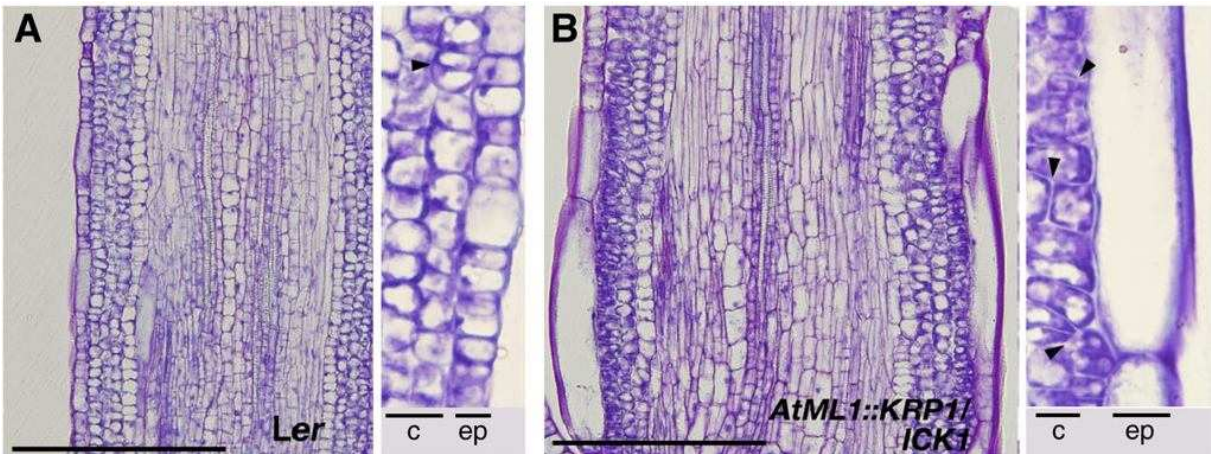

Figure 15 : Longitudinal section of stalk of (A) wild type plant and (B) transformed plant ML1: KRP1. Arrows point to cortex cells organization disrupted due to anticline divisions, from Bemis *et al.*(2007)

These results show, in this case, the autonomy of a cell layer to another, in terms of cell cycle. Thus, inhibition of cell division in the epidermis is not sufficient to induce modification of intercellular signals that would adjust the development in the rest of the organ.

It is most interesting to note that during this study, the over-expression of KRP in the L1 layer of shoot meristem does not induce a phenotype in the organization of the shoot itself, showing that the KRPs effect is context dependent. Interestingly, Le Foll *et al.*, (2008) have shown that the fluorescent signal of NtKIS1a overexpressed under the constitutive promoter 35S can not be detected in the shoot apical meristem. The

absence of phenotype associated with over-expression of a KRP inside the shoot meristem could thus be due to degradation of the inhibitor.

Another study, involving over-expression of AtKRP1 specifically in the trichomes of leaves of *Arabidopsis*, provides different conclusions:

Trichomes over-expressing AtKRP1 are smaller, have fewer branches and are less endoreduplicated. In addition, the authors have shown that AtKRP1 over-expressing trichomes enter into programmed cell death (Schnittger *et al.*, 2003; see **Figure 16**).

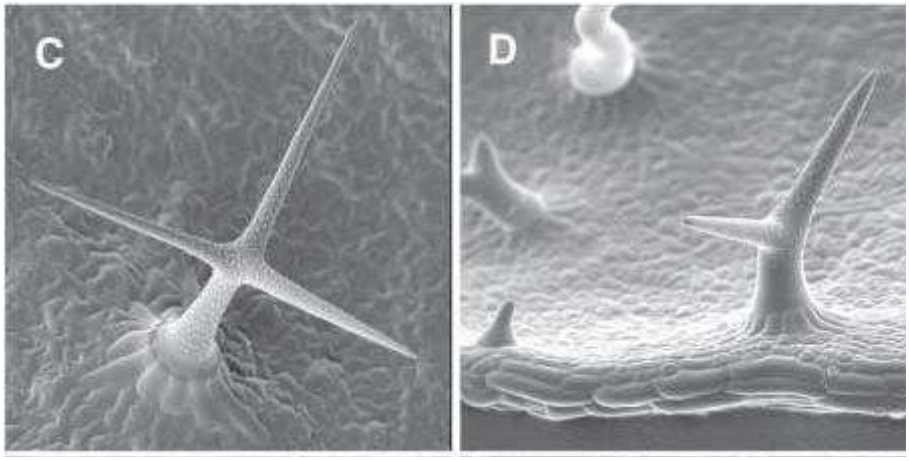

Figure 16 : Electron microscopy image centered on a wild plant trichome (left) and transformed plant GL2:: AtKRP1 from Schnittger *et al.* (2003)

If the lower level of endoreduplication is easily explained by parallel with previous studies, the fact that the cells decrease in size is contradictory to what has been seen previously. This can certainly be explained by the particular tissue context of the trichome that do not participate to organ size and could thus be excluded from any control and any compensation at the organic scale.

Thus, in this particular context, the over-expression of KRP leads to smaller cells. As the discrepancy of endoreduplication was not linearly followed by cell size, which remained bigger than one would expect, the authors hypothetized that trichome size is conditioned by both the endoreduplication level and an other factor.

It is interesting to note that co-overexpression of AtCycD3,1 compensates the phenotype, unlike the co-overexpression of AtCycB1;2 which induces the division of these abnormal trichomes.

The same authors have also shown that KRP1 when expressed in trichomes induces an additional phenotype in cells surrounding trichomes: they are broader and more endoreduplicated. This phenotype is explained by the transport of the protein over-expressed to adjacent cells (Weinl *et al.*, 2005; see Figure 17).

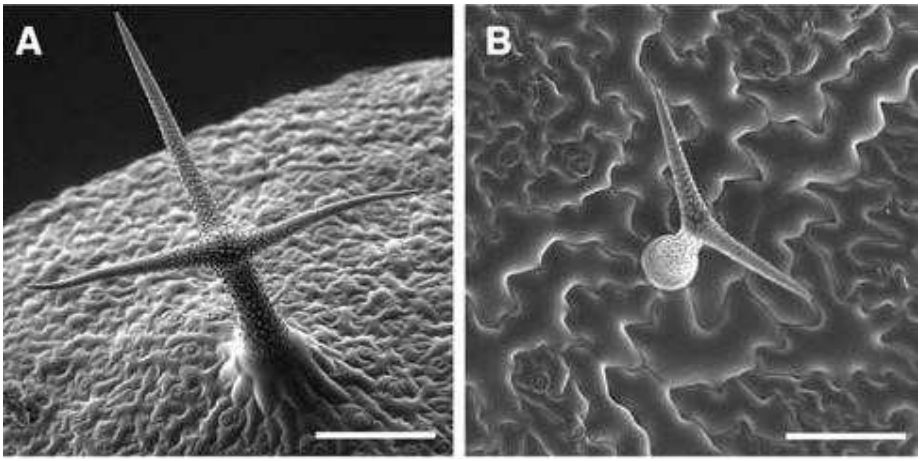

Figure 17 : Electron microscopy images centered on a wild plant trichome (left) and transformed plant GL2:: AtKRP1Δ1-108, from Weinl *et al*. (2005)

The difference between the phenotypes of trichomes (small and less endoreduplicated) and neighbouring cells (larger and more endoreduplicated) can be explained by a difference in the amount of KRPs present and the specific cell cycle state of each cell. Thus, neighbouring cells with a lower amount of KRP have their mitotic CDK/cyclin inhibited, inducing an increase of endoreduplication at the expense of the divisions. These cells compensate for their small numbers by expansion, specifically in their tissue context. Interestingly, when over-expressor trichomes die, surrounding endoreduplicated cells resume divisions, showing that cessation of division for endoreduplication is not necessarily irreversible.

3.4.4 Phenotypic effect of misregulation of genes from the SIM family

Discovered more recently, the SIM genes family has been little studied in comparison with the genes coding for KRPs. There are however two studies dealing on this protein family, in *Arabidopsis* and rice (Churchman *et al.*, 2006; Peres *et al.*, 2007).

The SIAMESE (SIM) gene, the first family member discovered, was initially studied because of the phenotype induced in *Arabidopsis thaliana* trichomes by its mutation. Contrary to KRPs mutations without phenotype, probably due to compensation by

other family members, mutation of SIM can induce a phenotype: mutation of this gene leads to multicellular trichomes with low endoreduplication (Churchman *et al.*, 2006; Peres *et al.*, 2007; see Figure 18).

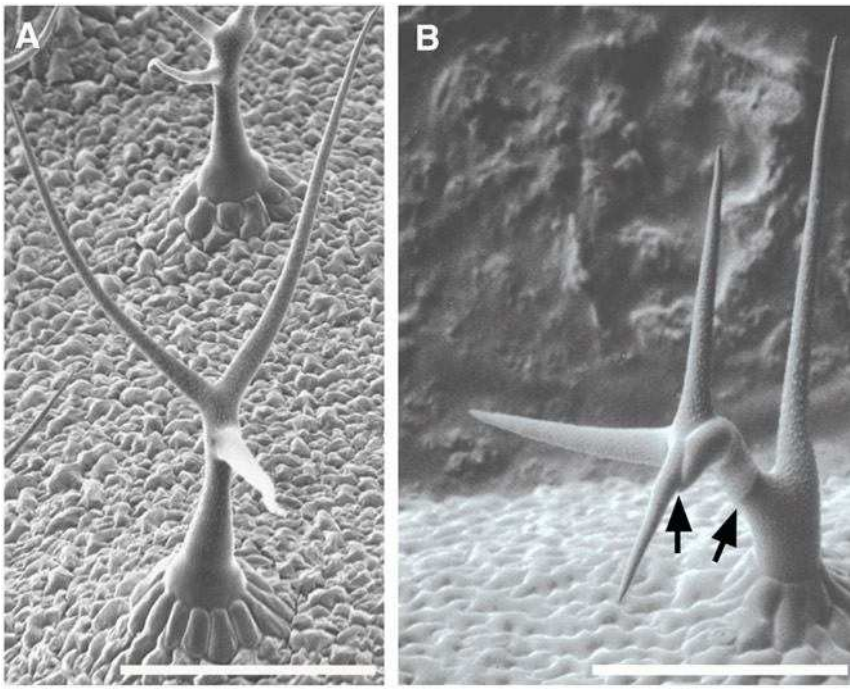

Figure 18 : Electron microscopy images centered on a wild plant trichome (left) and mutant plant sim (right), from Churchman *et al.* (2006)

The plants over-expressing constitutively SIM suffer from dwarfism, and have larger and more endoreduplicated cells than control plants (see Figure 19).

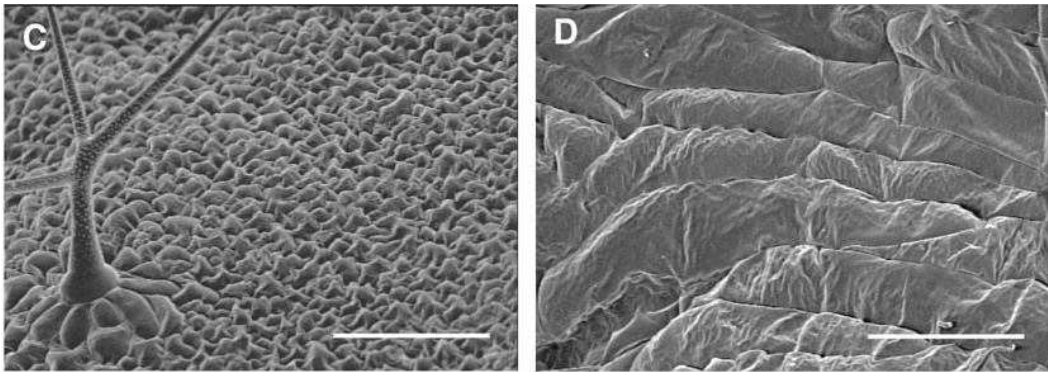

Figure 19 : Electron microscopy images of the adaxial side of a wild type plant (left) and transformed plant 35S::SIM, from Churchman *et al.* (2006)

Chuchman *et al.* (2006) showed by FRET that SIMs like KRPs are able to interacting with different cyclins D and CDKA1. In addition, it has been shown that OsEL2, a SIM from rice, is able to inhibit CDKA/cyclin complex kinase activity. The function of the

SIM seems partially redundant with that of KRPs, especially since in *Arabidopsis* the phenotype due to the *sim* mutation can be compensated by GL2::KRP1 over-expression (Weinl *et al.*, 2005).

From the study of phenotypes associated with mutation or overexpression of SIM (Churchman *et al.*, 2006), it is important to note that SIM negatively controls the division level for the benefit of endoreduplication. These proteins are probably involved in the specific repression of G2/M CDK/Cyclin complexes.

4 Context and objectives of the present thesis

4.1 Tomato as a model for studying endoreduplication

4.1.1 Presentation of the endoreduplication cycle

Endoreduplication is a modified cell cycle characterized by the absence of M phase. After DNA replication, cells do not divide but can enter in a new phase of DNA synthesis. Cells can therefore increase their DNA content by a 2-fold factor after each new endoreduplication cycle. This phenomenon has been characterized in mammals, in placental trophoblasts cells and in megakaryocytes, and is quite frequent in insects (Edgar and Orr-Weaver, 2001). Endoreduplication is widespread in plants, and its intensity varies from species to species, and from tissue to tissue. The ploidy level can vary from 4C to 32C in *Arabidopsis thaliana*, and up to 24576C in endosperm cells of *Arum maculatum* (Joubès and Chevalier, 2000, Sugimoto-Shirasu and Roberts, 2003).

The function of endoreduplication is not understood at present. However, several hypotheses have been proposed concerning its role:

- Endoreduplication could compensate a small genome size. Indeed, an inverse correlation between genome size and endoreduplication has been observed.

- Endoreduplication could allow the increase in the transcription level of key genes, and therefore of particular metabolites. However, the decrease in endoreduplication in cells of maize endosperm drives only a small decrease in accumulation of starch and storage proteins (Leiva-Neto *et al.*, 2004).

- Endoreduplication could protect from DNA damages by increasing the number of available gene copies.

- Endoreduplication could support an optimal ratio between genomic DNA and organite DNA.

- At last, endoreduplication could play a role as an engine for cell growth: a positive correlation has been found between endoreduplication and cell size (Cheniclet *et al.*, 2005).

4.1.2 Introduction to tomato fruit development

Tomato fruit is nowadays the main model for fleshy fruits studies. It comprises four main tissues. From the outside to the inside of the fruit, there are (Figure 20):

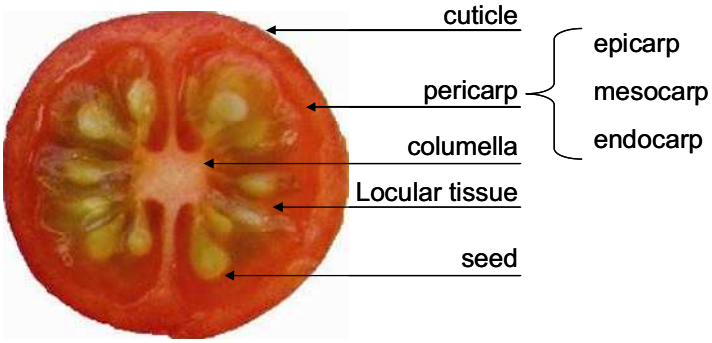

Figure 20 : Dissection of mature WVA106 tomato fruit

- The cuticle;

- The pericarp, composed of 12-17 cell layers; the three most external layers being the epicarp, the central layers being the mesocarp, and the most internal layers the endocarp

- The locular tissue or jelly, which contains the seeds;

- And at the centre of the fruit the columella to which seeds are attached.

Fruit development is composed of four phases (Cheniclet *et al.*, 2005, see Figure 21):

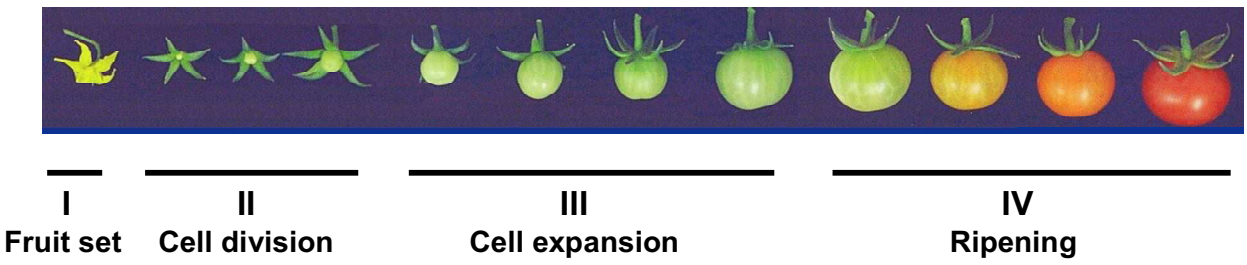

Figure 21 : WVA106 tomato fruit development

1/ Fruit set, which corresponds to the decision to form a fruit following proper flower fertilization.

2/ Division phase: fruit grows slowly by cell divisions. This phase is about 5 to 10 days long.

3/ Expansion phase: the rate of fruit growth increases, mainly because of cell expansion. During this period, cells highly endoreduplicate, and more particularly cells from the pericarp, previously limited to 16C. This phenomenon continues until around 35 days post-anthesis.

4/ Maturation phase or ripening: fruit houses important biochemical and structural changes responsible of its aroma, colour and texture. It is an important phase of production of secondary compounds concomittant to cell wall degradation leading to fruit softness. At this phase, fruit growth ceases. The fruit is considered mature at around 45 days post-anthesis.

At the end of the maturation phase, pericarp cells can reach high level of ploidy, up to 512C, and some cells will have had their volume increased by a 1000 fold factor.

The final fruit size is hence determined by two factors: the number of cells in the fruit, and cell size increase, particularly during the expansion phase.

Fruit size control is due at least in part by phytohormones: giberellins as well as cytokinins produced by seeds activate cell multiplication, particularly during the division phase, while auxin would be responsible of cell growth, during the expansion phase. At last, ethylene is a fruit maturation signal (Gillaspy *et al.*, 1993, Varga et Bruinsma, 1986).

Genetic variability also plays an important role in determining fruit size. Indeed, more than 30 quantitative trait loci (QTL) of fruit size have been mapped. Among them, the most important QTL, FW2.2, responsible of 30% of fruit final size variation between cultivated species and wild type species, has been mapped and identified (Frary *et al.*, 2000). The mutation responsible of the QTL is located at the level of the promoter of the gene (Nesbitt and Tanksley, 2002). The product of this gene, expressed from flowering to the end of the division phase, has a negative action over cell divisions

(Liu *et al*., 2003). The molecular mechanism by which it is implicated is still unknown but would be linked with the function of a casein kinase (Cong *et al.*, 2006).

4.1.3 Book Chapter: Endoreduplication and Growth of Fleshy Fruits

Endoreduplication and Growth of Fleshy Fruits

Matthieu Bourdon, Nathalie Frangne, Elodie Mathieu-Rivet, Mehdi Nafati, Catherine Cheniclet, Jean-Pierre Renaudin, and Christian Chevalier

Contents

Abstract The fruit is a specialized organ, which results from the development of the ovary after successful flower pollination and fertilization, and provides a suitable environment for seed maturation and seed dispersal mechanisms. Due to

M. Bourdon, E. Mathieu-Rivet, M. Nafati, C. Cheniclet and C. Chevalier (✉)
INRA (Institut National de la Recherche Agronomique), UMR619 Biologie du Fruit, F-33883, Villenave d'Ornon, France
e-maill: chevalie@bordeaux.inra.fr

M. Bourdon, N. Frangne, E. Mathieu-Rivet, M. Nafati and J.-P. Renaudin
Université de Bordeaux, UMR619 Biologie du Fruit, F-33883, Villenave d'Ornon, France

U. Lüttge et al. (eds.), *Progress in Botany* 71,
DOI 10.1007/978-3-642-02167-1_4,

their importance in human nutrition and their economic inference, fleshy fruit species have been the subject of developmental studies, mostly devoted to ovary formation, fruit set, and fruit maturation. The growth phase of the fruit has been much less addressed, although the complex interplay between cell division and cell expansion during this period is a crucial determinant of the final size, weight and shape of fruits. This chapter aims at reviewing our current knowledge on fleshy fruit development and addresses the cellular and molecular mechanisms involved in their growth, with a special emphasis on the cell expansion associated process of endoreduplication, with tomato fruit as the model species for fleshy fruits.

1 Introduction

The fruit is a plant organ specific to Angiosperms, which typically contains the seeds. At the botanical level, most fruits develop from mature ovaries and, therefore, include carpel tissues in part or whole. Additionally, many species develop mature fruit tissues from extracarpellary floral components, e.g., strawberry, pineapple, mulberry, and pome fruits (apple, pear), in which the receptacle, bracts, calyx, and floral tube (the fused base of floral organs), respectively constitute the majority of mature fruit tissue (Coombe 1976; Gillaspy et al. 1993; Nitsch 1953). The fruit has evolved in Angiosperms to fulfill ovule and seed protection during embryo development, and seed dispersal after maturation. This important physiological function accounts for a significant part of the adaptive success of Angiosperms. As such, the fruit has been under strong selective pressure, which accounts for the very wide diversity of fruit size, form and composition, and of seed and fruit dispersion mechanisms. These mechanisms range from the small, nondehiscent akene dry fruit, dispersed by wind, to the large, fleshy, and juicy berry and drupe fruits, which have to be eaten by animals, such as mammals or birds for seed dispersion and germination. As an example, the Solanaceae family, which encompasses nearly 10,000 species, has very diverse types of fruits, with capsules, drupes, pyrenes, berries, and several sorts of dehiscent noncapsular fruits occurring in more than 90 genera (Knapp 2002).

According to common use, fruit refers to the fleshy, edible fruits, such as grape, banana, tomato, citrus, cucurbits, pomes, stone fruit, and mango. These species are subjected to major agricultural production, which rely on permanent selection and improvement in yield and quality. Their common feature is tissues that accumulate water and many organic compounds, such as sugars, organic acids, pigments, flavor and aromas, and vitamins, which bestow their juiciness and attractiveness. Most fundamental knowledge exists about the control of maturation of fleshy fruit (Giovannoni 2001, 2004), and their postharvest handling (Brecht et al. 2003; Soliva-Fortuny and Martin-Belloso 2003), and more recently, about the processes involved in carpel morphogenesis and fruit set by using the model dry fruit of

Arabidopsis thaliana (Ferrandiz 2002; Ferrandiz et al. 1999; Roeder and Yanofsky 2006). Surprisingly, in the past 50 years, only a few reviews have addressed the molecular, cellular, and physiological events that control growth and differentiation in fleshy fruits (Bollard 1970; Coombe 1976; Gillaspy et al. 1993; Nitsch 1953, 1965, 1970; Varga and Bruinsma 1986). However, this developmental phase represents by far most of the total duration of fruit development, and is obviously associated with many parameters determining fruit quality, such as fruit size, shape, and composition.

Most recent studies on fleshy fruit growth have focused on tomato, Solanum lycopersicum (Gillaspy et al. 1993; Giovannoni 2004; Srivastava and Handa 2005; Tanksley 2004), a crop of the Solanaceae, which produces a multicarpellar berry. This crop is of strong economical importance, and for which numerous genetic (http://tgrc.ucdavis.edu/) and molecular (http://compbio.dfci.harvard.edu/tgi/) resources have been developed. In tomato, high levels of endopolyploidy occur in the course of fruit growth (Bergervoet et al. 1996; Bertin et al. 2007; Cheniclet et al. 2005; Joubès et al. 1999). This review deals with the cellular and molecular mechanisms involved in the growth of fleshy fruit, with a special emphasis on endopolyploidy and tomato fruit development.

2 Fruit Development and Growth

2.1 Carpel Morphogenesis and Fruit Set

Fruits typically develop from pre-existing organs, such as carpels inside flowers. The first phase of fruit development represents the morphogenesis and growth of carpels and ovules, from flower initiation to the double fecundation occurring in ovules (Gillaspy et al. 1993; Tanksley 2004). The ontogenic relationship between carpel and leaf has been emphasized (Gillaspy et al. 1993) and the genetic network responsible for carpel and ovule development has been thoroughly analyzed in *A. thaliana* (Ferrandiz et al. 1999). In grape, tomato, and apple, carpels are formed by ca. 17–20 rounds of cell divisions during this prebloom period, with virtually no cell expansion (Coombe 1976; Ho 1992). These divisions occur in the L3 layer of the floral meristem in a coordinated developmental pattern.

The number of cells formed in the ovary before anthesis is an important determinant of the potential final size in many fruits. This explains why fruits from early opening flowers are larger at maturity than those from later blooms (Coombe 1976). In addition, in many species including tomato (Bohner and Bangerth 1988a, 1988b; Frary et al. 2000; Tanksley 2004) and kiwi fruit (Cruz-Castillo et al. 2002), ovary size at anthesis and mature fruit size are frequently correlated positively. More work is needed to unravel the effect of internal cues,

e.g., sink effects (Ho 1992), and external ones, e.g., temperature (Bertin 2005; Higashi et al. 1999) on this phenomenon.

2.2 Fruit Growth

Shortly before anthesis, growth usually stops in the ovary. The second phase of fruit development, i.e., fruit growth, resumes only after pollination by compatible pollen and then fertilization (i.e., at fruit set). A major issue for understanding fruit growth is to decipher the signals and their mode of action, which simultaneously induce corolla and stamen senescence and fruit set after pollination and fertilization. Recent results in tomato suggest a function of abscisic acid (ABA) and ethylene before fruit set, to keep the ovary in a temporally protected and dormant state (Balbi and Lomax 2003; Vriezen et al. 2008).

The involvement of plant hormones in fruit set has long been postulated from the efficiency of externally applied auxins or gibberellins to replace pollination and fertilization in inducing fruit set and growth (Crane 1964; Nitsch 1965; Nitsch 1970; Vivian-Smith and Koltunow 1999). When the auxin signaling pathway is altered, fruit set and development can occur without fertilization, i.e., parthenocarpy (Carmi et al. 2003; Goetz et al. 2006; Goetz et al. 2007; Pandolfini et al. 2007; Wang et al. 2005). Auxin action on fruit set may also be through gibberellic acid (GA) synthesis (Serrani et al. 2008) and GA action (Martí et al. 2007). Fruit set has also been related to the strong increase of sucrose import capacity in young tomato fruit (Ho 1996; D'Aoust et al. 1999).

Fruit growth is by far the longest phase of fruit development. It ranges from 1 week for *A. thaliana*, 3–5 weeks for strawberry, 5–8 weeks for tomato, to 60 weeks for many citrus fruits with an average of 15 weeks for most fleshy fruits (Coombe 1976) (Table 1). Two distinctive types of fruit growth curves have been reported on cumulative and/or rate bases according to fruit species (Coombe 1976). Single S-shaped (sigmoidal) growth curves occur in most species including tomato. In few-seeded-fruit, such as stone fruit (drupes) and some berries, such as grape, growth curves fit a double-sigmoid pattern, which involves two successive phases of growth with physiologically distinct sink activity and a transition in between (DeJong and Goudriaan 1989). The type of growth curve for several fruit species is indicated in Table 1.

In general, fruit growth starts by a period of intense cell divisions. Then, before the frequency of cell division declines, cells begin to enlarge rapidly; the final period of fruit growth relies uniquely on cell expansion. As already pointed out more than 50 years ago, "fruit growth curves do not indicate when the transition of cell multiplication to cell enlargement occurs, so that, from the point of view of the growth process, distinction between both is not considered to be important. The important entity seems to be the organ rather than its constituents" (Nitsch 1953). Thus, although they offer convenient data for phenological studies, most growth curves are inadequate for the analysis of the components of growth (Coombe 1976).

Table 1 Characteristics of fruit growth in 22 species undergoing or not endopolyploidization, and sorted according to fruit growth duration

Family	Speciesenglish name	Speciesbotanical name	DNA contentpg/ 1C[a]	Dev. Curve[b]	Growth duration[c]	Max nb endo-cycles[d]	Cell diameter (m)[e]	References[f]
Brassicaceae	Arabidopsis	*Arabidopsis thaliana*	0.16	S	1	3	25	Vivian-Smith and Koltunow (1999)
Rosaceae	Strawberry	*Fragaria sp.*	0.4*	S	3–5	5	50	Suutarinen et al. (1998)
Cucurbitaceae	Melon	*Cucumis melo*	1.05	S	5–6	6	450	Kano (2007)
Solanaceae	Potato	*Solanum tuberosum*	0.88 or 2.10	n.d.	6	4	n.d.	-
Fabaceae	Common Bean	*Phaseolus vulgaris*	1.43	n.d.	6	4–5	n.d.	-
Cucurbitaceae	Cucumber	*Cucumis sativus*	1.77	S	6	6	>200	Boonkorkaew et al. (2008)
Solanaceae	Tomato	*Solanum lycopersicum*	1.0*	S	5–8	7–8	600–1,000	Cheniclet et al. (2005)
Solanaceae	Pepper	*Capsicum annuum*	4.00	S	8	6	800	Rygol and Lüttge (1983)
Rosaceae	Cherry	*Prunus avium*	0.35	D	9–11	4–5	65	Stern et al. (2007)
Rosaceae	Raspberry	*Rubus sp.*	0.3*	D	12	5	n.d.	-
Vitacaee	Grape	*Vitis vinifera*	0.43	D	14	0	350	Schlosser et al. (2008)
Rosaceae	Apricot	*Prunus armeniaca*	0.30	D	16	5	n.d.	-
Rosaceae	Peach	*Prunus persica*	0.28	D	16–26	5	120	Ognjanov et al. (1995)
Musaceae	Banana	*Musa sp.*	0.6*	Other	17–18	0	n.d.	
Rosaceae	Plum	*Prunus domestica*	0.93	D	19–22	4	100	Stern et al. (2007)
Rosaceae	Pear	*Pyrus communis*	0.55	S	18–25	0	n.d.	-
Rosaceae	Apple	*Malus domesticaor M. communis*	4.50	S	21–22	0	n.d.	-
Ebenaceae	Persimmon	*Diospyros kaki*	1.2–1.7*	D	21–28	0	220	Hamada et al. (2008)
Actinidiaceae	Kiwi	*Actinidia chinensis*	4.19	D	23–26	0	200	Hopping (1976)Cruz-Castillo et al. (2002)
Moraceae	Fig tree	*Ficus carica*	0.70	D	25	0	n.d.	-
Lauraceae	Avocado	*Persea americana*	0.93	S	40	0	n.d.	-
Rutaceae	Orange	*Citrus x sinensis*	0.63	S	60	0	n.d.	-

[a]DNA content per haploid genome (major source: Plant DNA C-values database, Royal Botanical Gardens, Kew, http://data.kew.org).
*mean of different varieties or data
[b]Type of development growth curve (S = single sigmoid, D = double-sigmoid)
[c]Length of fruit development from anthesis to ripe stage (in weeks) (literature and our personal data)
[d]Personal data on maximum number of endocycles undergone during fruit development. n.d.: non determined
[e]Approximate cell diameter of the largest mesocarp cells in mature fruit
[f]Main source of cell diameter data (p.d.: our personal data)

Fruit growth relies on a spatially and temporally organized pattern of cell division and of cell expansion. Remarkably, fleshy fruit tissues may have very various ontogenic origins (Coombe 1976), although they all share similar characteristics, with large, highly vacuolated cells with thin walls. In tomato, the ovary wall has seemingly a simple organization at anthesis, with ca. 11 layers of small isodiametric cells including two epidermal cell layers, and vascular bundles in the central pericarp (Cheniclet et al. 2005). During fruit organogenesis and growth, the fertilized ovary acquires a complex pattern of cells with various sizes and shapes, and various metabolic differentiations (Cheniclet et al. 2005; Gillaspy et al. 1993; Mohr and Stein 1969; Smith 1935) (Fig. 1a). How this spatio-temporal pattern of development is related to gene expression, metabolic profiles and cellular characteristics, such as endopolyploidy has only just started to be described (Lemaire-Chamley et al. 2005). This apparent slow progress has been due to the difficulty in correlating various cellular and molecular data at the level of given cell types in three-dimensionally complex organs, such as fruits. How this complexity relates to hormonal and nutritional regulation during fruit growth also remains largely ignored. Many data have been reported on the kinetics of hormone content in various fruit materials (reviewed in Gillaspy et al. 1993; Srivastava and Handa 2005), but their use for a proper understanding of their action in relation to growth mechanisms remains rather elusive. Fruit growth requires the combined presence of several growth-promoting plant hormones, such as auxin, gibberellins, cytokinins and brassinosteroids (Cowan et al. 2005; Ozga et al. 2002; Srivastava and Handa 2005). Many of these hormones appear to originate from the developing seeds, with a particular role for the endosperm in the secretion of these compounds.

2.3 Cell Division During Fruit Growth

Active cell division within the flesh is usually restricted to an initial period of 1–2 weeks after pollination and fertilization (e.g., cucurbits, tomato), 3 weeks in apple, 4–7 weeks in Japanese pear, peach, and plum. Cell divisions do not occur in the pericarp of Corynth grape, Rubus, or some Ribes species. However, divisions continue in avocado and in strawberry throughout the life of the fruit (Coombe 1976; Crane 1964; Nitsch 1965). In tomato and as in many fleshy fruits, cell divisions occur in various cells and with various division planes to allow fruit growth, but they also occur in discrete cell layers with definite division planes for specific purposes. This is the case for tomato, where the two epidermal cell layers of the pericarp undergo anticlinal divisions, whereas the two subepidermal layers undergo several rounds of periclinal divisions leading to an increase in the number of pericarp cell layers to a varying extent according to the tomato line. These various types of cell divisions are differently regulated because cell-layer forming cell divisions occur only within 5–8 days post-anthesis in various tomato lines (Cheniclet et al. 2005; Cong et al. 2002; Mazzucato et al. 1998), whereas

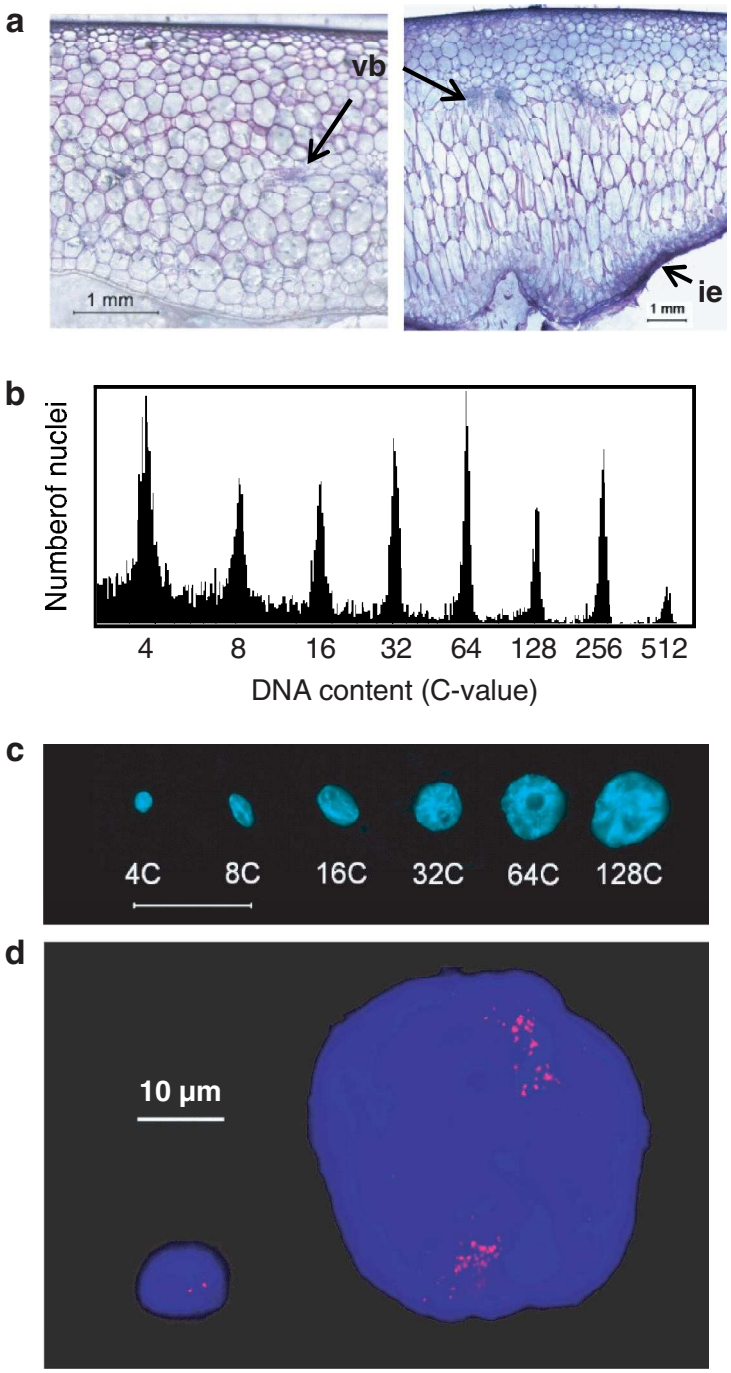

Fig. 1 Cellular aspects of endoreduplication in tomato fruit. (**a**) Pericarp histology in mature green fruits from two distinct tomato lines (*left*: Gardener's delight; *right*: Montfavet), showing the variability in pericarp tissue patterning resulting from differences in cell expansion. vb: vascular bundles; ie: inner epidermis. (**b**) Flow cytometry analysis of mature green fruit pericarp from a large-fruited line, showing the distribution of nuclei according to DNA content (C-value). (**c**) DAPI-stained nuclei isolated from mature green tomato pericarp (cherry line) and sorted according to their fluorescence intensity ; *from left to right*: 4C, 8C, 16C, 32C, 64C, 128C) ; note the increase in size and the increasing complexity of condensed chromatin distribution revealed by DAPI fluorescence. (**d**) FISH on two nuclei isolated from mature green pericarp tomato and flow cytometry sorted according to their ploidy class (*left*: 2C, *right*: 64C); DAPI-stained DNA appear in *blue*, and hybridization spots of a BAC probe specific for chromosome 7 appear in *red* after Texas-red revelation

randomly-oriented cell divisions occur for longer periods up to 10–18 days post-anthesis (Gillaspy et al. 1993; Tanksley 2004). Moreover, two different modified genetic backgrounds affect cell divisions in tomato pericarp, excluding cell-layer forming divisions (Cong et al. 2002; Jones et al. 2002). Commonly, tissues closest to the ovules (e.g., placenta in tomato or fruit surface in strawberry) cease division earlier than other tissues (Coombe 1976). All these data indicate spatially and temporally complex regulation of cell divisions in growing fruit.

After anthesis, the locular cavities in fruit are usually filled as a result of intense cell division activity from one or more of the locule surface areas (e.g., placenta in tomato, septum in banana and grape, endodermis in banana and orange, and seed aril in lychee). Cell expansion then contributes to the filling of the locule, which behaves in concert with the neighboring flesh to form fruit pulp or, as in tomato, to form a jelly-like tissue with distinct properties from the pericarp (Coombe 1976).

In conclusion, the fruit as a whole is composed of cells, which were present at anthesis and of newly formed cells during fruit growth. The ratio between both kinds of cells is a function of the number of doublings at these two phases. After anthesis, 80–97% of fruit cells in apple, strawberry, peach, apricot and tomato are produced, whereas ca. 70% of fruit cells are formed before anthesis in cucumber and blueberry (Cano-Medrano and Darnell 1997). The modulation of cell division in fruit either pre- or post-anthesis has repeatedly been associated with strong variations in fruit size. As an illustration, strong differences in overall anticlinal, but not periclinal, cell division in the pericarp are associated with varying levels of *fw2.2* transcripts corresponding to the major quantitative trait locus (QTL) for tomato fruit size, which accounts for as much as a 30% difference in fruit fresh weight between small-fruited and large-fruited tomatoes (Cong et al. 2002; Liu et al. 2003).

2.4 Cell Expansion During Fruit Growth

In eukaryotic cells, cell enlargement results from two processes: cell growth by increase in cytoplasmic volume and cell expansion through vacuolation. Cell growth by cytoplasmic volume increase may occur in all types of cells and is responsible for moderate increases in cell volume, by less than tenfold (Sugimoto-Shirasu and Roberts 2003). Cell expansion through vacuolation is a specific property of plant cells because of their large vacuolar compartment, and it leads to an increase in cell volume by more than one hundredfold (Sugimoto-Shirasu and Roberts 2003). Cell expansion through vacuolation typically starts in young organs, once cells have stop dividing, exit the cell cycle, and differentiate.

Some of the largest cells found in plants occur in the flesh of ripe fruit, with cell length between 150 and 700 μm, and in some cases more than 1 mm. The volume of cells in ovary wall is only ca. 10^{-3}–10^{-2} nL at anthesis whereas it is in the range of 1–10 nL, up to 100 nL in mature fruit (Coombe 1976). Because cell volume may be increased by 10^{2}–10^{4} times during the growth of fleshy fruit, this phenomenon

makes by far the greatest contribution to the total expansion of the fruit. Cell size has been recognized as a critical component of fruit size in cucumber, blueberry, and grape (Cano-Medrano and Darnell 1997).

When expressed on an arithmetic scale, cell expansion, by several orders of magnitude, has often been considered to occur after the cell division phase in fleshy fruit (Gillaspy et al. 1993). In fact, cell expansion starts in the very few days after fruit set, concomitantly with cell division (Boonkorkaew et al. 2008; Cheniclet et al. 2005), and it lasts for the entire period of fruit growth. However, whether initial cell growth occurs through cytoplasmic growth while the cells are actively cycling in the mitotic cycle remains poorly understood. The most intense cell growth phase then occurs through dramatic increases in the vacuolar volume and vacuolation index of fruit cells.

Cell size is typically described by linear cell dimensions, e.g., diameter or perimeter in fruit sections, which gives only an approximation of cell volume, and thus, requires deeper sectional analyses to take cell shape into account. The absolute measurement of cell size and shape in the growing grape fruit revealed that cell shape was irregular and cell volumes in the inner mesocarp of a grape berry exhibited a 14-fold range variation, with polysigmoidal distribution and clusterings around specific cell size classes (Gray et al. 1999). Obviously, more measurements of this type are required to fully understand the patterning of fleshy parenchymatous fruit tissues.

In the course of fleshy fruit development, the extent of cell expansion is influenced by cell wall behavior, turgor, and constraints imposed upon the flesh by the extensibility of the skin. Auxin is generally considered responsible for cell expansion during fruit growth, although this effect may not be direct but mediated through ill-defined compounds mediating sink activity.

3 Endopolyploidization

3.1 Definitions

Polyploidy can be defined as the addition of a complete set of chromosomes to one genome, which results from either sexual reproduction via 2n gametes or somatic chromosome doubling. According to the mode of polyploidy formation, allopolyploidy and autopolyploidy can be distinguished as originating respectively from interspecific hybridization between divergent progenitor species, thus giving rise to the presence of distinct subgenomes, and from intraspecific hybridization (or self-fertilization) or somatic chromosome doubling, thus resulting in identical subgenomes (Otto 2007). Related to autopolyploidy, endopolyploidy corresponds to the occurrence of different ploidy levels within an organism.

Endopolyploidy can result from the generation of multinucleate cells originating from acytokinetic mitosis, from nuclear fusion, from endomitosis, or from endoreduplication. Multinucleate cells in plants are found during the formation of the

syncitial female gametophyte (Yadegari and Drews 2004), in anther tapetum (D'Amato 1984) and seed endosperm (Berger 2003), while nuclear fusion may also contribute to polyploidization of the chalazal domain of the endosperm in Arabidopsis (Baroux et al. 2004). Endomitosis corresponds to a doubling of the chromosome number in nucleus. Chromosomes double and condense, sister chromatids separate normally, but return to the interphase state within an intact nuclear envelope, thus generating nuclear endopolyploidy. Although endomitosis mainly occurrs in animals, it is only rarely encountered in plants (D'Amato 1984).

Endoreduplication represents the most common mode of cell endopolyploidization in plants and is estimated to occur in over 90% of Angiosperms (Nagl 1976; D'Amato 1984). This process is an endonuclear chromosome duplication, which occurs in the absence of any obvious condensation and decondensation steps leading to the production of chromosomes with 2n chromatids without any change in chromosome number (Joubès and Chevalier 2000; Edgar and Orr-Weaver 2001). As a consequence, hypertrophying nuclei arise from successive cycles of DNA replication without segregation of sister chromatids, and in extreme cases "giant" polytene chromosomes are generated as observed for embryo suspensor cells of *Phaseolus* species (D'Amato 1984) or giant hair cells of *Bryonia* anthers (Barlow 1975).

3.2 Occurrence of Endopolyploidization in Fruit Species

As stated by D'Amato (1984), endopolyploidy is "of such a widespread occurrence in plants, that it can be regarded as the rule rather than the exception." A recent survey performed on several vegetative organs of 54 seed plant species different in term of genome size and belonging to two Gymnosperm and 14 Angiosperm families by Barow and Meister (2003) indicated that endopolyploidy occurred in 33 species taken from ten different families. Though absent in Gymnosperms, the frequent occurrence of endopolyploidy within Angiosperms seems restricted, however, to certain phylogenetic groups (Barow 2006).

Though largely documented in vegetative organs (Barow and Meister 2003), the occurrence of endopolyploidy in reproductive organs, especially in fruit tissues, and its extent in different species has gained little attention so far. Endopolyploidization was found in ovular tissues (antipodal cells, synergids, endosperm and embryo suspensor cells) and in anther cells (anther hair, glandular hair and anther tapetal cells), where endoreduplication seems to be the preferential way of polyploidization (D'Amato 1984; Carvalheira 2000; Bauer and Birchler 2006).

More than 60 years ago, endopolyploidization was reported initially in cucumber and other fruit materials (cited in Coombe 1976 and Barow 2006) and then in the mesocarp parenchyma cells in apricot (Bradley and Crane 1955). However, in this latter report the natural and/or physiological occurrence of the phenomenon in this fruit could be questioned as these authors observed polysomaty (increase in chromosome number according to endomitosis), after an auxin treatment and subsequent

needle wounding of the fruit mesocarp. More recently, some reports described the occurrence of endopolyploidization in the pericarp of *Sorghum bicolor* (Kladnik et al. 2006), *Ornithogalum umbellatum* ovary epidermal cells (Kwiatkowska et al. 2007), and sugar-beet pericarp (up to 32C in diploid and to 16C in triploid and tetraploid plants) (Lukaszewska and Sliwinska 2007). Most of the reports dealing with endopolyploidy in fruit so far concerned tomato (Bergervoet et al. 1996; Bertin et al. 2007; Cheniclet et al. 2005; Joubès et al. 1999) (Fig. 1b). On the contrary, endopolyploidy has been reported neither for grape (Ojeda et al. 1999) nor for apple (Harada et al. 2005).

To provide more data about the occurrence of endopolyploidization in fruits, we initiated a large scale analysis of ploidy levels in fruit of different species, focusing mainly on fleshy fruits. DNA content of nuclei isolated from whole ovaries at anthesis and from pericarp of fully developed fruits were analyzed by flow cytometry, and the maximum number of endocycles (corresponding to the number of DNA duplications, cf. Sect. 5.2) made during fruit development was determined. These data are presented in Table 1, together with additional parameters, such as the DNA content per haploid genome, the average cell diameter in fruit flesh (available data from the literature), and the type and duration of growth. The ordering of phylogenetic families and species within the table is based on the duration of growth accordingly.

From this table and additional data not shown, endopolyploidization in fruit appears to be dependent in part from the phylogenetic position of species, as observed for vegetative organs by Barow and Meister (2003). In some families (e.g., Rutaceae), no endopolyploidization was observed, while in others, such as in Brassicaceae, Cucurbitaceae, Fabaceae, and Solanaceae, most of the fruit species displayed a high degree of endopolyploidization. According to Barow and Meister (2003), a high frequency of endopolyploidization was also reported in vegetative organs of these families. Amongst Rosaceae, pome fruits (apple, pear) do not exhibit endopolyploidization, while stone fruits (*Prunus* sp.) as well as strawberry and raspberry undergo several rounds of DNA duplication.

Of the vegetative organs reported to display endopolyploidization, the number of endocycles that cells undergo is predominantly, 2–3, less frequently 4 and rarely 5 (corresponding respectively to ploidy levels of 8C, 16C, 32C and 64C for diploid species, where C is the DNA content of the unreplicated haploid genome of a gamete). Higher ploidy levels appear to occur more frequently in fleshy fruits for which 4–5 endocycles can often be observed (Table 1). In maize endosperm, fertilization gives rise to 3C cells, which undergo up to 5 endocycles in the course of development, resulting in a maximum ploidy level of 96C (Leiva-Neto et al. 2004). In fruits of Cucurbitaceae and Solanaceae, mesocarp cells commonly undergo 6 endocycles, the highest ploidy levels for these cells being reached in tomato where 8 endocycles (up to 512C) can be observed. This high level of endopolyploidy in tomato and the numerous data reported on this process in this species (Bergervoet et al. 1996; Joubès et al. 1999; Cheniclet et al. 2005) makes it an outstanding model for studying endopolyploidization and its physiological role during fruit development.

3.3 Cellular Aspects of Endoreduplication

3.3.1 Cell Size

Endopolyploidization and cell expansion often occur simultaneously in developing organs, and high ploidy level have long been reported as associated with large cell size (Joubès and Chevalier 2000; Sugimoto-Shirasu and Roberts 2003). An ultimate demonstration of a direct correlation between ploidy level and size in single cells requires simultaneous in situ determination of DNA ploidy level and size in individual cells. This has been achieved only in a limited number of vegetative tissues, such as leaf epidermis (Melaragno et al. 1993), hypocotyl (Gendreau et al. 1997), and symbiotic root nodules (Cebolla et al. 1999), and of floral tissues (Kudo and Kimura 2002; Lee et al. 2004). In tomato, Bünger-Kibler and Bangerth (1982) showed that the ploidy level in fruit pericarp cells increases from 4 to 10 days after anthesis. At this stage, small cells localized around vascular bundles and hypodermis display nuclei with a 4C level, while in the large parenchyma cells, the ploidy level was between 16 and 32C, thus arguing for cell enlargement that is correlated with DNA content. Subsequently, such an observation was also reported by Bergervoet et al. (1996) and Joubès et al. (1999), while Cheniclet et al. (2005) established clearly a direct correlation between mean cell size and mean C-level during the development of tomato fruit pericarp.

3.3.2 Nuclear Size

Obviously as the nuclear DNA content undergoes exponential amplification through endoreduplication, the nuclear volume is expected to increase accordingly. In tomato fruit, an increase in nuclear size was observed in most pericarp cell-layers in the course of development (up to 6-fold in diameter) (Bergervoet et al. 1996; Joubès et al. 1999). Nuclei sorted by flow cytometry according to their DNA content show a strong positive correlation between nuclear size and ploidy level as far as the lower ploidy levels are concerned, but this correlation becomes weaker for higher ploidy levels, due to a larger variation of nuclear sizes (Bourdon et al. personal communication) (Fig. 1c). The heterogeneity in nuclear size of highly polyploid nuclei suggests that the nuclear volume depends not only on its DNA content, but also on other parameters, such as the amount and conformation of nuclear proteins, RNA molecules, and the degree of chromatin condensation. Therefore, one cannot deduce the precise ploidy level of a nucleus merely from its relative volume in a given tissue. It is noteworthy that a positive relationship between nuclear size and ploidy level has also been demonstrated in various endoreduplicating plant tissues, such as metaxylem in maize roots, *Aloë arborea* (Agavaceae) and *Zebrina pendula* (Commelinaceae) (List 1963), endosperm in *S. bicolor* (Kladnik et al. 2006), and in species encompassing a wide variation in endopolyploidy (Barow 2006).

3.3.3 Nuclear Morphology

In most studies dealing with histological aspects of endopolyploidy, the overall morphology of nuclei has been observed in whole tissue or epidermal layers, but quite often the fine structure of nuclei was not described.

In tomato fruit, observations were made on mature pericarp nuclei by confocal microscopy, bright field microscopy and transmission electron microscopy (Frangne et al. personal communication). A gradual increase in nuclear size is observed between the epidermal cell-layer and the central cell-layers of pericarp. Nuclei also present differences in term of shape. In the epidermal cell layer, the nuclei display a regular shape, whilst in the central cell layers they acquire a complex shape, with numerous deep grooves and digitations. When these nuclei are observed with conventional fluorescence microscopy after DAPI-staining, the grooves in their DNA are barely visible, but are suggested by the complex distribution of condensed chromatin (Fig. 1c). The gradient of nuclear size and shape observed in situ from the epidermis to the central layers of pericarp is similar to the gradient observed in ploidy-sorted nuclei, thus strongly suggesting that the most central nuclei are the most polyploid. Whether or not this particular morphology of nuclei observed in tomato fruit results from their high ploidy level has not yet been determined. Such a variation in the shape of the nucleus according to ploidy levels has also been reported in different cell types of *A. thaliana* (Barow 2006).

3.3.4 Chromatid Organization in Fruit Polyploid Nuclei

As pointed out in Table 1, endopolyploidization is a widespread phenomenon in various fruit species. However to our knowledge, not a single report focused so far on elucidating the chromosome organization in endopolyploid fruits' cells, except the study of Bradley and Crane (1955), who demonstrated the occurrence of endomitoses in the mesocarp of apricot. In an effort to identify chromosome organization in polyploidy tissues of tomato fruit, we performed a fluorescence in situ hybridization (FISH) analysis of tomato pericarp nuclei sorted by flow cytometry according to their DNA content. A biotin-labeled bacterial artificial chromosome (BAC) DNA sequence specific for tomato chromosome 7 (O. Coriton, personal communication) was used as a probe.

As illustrated in Fig. 1d, a 2C nucleus displayed two spots of hybridization as expected for the two copies of chromosome 7, while the hybridization on a 64C nucleus resulted in a uneven distribution of spots throughout the whole nuclear volume, but a clustering in two separated areas. The spatial proximity of the hybridization spots within these two areas suggests that the sister chromatids stay closely associated during endopolyploidization, thus accounting for a polytene structure of chromosomes and consequently for endoreduplication in tomato fruit. Such polytenic structures were also observed in maize endosperm (Bauer and Birchler 2006), Arabidopsis root tips and mature leaves (Lermontova et al. 2006), and cabbage root tips (Sesek et al. 2005).

Even if polyteny seems to be widespread in various plant organs, differences in chromatin organization can be observed between cell types during endoreduplication. These differences lie mainly in a more or less complete pairing of sister chromatids and in the state of chromatin condensation. Sister chromatid pairing can be observed along the entire length of chromosomes, such as for giant hair cells in *Bryona* anthers (Barlow 1975) or just in part of them, such as the embryo suspensor cells in *Phaseolus coccineus* (Nenno et al. 1994). Recently, Schubert et al. (2006) provided evidence for a differential alignment of sister chromatids pairing along Arabidopsis chromosome 1, and thus, for polyteny in Arabidopsis vegetative tissues. In addition, the condensation state of centromeres in Arabidopsis endoreduplicated cells was shown to be variable and cell type-dependent (Fang and Spector 2005). Decondensation could also account for a greater range of chromatin movement in endoreduplicated cells (Kato and Lam 2003). Hence, further investigations are needed to determine the biological significance of chromosome and chromatin organization in endoreduplicated cells.

Since endoreduplication appears to be the preferred mode of endopolyploidization in most plant organs and notably in tomato fruit, we shall use this term from here onwards.

4 Proposed Physiological Roles for Endoreduplication

4.1 Endoreduplication and the Determination of Cell- and Organ Size

The frequent positive correlation between endoreduplication and cell size in many different plant species, organs, and cell types (Joubès and Chevalier 2000; Sugimoto-Shirasu and Roberts 2003; Kondorosi and Kondorosi 2004) is commonly interpreted as endoreduplication as the driver for cell expansion. The successive rounds of DNA synthesis during endoreduplication induce a consequent hypertrophy of the nucleus. This can influence the final size of the cell, which, therefore, may adjust its cytoplasmic volume with respect to the DNA content of the nucleus (according to the "karyoplasmic ratio" theory; Sugimoto-Shirasu and Roberts 2003). Cell expansion proceeds further through vacuolation, to adjust the size of the vacuolar compartment in accordance with the cytoplasmic volume, and even to increase the vacuolation index of the plant cell.

Cheniclet et al. (2005) provided evidence for such a positive correlation between cell size and ploidy level in pericarp tissue during fruit development. However insufficient comparison has been performed so far in other fruit species, and even in tomato, opposing results were reported in two tomato isogenic lines differing by fruit weight and sugar content QTLs (Bertin et al. 2003) and between large fruits of

lines cultivated at different temperatures (Bertin 2005). To gain further insight about the possible relationship between endoreduplication and cell size in fruit, we collected data from the literature and performed additional measurements of cell size in fully-grown fruit displaying or not displaying endopolyploidization (Table 1). This analysis indicated no clear-cut relationship between these two parameters. For example, nonendopolyploidizing fruits like kiwi, persimmon, and grape display cell diameters of ca. 200 μm, 220 μm, and 350 μm respectively, while smaller cell diameters are observed in endopolyploidizing fruits, such as the Arabidopsis silique (25 μm), strawberry (50 μm), cherry (65 μm), and peach (120 μm). Therefore the ability to develop large cells as measured by their diameters, is not restricted to endopolyploidizing fruits. Nevertheless when endopolyploidizing fruits are compared, it also appears that the largest cells are present in fruits that undergo the highest number of endocycles (diameters of 600–1,000 μm in tomato, 800 μm in pepper, and 450 μm in melon), which suggests that endopolyploidization might be necessary for plant cells to reach very large sizes.

However, various examples show that endoreduplication can occur in the absence of dramatic cell expansion. For instance, Gendreau et al. (1998) reported that a small cell size in some Arabidopsis mutants did not prevent the occurrence of the same number of endocycles as in larger cells present in wild-type. Endoreduplication is, thus, obviously not the only parameter either signifying or favoring cell expansion.

The mean level of endoreduplication of various plant organs has repeatedly been found correlated with organ size, as exemplified in Arabidopsis leaves (Cookson et al. 2006), pea cotyledons (Lemontey et al. 2000) and tomato fruit (Cheniclet et al. 2005). However, the function of endoreduplication in organ growth remains open to various hypotheses. Organ growth can be considered as the result either of a given balance of cell-based (autonomous) mechanisms relying on division, expansion, and endoreduplication or according to the opposite, of organismal level of regulation (Mizukami 2001; John and Qi 2008). In view of the organismal control, the synthesis of cytoplasm is the primary process and DNA endoreduplication would come second to maintain the karyoplasmic ratio (Cookson et al. 2006; John and Qi 2008). This latter parameter is difficult to estimate because of technical constraints, although it is a common observation that fruits with endopolyploidy such as tomato have larger protein contents linked to a larger cytoplasmic compartment, than fruits without endopolyploidy, such as apple (Harada et al. 2005).

Although the correlation between cell size and endoreduplication is obvious, which process triggers the other is still a matter of debate, as a kind of Chicken or the egg causality dilemma. Since endoreduplication corresponds to successive rounds of DNA duplication in the absence of mitosis as defined below (cf. Sect. 5), it is therefore likely that a minimal cell size must be required to commit to the following round of DNA replication, thus implying cell growth. However, once DNA synthesis is completed, the doubling of the DNA quantity can in turn promote cell growth, according to the "karyoplasmic ratio" theory (Sugimoto-Shirasu and Roberts 2003).

4.2 Endoreduplication and Cell Differentiation

In the model plant Arabidopsis, the influence of endoreduplication in forming large specialized cells was best characterized in epidermal cells of mature leaves (Melaragno et al. 1993), during hypocotyl development in which the ploidy levels vary according to light conditions (Gendreau et al. 1997), and in leaf single-celled trichomes (Larkin et al. 2007). The growth of trichomes was shown to be dependent on the succession of endocycles. The formation of a two-branched trichome cell requires three rounds of endocycle, leading to a 16C DNA ploidy level. A supplementary endocycle may eventually occur to give rise to the formation of a third branch and 32C DNA content. Moreover, cell growth and differentiation of trichomes is a genetically regulated process, since mutants affecting the nuclear ploidy level impacts positively or negatively on trichome cell size.

As illustrated for trichomes, endoreduplication often occurs during the differentiation of cells that are highly specialized in their morphology or metabolism. This is the case for cells from tomato fruit pericarp and jelly-like locular tissues (Cheniclet et al. 2005; Lemaire-Chamley et al. 2005; Chevalier 2007) as described above, for symbiotic host cells during the formation of nitrogen-fixing root nodules in legumes (Cebolla et al. 1999) and/or for the endosperm cells of maize kernels (Kowles and Phillips 1985; Kowles et al. 1990).

4.3 Endoreduplication and Metabolism

There are instances where endoreduplication is linked to endogenous metabolism. For example, nodule development on legume roots is initiated in response to interaction with the symbiotic bacterium *Sinorhizobium meliloti*. During their differentiation process, symbiotic nodule cells, programmed to fix nitrogen, develop into very large and highly endoreduplicated cells (Cebolla et al. 1999; Vinardell et al. 2003) and display an important transcriptional activity that is remarkably specific to the nodule (Mergaert et al. 2003). Also, in *Zea mays*, endosperm cells accumulate large amounts of starch and storage proteins, concomitantly with multiple and successive endocycles during seed development (Lopes and Larkins 1993).

Since a correlation exists between endoreduplication and cell differentiation-specific metabolism, it is tempting to speculate that one role of endoreduplication would be to modulate transcriptional activity by increasing the availability of DNA templates for gene expression as the gene copy number is obviously multiplied, and therefore, to modulate subsequent translational and metabolic activities. However, this hypothesis has neither been convincingly demonstrated nor negated in plant cells. For example, Leiva-Neto et al. (2004) showed that endoreduplication levels did not clearly impact on the expression level of some endosperm-specific genes, which led them to propose that endoreduplication in maize endosperm functions primarily to provide a store of nitrogen and nucleotides during embryogenesis and/or germination.

4.4 Endoreduplication in Response to Environmental Factors

An important physiological role of endoreduplication might be in the adaptation to adverse environmental factors, especially maintenance of growth under stress conditions. For instance, amplification of DNA may provide a means to protect the genome from DNA damaging conditions, such as uneven chromosome segregation or UV damage. In Arabidopsis, the *UV-B-insensitive 4* mutation (*uvi4*) promotes the progression of endoreduplication in hypocotyl and leaf development, and confers an increased UV-B tolerance (Hase et al. 2006). Endoreduplication was also demonstrated to be an adaptation factor in plant responses to high salt concentration (Ceccarelli et al. 2006). Moreover, an increase in the extent of endoreduplication reduced the impact of water deficit on epidermal cell size, leaf expansion rate and final leaf size (Cookson et al. 2006), and facilitated growth at low temperatures (Barow 2006), thus suggesting that an increase in DNA content can be of advantage in a given environment.

4.5 Endoreduplication and Growth Rate

As described above (cf. Sect. 4.1) endoreduplication does not seem to be necessary for cell expansion. However, it could participate in modulating the rate or organ growth and/or cell expansion. We previously demonstrated a clear correlation between mean ploidy level in fully developed pericarp and final fruit size and weight, when 20 tomato lines displaying a large range in fruit weight were compared (Cheniclet et al. 2005).

To investigate whether endoreduplication influences the fruit growth rate, we recorded the time of anthesis (full bloom in the case of trees) and fruit maturity (harvest time) for different fruit species and compared the determined length of development with the extent of endoreduplication (Table 1). From this analysis, it has been concluded that (1) in all species where fruit development lasts for a very long period of time (over 17 weeks), endoreduplication does not occur in fruit tissues; (2) in species displaying middle-length fruit development (10–16 weeks), some fruits do not display endoreduplication (e.g., grape), while others undergo 4–5 endocycles (e.g., fruits of many Prunus sp.); (3) in fruits, which develop rapidly (in less than 10 weeks) undergo several rounds of endocycle (3–8). Moreover, the formation of cells of similar size, and even larger ones, takes far less time in endopolyploidizing fruits than in nonendopolyploidizing fruits. Assuming that the ovary cells display roughly similar sizes at anthesis in the different species, these observations support the assertion that endoreduplication is likely to influence not only the rate of fruit development but also the rate of cell expansion in species exhibiting rapid fruit development. This would be consistent with the analysis of Barow (2006), who suggested that endoreduplication contributes to a greater extensive growth than in nonendopolyploid plants.

The rate of organ growth could be also under the influence of genome size. From the data presented in Table 1, no obvious relationship between genome size and length of fruit growth could be observed. For instance, pear and apple (nonendoreduplicating species) have respectively a small (C-value = 0.55 pg) and large (C-value = 4.50 pg) genome size and display similar fruit growth lengths of around 21 weeks. The same observation is also true for endoreduplicating species, such as tomato (C-value = 1 pg) and pepper (C-value = 4 pg), whose fruit both develops in 6–8 weeks. Thus, the positive correlation between genome size and life cycle shown by Bennett (1972) may not be applicable if confined to fruit development, at least in this range of genome size.

We also examined if the ability to exhibit endoreduplication was favored by a small genome size, owing to the fact that a higher nuclear DNA content as a result of autopolyploidy requires more time to replicate (Bennett 1972). From the 22 different fruit species analyzed in Table 1, it seems that the occurrence and extent of endoreduplication is not related to genome size, since endopolyploidizing fruits display genome sizes ranging from 0.16 to 4 pg and nonendopolyploidizing ones from 0.43 to 4.50 pg.This result is in accordance with the findings of Barow and Meister (2003) who observed only a low negative correlation between genome size and endopolyploidization, which was contrary to a previous claim based on fewer species (Nagl 1976).

5 Molecular Control of Endoreduplication

5.1 The Canonical Cell Cycle

The canonical eukaryotic cell cycle is composed of four distinct phases: an undifferentiated DNA presynthetic phase with a 2C nuclear DNA content, termed the G1 phase; the S-phase, during which DNA is synthesized, with a nuclear DNA content intermediate between 2C and 4C; a second undifferentiated phase (DNA postsynthetic phase) with a 4C nuclear DNA content, termed the G2 phase; and the ultimate M-phase or mitosis. Mitotic cell division is the ultimate step in the cell cycle, and leads to the transmission of the genetic information from one mother cell to two daughter cells. The classical cell cycle thus involves the accurate duplication of the chromosomal DNA stock in S-phase and its subsequent equal segregation in each nascent cell as a result of mitosis.

The progression within the four phases of the plant cell cycle is regulated by a class of conserved heterodimeric protein complexes consisting of a catalytic subunit referred to as cyclin-dependent kinase (CDK) and a regulatory cyclin (CYC) subunit whose association determines the activity of the complex, its stability, its localization and substrate specificity (Inzé and De Veylder 2006). The canonical A-type CDK (CDKA; Joubès et al. 2000) harboring the PSTAIRE hallmark in the cyclin-binding domain displays a pivotal role during the cell cycle as it participates

in different CDKA/CYC complexes to trigger the specific phosphorylation of numerous protein substrates at the boundaries between the G1 and the S phases, and between the G2 and M phases, thus allowing the commitment to DNA replication and mitosis respectively. The availability and binding of the regulatory cyclin subunit to a CDK partner is thus of prime importance for the regulation of the cell cycle. However, other levels of complexity in the regulation occur at the posttranslational level affecting the components of the CDK/CYC complexes. The kinase activity of the complexes is dependent on the phosphorylation/dephosphorylation status of the kinase itself, and also on the binding of CDK inhibitors and/or recruitment of additional regulatory factors (Inzé and De Veylder 2006).

5.2 The Endocycle

The endoreduplication cycle (endocycle) is made of the succession of S- and undifferentiated G-phase without mitosis, thus accounting for the cessation of cell division and the increase in ploidy level (Joubès and Chevalier 2000; Edgar and Orr-Weaver 2001; Vlieghe et al. 2007). As a result, part of the molecular control existing for the classical cell cycle regulation is conserved in the endocycle.

5.2.1 The Mitosis-to-Endoreduplication Transition

The commitment to endocycle and the consequent lack of mitosis has been proposed to occur in the absence of a mitosis inducing factor (MIF) which normally governs the passage through the G2-M transition. In addition, down-regulation of M-phase-associated CDK activity is sufficient to drive cells into the endoreduplication cycle (Vlieghe et al. 2007). The M-phase CDKB1;1 activity is required to prevent a premature entry in the endocycle. Hence, CDKB1;1 is the likely candidate kinase to be part of the MIF. Though the cyclin partner of CDKB1;1 inside MIF still awaits a definite identification, convincing in planta functional analyses highlighted the A-type cyclin CYCA2;3 to be the most appropriate candidate (Yu et al. 2003; Imai et al. 2006).

5.2.2 Relicensing of Origins of Replication

The control of MIF activity cannot account solely for the progression within the endocycle, since it requires the fluctuation in the activity of S-phase CDK between DNA synthesis and the undifferentiated G-phase as to allow relicensing of origins of replication. In eukaryotes, the initiation of DNA replication occurs only once during each cell cycle from multiple sites throughout each chromosome (Kelly and Brown 2000). These origins of replication trigger the assembly of prereplication complex (pre-RC) harboring several components, such as the ORC, CDC6, CDT1, and MCMs proteins (Bryant and Francis 2008). During the cell cycle, the control of the G1-to-S

transition in plant cells is exerted through the retinoblastoma-related protein (RBR) pathway (de Jager and Murray 1999; Gutierrez et al. 2002), where the hypophosphorylated form of RBR binds to the E2F-DP dimeric transcription factor, thereby repressing the E2F-responsive genes required for the commitment to the S-phase, such as those encoding the pre-RC components. Interestingly, the ectopic expressions of either *CDC6* (Castellano et al. 2001) or *CDT1* (Castellano et al. 2004), or E2Fa with its dimerization partner DPa (De Veylder et al. 2002) are sufficient to trigger extra endocycles, as well as the inhibition of RBR function, consistent with the inhibitory function of RBR on E2F (Park et al. 2005). It is noteworthy that the activation of DNA replication in all these transgenic plants results in extra endocycles and also causes prolonged cell proliferation activity. These data illustrate the conservation of molecular controls between the endocycle and the canonical cell cycle, but more importantly the importance of regulating the CDK activity, including the pivotal role of MIF at the onset of endoreduplication. It was thus proposed as a quantitative model that the amount of CDK activity controls the differentiation – and obviously the endoreduplication – status of a cell (De Veylder et al. 2007).

5.2.3 Regulation of CDK Activity in Endoreduplication During Fruit Development

Among the potential mechanisms regulating the CDK activities in endoreduplicating tissues, three distinct mechanisms are proposed to be affecting the components of the CDK/CYC complexes at the posttranslational level: (1) the WEE1 kinase regulates negatively the CDK activity by phosphorylation of residue Tyr15 before the commitment to mitosis as to ensure that DNA replication and repair on damaged DNA have been completed; (2) the active CDKA/CYCD complexes may be inhibited by specific CDK inhibitors, termed ICK/KRPs (for Interactor of cyclin-dependent kinase/Kip-related protein); (3) loss of CDK activity occurs upon the proteolytic destruction of the cyclin subunits via the ubiquitin proteasome pathway, involving the activation of the anaphase-promoting complex (APC) through its association with the CCS52.

Since endoreduplication plays such an important part during fruit development (Chevalier 2007), the relative contribution of these different control mechanisms on CDK activity has been addressed in tomato.

Role of WEE1

Homologues to *WEE1* have been isolated from various plant species (Shimotohno and Umeda 2007). While functional analyses performed in *Schizosaccharomyces pombe* indicated that expression of the maize or Arabidopsis gene led to the inhibition of cell division and significant cell enlargement (Sun et al. 1999; Sorrell et al. 2002), Arabidopsis knock-out mutants for *WEE1* grow perfectly well under nonstress conditions (De Schutter et al. 2007). Neither cell division nor endoreduplication was affected in these mutants, thus indicating that *WEE1* is not rate-limiting for cell cycle

progression under normal growth conditions. However, *WEE1* was shown to be a critical target of the DNA replication and DNA damage checkpoints, which operates in the G2 phase by arresting the cell cycle in response to DNA damage.

Since the *WEE1* gene is significantly expressed in endoreduplicating cells of maize endosperm (Sun et al. 1999) and tomato fruit tissues (Gonzalez et al. 2004), the function of the WEE1 kinase in the onset of endoreduplication *in planta* appears to conflict with the work of De Schutter et al. (2007). During tomato fruit development, i.e., in a highly endoreduplicating cell context, we provided evidence that *WEE1* is involved in the determination of endoreduplication and thus, participates in the control of cell size during tomato fruit development through its expected negative regulation on CDK activity (Gonzalez et al. 2007).

In Arabidopsis, the WEE1 Kinase controls the cell cycle arrest in response to activation of the DNA integrity checkpoint, thus targeting the CDKA/Cyclin complex, resulting in a stop of the cell cycle in the G2 phase until DNA is repaired or replication is completed (De Schutter et al. 2007). Unlike its Arabidopsis counterpart, the down-regulation of tomato *WEE1* induced a small-fruit phenotype originating from a reduction in cell size associated with a lowering of endoreduplication (Gonzalez et al. 2007), suggesting that *WEE1* acts on endoreduplication in a species-dependent manner, especially in the context of highly endoreduplicating tissues. Within the endocycles, a minimal cell size must be required to pass the checkpoint in the G-phase prior to the following round of DNA replication. Hence, WEE1 activity could contribute to inhibit the CDK/cyclin complexes driving the G-to-S transition, preventing a premature entry into the S-phase of the following endocycle by regulating the length of the G-phase and thus allowing cell enlargement (Gonzalez et al. 2007).

Role of ICK/KRP

Plant specific CDK inhibitors called ICK/KRPs bind and inhibit or sequester CDKs (Verkest et al. 2005b). In *A. thaliana*, when ICK/KRPs are constitutively expressed slightly above their endogenous level, only mitotic cell cycle specific CDKA;1 complexes are affected, thus blocking the G2/M transition, while the endoreduplication cycle specific CDKA;1 complexes are unaffected (Verkest et al. 2005a; Weinl et al. 2005). The fine tuning of the ICK/KRP protein abundance was demonstrated as a key feature for cell cycle control, and especially to trigger the onset of the endoreduplication cycle (Verkest et al. 2005a). The activity of the G2-to-M specific CDKB1;1 in dividing cells triggers the phosphorylation of Arath; KRP2, thus mediating its degradation by the proteasome, and consequently controls the level of CDKA;1 activity. Therefore, when CDKB1;1 activity decreases, Arath; KRP2 protein level increases, leading cells to enter the endoreduplication cycle.

Four different KRP inhibitors have been identified so far in tomato, namely Solly;KRP1 to Solly;KRP4. The respective expression of Solly;*KRP1* and Solly; *KRP2* displayed distinct behaviors, since Solly;*KRP1* is preferentially expressed at 20 DPA (both at the transcription and translation levels), when the endoreduplication process is maximal in the pericarp and the gel tissues, while Solly; *KRP2*

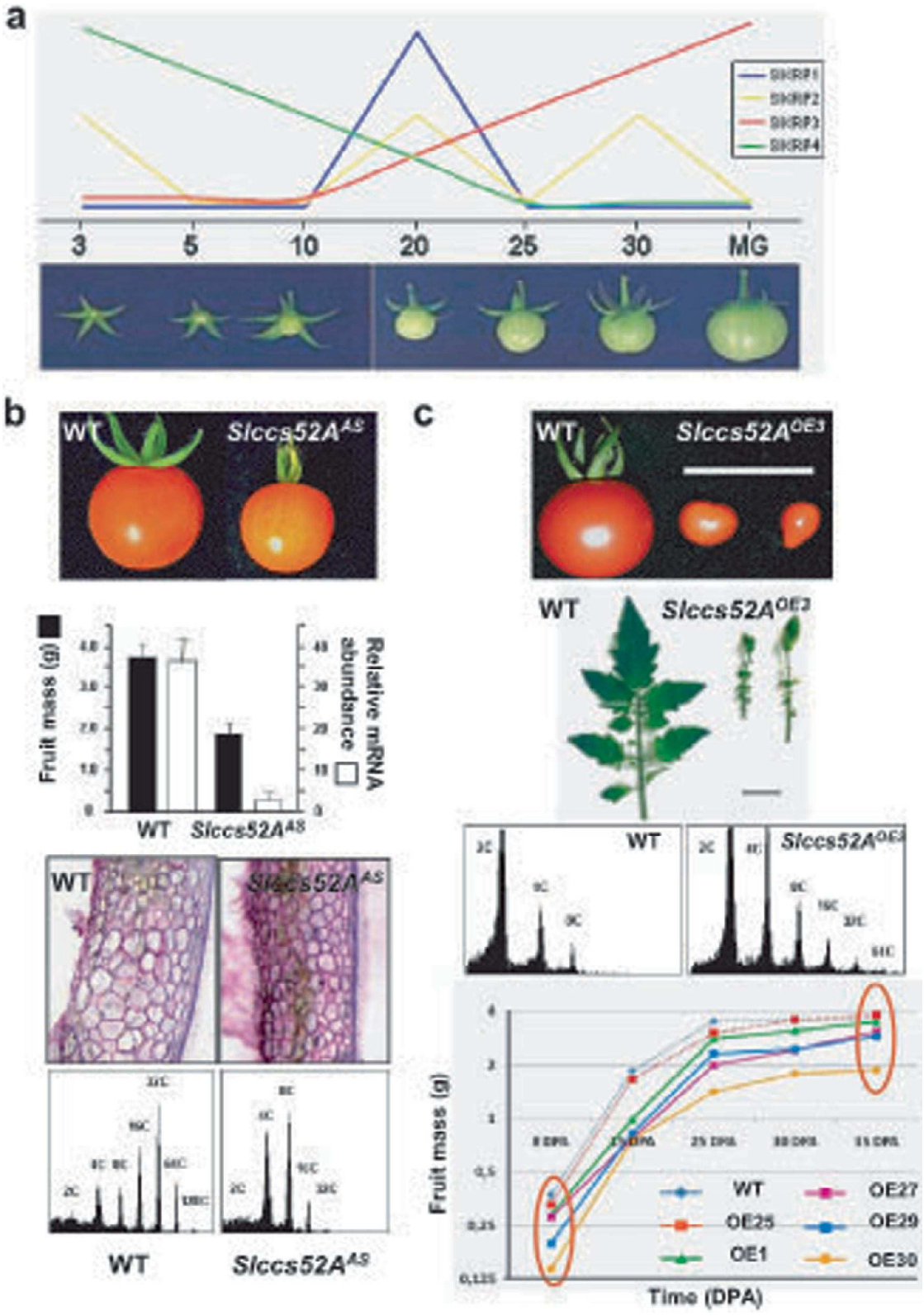

Fig. 2 Molecular and functional analysis of genes involved in the control of endoreduplication during tomato fruit development. (**a**) Schemed profile of mRNA expression for the four tomato KRP genes. The stages of fruit development are indicated in days post-anthesis. MG: Mature Green. (**b**) Phenotypic and molecular analysis of tomato *CCS52A* down-regulated *Pro35S: SlCCS52AAS* plants. Mature fruits (red ripe stage) were compared with untransformed control

expression peaks during fruit maturation (Bisbis et al. 2006). Using quantitative PCR following reverse transcription (RT-qPCR), we showed that the four tomato KRPs display unique expression profiles during tomato fruit development (Fig. 2a). Interestingly, Solly;*KRP4* is mostly expressed during the very early development of the fruit, i.e., when cell divisions predominantly drive fruit growth, while the expression of Solly;*KRP3* increases at the latest stages of fruit development, i.e., when cell expansion predominantly accounts for fruit growth. These data suggest that these KRPs may display distinct physiological and functional roles during the cell cycle and eventually, during the endoreduplication cycle.

During tomato fruit development, the large and hypervacuolarized cells constituting the jelly-like (gel) locular tissue undergo multiple rounds of endoreduplication. Within this particular tissue, mitosis is arrested after 20 DPA and only endoreduplication occurs until then concomitantly with a strong posttranslational inhibitory regulation of the CDKA activity (Joubès et al. 1999). The origin of this posttranslational regulatory mechanism resides in part in the accumulation of Solly; KRP1, which accounts for the inhibition of CDK/CYC kinase activity during the development of the gel tissue in tomato fruit (Bisbis et al. 2006).

Role of CCS52

The ubiquitin-dependent proteolysis of mitotic cyclins requires the involvement of a specific E3-type ubiquitin ligase named the anaphase-promoting complex/cyclosome (APC/C). In plants, the APC/C is activated by the CCS52A protein, homologous to the mammalian CDH1 and Drosophila FZR, which binds to cyclins to drive them towards the degradation process by the 26S proteasome (Capron et al. 2003). Like its eukaryotic counterparts, CCS52A was found to promote the onset and progression of endoreduplication (Cebolla et al. 1999; Vinardell et al. 2003). As far as the Arabidopsis CCS52A2 isoform is concerned, its transcriptional activity is under the control of the atypical E2Fe/DEL1 factor, which acts as a repressor of premature endocycle onset (Vlieghe et al. 2005; Lammens et al. 2008).

We have investigated the functional role of *CCS52* genes during tomato fruit development. Transgenic plants underexpressing *SlCCS52A* or *SlCCS52B* using the

Fig. 2 (continued) (WT) of the same age. Fruit mass measurements of 25 DPA-fruits harvested from *Slccs52A*^{AS} lines and WT. The corresponding transcript levels of 25 DPA-fruits were measured by real-time PCR, and the relative abundance of mRNA was normalized to Sl*βtubulin* and Sl*eiF4A*. Data are mean ± standard deviation ($n = 3$). The comparison of 25 DPA-pericarps from WT and *Slccs52A*^{AS} fruits reveals an alteration in cell size induced by the down-regulation of SlCCS52A, together with a shift towards lower DNA ploidy levels. (**c**) Phenotypic and molecular analysis of *Pro35S:SlCCS52AOE* plants overexpressing tomato *CCS52A*. Mature fruits (red ripe stage) and fully developed leaves from line *Pro35S:SlCCS52A*^{OE3} were compared with untransformed control (WT). In line *Pro35S:SlCCS52A*^{OE3} DNA ploidy levels in leaves were shifted towards greater levels as a result of CCS52A overexpression. The growth kinetics of fruits harvested from WT plants and *Pro35S:SlCCS52A*^{OE} plants (lines OE1, OE25, OE27, OE29 and OE30) was established by measuring fruit mass daily up to 35 DPA

CaMV 35S promoter as a primary approach were generated. While the Pro35S:*SlCCS52B*^{AS} plants showed no evident phenotype at all, the Pro35S:*SlCCS52A*^{AS} plants displayed smaller fruits than wild-type plants (Fig. 2b). The ploidy level of the Pro35S:*SlCCS52A*^{AS} fruits was reduced and correlated with a decrease in mean cell size and an increased cell number.

Gain-of-function transgenic tomato plants overexpressing *SlCCS52A* were also generated. In the most extreme case, the phenotype of the Pro35S:*SlCCS52A*^{OE} line OE3 exhibited gross changes in leaf development and morphology (Fig. 2c). The plant phenotype was characterized by the appearance of under-developed (small and curly) leaves, resembling those of Arabidopsis plants overexpressing CDK inhibitors (Wang et al. 2000; De Veylder et al. 2001; Schnittger et al. 2003), thus suggesting that cell division was deeply impaired in these plants. Interestingly, the ploidy level in these plants was increased towards high DNA levels. Five more *SlCCS52A* overexpressing plants were analyzed for which the overall phenotypes were less affected allowing subsequent analyses, especially fruit growth characteristics (Fig. 2c). In accordance with the level of *SlCCS52A* expression, which was not significantly different from that of WT, fruits from line OE25 did behave like WT. On the contrary, the growth of fruits from the four other lines expressing greater levels of *SlCCS52A* transcripts displayed a slower kinetics. However, fruits from these transgenic lines at 35 DPA tended to reach almost the same size as WT fruit.

To explain these data, the effects of a *SlCSS52A* overexpression during very early fruit development are essentially, likely to affect the cell division process thus leading to very small fruits. Thereafter, and in accordance with the functional specificity of *SlCSS52A* in the control of endoreduplication, fruit growth is then accelerated during the endoreduplication-driven cell expansion phase to recover an optimum final fruit size close to that of WT. A kinetic study of the appearance of highly polyploid nuclei during fruit growth in these Pro35S:*SlCCS52A*^{OE} lines does support strongly this hypothesis (Mathieu-Rivet et al. submitted).

The functional analysis of endoreduplication-promoting genes, such as *WEE1* and *CCS52A* thus demonstrates the physiological role of endoreduplication in fleshy fruit growth, since a reduction in cell size originating from a decrease in DNA ploidy levels impacts the whole fruit development and final fruit size. We cannot make short work of the above stated causality dilemma, and whether endoreduplication is as a driving regulator for cell expansion. Nonetheless *WEE1* is thought to control the endocycle G-phase length as to allow the sufficient cell growth prior to commitment to the next nuclear DNA amplification, and accordingly cell enlargement becomes determining for subsequent DNA reduplication. At the organ level, manipulating endoreduplication through *CCS52A* overexpression highlights the function of endoreduplication as an ultimate driving force for fruit growth, and even an enhancer of cell growth rate facilitating and/or accelerating fruit growth or bigger fruit size. As shown in our cytological analysis in Table 1, endoreduplication is strong when fruit development is short and, therefore, endoreduplication is a way to get big fruits rapidly as supported by our molecular data.

6 Concluding Remarks

Fleshy fruit organogenesis represents an interesting plant system to study at the molecular and functional level the regulation of cell division and cell expansion processes, and especially, the interplay between the classical cell cycle and the endoreduplication cycle. Among the different plant models, tomato is especially well suited to address this question. Indeed, the final size of the fruit depends upon both the cell number and cell size, which is strongly associated with endoreduplication. The originality of the tomato fruit model resides in the cellular and structural diversity of tissues that compose the fruit, and very importantly final cell size (cell diameter higher than 0.6 mm at the end of fruit development) and ploidy levels (up to 512C in some genotypes) (Cheniclet et al. 2005). Such levels of endopolyploidy represent values unmatched in other model plants, such as Arabidopsis or maize where the maximum physiological ploidy is limited respectively to 32C (epidermal cells of the hypocotyls) or 96C (seed endosperm). Why such high levels of endopolyploidy in tomato represents a crucial interrogation.

As reviewed in this chapter, several physiological traits have been attributed to endoreduplication in plants, and as far as fleshy fruits are concerned, the complete elucidation of the functional role of endoreduplication during their growth still awaits us. As discussed herein, we believe that endoreduplication facilitates the growth of fleshy fruits by driving an extended cell expansion process. Obviously, it is also tempting to speculate that endoreduplication is associated with cell differentiation and metabolic specialization cell in fruit cells in the course of fleshy fruit development. The biochemical composition of fruit is mainly determined during the growth period sustained by cell expansion: starch, organic acids, secondary metabolites and aroma precursors accumulate and thus contribute to the organoleptic and nutritional quality of fruit such as tomato. These metabolic modifications during fruit growth originate from a profound change in the cellular behavior and gene expression program of fruit cells and are concomitant with endoreduplication as recently analyzed (e.g., Lemaire-Chamley et al. 2005; Mounet et al. 2009). However, the direct link between endoreduplication and gene expression control still awaits a definitive demonstration.

Acknowledgements Part of the research described in this chapter was supported by the 6th Framework Program of the European Commission, within the European Solanaceae Integrated project, EU-SOL (grant no. FOOD-CT-2006-016214), and by fundings from the Region Aquitaine. M. B., E.M.-R. and M.N. were supported respectively by grants n°26855-2007, n°19061-2005 and n°24220–2006 from the Ministère de l'Enseignement Supérieur et de la Recherche (France).
We express our deepest thanks to Dr Theresa Barreneche and Dr Hélène Christmann (Research Unit 419 on Fruit Species, INRA Bordeaux, France), for having provided fruit samples of 25 varieties from the Prunus species and the corresponding data for bloom and maturity time. The Prunus species are conserved in the Prunus, Castanea, Juglans Genetic Resources Centre of INRA Bordeaux.

Dr Spencer Brown and Olivier Catrice (Plant Science Institute, UPR 2355, CNRS, Gif-sur-Yvette, France) are acknowledged for flow cytometry sorting of tomato nuclei and helpful discussions, and Dr Olivier Coriton (Plant Cytogenetics Plateform, INRA Le Rheu, France) for his precious help in performing FISH analyses.
We acknowledge the excellent technical assistance from Valérie Rouyère. Part of the cytological work was done on the Imaging Cytology facility (Plateau Technique Imagerie Cytologie, IFR103) at INRA Bordeaux with the help of Martine Peypelut for confocal image acquisition of hybridized nuclei.

References

Balbi V, Lomax TL (2003) Regulation of early tomato fruit development by the *Diageotropica* gene. Plant Physiol 131:186–197

Barlow PW (1975) The polytene nucleus of the giant cell of *Bryonia* anthers. Protoplasma 83:339–349

Baroux C, Fransz P, Grossniklaus U (2004) Nuclear fusions contribute to polyploidization of the gigantic nuclei in the chalazal endosperm of Arabidopsis. Planta 220:38–46

Barow M (2006) Endopolyploidy in seed plants. BioEssays 28:271–281

Barow M, Meister A (2003) Endopolyploidy in seed plants is differently correlated to systematics, organ, life strategy and genome size. Plant Cell Environ 26:571–584

Bauer MJ, Birchler JA (2006) Organization of endoreduplicated chromosomes in the endosperm of Zea mays L. Chromosoma 115:383–394

Bennett MD (1972) Nuclear DNA content and minimum generation time in herbaceous plants. Proc R Soc Lond Ser B Biol Sci 181:109–135

Berger F (2003) Endosperm: the crossroad of seed development. Curr Opin Plant Biol 6: 42–50

Bergervoet JHW, Verhoeven HA, Gilissen LJW, Bino RJ (1996) High amounts of nuclear DNA in tomato (*Lycopersicon esculentum* Mill.) pericarp. Plant Sci 116:141–145

Bertin N (2005) Analysis of the tomato fruit growth response to temperature and plant fruit load in relation to cell division, cell expansion and DNA endoreduplication. Ann Bot 95:439–447

Bertin N, Borel C, Brunel B, Cheniclet C, Causse M (2003) Do genetic make-up and growth manipulation affect tomato fruit size by cell number, or cell size and endoreduplication? Ann Bot 92:415–424

Bertin N, Lecomte A, Brunel B, Fishman S, Genard M (2007) A model describing cell polyploidization in tissues of growing fruit as related to cessation of cell proliferation. J Exp Bot 58:1903–1913

Bisbis B, Delmas F, Joubès J, Sicard A, Hernould M, Inzé D, Mouras A, Chevalier C (2006) Cyclin-Dependent Kinase Inhibitors are involved in endoreduplication during tomato fruit development. J Biol Chem 281:7374–7383

Bohner J, Bangerth F (1988a) Cell number, cell size and hormone levels in semi-isogenic mutants of *Lycopersicon pimpinellifolium* differing in frut size. Physiol Plant 72:316–320

Bohner J, Bangerth F (1988b) Effect of fruit-set sequence and defoliation on cell number, cell size and hormone levels of tomato fruits (*Lycopersicon esculentum* Mill.) within a truss. Plant Growth Regul 7:141–155

Bollard EG (1970) The physiology and nutrition of developing fruits. In: Hulme AC (ed) The biochemistry of fruit and their products, vol 1. Academic, London, pp 387–425

Boonkorkaew P, Hikosaka S, Sugiyama N (2008) Effect of pollination on cell division, cell enlargement, and endogenous hormones in fruit development in a gynoecious cucumber. Sci Hortic 116:1–7

Bradley MV, Crane JC (1955) The effect of 2,4,5-trichlorophenoxyacetic acid on cell and nuclear size and endopolyploidy in parenchyma of apricot fruits. Am J Bot 42:273–281

Brecht JK, Chau KV, Fonseca SC, Oliveira FAR, Silva FM, Nunes MCN, Bender RJ (2003) Maintaining optimal atmosphere conditions for fruits and vegetables throughout the postharvest handling chain. Postharvest Biol Technol 27:87–101

Bryant JA, Francis D (2008) Initiation of DNA replication In: Bryant JA, Francis D (eds) The eukaryotic cell cycle. Taylor and Francis, Abingdon, UK, pp 29–44

Bünger-Kibler S, Bangerth F (1982) Relationship between cell number, cell size and fruit size of seeded fruits of tomato (Lycoperpsicon esculentum Mill.), and those induced parthenocarpically by the application of plant growth regulators. Plant Growth Regul 1:143–154

Cano-Medrano R, Darnell RL (1997) Cell number and cell size in parthenocarpic *vs.* pollinated Blueberry (Vaccinium ashei) fruits. Ann Bot 80:419–425

Capron A, Okrész L, Genschik P (2003) First glance at the plant APC/C, a highly conserved ubiquitin-protein ligase. Trends Plant Sci 8:83–89

Carmi N, Salts Y, Dedicova B, Shabtai S, Barg R (2003) Induction of parthenocarpy in tomato via specific expression of the rolB gene in the ovary. Planta 217:726–735

Carvalheira GMG (2000) Plant polytene chromosomes. Genet Mol Biol 3:1043–1050

Castellano MM, del Pozo JC, Ramirez-Parra E, Brown S, Gutierrez C (2001) Expression and stability of Arabidopsis CDC6 are associated with endoreduplication. Plant Cell 13:2671–2686

Castellano MM, Boniotti MB, Caro E, Schnittger A, Gutierrez C (2004) DNA replication licensing affects cell proliferation or endoreplication in a cell type–specific manner. Plant Cell 16:2380–2393

Cebolla A, Vinardell JM, Kiss E, Olah B, Roudier F, Kondorosi A, Kondorosi E (1999) The mitotic inhibitor ccs52 is required for endoreduplication and ploidy-dependent cell enlargement in plants. EMBO J 18:4476–4484

Ceccarelli M, Sanantonio E, Marmottini F, Amzallag GN, Cionini PG (2006) Chromosome endoreduplication as a factor of salt adaptation in *Sorghum bicolor*. Protoplasma 227:113–118

Cheniclet C, Rong WY, Causse M, Bolling L, Frangne N, Carde JP, Renaudin JP (2005) Cell expansion and endoreduplication show a large genetic variability in pericarp and contribute strongly to tomato fruit growth. Plant Physiol 139:1984–1994

Chevalier C (2007) Cell cycle control and fruit development. In: Inzé D (ed) Cell cycle control and plant development. Annual plant reviews, vol 32. Blackwell, Oxford, pp 269–293

Cong B, Liu J, Tanksley SD (2002) Natural alleles of a tomato QTL modulate fruit size through heterochronic regulatory mutations. Proc Natl Acad Sci U S A 99:13606–13611

Cookson SJ, Radziejwoski A, Granier C (2006) Cell and leaf size plasticity in *Arabidopsis*: what is the role of endoreduplication? Plant Cell Environ 29:1273–1283

Coombe B (1976) The development of fleshy fruits. Annu Rev Plant Physiol 27:507–528

Cowan AK, Taylor NJ, van Staden J (2005) Hormone homeostasis and induction of the small-fruit phenotype in a "Hass" avocado. Plant Growth Regul 45:11–19

Crane JC (1964) Growth substances in fruit setting and development. Annu Rev Plant Physiol 15:303–326

Cruz-Castillo JG, Woolley DJ, Lawes GS (2002) Kiwifruit size and CPPU response are influenced by the time of anthesis. Sci Hortic 95:23–30

D'Amato F (1984) Role of polyploidy in reproductive organs and tissues. In: Johri BM (ed) Embryology of Angiosperms. Springer, New York, pp 519–566

D'Aoust MA, Yelle S, Nguyen-Quoc B (1999) Antisense inhibition of tomato fruit sucrose synthase decreases fruit setting and the sucrose unloading capacity of young fruit. Plant Cell 11:2407–2418

De Schutter K, Joubès J, Cools T, Verkest A, Corellou F, Babiychuk E, Van Der Schueren E, Beeckman T, Kushnir S, Inzé D, De Veylder L (2007) Arabidopsis WEE1 kinase controls cell cycle arrest in response to activation of the DNA integrity checkpoint. Plant Cell 19:211–25

De Veylder L, Beeckman T, Beemster GTS, Krols L, Terras F, Landrieu I, Van Der Schueren E, Maes S, Naudits M, Inzé D (2001) Functional analysis of cyclin-dependent kinase inhibitors of Arabidopsis. Plant Cell 13:1–15

De Veylder L, Beeckman T, Beemster GTS, de Almeida Engler J, Ormenese S, Maes S, Naudts M, Van Der Schueren E, Jaqmard A, Engler G, Inzé D (2002) Control of proliferation, endoreduplication and differentiation by the *Arabidopsis* E2Fa-DPa transcription factor. EMBO J 21:1360–1368

De Veylder L, Beeckman T, Inzé D (2007) The ins and outs of the plant cell cycle. Nat Rev Mol Cell Biol 8:655–665

DeJong T, Goudriaan J (1989) Modeling peach fruit growth and carbohydrate requirements: reevaluation of the double-sigmoid growth pattern. J Am Soc Hortic Sci 114:800–804

Edgar BA, Orr-Weaver TL (2001) Endoreplication cell cycles: more for less. Cell 105:297–306

Fang Y, Spector DL (2005) Centromere positioning and dynamics in living Arabidopsis plants. Mol Biol Cell 16:5710–5718

Ferrandiz C (2002) Regulation of fruit dehiscence in Arabidopsis. J Exp Bot 53:2031–2038

Ferrandiz C, Pelaz S, Yanofsky MF (1999) Control of carpel and fruit development in *Arabidopsis*. Annu Rev Biochem 68:321–354

Frary A, Nesbitt TC, Frary A, Grandillo D, van der Knapp E, Cong B, Liu J, Meller J, Elber R, Alpert KB, Tanksley SD (2000) *fw2.2*: a quantitative trait locus key to the evolution of tomato fruit size. Science 289:85–88

Gendreau E, Traas J, Desnos T, Grandjean O, Caboche M, Höfte H (1997) Cellular basis of hypocotyl growth in Arabidopsis thaliana. Plant Physiol 114:295–305

Gendreau E, Höfte H, Grandjean O, Brown S, Traas J (1998) Phytochrome controls the number of endoreduplication cycles in the *Arabidopsis thaliana* hypocotyl. Plant J 13:221–230

Gillaspy G, Ben-David H, Gruissem W (1993) Fruits: a developmental perspective. Plant Cell 5:1439–1451

Giovannoni J (2001) Molecular biology of fruit maturation and ripening. Annu Rev Plant Physiol Plant Mol Biol 52:725–749

Giovannoni J (2004) Genetic regulation of fruit development and ripening. Plant Cell 16: S170–S180

Goetz M, Vivian-Smith A, Johnson SD, Koltunow AM (2006) Auxin response factor8 is a negative regulator of fruit initiation in Arabidopsis. Plant Cell 18:1873–1886

Goetz M, Hooper LC, Johnson SD, Rodrigues JCM, Vivian-Smith A, Koltunow AM (2007) Expression of aberrant forms of AUXIN RESPONSE FACTOR8 stimulates parthenocarpy in Arabidopsis and tomato. Plant Physiol 145:351–366

Gonzalez N, Hernould M, Delmas F, Gévaudant F, Duffe P, Causse M, Mouras A, Chevalier C (2004) Molecular characterization of a *WEE1* gene homologue in tomato (*Lycopersicon esculentum* Mill.). Plant Mol Biol 56:849–861

Gonzalez N, Gévaudant F, Hernould CC, Mouras A (2007) The cell cycle-associated protein kinase WEE1 regulates cell size in relation to endoreduplication in developing tomato fruit. Plant J 51:642–655

Gray JD, Kolesik P, Hoj PB, Coombe BG (1999) Confocal measurement of the three-dimensional size and shape of plant parenchyma cells in a developing fruit tissue. Plant J 19:229–236

Gutierrez C, Ramirez-Parra E, Mar Castellano M, del Pozo JC (2002) G1 to S transition: more than a cell cycle engine switch. Curr Opin Plant Biol 5:480–486

Hamada K, Hasegawa K, Ogata T (2008) Strapping and a synthetic cytokinin promote cell enlargement in 'Hiratanenashi' Japanese persimmon. Plant Growth Regul 54:225–230

Harada T, Kurahashi W, Yanai M, Wakasa Y, Satoh T (2005) Involvement of cell proliferation and cell enlargement in increasing the fruit size of Malus species. Sci Hortic 105:447–456

Hase Y, Trung KH, Matsunaga T, Tanaka A (2006) A mutation in the uvi4 gene promotes progression of endoreduplication and confers increased tolerance towards ultraviolet B light. Plant J 46:317–326

Higashi K, Hosoya K, Ezura H (1999) Histological analysis of fruit development between two melon (*Cucumis melo* L. *reticulatus*) genotypes setting a different size of fruit. J Exp Bot 50:1593–1597

Ho L (1992) Fruit growth and sink strength. In Marshall C and Grace J (eds) Fruit and seed production. Aspect of development, environmental physiology and ecology. Cambridge University Press, Cambridge, pp 101–124

Ho LC (1996) The mechanism of assimilate partitioning and carbohydrate compartmentation in fruit in relation to the quality and yield of tomato. J Exp Bot 47:1239–1243

Hopping ME (1976) Structure and development of fruit and seeds in chinese gooseberry (Actinidia chinensis Planch.). N Z J Bot 14:63–68

Imai KK, Ohashi Y, Tsuge T, Yoshizumi T, Matsui M, Oka A, Aoyama T (2006) The A-type cyclin CYCA2;3 is a key regulator of ploidy levels in Arabidopsis endoreduplication. Plant Cell 18:382–396

Inzé D, De Veylder L (2006) Cell cycle regulation in plant development. Annu Rev Genet 40:77–105

John PCL, Qi R (2008) Cell division and endoreduplication: doubtful engines of vegetative growth. Trends Plant Sci 13:121–127

Jones B, Frasse P, Olmos E, Zegzouti H, Li ZG, Latche A, Pech JC, Bouzayen M (2002) Down-regulation of DR12, an auxin-response-factor homolog, in the tomato results in a pleiotropic phenotype including dark green and blotchy ripening fruit. Plant J 32:603–613

Joubès J, Chevalier C (2000) Endoreduplication in higher plants. Plant Mol Biol 43:737–747

Joubès J, Phan T-H, Just D, Rothan C, Bergounioux C, Raymond P, Chevalier C (1999) Molecular and biochemical characterization of the involvement of Cyclin-dependent kinase CDKA during the early development of tomato fruit. Plant Physiol 121:857–869

Joubès J, Chevalier C, Dudits D, Heberle-Bors E, Inzé D, Umeda M, Renaudin J-P (2000) Cyclin-dependent kinases related protein kinases in plants. Plant Mol Biol 43:607–621

Kano Y (2007) Comparison of Cell Size and Kind of Sugars Accumulated in Grape Berries vs Melon Fruits. Environ Control Biol 45:95–101

Kato N, Lam E (2003) Chromatin of endoreduplicated pavement cells has greater range of movement than that of diploid guard cells in Arabidopsis thaliana. J Cell Sci 116:2195–2201

Kelly TJ, Brown GW (2000) Regulation of chromosome replication. Annu Rev Biochem 69:829–880

Kladnik A, Chourey PS, Pring DR, Dermastia M (2006) Development of the endosperm of Sorghum bicolor during the endoreduplication-associated growth phase. J Cereal Sci 43:209–215

Knapp S (2002) Tobacco to tomatoes: a phylogenetic perspective on fruit diversity in the Solanaceae. J Exp Bot 53:2001–2022

Kondorosi E, Kondorosi A (2004) Endoreduplication and activation of the anaphase-promoting complex during symbiotic cell development. FEBS Lett 567:152–157

Kowles RV, Phillips RL (1985) DNA amplification patterns in maize endosperm nuclei during kernel development. Proc Natl Acad Sci USA 82:7010–7014

Kowles RV, Srienc F, Phillips RL (1990) Endoreduplication of nuclear DNA in the developing maize endosperm. Dev Genet 11:125–132

Kudo N, Kimura Y (2002) Nuclear DNA endoreduplication during petal development in cabbage: relationship between ploidy levels and cell size. J Exp Bot 53:1017–1023

Kwiatkowska M, Popłonska K, Kazmierczak A, Stepinski D, Rogala K, Polewczyk K (2007) Role of DNA endoreduplication, lipotubuloids, and gibberellic acid in epidermal cell growth during fruit development of Ornithogalum umbellatum. J Exp Bot 58:2023–2031

Lammens T, Boudolf V, Kheibarshekan L, Panagiotis Zalmas L, Gaamouche T, Maes S, Vanstraelen M, Kondorosi E, La Thangue NB, Govaerts W, Inze D, De Veylder L (2008) Atypical E2F activity restrains APC/CCCS52A2 function obligatory for endocycle onset. Proc Nat Acad Sci U S A 105:14721–14726

Larkin JC, Brown ML, Churchman ML (2007) Insights into he endocycle from trichome development. In: Inzé D (ed) Cell cycle control and plant development. Annual plant reviews, vol 32. Blackwell, Oxford, pp 249–268

Lee HC, Chiou DW, Chen WH, Markhart AH, Chen YH, Lin TY (2004) Dynamics of cell growth and endoreduplication during orchid flower development. Plant Sci 166:659–667

Leiva-Neto JT, Grafi G, Sabelli PA, Dante RA, Woo YM, Maddock S, Gordon-Kamm WJ, Larkins BA (2004) A dominant negative mutant of Cyclin-Dependent Kinase A reduces endoreduplication but not cell size or gene expression in maize endosperm. Plant Cell 16:1854–1869

Lemaire-Chamley M, Petit J, Garcia V, Just D, Baldet P, Germain V, Fagard M, Mouassite M, Cheniclet C, Rothan C (2005) Changes in transcriptional profiles are associated with early fruit tissue specialization in tomato. Plant Physiol 139:292–299

Lemontey C, Mousset-Declas C, Munier-Jolain N, Boutin JP (2000) Maternal genotype influences pea seed size by controlling both mitotic activity during early embryogenesis and final endoreduplication level/cotyledon cell size in mature seed. J Exp Bot 51:167–175

Lermontova I, Schubert V, Fuchs J, Klatte S, Macas J, Schubert I (2006) Loading of Arabidopsis centromeric histone CENH3 occurs mainly during G2 and requires the presence of the histone fold domain. Plant Cell 18:2443–2451

List A (1963) Some observations on DNA content and cell and nuclear volume growth in the developing xylem cells of certain higher plants. Am J Bot 50:320–329

Liu J, Cong B, Tanksley SD (2003) Generation and analysis of an artificial gene dosage series in tomato to study the mechanisms by which the cloned quantitative trait locus *fw2.2* controls fruit size. Plant Physiol 132:292–299

Lopes MA, Larkins BA (1993) Endosperm origin, development, and function. Plant Cell 5:1383–1399

Lukaszewska E, Sliwinska E (2007) Most organs of sugar-beet (Beta vulgaris L.) plants at the vegetative and reproductive stages of development are polysomatic. Sexual Plant Reprod 20:99–107

Martí C, Orzáez D, Ellul P, Moreno V, Carbonell J, Granell A (2007) Silencing of DELLA induces facultative parthenocarpy in tomato fruits. Plant J 52:865–876

Mazzucato A, Taddei AR, Soressi GP (1998) The parthenocarpic fruit (pat) mutant of tomato (*Lycopersicon esculentum* Mill.) sets seedless fruits and has aberrant anther and ovule development. Development 125:107–114

Melaragno JE, Mehrotra B, Coleman AW (1993) Relationship between endopolyploidy and cell size in epidermal tissue of *Arabidopsis*. Plant Cell 5:1661–1668

Mergaert P, Nikovics K, Kelemen Z, Maunoury N, Vaubert D, Kondorosi A, Kondorosi E (2003) A novel family in Medicago truncatula consisting of more than 300 nodule-specific genes coding for small, secreted polypeptides with conserved cysteine motifs. Plant Physiol 132:161–173

Mizukami Y (2001) A matter of size: developmental control of organ size in plants. Curr Opin Plant Biol 4:533–539

Mohr WP, Stein M (1969) Fine structure of fruit development in tomato. Can J Plant Sci 49:549–553

Mounet F, Moing A, Garcia V, Petit J, Maucourt M, Deborde C, Bernillon S, Le Gall G, Colquhoun I, Defernez M, Giraudel JL, Rolin D, Rothan C, Lemaire-Chamley M (2009) Gene and metabolite regulatory network analysis of early developing fruit tissues highlights new candidate genes for the control of tomato fruit composition and development. Plant Physiol 149:1505–1528

Nagl W (1976) DNA endoreduplication and polyteny understood as evolutionary strategies. Nature 261:614–645

Nenno M, Schumann K, Nagl W (1994) Detection of rRNA and phaseolin genes on polytene chromosomes of Phaseolus coccineus by fluorescence in situ hybridization after pepsin pretreatment. Genome 37:1018–1021

Nitsch JP (1953) The physiology of fruit growth. Annu Rev Plant Physiol 4:199

Nitsch JP (1965) Physiology of flower and fruit development. In: Ruhland W (ed) Encyclopedia of plant physiology. Springer, Berlin, Heidelberg, New York, pp 1537–1647

Nitsch JP (1970) Hormonal factors in growth and development. In: Hulme AC (ed) The biochemistry of fruits and their products 2. Academic, London, pp 427–472
Ognjanov V, Vujanic-Varga D, Misic PD, Veresbaranji I, Macet K, Tesovic Z, Krstic M, Petrovic N (1995) Anatomical and biochemical studies of fruit development in peach. Sci Hort 64:33–48
Ojeda H, Deloire A, Carbonneau A, Ageorges A, Romieu C (1999) Berry development of grapevines: Relations between the growth of berries and their DNA content indicate cell multiplication and enlargement. Vitis 38:145–150
Otto SP (2007) The evolutionary consequences of polyploidy. Cell 131:452–462
Ozga JA, van Huizen R, Reinecke DM (2002) Hormone and seed-specific regulation of pea fruit growth. Plant Physiol 128:1379–1389
Pandolfini T, Molesini B, Spena A (2007) Molecular dissection of the role of auxin in fruit initiation. Trends Plant Sci 12:327–329
Park JA, Ahn JW, Kim YK, Kim SJ, Kim JK, Kim WT, Pai HS (2005) Retinoblastoma protein regulates cell proliferation, differentiation, and endoreduplication in plants. Plant J 42:153–163
Roeder AHK, Yanofsky MF (2006) Fruit development in Arabidopsis. The Arabidopsis Book 52:1–50
Rygol J, Lüttge U (1983) Water-relation parameters of giant and normal cells of Capsicum annuum pericarp. Plant Cell Environ 6:545–553
Schlosser J, Olsson N, Weis M, Reid K, Peng F, Lund S, Bowen P (2008) Cellular expansion and gene expression in the developing grape (Vitis vinifera L.). Protoplasma 232:255–265
Schnittger A, Weinl C, Bouyer D, Schöbinger U, Hülskamp M (2003) Misexpression of the cyclin-dependent kinase inhibitor *ICK1*/*KRP1* in single-celled Arabidopsis trichomes reduces endoreduplication and cell size and induces cell death. Plant Cell 15:303–315
Schubert V, Klatte M, Pecinka A, Meister A, Jasencakova Z, Schubert I (2006) Sister chromatids are often incompletely aligned in meristematic and endopolyploid interphase nuclei of Arabidopsis thaliana. Genetics 172:467–475
Serrani J, Ruiz-Rivero O, Fos M, Garcia-Martinez JM (2008) Auxin-induced fruit-set in tomato is mediated in part by gibberellins. Plant J 56:922–934
Sesek P, Kump B, Bohanec B (2005) Interphase structure of endoreduplicated nuclei in diploid and tetraploid Brassica oleracea L. Acta Biol Cracov Ser Bot 47:93–99
Shimotohno A, Umeda M (2007) CDK phosphorylation. In: Inzé D (ed) Cell cycle control and plant development, Annual Plant Reviews, vol 32. Blackwell, Oxford, pp 114–137
Smith O (1935) Pollination and life-history studies of the tomato (Lycopersicon esculentum Mill.). Cornell Univ Agric Exp Stn Mem 184:3–16
Soliva-Fortuny RC, Martin-Belloso O (2003) New advances in extending the shelf-life of fresh-cut fruits: a review. Trends Food Sci Technol 14:341–353
Sorrell DA, Marchbank A, McMahon K, Dickinson JR, Rogers HJ, Francis D (2002) A WEE1 homologue from Arabidopsis thaliana. Planta 215:518–522
Srivastava A, Handa AK (2005) Hormonal regulation of tomato fruit development: a molecular perspective. J Plant Growth Regul 24:67–82
Stern RA, Flaishman M, Applebaum S, Ben-Arie R (2007) Effect of synthetic auxins on fruit development of 'Bing' cherry (Prunus avium L.). Sci Hortic 114:275–280
Sugimoto-Shirasu K, Roberts K (2003) "Big it up": endoreduplication and cell-size control in plants. Curr Opin Plant Biol 6:544–553
Sun Y, Dilkes BP, Zhang C, Dante RA, Carneiro NP, Lowe KS, JUNG R, Gordon-Kamm WJ, Larkins BA (1999) Characterization of maize (*Zea mays* L.) Wee1 and its activity in developing endosperm. Proc Nat Acad Sci U S A 96:4180–4185
Suutarinen J, Änäkäinen L, Autio K (1998) Comparison of Light Microscopy and Spatially Resolved Fourier Transform Infrared (FT-IR) Microscopy in the Examination of Cell Wall Components of Strawberries. Lebensm Wiss Technol 31:595–601
Tanksley SD (2004) The genetic, developmental, and molecular bases of fruit size and shape variation in tomato. Plant Cell 16:S181–S189

Varga A, Bruinsma J (1986) Tomato. In: Monselise SP (ed) CRC Handbook of fruit set and development. CRC, Boca Raton, FL, pp 461–480

Verkest A, Weinl C, Inzé D, De Veylder L, Schnittger A (2005a) Switching the cell cycle. Kip-related proteins in plant cell cycle control. Plant Physiol 139:1099–1106

Verkest A, de Manes CLO, Vercruysse S, Maes S, Van Der Schueren E, Beeckman T, Genschik P, Kuiper M, Inzé D, De Veylder L (2005a) The Cyclin-Dependent Kinase inhibitor KRP2 controls the onset of endoreduplication cycle during Arabidopsis leaf development through inhibition of mitotic CDKA;1 kinase complexes. Plant Cell 17:1723–1736

Vinardell JM, Fedorova E, Cebolla A, Kevei Z, Horvath G, Kelemen Z, Tarayre S, Roudier F, Mergaert P, Kondorosi A, Kondorosi E (2003) Endoreduplication mediated by the Anaphase-Promoting Complex Activator CCS52A is required for symbiotic cell differentiation in Medicago truncatula nodules. Plant Cell 15:2093–2105

Vivian-Smith A, Koltunow AM (1999) Genetic analysis of growth-regulator-induced parthenocarpy in Arabidopsis. Plant Physiol 121:437–451

Vlieghe K, Boudolf V, Beemster GTS, Maes S, Magyar Z, Atanassova A, de Almeida Engler J, De Groodt R, Inzé D, De Veylder L (2005) The DP-E2F-like gene *DEL1* controls the endocycle in *Arabidopsis thaliana*. Curr Biol 15:59–63

Vlieghe K, Inzé D, De Veylder L (2007) Physiological relevance and molecular control of the endocycle in plants. In: Inzé D (ed) Cell cycle control and Plant development. Annual plant reviews, vol 32. Blackwell, Oxford, pp 227–248

Vriezen WH, Feron R, Maretto F, Keijman J, Mariani C (2008) Changes in tomato ovary transcriptome demonstrate complex hormonal regulation of fruit set. New Phytol 177:60–76

Wang H, Zhou Y, Gilmer S, Whitwill S, Fowke LC (2000) Expression of the cyclin-dependent protein kinase inhibitor ICK1 affects cell division, plant growth and morphology. Plant J 24:613–623

Wang H, Jones B, Li Z, Frasse P, Delalande C, Regad F, Chaabouni S, Latché A, Pech J-C, Bouzayen M (2005) The tomato *Aux/IAA* transcription factor *IAA9* is involved in fruit development and leaf morphogenesis. Plant Cell 17:2676–2692

Weinl C, Marquardt S, Kuijt SJH, Nowack MK, Jakoby MJ, Hülskamp M, Schnittger A (2005) Novel functions of plant Cyclin-Dependent Kinase inhibitors, ICK1/KRP1, can act non-cell-autonomously and inhibit entry into mitosis. Plant Cell 17:1704–1722

Yadegari R, Drews GN (2004) Female gametophyte development. Plant Cell 16:S133–S141

Yu Y, Steinmetz A, Meyer D, Brown S, Shen WH (2003) The tobacco A-type cyclin, Nicta; CycA2;3, at the nexus of cell division and differentiation. Plant Cell 15:2763–2777

4.2 Presentation of thesis

In the UMR619 “Biologie du Fruit”, the team G1 "Organogenesis of the Fruit and endoreduplication" explores the role of the cell cycle in the development of tomato fruit, with a focus on the endoreduplication phenomenon. Having discovered and described CDKs and cyclins present in tomato (Joubès *et al.*, 1999; Joubès *et al.*, 2000; Joubès *et al.*, 2001), the laboratory has been particularly interested in the different CDK inhibitory mechanisms that could account for the endoreduplication process during tomato fruit development. Hence, the laboratory described the biochemical and physiological functions of WEE1 (Gonzalez *et al.*, 2004; Gonzalez *et al.*, 2007), CCS52a and CCS52b genes (Rivet-Mathieu *et al.*, 2010) and demonstrated the inhibitory activity of SlKRP1 on CDKA/cyclin complexes in endoreduplicating tissues (Bisbis *et al.*, 2006). However, the latter study lacked an *in planta* description of the physiological role of KRPs.

The objective of this thesis was to further study the genes of the Kip-Related Proteins family in tomato. Because SlKRP1 was the best known gene at the start the thesis, he served as a model for the study.

The thesis was conducted in two areas:

- The study of the primary structure of SlKRP1 to discover and locate the various sites carrying function in the protein.

- The annalysis of the physiological role of KRPs during tomato fruit development, especially during the phase of cell expansion, through the study of transgenic plants aimed at over-expressing SlKRP1 in the appropriate developmental stage.

CHAPTER 2 : RESULTS/DISCUSSION

1 Functional Analysis of motifs in SlKRP1

1.1 Primary structure of the different tomato KRPs

At the start of the thesis, two tomato KRPs were already identified: SlKRP1 and SlKRP2. Two additional KRPs have been identified, SlKRP3 and SlKRP4, by consulting the Sol Genomics Network database. Sequence comparison of the different KRPs allowed to distinguish, outside motifs 1 and 2 (see introduction 3.1.2) different protein motifs conserved within SlKRP1, SlKRP2 and SlKRP3, which were absent in SlKRP4 (see Figure 22).

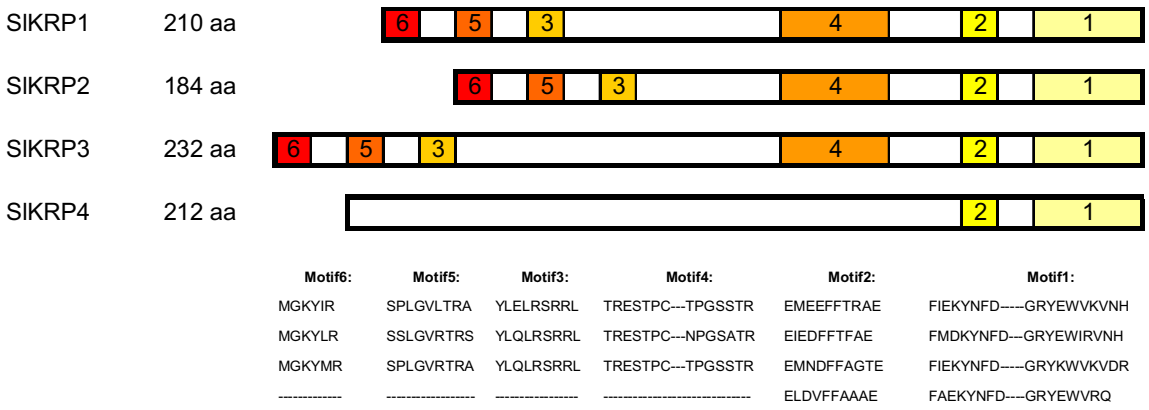

Motif6:	Motif5:	Motif3:	Motif4:	Motif2:	Motif1:
MGKYIR	SPLGVLTRA	YLELRSRRL	TRESTPC---TPGSSTR	EMEEFFTRAE	FIEKYNFD-----GRYEWVKVNH
MGKYLR	SSLGVRTRS	YLQLRSRRL	TRESTPC---NPGSATR	EIEDFFTFAE	FMDKYNFD---GRYEWIRVNH
MGKYMR	SPLGVRTRA	YLQLRSRRL	TRESTPC---TPGSSTR	EMNDFFAGTE	FIEKYNFD-----GRYKWVKVDR
----------	----------	----------	----------	ELDVFFAAAE	FAEKYNFD----GRYEWVRQ

Figure 22 : Conserved motifs within tomato KRPs. (A) Representation of different primary sequences of KRPs tomato. The conserved motifs are numbered from 1 to 6. (B) Protein sequence associated to motifs in each tomato KRPs

Using the recently published tomato genome sequence, we could investigate the number and the position of introns in the transcribed region of each KRP gene identified by comparison with the corresponding cDNA sequences (see Figure 23).

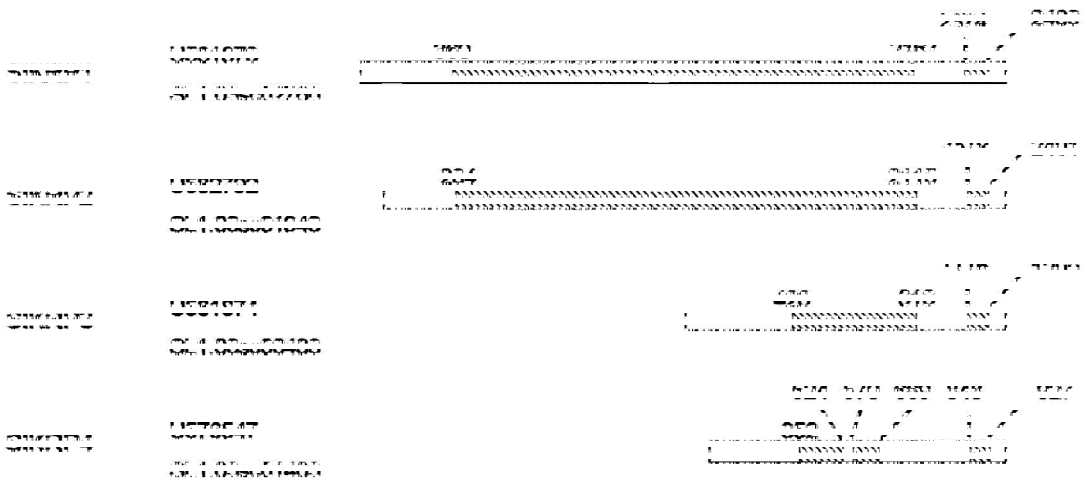

Figure 23 : Genomic sequences of the different KRPs identified in tomato from start to stop codons. Sequence references corresponding to the cDNA and genomic DNA are given in front of each KRP. Intronic regions are shaded

When comparing the different intronic and exonic sequences of the different KRPs, the most striking finding is the presence of an intron in the 3' part of the different genomic sequences starting exactly at the same position. Indeed, the start position of each intron is located at the corresponding start of motif 1 in the primary sequence (cutting motif KYNFD after the K). It is noteworthy that in tobacco, Jasinski et al. (2002) discovered that Ntkis1 can be found as two differently spliced variants, Ntkis1a and Ntkis1b, which diverge at the very same relative position. The presence of this last intron at the same position in all tomato KRPs investigated so far may argue for a common mechanism of alternative splicing between full length KRPs and their spliced variants lacking motif 1 and hence inactive as CDK inhibitors. Most of the other motifs present in tomato KRPs being of unknown function, the protein sequences of the 4 tomato KRPs have been studied by bioinformatics, using tools for predicting function. One of these tools, ELM, has put forward several putative sites of protein-protein interaction (seeTable 4: Prediction of functional sites in the different tomato KRPs using the ELM server).

Table 4: Prediction of functional sites in the different tomato KRPs using the ELM server

colour code

1
2
3
4
5
6

Elm Name	Elm Description	Cell Compartment	Pattern	KRP1		KRP2		KRP3		KRP4	
LIG_14-3-3_2	Longer mode 2 interacting phospho-motif for 14-3-3 proteins with key conservation RxxxSfp.	nucleus, mitochondrion, cytosol, internal side of plasma membrane	R.{*P}[ST][!VLM].	RVPNSIQ	155-161	RLQSSS HSASVD	30-35 74-79	RQNRSLR RDPPDSIP	86-92 154-160	HAKSCR	155-160
LIG_CYCLIN_1	Substrate recognition site that interacts with cyclin and thereby increases phosphorylation by cyclin/cdk complexes. Predicted protein should have the MOD_CDK site. Also used by cyclin inhibitors.	nucleus, cytosol	[RK]-L.{0,1}[FYLIVMP]	KALAL RRLV KPLP	24-28 42-45 197-200			KTLAL KPLV RSLRV KPLP	32-36 67-70 89-93 219-222	KFLDL	112-116
LIG_FHA_1	Phosphothreonine motif binding a subset of FHA domains that show a preference for a large aliphatic amino acid at the pT+3 position.	nucleus	..(T)..[ILV].	RKTEDVS	9-15	STTLALQ	23-29	KATGEVV AKTLALK	11-17 31-37		
LIG_FHA_2	Phosphothreonine motif binding a subset of FHA domains that have a preference for an acidic amino acid at the pT+3 position.	nucleus, Replication fork	..(T)..[DE].	PFTVLEG KRTTRES IPTDLEM FFTRAEK	47-53 119-125 164-170 173-179	FFTFAEQ	148-154	ERTTRES IPTAHEM	141-147 186-192		
LIG_MAPK_1	MAPK interacting molecules (e.g. MAPKKs, substrates, phosphatases) carry docking motif that help to regulate specific interaction in the MAPK cascade. The classic motif approximates (R/K)xxxfxfxf where # is a hydrophobic residue.	nucleus, cytosol	[KR]{0,2}[KR].{0,2}[KR].{2,4}[LVM].[LVF]			RTRSTTLAL	20-28	RTRAKTLAL RRLEKPLVGF RLEKPLVGF KRQNRSLRV	28-36 63-72 64-72 85-93	KMTREREVLEV REREVLEV	27-37 30-37
LIG_USP7_1	The USP7 NTD domain binding motif variant based on the MDM2 and P53 interactions.	nucleus	[PA][^PP][^PYW1]S[^P]	PEDSF PGSST	104-108 140-144	PSASD ASDSC	44-48 46-50	PGSST	162-166	PAVSS AVSSN	84-88 85-89
LIG_WW_4	Class IV WW domains interaction motif; phosphorylation-dependent interaction.	nucleus, cytosol	...[ST]P.	EDVSPL RESTPC NIQTPG	12-17 123-128 136-141	SSSTPP KPPTPI RESTPC	35-40 61-66 98-103	LDVSPL RESTPC SIPTPG	20-25 145-150 158-163	LEMSPT ISESPA FQSTPK	50-55 65-70 147-152
MOD_CK1_1	CK1 phosphorylation site	nucleus, cytosol	S..{(ST)}...			SSSSSTP SSSSTPP SSSTPPP SLPSASD	33-39 34-40 35-41 42-48	SWNSGSG SIPTPGS	100-106 158-164	SVISESP SPASELS SELSSQG SNVTKGS	63-69 68-74 71-77 104-110
MOD_CK2_1	CK2 phosphorylation site	nucleus, cytosol, protein kinase CK2 complex	...{(ST)}..E	DGGSYLE KPPTVLE PEDSFGE RKRTTRE TIPTDLE EPFTRAE	32-38 46-52 104-110 118-124 163-169 172-178	HSASVDE THRSTRE NIPSAHE DFTTFAE	74-80 93-99 138-144 147-153	RERTTRE IIPTAHE	140-146 185-191	IATSYSE TMPSEAE	123-129 167-173
MOD_GSK3_1	GSK3 phosphorylation recognition site	nucleus, cytosol	...{(ST)}...[ST]	TRKTEDVS RKRTTRES KRTTREST TRESTPCS NIQTPGSS PGSSTRRT VPNSIQPT	8-15 118-125 119-126 122-129 136-143 140-147 156-163	GVRTRSTT RLQSSSSS LQSSSSST SSSTPPPS SLPSASDS CPNSHPHS FQHTHRST THRSTRES HRSTREST TRESTPCS TRQTELNT	18-25 30-37 31-38 35-42 42-49 68-75 90-97 93-100 94-101 97-104 119-126	GVRTRAKT RERTTRES ERTTREST SIPTPGSS	26-33 140-147 141-148 158-165	SPASELSS ELSSQQNT DNESSNVT SNVTKGSS	68-75 72-79 100-107 104-111
MOD_PIKK_1	(ST)Q motif which is phosphorylated by PIKK family members	nucleus	...([ST])Q..			NTTTQRR	125-131			ELSSQGN	72-78
MOD_ProDKin_1	Proline-Directed Kinase (e.g. MAPK) phosphorylation site in higher eukaryotes.	nucleus, cytosol	...([ST])P..	EDVSPLG RESTPCS NIQTPGS	12-18 123-129 136-142	SSSTPPP KPPTPIP RESTPCS	35-41 61-67 98-104	LDVSPLG RESTPCN SIPTPGS	20-26 145-151 158-164	LEMSPTV ISESPAS FQSTPKP	50-56 65-71 147-153
LIG_APCC_Dbox_1	An RxaL-based motif that binds to the Cdh1 and Cdc20 components of APC/C thereby targeting the protein for destruction in a cell cycle dependent manner	nucleus, cytosol	.R.L..[LIVM].							EREVLEVVD	31-39
LIG_BRCT_BRCA1_1	Phosphopeptide motif which directly interacts with the BRCT (carboxy-terminal) domain of the Breast Cancer Gene BRCA1 with low affinity	nucleus, BRCA1-BARD1 complex	.S..F							VSSNF GSSKF SSSKF	86-90 109-113 139-143
LIG_PP1	Protein phosphatase 1 catalytic subunit (PP1c) interacting motif binds targeting proteins that dock to the substrate for dephosphorylation. The motif defined is [RK]{0,1}[VI][^P][FW].	protein phosphatase type 1 complex, nucleus, cytosol	.[RK]{,0,1}[VI][^P][FW].							KFKVEFQ	142-148
MOD_SUMO	Motif recognised for modification by SUMO-1	nucleus, PML body	[VILMAFP]K.E							FKVE AKEE	143-146 198-201

Because the software is based on conservness on few amino acids, most of the time sites can be recognized for different functions. However, the software detects a large proportion of putative interaction motifs at different conserved sites between different KRPs. This may be an additional argument that these motifs do have a functional role, in addition to the conservation of these motifs between different KRPs.

Another interesting point is the presence of specific putative motifs for SlKRP4, most of which fall within the theme of "DNA damage checkpoint". Thus, there are 3 putative binding motifs for BRCT-type proteins, present in various proteins involved in DNA damage checkpoint: one putative motif recognized by CDH1/CDC20 is responsible for the selection of targets to be degraded by the Anaphase Promoting Complex and a PIKK phosphorylation site, a motif recognized by a family of kinases involved in DNA repair and DNA damage checkpoints. Regarding the latter, it is also interesting to note that the targets of BRCT also often seem to be PIKK targets. So, the hypothesis of a role for SlKRP4 in the machinery of DNA damage checkpoint is to be considered.

In addition, the study of the tomato KRPs expression during plant development showed that SlKRP4 has a particular expression profile: indeed, SlKRP4 is highly expressed in the first phase of fruit development (division phase), and in young expanding leaves, which could be an argument for M phase specific expression of SlKRP4 (see 2.2). This expression pattern may suggest a different function between these KRPs. Moreover, in *Arabidopsis thaliana*, AtKRP3, -4 and -5 which have the same motifs that SlKRP1, -2 and -3, are preferentially expressed around the S phase (see Introduction 3.2.2). Furthermore, it has been shown in *Arabidopsis thaliana* that motif 3 is potentially responsible for a particular nuclear localization (Bird *et al.*, 2007, see Introduction 3.2.3). This motif is present in tomato KRP-1, -2 and -3, but not in SlKRP4. The sub-nuclear localization of *Arabidopsis* KRPs with motif 3 and the timing of expression of these genes allow us to make the hypothesis of a particular function of the specific motifs for this class of protein.

This problem has led to the study of different motifs of SlKRP1, as a representative tomato KRP.

1.2 **Article 1** Published in The New Phytologist (2010) 188:136-149

New Phytologist

Functional characterization of the tomato cyclin-dependent kinase inhibitor SlKRP1 domains involved in protein–protein interactions

Mehdi Nafati, Nathalie Frangne, Michel Hernould, Christian Chevalier and Frédéric Gévaudant

Institut National de la Recherche Agronomique (INRA), Université de Bordeaux, Unité Mixte de Recherche 619 sur la Biologie du Fruit, BP 81, F–33883 Villenave d'Ornon Cedex, France

Author for correspondence:
Christian Chevalier
Tel: +33 557 122693
Email: chevalie@bordeaux.inra.fr

Received: *16 April 2010*
Accepted: *23 May 2010*

New Phytologist (2010) **188**: 136–149
doi: 10.1111/j.1469-8137.2010.03364.x

Key words: cell cycle, cyclin-dependent kinase, cyclin-dependent kinase inhibitor, kip-related protein, plant, tomato (*Solanum lycopersicum*).

Summary

• Cyclin-dependent kinase (CDK) inhibitors (kip-related proteins, KRPs) play a major role in the regulation of plant cell cycle in antagonizing its progression, and are thus regulators of development. The primary sequence of KRPs is characterized by the existence of conserved motifs, for which we have limited information on their functional significance.

• We performed a functional analysis of various domains present in KRPs from tomato. A series of deletion mutants of SlKRP1 was generated and used in transient expression assays to define the relevance of conserved protein domains in subcellular and subnuclear localizations. Specific interactions of SlKRP1 and its deletion variants with cell cycle proteins were investigated using two-hybrid assays and bimolecular fluorescent complementation.

• Plant KRPs are distributed into two phylogenetic subgroups according to the presence of conserved motifs. Members of subgroup 1 represented by SlKRP1 share 6 conserved motifs whose function in protein localization and protein–protein interactions could be identified. A new interaction motif was localized in the central part of SlKRP1 that targets SlCDKA1 and SlCYCD3;1 to the nucleus.

• Our results bring new insights to the functional role of particular domains in KRPs relative to subcellular localization or proteolytic degradation.

Introduction

Progression of the eukaryotic cell cycle relies on remarkably conserved molecular mechanisms. It involves kinase activities from cyclin-dependent kinase (CDK)/cyclin (CYC) complexes that coordinate the transition from one phase of the cell cycle to the next. Several types of CDKs and cyclins exist in plants reflecting the complexity of the plant cell cycle. Twenty-nine CDK-related sequences have been identified in Arabidopsis and classified into seven distinct classes (CDKA to CDKF plus a group of CDK-like proteins, CKL), defined according to phylogenetic, structural and functional similarities with animal and yeast CDKs (Joubès *et al.*, 2000a; Vandepoele *et al.*, 2002; Menges *et al.*, 2005). CDKAs are functional homologues of the yeast $p34^{CDC2/CDC28}$ protein and thus correspond to the canonical CDK that regulate both the G1–S and G2–M transitions whereas CDKBs are plant-specific CDKs that regulate the G2–M transition (Mironov *et al.*, 1999). The Arabidopsis genome encodes 49 cyclins that have been classified into eight classes and 23 subgroups (CYCA1-3, CYCB1-3, CYCC, CYCD1-7, CYCH, CYCL, CYCP1-4 and CYCL) (Wang *et al.*, 2004). From this complex family of regulators, the A- and B-type cyclins are known as mitotic cyclins regulating the progression through the S-, G2- and early M-phase, while D-type cyclins control the progression through the G1 phase in response to growth factors and nutrients (Inzé & De Veylder, 2006).

CDK/CYC complex activity is under tight post-translational regulations through phosphorylations mediated both positively by CDK/CYC activating kinases (CAK) on residue Thr161 or negatively by the WEE1 kinase on residue Tyr15 (Shimotohno *et al.*, 2006), through the proteolytic degradation of the cyclin moiety (Genschik & Criqui, 2007) or the stable binding of specific CDK inhibitors (CKI) (Wang *et al.*, 2007).

In plants, two families of CKI proteins have been identified to date, and are referred to as the interactor of Cdc2 kinase (ICK)/kip-related protein (KRP) family (Wang *et al.*, 1997; De Veylder *et al.*, 2001), and the SIAMESE protein family (SIM) (Churchman *et al.*, 2006). ICK/KRPs were identified on the basis of a slight sequence homology with one type of animal CKI, namely the $p27^{KIP1}$ protein, localized at the *C*-terminal end and corresponding to the motif of interaction with CDK/CYC complexes. Outside of this functional domain, ICK/KRPs show no significant homology with their animal counterparts (Wang *et al.*, 2007). All ICK/KRPs studied so far are able to bind CDKA and D-type cyclins. The interaction with D-type cyclins can occur within complexes or with the cyclin subunit on its own (Nakai *et al.*, 2006). In addition, putative binding to and inhibition of CDKB complexes have also been reported *in vitro* (Nakai *et al.*, 2006).

Single mutations in *ICK/KRP* genes or loss-of-function strategies do not produce any phenotype, mostly because of gene redundancy. In contrast, the overexpression of ICK/KRPs leads to plant dwarfism as the progression within the cell cycle is deeply altered (Wang *et al.*, 2000; Jasinski *et al.*, 2002a; Verkest *et al.*, 2005). This phenotype can be partly complemented by the co-overexpression of a D-type cyclin (Jasinski *et al.*, 2002b; Schnittger *et al.*, 2003). Interestingly, the phenotypes reported at the cytological level in ICK/KRP overexpressor plants can be classified into two categories according to the level of the ICK/KRP expression (Verkest *et al.*, 2005). A low level of overexpression leads to an increase in nuclear ploidy, according to the process of endoreduplication, at the expense of cell divisions, but with only slight cell size modifications. Conversely, a high overexpression levels leads to a decrease in both mitotic activity and endoreduplication level, concomitantly with an increase in cell size, probably owing to an organismal control tending to achieve a proper organ size. This relationship between the level of ICK/KRP overexpression and the cell cycle alteration led to the hypothesis that G2/M-specific CDK/CYC complexes are more sensitive to ICK/KRP inhibition than G1/S complexes (Verkest *et al.*, 2005; Pettko-Szandtner *et al.*, 2006).

In animal cells, the regulation of $p27^{KIP1}$ at the post-translational level has been extensively studied because many types of cancer originate in a deregulation of its inhibitory function (Vervoorts & Luscher, 2008). In plants, the first evidence of a post-translational activation of ICK/KRP has been reported in *Medicago*, as a calmodulin-like kinase is able to stimulate the inhibitory activity of MtKRP (Pettko-Szandtner *et al.*, 2006). A CDK/CYC complex harbouring CDKB1;1 has been shown to phosphorylate ICK2/KRP2 in *Arabidopsis thaliana*, thus leading to its proteolytic degradation, in order to prevent exit from the cell cycle towards endoreduplication (Verkest *et al.*, 2005). Substantial evidence has recently emerged arguing for ICK/KRP degradation via the E3-ubiquitin ligase SCF pathway involving the 26S proteasome (Kim *et al.*, 2008; Liu *et al.*, 2008; Ren *et al.*, 2008). However, the motifs responsible for the post-translational regulation of ICK/KRPs are yet to be described, although it has been reported that the first 108 amino acids of ICK1/KRP1 (Zhou *et al.*, 2003b) as well as a *C*-terminus located putative motif (Jakoby *et al.*, 2006) could be responsible for the protein instability.

In the proteolytic degradation and signal transduction pathways the signalosome subunit, JAB1/CSN5 (for COP9 SigNalosome subunit 5), is responsible for the nucleus-to-cytoplasm translocation of $p27^{KIP1}$ at the G0/G1 transition in animal cells, to promote this CKI degradation (Tomoda *et al.*, 1999). Again, a deregulation in $p27^{KIP1}$ cellular compartmentalization is associated with cancers, which emphasizes the importance of this process in proper cell cycle regulation (Vervoorts & Luscher, 2008). Whether this type of regulation for ICK/KRP degradation and/or subcellular addressing occurs in plants is highly probable, as an interaction between the tobacco NtKIS1a protein and the NtCSN5 signalosome subunit has been reported (Le Foll *et al.*, 2008). All ICK/KRPs studied to date show a clear nuclear localization (Wang *et al.*, 2007). However, the pattern of localization inside the nucleus varies among the different ICK/KRPs: in Arabidopsis, ICK2/KRP2, ICK4/KRP6 and ICK5/KRP7 are homogeneously localized within the nucleus, while ICK1/KRP1, ICK6/KRP3, ICK7/KRP4 and ICK3/KRP5 show punctuate subnuclear distributions (Bird *et al.*, 2007).

We have previously reported the isolation and biochemical characterization of two ICK/KRPs in tomato, namely SlKRP1 and SlKRP2, and have shown that SlKRP1 contributes to the control of endoreduplication through the inhibition of mitotic CDKA/CYC complex activity during tomato fruit development (Bisbis *et al.*, 2006). To expand our knowledge on the regulatory role of CDK-specific inhibitors in tomato fruit development, we performed a functional analysis of the conserved protein domains present in tomato ICK/KRPs. We showed that ICK/KRPs can be classified into two phylogenetic groups correlated with the existence of short conserved motifs. In the present study, we describe the role of several of these motifs in the subcellular and subnuclear localization of tomato ICK/KRPs and investigate the extent of their putative interaction with candidate cell cycle proteins.

Materials and Methods

Phylogenetic analysis of plant ICK/KRPs

The sequence alignment of ICK/KRPs was performed using CLUSTALW (http://align.genome.jp/) and manually adjusted to improve the best fit of short conserved motifs.

The phylogenetic tree was constructed with the minimum evolution algorithm using MEGA3 (Kumar *et al.*, 2004). Bootstrap analysis with 1000 replicates was performed to test the significance of the nodes.

Plasmid and construct preparation

cDNAs encoding the different target genes were ordered from the Sol Genomics Network Database (http://www.sgn.cornell.edu/search/clone-order.pl), amplified with attB-flanked specific primers and cloned into pDonr201 plasmid using the BP clonase reaction (Invitrogen).

For each mutant form of SlKRP1, either deleted or mutated inside the original sequence, two independent PCRs were first made to amplify the two different portions of the cDNA. The purified PCR products were then mixed at equal molarities and used as template for a third PCR with attB-flanked specific primers. The PCR conditions were standard using a temperature of 50°C for annealing and combinations of gene-specific primers for the different constructs.

cDNAs inserted in the pDonr201 plasmid were then cloned into different sets of destination vectors : pDest22 and pDest32 (Invitrogen) for two-hybrid assays; pBS-35S-YFP-attR and pBS-35S-attR-YFP (kindly provided by Dr Von Arnim, University of Tennessee, Knoxville, USA) for yellow fluorescent protein (YFP) fusions; p2CGW7 and p2GWC7 (purchased from the Plant Systems Biology Laboratory, VIB, Ghent University, Belgium) for cyan fluorescent protein (CFP) fusions; and nEYFP/pUGW2, cEYFP/pUGW2, nEYP/pUGW0 and cEYFP/pUGW0 (kindly provided by Dr Tsuyoshi Nakagawa, Shimane University, Japan) for bimolecular fluorescent complementation (BiFC) assays.

Transient expression in tomato leaf protoplasts and cultured cells, and in onion epidermal cells

Transient expression analyses were performed using homologous systems, namely leaf protoplasts and cultured cells from tomato, and onion epidermal cells as a heterologous system.

Protoplasts were prepared from 7-d-old leaves from tomato plants and transformed using polyethylene glycol (PEG) according to Di Sansebastiano *et al.* (1998). To perform biolistic transformations, 1 ml of 4-d-old tomato SWEET 100 cultured cells (Rontein *et al.*, 2002) or onion epidermis were placed on Murashige and Skoog (MS) basal medium in Petri dishes. For subsequent bombardment, 1 μm and 1.6 μm gold particles (60 mg ml^{-1}) were used for SWEET100 cells and onion epidermal cells, respectively. Gold particles were suspended in 50% ethanol and 25 μl of the suspension were mixed with 5 μl (5 μg) plasmid DNA, 25 μl of 2.5 M $CaCl_2$, 10 μl of 0.1 M spermidine. Pelleted gold particles were washed with consecutively 70% and 100% ethanol and resuspended in 30 μl of 100% ethanol, loaded on macrocarriers (8 μl of gold particle suspension per macrocarrier) for transformation with the particle delivery system using a rupture disc of 1100 psi (7.58 MPa) (PDS-1000/He; Bio-Rad). The distance between macrocarrier and the tissue was 6 cm. After gene delivery, cultured cells or epidermal tissue slices were incubated overnight on MS basal medium at room temperature in the dark, before analysis. Each transformation assay was performed in triplicate and each experiment was replicated at least twice.

For 4,6-diamidino-2-phenylindole (DAPI) treatment experiments, the onion epidermis tissues were incubated in 1 μg ml^{-1} DAPI for 2 min and washed in distilled water before visualization.

Microscopy techniques and imaging

Images for subcellular localization, protein colocalization and BiFC assays were obtained by using the TCS SP2 AOBS confocal scanning microscope from Leica (Gennevilliers, France). CFP was excited using an argon laser at 458 nm and emissions were collected from 465 to 500 nm; YFP was excited by an argon laser at 514 nm and the emission collected from 525 to 600 nm. A 406 nmHg lamp was used for DAPI and emissions were collected from 465 to 500 nm. Images of DAPI colocalization were obtained by using a Nikon Eclipse E800 epifluorescence microscope (Nikon, Champigny sur Marne, France). YFP was visualized using a GFP filter (Ex: 460–500 nm, DM: 505 nm, BA: 510 nm), DAPI was visualized using a DAPI filter (Ex: 340–380 nm, DM: 400 nm, BA: 435–485 nm) and images were recorded using a camera Spot RTke (Diagnostic Instruments Inc., Sterling Heights, MI, USA). All images were processed using Photoshop Software

Fig. 1 Phylogenetic tree of interactor of Cdc2 kinase/kip-related proteins (ICK/KRP). Sequence alignments were created using CLUSTALW, and the tree was derived by minimum evolution analysis. The statistical reliability of the inferred tree topology was assessed by bootstrap test (1000 replicates). The tree was condensed with a cut-off value of 50. Conserved motifs present in each sequence, as referred to in the text, are represented on the right-hand side of the tree. According to the tree branches, ICK/KRPs are clustered in two subgroups, namely subgroup 1 proteins, tinted light grey, and subgroup 2 proteins, tinted dark grey. Accession numbers corresponding to the different *ICK/KRP* genes are given in the Supporting Information Table S1. At, *Arabidopsis thaliana*; Cp, *Carica papaya*; Cr, *Chenopodium rubum*; Ee, *Euphorbia esula*; Gm, *Glycine max*; Mt, *Medicago truncatula*; Nta, *Nicotiana tabacum*; Nto, *Nicotiana tomentosiformis*; Os, *Oryza sativa*; Ps, *Pisum sativum*; Pt, *Populus trichocarpa*; Sl, *Solanum lycopersicum*; Sb, *Sorghum bicolor*; Vt, *Vitis vinifera*; Zm, *Zea mays*.

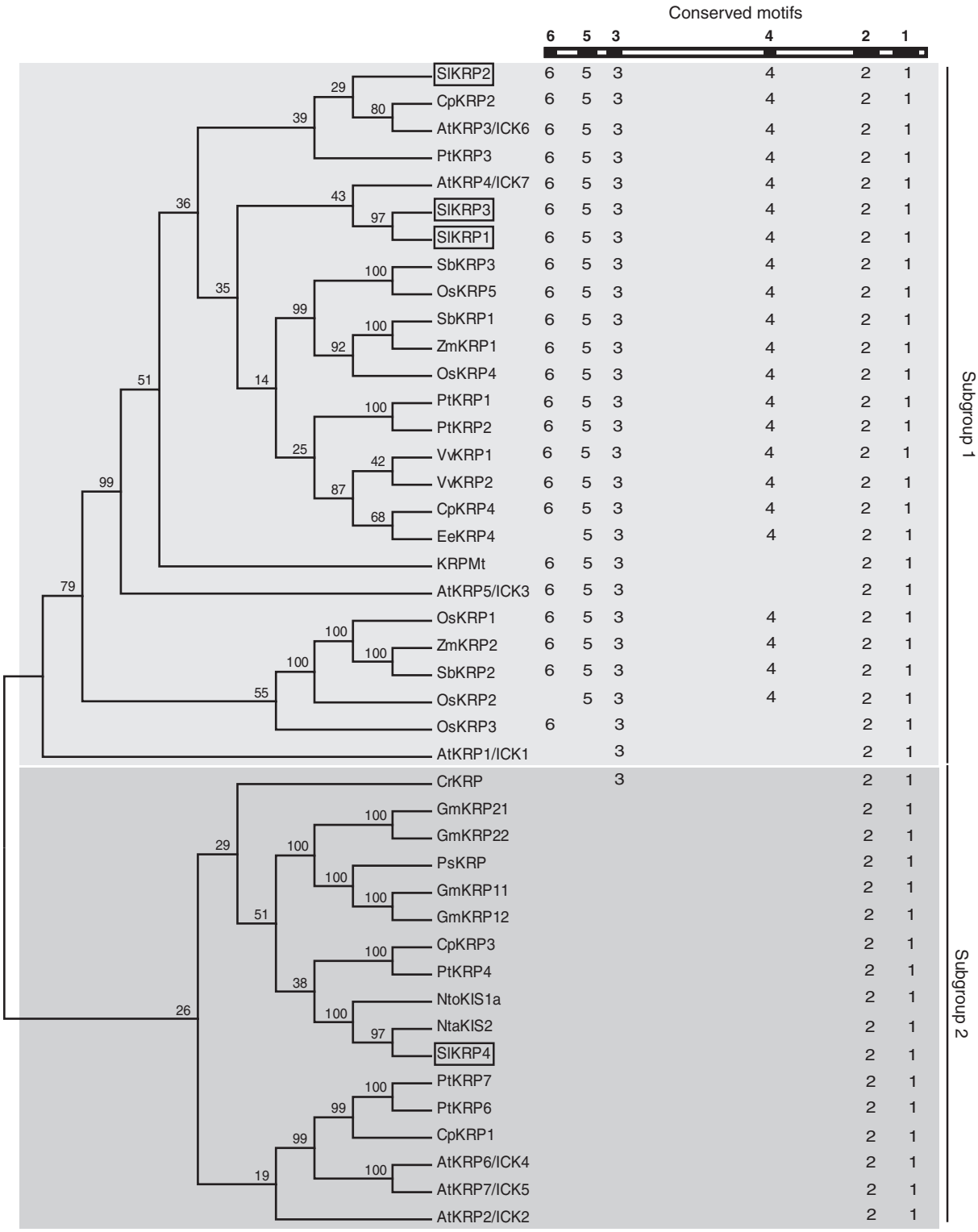

Motif 3 36-YLQLRSRRL
Motif 5 17-LGVRTRA(K/R)(S/T)LAL
Motif 6 1-MGKYM(R/K)K

Motif 1 185-FXKYNFDPVN(D/E)XPL(P/S)R(Y/F)W
Motif 2 169-E(M/I)EEFFAXAEAE
Motif 4 122-TRESTPCSLIR(X_{10})TPGS(S/T)TR

(version CS3, Adobe Systems Incorporated, San José, USA). During subcellular and BiFC assay, the YFP signal was false coloured in glow. During colocalization experiments, the YFP signal was false coloured in yellow and the CFP signal was false coloured in cyan.

Two-hybrid assay

Yeast strains (MAV203) were transformed using the Proquest two-hybrid system for GATEWAY technology according to the manufacturer's instruction (Invitrogen). After transformation, the Petri dishes were incubated for 3 d at 30°C, and isolated colonies were diluted in 40 µl water. Four microlitre of each diluted colony were then deposited on a Petri dish containing SD-LTH medium supplemented with a variable amount of 3-amino1,2,4triazol (3-AT) (20–80 mM) and reincubated for three further days before evaluation of growth.

Results

Identification of KRPs from tomato

Previously we described the characterization of two KRPs from tomato SlKRP1 and SlKRP2 (Bisbis *et al.*, 2006). We report here the identification of two new tomato KRP sequences by BLAST searches using the Solanaceae Genomics Network (SGN) Unigene database (http://sgn.cornell.edu/). These two sequences were named SlKRP3 (SGN-U320533) and SlKRP4 (SGN-U318507) and assigned the GenBank database accession numbers FN794406 and FN794407, respectively.

Alignments of ICK/KRP primary sequences isolated from various plant species highlighted the presence of six conserved motifs (see the Supporting Information, Table S1 and Fig. S1). Motif 1 corresponds to the CDK/CYC binding motif at the protein *C*-terminus, which originally allowed the identification of the first plant CDK inhibitor sequence (Wang *et al.*, 1997). This sequence is now used routinely as a marker for the identification of CDK inhibitors both in plants and animals. Motif 2 is found in all published ICK/KRP sequences or in databases, as well as in inhibitors of the SIM/EL2 family. A putative role as a D-type cyclin binding domain was proposed in SIM/EL2 proteins, (Peres *et al.*, 2007). Similarly, motifs 3–6 are plant specific and of unknown function, but they only occur in a subset of ICK/KRPs (Fig. S1).

Phylogenic classification of KRPs

To investigate the relationships between known ICK/KRPs and the two newly isolated SlKRPs, a phylogenic tree was generated using the full-length sequences of ICK/KRPs from various species found in literature or in databases (Table S1 and Fig. 1). The ICK/KRPs fall into two distant subgroups that will be referred to as subgroup 1 and subgroup 2. Arabidopsis ICK1/KRP1, ICK6/KRP3, ICK7/KRP4 and ICK3/KRP5 lie within subgroup 1, together with tomato SlKRP1, SlKRP2 and SlKRP3. Subgroup 2 hosts ICK2/KRP2, ICK4/KRP6, ICK5/KRP7 from Arabidopsis and SlKRP4. Hence within subgroup 1, SlKRP1 and SlKRP3 share clear sequence homologies with ICK7/KRP4, while SlKRP2 is closer to ICK6/KRP3. The primary sequence of SlKRP4 is highly divergent from that of the three other tomato KRPs because it shares only 19% of identity with SlKRP1, SlKRP2 and SlKRP3, and is only slightly related to ICK1/KRP1 and ICK2/KRP2.

Notably, among the different ICK/KRPs originating from monocotyledonous species to be found in databases and in the literature, not a single one belongs to subgroup 2, while more than half of ICK/KRP sequences from dicotyledonous species used to construct the phylogenetic tree fall into subgroup 2 (Fig. 1). While the two subgroups are composed of sequences from evolutionary distant species, branches inside each group tend to encompass proteins from evolutionary close plants. For example, maize ICK/KRPs are on the same subbranches as rice ICK/KRPs, and tobacco ICK/KRPs are close to tomato ICK/KRPs.

The present description of ICK/KRPs into two subgroups reveals a phylogenetic separation according to the presence of conserved motifs in the primary sequences of ICK/KRPs (Figs 1, S1). Indeed, ICK/KRPs belonging to subgroup 1 display the presence of nearly all of the six defined conserved motifs with some exceptions lacking motif 4, 5 or 6. By contrast, ICK/KRPs from subgroup 2 harbour only motifs 1 and 2 and display their own specific motifs (Fig. S1).

Subcellular localization analysis of SlKRP1 and SlKRP4

To address the subcellular localization of tomato ICK/KRPs and other candidate proteins, transient expression assays were performed in tomato leaf protoplasts and cultured cells derived from fruit pericarp of the SWEET100 variety, using various constructs encoding YFP fused in-frame to the *N*-terminus of the proteins tested under the control of the CaMV 35S promoter. As representative members of each subgroup of ICK/KRPs, the sub-cellular localization of SlKRP1 and SlKRP4 was tested first. The protein constructs YFP-KRP1 and YFP-KRP4 were both localized in the nuclei of tomato leaf protoplasts (Fig. S2), as expected for ICK/KRPs (Bird *et al.*, 2007). Similar results were obtained in cultured cells. However, the use of these two biological materials caused technological difficulties, hampering the observations. Nuclei from leaf protoplasts tend to be overlaid by the surrounding plastids, thus greatly affecting the interpretation of results, and the efficiency in cell transformation using the SWEET100 tomato cultured cells was very low, thus leading to poor reproducibility.

We therefore decided to use onion epidermal cells as a model of choice for plant subcellular localization studies because of the presence of a unique large-sized cell layer. Onion epidermal cells are characterized by the presence of a large vacuole occupying most of the cell volume, squeezing the cytoplasm and nucleus to the outer perimeter of the cell. Nevertheless onion epidermal cells allow a good microscopic visualization of nuclei. After transient transformation of onion epidermal cells by biolistics using the corresponding constructs, YFP-KRP1 and YFP-KRP4 were both localized in the nucleus (Fig. 2a). Alternative fusion of YFP at the *C*-terminal end of SlKRPs gave similar results (data not shown). As shown in Fig. 2(a), the subnuclear distribution of YFP-KRP1 and YFP-KRP4 was different as YFP-KRP1 was localized reproducibly, according to a punctuate distribution similar to all ICK/KRPs belonging to the first phylogenetic subgroup (Fig. 1; Bird *et al.*, 2007), while YFP-KRP4 was distributed uniformly all over the nucleoplasm (Fig. 2a).

To investigate whether the particular localization of YFP-KRP1 is linked to DNA, onion epidermal cells were stained with DAPI following the transient transformation with YFP-KRP1 (Fig. 2b). We found YFP-KRP1 to localize in the vicinity to chromatin DNA, as well as in nuclear bodies of *c.* 2 μm in diameter physically unlinked to DNA. Conversely, YFP-KRP4 appeared to be uniformly distributed in the nucleus, while DNA had a heterogeneous distribution.

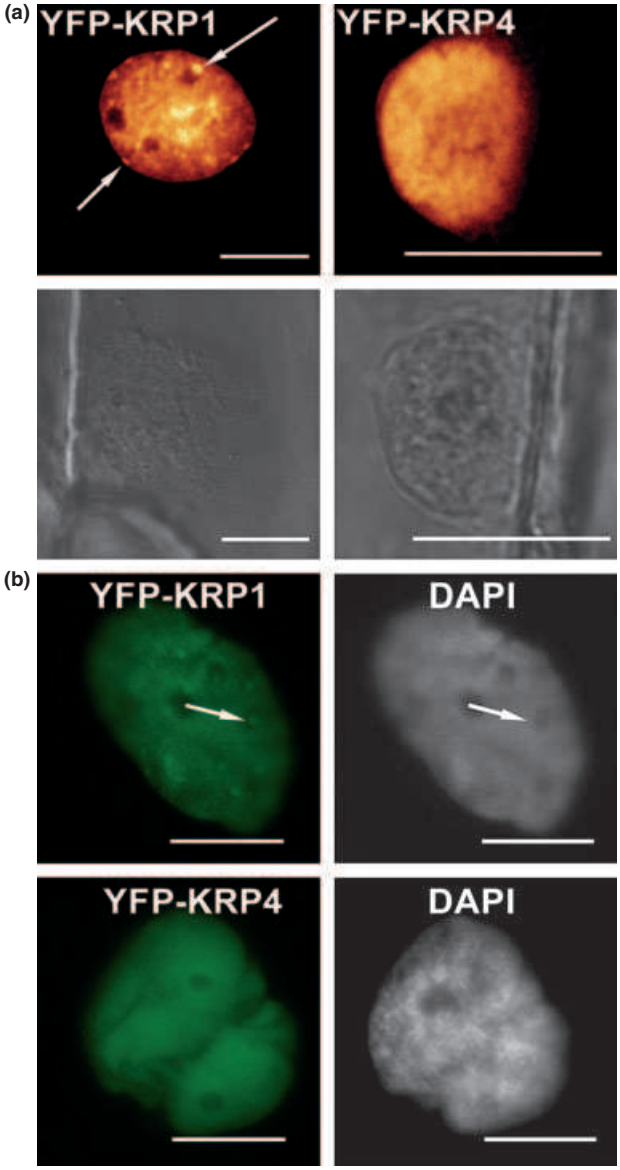

Fig. 2 Subcellular localization of SlKRP1 and SlKRP4. (a) Yellow fluorescent protein (YFP)-tagged SlKRP1 and SlKRP4 were transiently expressed in onion epidermal cells. Corresponding bright-field images are shown below. Arrows point to subnuclear punctuations. (b) Colocalization between YFP-tagged SlKRP1 or SlKRP4 and 4,6-diamidino-2-phenylindole (DAPI). The arrow points to a typical 2 μm nuclear body. Bar, 20 μm.

Functional analysis of protein motifs responsible for SlKRP1 subnuclear localization

To determine the primary sequence motifs in SlKRP1 responsible for nuclear localization, we generated different constructs corresponding to a deletion series of SlKRP1 variants (Fig. 3).

Deleting the *C*-terminal part of SlKRP1 (construct referred to as SlKRP1$^{\Delta 165–210}$) had no effect on the nuclear localization of the protein, while the SlKRP1$^{\Delta 1–44}$ variant lacking the first *N*-terminal 44 amino acids was spread in both the nucleus and cytoplasm (Figs 4a, S3). To confirm whether the *N*-terminal end of SlKRP1 plays a part in nuclear localization, the SlKRP1$^{\Delta 54–210}$ variant was generated. As shown in Fig. 4(a), the 53 aa-long *N*-terminal end of SlKRP1 was sufficient to locate the protein with a punctuate distribution in the nucleus.

The *N*-terminal part of SlKRP1 harbours the conserved motifs 6, 5 and 3 (Figs 1, S1). Alternative forms of the protein lacking one of these motifs (SlKRP1$^{\Delta 1–4}$ lacking motif 6, SlKRP1$^{\Delta 18–28}$ lacking motif 5 and SlKRP1$^{\Delta 36–44}$ lacking motif 3) did not disturb the nuclear localization (Fig. 4a); neither did the concomitant deletion of motifs 6 and 5 or 6 and 3 (data not shown). However, the deletion of both motifs 5 and 3 (SlKRP1$^{\Delta 18–28\ \Delta 36–44}$) induced the reallocation of much of the protein outside of the nucleus, as revealed by the localization along the cytoplasmic stands shown in Fig. 4(a). Such a modification in sub-cellular localization of SlKRP1 was also observed when the deletion of motif 5 was combined with a mutation of the highly conserved Tyrosine^{36} to Alanine (Y36A) within motif 3 (SlKRP1$^{\Delta 18–28\ Y36A}$).

We then performed a coexpression assay of the variants of SlKRP1 lacking motif 5 on the one hand and motif 3 on

New Phytologist

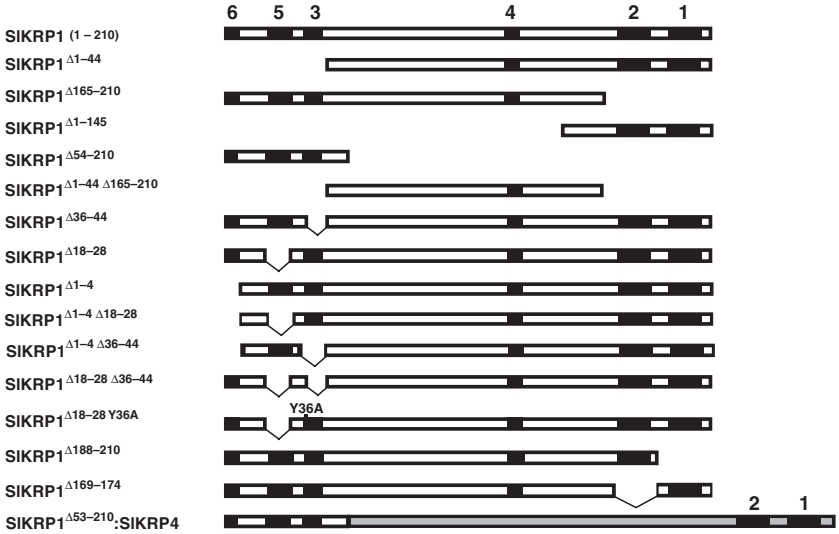

Fig. 3 Schematic view of the series of SlKRP1 deletion mutants used for subcellular localization, bimolecular fluorescent complementation (BiFC) and two-hybrid experiments. Conserved motifs are shown as black boxes and numbered above. The sequence for SlKRP4 used in the SlKRP1$^{\Delta 53-210}$:SlKRP4 chimeric construct is tinted grey.

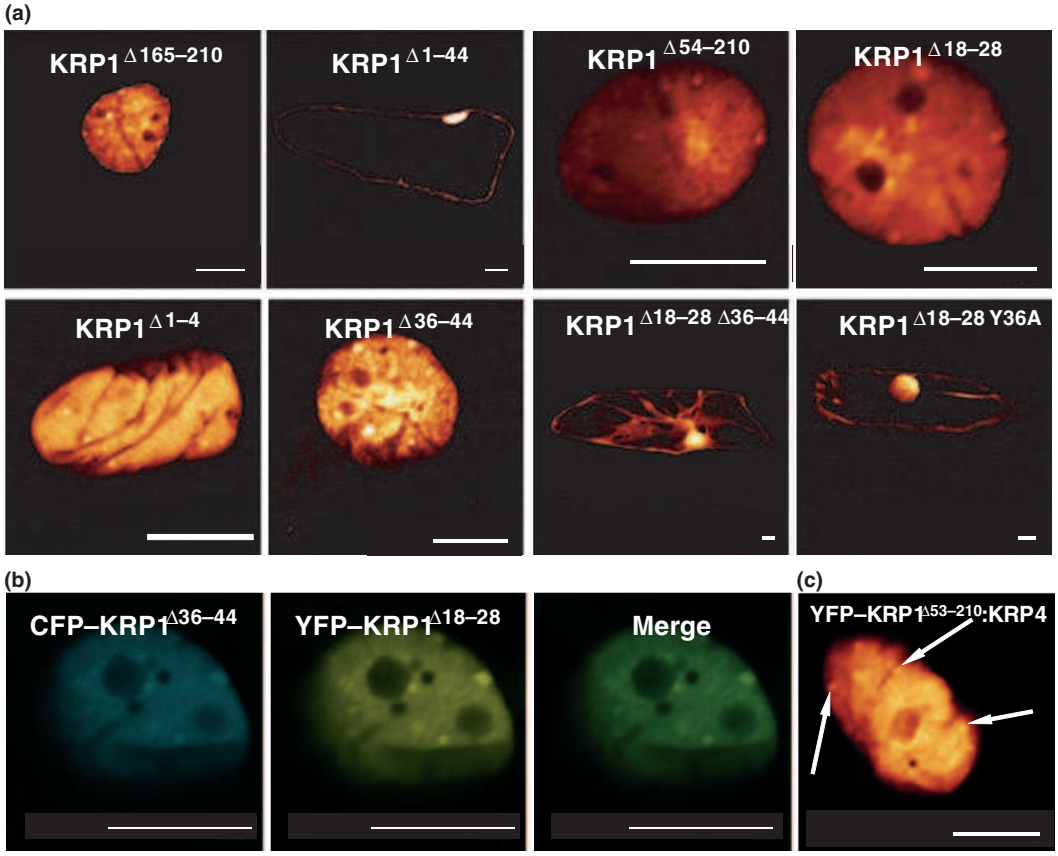

Fig. 4 Identification of domains and sequences affecting SlKRP1 subnuclear targeting. Onion epidermal cells were transformed with fluorescently tagged SlKRP1 variants and analysed by confocal laser scanning microscopy. (a) Subcellular localization of yellow fluorescent protein (YFP)-tagged SlKRP1. (b) Colocalization of cyan fluorescent protein (CFP)-tagged SlKRP1$^{\Delta 36-44}$ and YFP-tagged SlKRP1$^{\Delta 18-28}$. (c) YFP-KRP1$^{\Delta 53-210}$:KRP4 chimeric protein comprising the *N*-terminal part of SlKRP1 (KRP1$^{\Delta 54-210}$) followed by full-length SlKRP4. Arrows point to subnuclear punctuations. Bar, 20 μm.

the other using CFP-KRP1$^{\Delta 36–44}$ and YFP-KRP1$^{\Delta 18–28}$ fusions respectively. Both variants colocalized perfectly (Fig. 4b). We thus conclude that motifs 5 and 3 are together involved in the nuclear localization of SlKRP1 according to the same punctuate distribution within the nucleus.

As SlKRP1 and SlKRP4 display different subnuclear localization patterns, we fused the *N*-terminal part of SlKRP1 to the full-length sequence of SlKRP4 (YFP-KRP1$^{\Delta 53–210}$:KRP4). This chimeric protein displayed a punctuate pattern of localization identical to that of native SlKRP1 (Figs 4c, S3), and thus differed from the uniform nuclear distribution of native SlKRP4 (Fig. 2a). Hence it demonstrated that not only the *N*-terminal part of SlKRP1 is necessary and sufficient to drive its nuclear localization, but also that it is associated with the punctuate distribution of the protein within the nucleus.

SlKRP1 contributes in housing SlCDKA1 and SlCYCD3;1 in the nucleus

Previously, we showed that SlCDKA;1 and SlCYCD3;1 interact with SlKRP1 and SlKRP2 (Bisbis *et al.*, 2006). To investigate whether SlKRP3 and SlKRP4 share the same protein partnership, targeted yeast two-hybrid experiments were performed using the different cell cycle proteins that have been reported so far in tomato (Joubès *et al.*, 1999; Joubès *et al.*, 2000b, 2001). We showed that SlKRP3 and SlKRP4 interact specifically with SlCDKA;1 and SlCYCD3;1, alongside SlKRP1 and SlKRP2 (Table 1).

Table 1 Analysis of putative interactions between tomato kip-related proteins (KRPs) and candidate cell cycle proteins as determined by yeast two-hybrid assays

	None	KRP1	KRP2	KRP3	KRP4	RAS
None	–	–	–	–	–	–
CDKA1	–	++	+	+	+	–
CDKB1	–	–	–	–	–	–
CDKB2	–	–	–	–	–	–
CDKC	–	–	–	–	–	–
CycA1;1	–	–	–	–	–	–
CycA2;1	–	–	–	–	–	–
CycA3;1	–	–	–	–	–	–
CycB1;1	–	–	–	–	–	–
CycB1;1	–	–	–	–	–	–
CycD3;1	–	+++	+++	+	++	–
CSN5A	–	+	+	+	+	–
RAF	–	–	–	–	–	+++

Yeasts were cotransformed with the combination of bait and prey vectors as indicated. Transformants were then cultured on SD-LTH for 36 h at 30°C. –, No specific growth; +, weak growth (in the presence of 20 mM of 3-AT (3-amino 1,2,4 triazol)); ++, moderate growth (in the presence of 40 mM of 3-AT); +++, strong growth (in the presence of 80 mM of 3-AT). RAS and RAF proteins were used as a positive control of interaction.

However, differences in yeast growth as an indicator of the interaction strength were observed among the yeast transformants. Yeasts cotransformed with constructs harbouring SlKRP1 and SlCDKA;1 were able to grow on 40 mM of 3-AT, while growth of yeasts cotransformed with SlKRP2 and SlCDKA1, SlKRP3 and SlCDKA1 or SlKRP4 and SlCDKA1 could only be visualized on plates supplemented with 20 mM of 3-AT. Except for SlKRP3, growth was induced when all KRPs were coexpressed with SlCYCD3;1, despite the presence of high concentrations of 3-AT (40 mM). Yeasts cotransformed with SlKRP3 and CYCD3;1 could only grow under a 20 mM 3-AT pressure. We then used BiFC assays as an *in vivo* technique to confirm these results. Positive signals of interaction between YFP^N-SlKRP1 and SlCDKA;1-YFP^C and between YFP^N-SlKRP1 and SlCYCD3;1-YFP^C were found within the nucleus (Fig. 5a). Interestingly, SlCDKA;1 and SlCYCD3;1 were also found mainly in the nucleus when co-expressed, as to reconstitute a CDKA/CYCD3;1 complex (Fig. 5a), while on their own they both localized in the nucleus and the cytoplasm (Figs 5b, S3).

In *Arabidopsis*, it was reported that ICK1/KRP1 drives AtCDKA1 into the nucleus (Zhou *et al.*, 2006). In coexpression experiments using SlKRP1 fused to YFP (YFP-KRP1) and SlCDKA;1 fused to CFP (CFP-CDKA;1) or SlCYCD3;1 fused to CFP (CFP-CYCD3;1), we showed that the signals associated to SlCDKA;1 and SlCYCD3;1 were clearly much more abundant within the nucleus than within the cytoplasm (Fig. 5c) compared with their cellular distribution when expressed alone (Fig. 5b). To confirm these results we used the SlKRP1$^{\Delta 54–210}$ variant deleted for the *C*-terminal domain necessary for the interaction with CDK–CYC complexes as a negative control for coexpression experiments (Fig. S4). This allowed us to demonstrate that the interaction of SlKRP1 with either SlCDKA;1 or SlCYCD3;1 does contribute to concentrating both SlCDKA;1 and SlCYCD3;1 inside the nucleus, as the CFP-tagged CycD3;1 or CDKA1 retained their original localization (both in nucleus and cytoplasm), while YFP-KRP1$^{\Delta 54–210}$ showed the expected exclusive nuclear localization.

A new domain of interaction between CDKA;1 and CYCD3;1 is functional for their translocation into the nucleus

Yeast two-hybrid assays were performed taking advantage of the deletion series of SlKRP1 variants generated (Fig. 3) to unravel putative functional domains necessary for the interaction of SlKRP1 with different candidate proteins. As expected, the *C*-terminal part of SlKRP1 (KRP1$^{\Delta 1–145}$) is necessary for the interaction with both SlCDKA;1 and SlCYCD3;1 (Table 2) because the evolutionary conserved motif 1 at the *C*-terminus of KRPs is involved in the binding to CDK/CYC complexes in plants (Wang *et al.*, 1998).

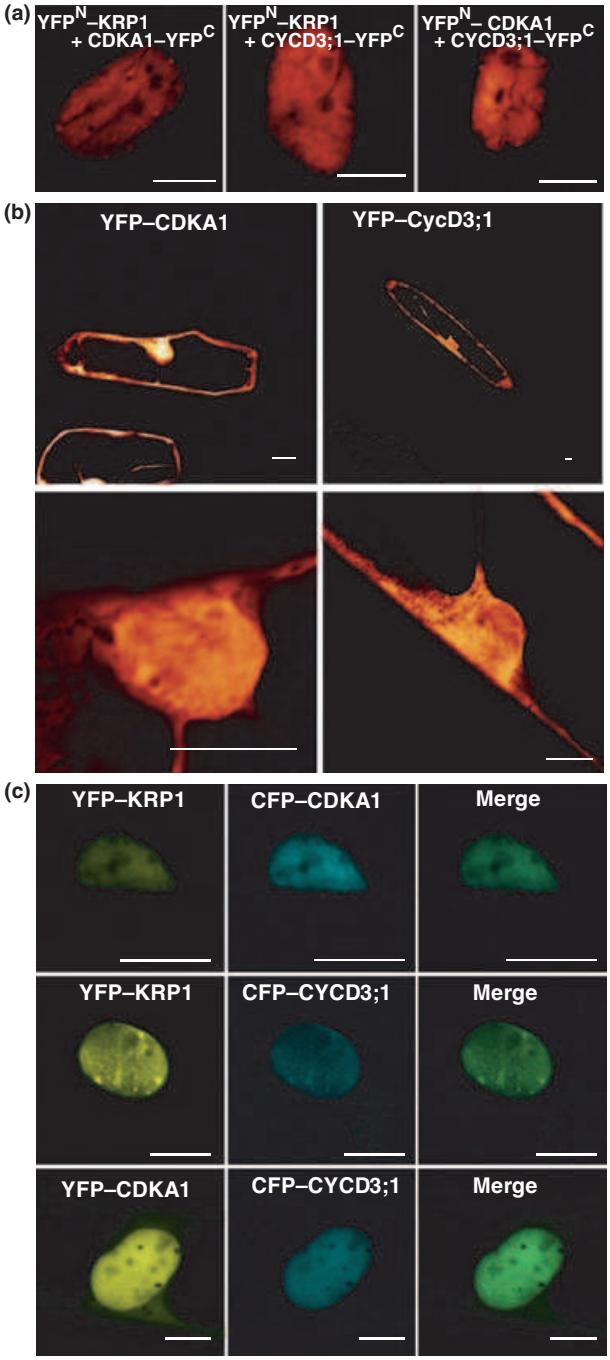

Fig. 5 *In cellulo* interaction between SlKRP1 and SlCDKA;1 or SlCycD3;1. (a) Bimolecular fluorescent complementation (BiFC) analyses in onion epidermal cells of the SlKRP1-SlCDKA;1 (YFP^N-KRP1 + CDKA1-YFP^C), SlKRP1-SlCycD3;1 (YFP^N-KRP1 + CYCD3;1-YFP^C) and SlCDKA1-SlCycD3;1 (YFP^N-CDKA1 + CYCD3;1-YFP^C) interactions. (b) Localization of yellow fluorescent protein (YFP)-tagged SlCDKA1 and SlCycD3;1. Enlarged views (× 6.0) of the nucleus regions are provided below to show the localization of both proteins in the nucleus and cytoplasm. (c) Colocalization experiments of YFP-KRP1 with CFP-CDKA;1 or CFP-CycD3;1. The colocalization of YFP-CDKA;1 with CFP-CycD3;1 was shown as a positive control. Bar, 20 μm.

We determined that SlKRP1 possesses a second site of interaction with SlCYCD3;1 because the variant $KRP1^{\Delta 165–210}$ (lacking the *C*-terminal CDK/CYC binding motifs 1 and 2) still interacted with SlCYCD3;1 (Table 2). Even if this interaction seemed weaker (yeast growth was impaired over 20 mM of 3-AT selection pressure), it was still significant and the interaction was indeed confirmed using BiFC (Fig. 6a). This interaction domain is probably localized in the central part of the SlKRP1 sequence, between residues 45 and 164, because the interaction between SlCYCD3;1 and $KRP1^{\Delta 1–44\ \Delta 165–210}$ was still positive (Table 2) while the $KRP1^{\Delta 54–210}$ variant (harbouring only the *N*-terminal end) could not interact with SlCYCD3;1 according to the yeast two-hybrid assay (Table 2) or BiFC despite repeated experiments (data not shown).

Although the interaction between SlCDKA;1 and $SlKRP1^{\Delta 165–210}$ was not observed in yeast two-hybrid assays (Table 2), the truncated $SlKRP1^{\Delta 165–210}$ variant (YFP^N-$SlKRP1^{\Delta 165–210}$) lacking the classical CDK–CYC interaction motif was still able to interact with both SlCDKA;1-YFP^C and SlCYCD3;1-YFP^C according to the reconstituted YFP signal observed in BiFC experiments (Fig. 6a). When compared with the full-length SlKRP1 (Fig. 5c), $SlKRP1^{\Delta 165–210}$ could also contribute to the concentration of both SlCDKA;1 and SlCYCD3;1 inside the nucleus, as demonstrated in coexpression assays (Fig. 6b). Together, these data suggest that a new motif present in the central part of the SlKRP1 sequence is involved in the binding to SlCYCD3;1 which appears sufficient to allow the reconstitution of a CDKA/CYCD3;1 complex to be imported into the nucleus.

Motif 2 in SlKRP1 is involved in the interaction with SlCSN5A

Le Foll *et al.* (2008) revealed that the COP9 signalosome subunit CSN5A interacts with either the full-length sequence of the tobacco KRP NtKIS1a or its spliced variant NtKIS1b (lacking motif 1). We confirmed that the tomato SlCSN5A protein interacts with all tomato KRPs using yeast two-hybrid assays (Table 1). Using BiFC, the relevance of this interaction was demonstrated in tomato leaf protoplast or onion epidermal cells (at least for SlKRP1 and SlCSN5A) (Figs 7a, S3). When compared with the uniform distribution of YFP-CSN5A in nucleus and cytoplasm (Fig. 7b), the interaction between SlKRP1 and SlCSN5A was exclusively localized within the nucleus (Fig. 7a, left panel). SlCSN5A could also interact with the truncated form of SlKRP1, $KRP1^{\Delta 1–145}$, only harbouring the *C*-terminal motifs 1 and 2 (Table 2), according to a uniform cellular distribution (Fig. 7a, right panel), thus confirming the role of motifs 3 and 5 in nuclear localization. Similar results were obtained in coexpression experiments

Table 2 Functional analysis of structural domains in SlKRP1 putatively involved in the interactions with candidate proteins as determined by yeast two-hybrid assays

	None	KRP1 Δ1–44	KRP1 Δ165–210	KRP1 Δ54–210	KRP1 Δ1–145	KRP1 Δ1–44 Δ165–210	KRP1 Δ188–210	KRP1 Δ169–174	Control
None	–	–	–	–	–	–	–	–	–
CDKA1	–	++	–	–	++	–	–	–	–
CycD3;1	–	+++	+	–	+++	+	+	+	–
CSN5A	–	+	–	–	+	–	+	–	–
Control	–	–	–	–	–	–	–	–	+++

Yeasts were cotransformed with the combination of bait and prey vectors as indicated. Transformants were then cultured on SD-LTH for 36 h at 30°C. –, No specific growth; +, weak growth (in the presence of 20 mM of 3-AT (3-amino 1,2,4 triazol)); ++, moderate growth (in the presence of 40 mM of 3-AT); +++, strong growth (in the presence of 80 mM of 3-AT).

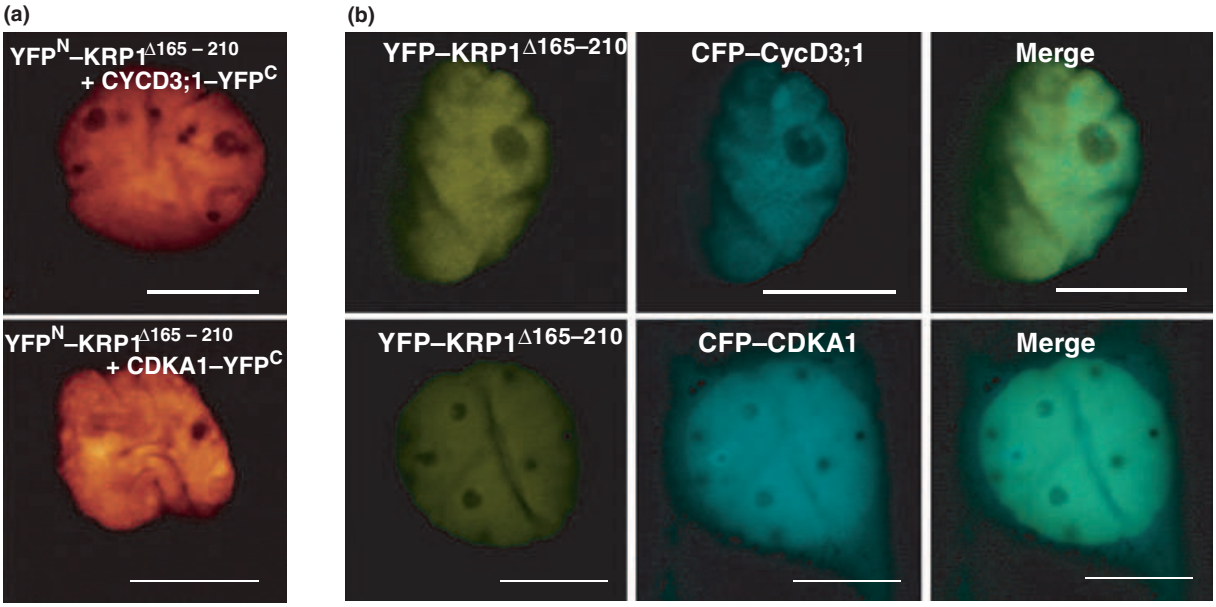

Fig. 6 Functional identification of a new motif of interaction between SlKRP1 and SlCDKA;1 and SlCycD3;1. (a) Bimolecular fluorescent complementation (BiFC) analyses in onion epidermal cells of the KRP1$^{\Delta165–210}$-SlCycD3;1 and KRP1$^{\Delta165–210}$-SlCDKA;1 interactions. (b) Colocalization experiments of YFP-KRP1$^{\Delta165–210}$ with CFP-CDKA;1 or CFP-CycD3;1. Bar, 20 μm.

using YFP-SlKRP1 and CFP-SlCSN5A or YFP-KRP1$^{\Delta1–145}$ and CFP-CSN5A (Fig. 7c), showing the exclusive nuclear or uniform cellular localization, respectively.

In addition, SlCSN5A could also interact with the truncated variant of SlKRP1, KRP1$^{\Delta188–210}$ lacking the last 22 residues encompassing motif 1 (Table 2). Conversely, the KRP1$^{\Delta165–210}$ variant lacking motifs 1 and 2 could no longer interact with SlCSN5A (Table 2). As KRP1$^{\Delta1–145}$ and KRP1$^{\Delta188–210}$ only share the presence of motif 2, we suspected the interaction of SlCSN5A with SlKRP1 occurred via motif 2. To confirm this hypothesis, the interaction was tested between SlCSN5A and the KRP1$^{\Delta169–174}$ variant only lacking the seven amino acids constituting motif 2. As a result, the interaction ceased (Table 2) and despite many different repeated experiments we could never demonstrate this interaction using BiFC.

Discussion

The phylogenic separation of ICK/KRPs in two subgroups correlates with sub-nuclear behaviour

The ICK/KRP primary sequences identified so far share very little similarities (De Clercq & Inze, 2006). As a common feature, they all display a highly conserved *C*-terminal functional domain similar to the *N*-terminal domain present in mammalian CIP/KIP CDK inhibitors that is required for the interaction with components of CDK/CYC complexes (Wang *et al.*, 1998; Zhou *et al.*, 2003b, 2006). A careful analysis of ICK/KRP sequence alignments has allowed the identification of other conserved domains that are restricted to short tracks of amino acid residues (De Veylder *et al.*, 2001; Wang *et al.*, 2007) for which very little

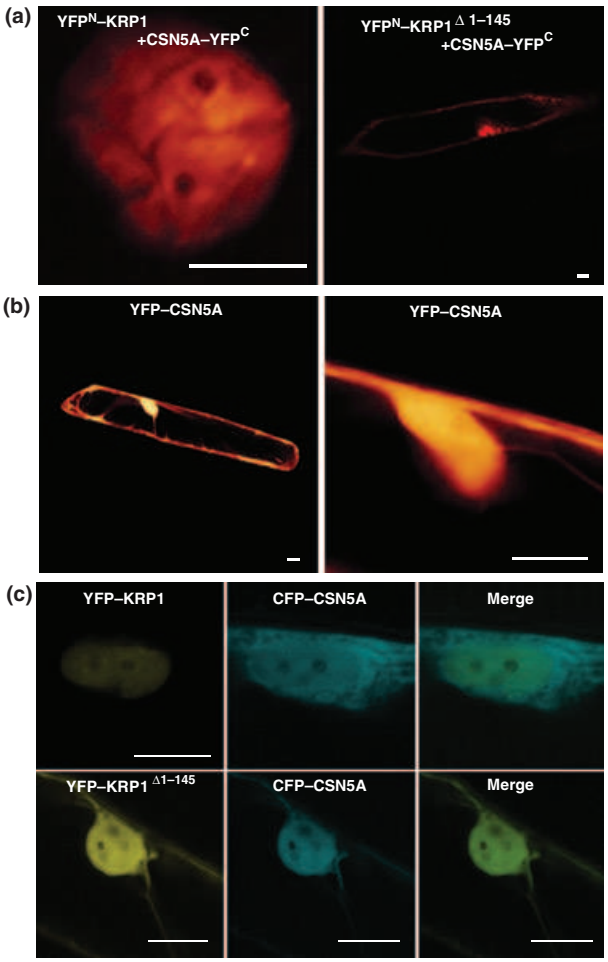

Fig. 7 *In cellulo* interaction between SlKRP1 and SlCSN5A. (a) Bimolecular fluorescent complementation (BiFC) analyses in onion epidermal cells of the SlKRP1-SlCSN5A (YFP^N-KRP1 + CSN5A-YFP^C) and SlKRP1$^{\Delta 1-145}$-SlCSN5A (YFP^N-KRP1$^{\Delta 1-145}$ + CSN5A-YFP^C) interactions. (b) Subcellular localization of yellow fluorescent protein (YFP)-tagged SlCSN5A. An enlarged view (×6.0) of the nucleus region is provided on the right side to show the localization of CSN5A in the nucleus and cytoplasm. (c) Colocalization experiments of YFP-KRP1 with CFP-CSN5A or KRP1$^{\Delta 1-145}$ with SlCSN5A. Bar, 20 μm.

functional information is currently available (Zhou *et al.*, 2006; Bird *et al.*, 2007).

No clear phylogenetic relationships have emerged from previous analyses of ICK/KRP sequences (Barroco *et al.*, 2006; Pettko-Szandtner *et al.*, 2006), most probably owing to their wide sequence variability. We provide in Fig. 1(a) new phylogenetic tree showing a clear partitioning of ICK/KRPs into two subgroups: subgroup 1 includes ICK/KRPs with more than the two *C*-terminal conserved motifs 1 and 2, and subgroup 2 gathers those displaying only motifs 1 and 2. Interestingly this partitioning correlates with the subnuclear behaviour of ICK/KRPs. Clearly, all ICK/KRPs are nuclear localized, but their distribution can be either uniform or accords with a punctuate pattern as observed in Arabidopsis (Bird *et al.*, 2007) and for SlKRP4 and SlKRP1, respectively (Fig. 3). The ICK/KRPs uniformly localized in nucleoplasm all belong to subgroup 2 (lacking motifs 3 to 6), and punctuate localized ICK/KRPs are all found within subgroup 1 (Fig. 1). According to Zhou *et al.* (2006), the motif responsible for the punctuate localization of ICK/KRPs lies within the *N*-terminal part of the protein and could be motif 3. However, when motif 3 is deleted in ICK6/KRP3, the punctuate localization still occurs, which implies the involvement of other motifs (Bird *et al.*, 2007). We found an apparent redundancy of function between motifs 3 and 5, which could putatively explain why ICK6/KRP3 lacking motif 3 is still localized in the nucleus according to a punctuate distribution. These results suggest the occurrence of an ancient separation between the two main subgroups during evolution, and argue for two separate functional roles for ICK/KRPs. The meaning of this punctuate localization for ICK/KRPs belonging to subgroup 1in relation to their precise function or mode of action in plants remains to be fully understood.

Some of the conserved motifs found in ICK/KRPs from subgroup 1 are probably part of the same functional domains. This hypothesis is supported by the observation of relative constant distances between motifs: motif 2 is always close to motif 1; motifs 3, 5 and 6 are all localized in the *N*-terminal part of the protein (Fig. S1). In addition, there is no constant distance between motif 4 and the other groups of motifs, suggesting that motifs 1 and 2, motif 4, and motifs 6, 5 and 3 may correspond to three different functional domains. Interestingly, some ICK/KRPs of subgroup 1 only share some of the conserved motifs like ICK1/KRP1 harbouring motif 3 but not motif 5 which suggests a partial functional redundancy of conserved domains among members of subgroup 1.

SlKRP1 interaction with CDKA;1 and CYCD3;1

Using yeast two-hybrid experiments and a BiFC approach, we showed the direct interaction of SlKRP1 with both SlCDKA;1 and SlCYCD3;1 (Fig. 5a). These data confirm what is observed in Arabidopsis (Wang *et al.*, 1998; Jakoby *et al.*, 2006; Zhou *et al.*, 2006). The interactions between ICK/KRP and D-type cyclins were also observed in two-hybrid targeted screens (Wang *et al.*, 1998; Jakoby *et al.*, 2006). Furthermore the *in planta* interaction was indirectly demonstrated by the simultaneous overexpression of AtCycD3;1 and NiKIS1a from tobacco, as a wild-type leaf phenotype was restored in the double overexpressing plants (Jasinski *et al.*, 2002b; Schnittger *et al.*, 2003; Zhou *et al.*, 2003a). In addition, SlKRP1 is able to import SlCDKA;1 into the nucleus (Fig. 5c), in full agreement with previous data obtained for ICK1/KRP1 and CDKA from Arabidopsis (Jakoby *et al.*, 2006; Zhou *et al.*, 2006).

However, we report here for the first time that SlKRP1 also helps in reallocating SlCYCD3;1 into the nucleus (Fig. 5c). The functional meaning of such an interaction is not fully understood, although Jasinski *et al.* (2002b) proposed that CycD3;1 and ICK/KRP operate as mutual antagonists.

Our results showed that SlKRP1 does not exclusively need the CDK/CYC interaction domain composed of motifs 1 and 2, localized between residues 165 and 210 ($SlKRP1^{\Delta 165–210}$), to drive both SlCDKA1 and SlCYCD3;1 into the nucleus (Fig. 6a). A second motif of interaction with SlCYCD3;1, outside of the already known *C*-terminal domain of SlKRP1, seems to occur within the central part of SlKRP1 between residues 45 and 164 (referred to as $KRP1^{\Delta 1–44\ \Delta 165–210}$; Table 2). Such a motif was putatively reported to exist in ICK1/KRP1 as a truncated variant comprising the first 108 amino acids interacted with AtCYCD3;1 in a yeast two-hybrid experiment (Jakoby *et al.*, 2006). Although SlCDKA1 does not interact with $KRP1^{\Delta 165–210}$ lacking motifs 1 and 2 in yeast two-hybrid assays, the *in cellulo* interaction was demonstrated using BiFC (Fig. 6a). Interestingly, SlCDKA1 is preferentially housed in the nucleus when coexpressed with the full-length SlKRP1 or its truncated variant $KRP1^{\Delta 165–210}$. To reconcile the absence of a detectable interaction in the yeast two-hybrid assay and the positive BiFC interaction between SlCDKA1 and $KRP1^{\Delta 165–210}$, we hypothesize that the SlKRP1-dependent allocation of SlCDKA1 into the nucleus is mediated in plant cells by an intermediary such as SlCYCD3;1, which is also driven into the nucleus by $SlKRP1^{\Delta 165–210}$ (compare Fig. 5 with Fig. 6).

Data obtained in animal cells indicate that $p27^{KIP1}$ may act as a CDK/CYC complex assembly factor when expressed at low level (Labaer *et al.*, 1997; Sherr & Roberts, 1999). As most of the transgenic plants overexpressing ICK/KRPs were generated using strong promoters like the CaMV 35S promoter, the relevance of such a role in plants has not yet been addressed. Interestingly, although ICK3/KRP5 is able to bind to CDKA/CYCD complexes, it does not display any significant inhibitory activity towards its targets *in vitro* (Nakai *et al.*, 2006), and may argue for such a role as an assembly factor.

Does SlKRP1 interact with CSN5 for subsequent degradation via the SCF pathway?

The COP9 signalosome (CSN) is an evolutionarily conserved multisubunit protease with a central role in the ubiquitin–proteasome pathway, as it regulates the activity of Cullin–Ring Ligase (CRL) families of ubiquitin E3 complexes (Wei *et al.*, 2008; Schweichheimer & Isono, 2010).

In animal cells, the post-translational regulation of $p27^{KIP1}$ has been extensively studied. At the G0/G1 checkpoint the CSN subunit 5 (CSN5), also called JAB1, interacts with $p27^{KIP1}$ to trigger its proteolytic degradation via the SCF pathway involving the Cullin1-containing SCF-type CRL (Tomoda *et al.*, 1999; Yang *et al.*, 2002). Here we demonstrate that SlKRP1 does interact with SlCSN5A (Fig. 7), thus confirming the observed interaction between NtKIS1a and NtCSN5 in tobacco (Le Foll *et al.*, 2008). In addition, this interaction took place through motif 2 in SlKRP1 (Table 2). As motif 2 is present in every ICK/KRP sequence analysed so far, it argues for a universal mechanism for the signalosome-mediated degradation of ICK/KRPs via the SCF pathway, which has been largely documented these last years (Kim *et al.*, 2008; Liu *et al.*, 2008; Ren *et al.*, 2008).

Motif 2 in ICK/KRPs is the only conserved motif also present in the second family of plant CDK inhibitors called the SIAMESE (SIM) proteins (Churchman *et al.*, 2006), which are able to interact with both CDKA and D-type Cyclins. Peres *et al.* (2007) showed that the rice SIM protein OsEL2 deleted for this consensus motif, loses its ability to interact with OsCYCD5;3, suggesting a putative role for this motif as a D-type cyclin-binding domain. It would be interesting to analyse whether SIM proteins are also CSN5 interactors and investigate the interplay between CYCD3 and CSN5 at the level of this particular motif.

The functional relevance of the reallocation of CDK/CYC complexes to the nucleus in the presence of ICK/KRPs could be associated to the proteolytic degradation of KRPs to take place in the nucleus. In early male germ cells from *A. thaliana*, the degradation of ICK4/AtKRP6 and ICK5/AtKRP7 coincides with the expression within the nucleus of the F-box protein AtFBL17, belonging to the SCF E3 ubiquitin ligase complex (SCF(FBL17)) (Kim *et al.*, 2008). Furthermore, AtFBL17 interacted physically with ICK4/AtKRP6 and ICK5/AtKRP7 using BiFC, and the signal of interaction was exclusively located within the nucleus.

Conclusion: towards a functional map-based model for plant ICK/KRPs

Despite the large amount of available data dealing with the biochemical activity and post-translational regulation of the animal $p27^{KIP1}$ (Vervoorts & Luscher, 2008), very little is known about the functional and structural characterization of ICK/KRP counterparts. So far only the function associated to the conserved motif 1 in ICK/KRPs can be transposed from animal studies (Wang *et al.*, 1997).

Based on the data described herein, we propose a functional map of ICK/KRPs belonging to subgroup 1 (Fig. 8), using SlKRP1 as a representative member. Motifs 3 and 5 within the *N*-terminal region allow the specific allocation within the nucleus and contribute to addressing the protein in nuclear bodies of a yet unidentified nature. A second region central to ICK/KRPs, encompassing motif 4, is still functionally uncharacterized, but is able to interact with

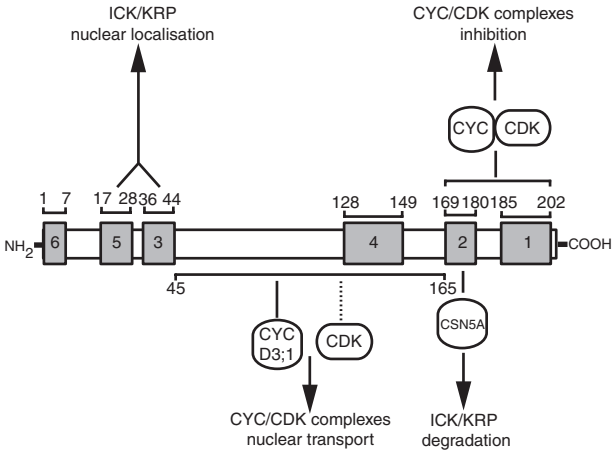

Fig. 8 Schematic representation of conserved functional domains present in SlKRP1. The different conserved domains are indicated as grey-tinted boxes. The positions of the first and last amino acid residues for each domain are indicated above delineating brackets. The interaction of cyclin D3;1 with SlKRP1 central region encompassing motif 4 (amino acids 45 to 165) was experimentally determined while the interaction with cyclin-dependent kinase (CDK) was deduced from colocalization experiments shown in Fig. 6b (indicated as a dotted line). Vertical arrows point to proposed functional roles for the different domains as deduced from the partner interaction or protein localization studies.

Cyclin D3;1 and drive it into the nucleus. Finally the *C*-terminal part of ICK/KRPs encompasses two functionally important domains: motif 1 is the binding domain to CDK/CYC complexes, and motif 2 binds to CSN5A for the putative post-translational regulation of ICK/KRPs via the 26S proteasome degradation pathway. This study offers a frame for future characterization studies of structurally and functionally important domains in plant ICK/KRPs.

Acknowledgements

This research was supported by the 6th Framework Program of the European Commission, within the European Solanaceae Integrated project, EU-SOL (grant no. FOOD–CT-2006-016214), and by funding from the Region Aquitaine; MN was supported by grant no. 24220-2006 from the Ministère de l'Enseignement Supérieur et de la Recherche (France). We express our deepest thanks to Dr Von Arnim (University of Tennessee, Knoxville, USA) and Dr Tsuyoshi Nakagawa (Shimane University, Japan) for the kind provision of vector constructs used in this study.

References

Barrôco RM, Peres A, Droual AM, De Veylder L, Nguyen Le SL, De Wolf J, Mironov V, Peerbolte R, Beemster GT, Inze D *et al.* 2006. The cyclin-dependent kinase inhibitor Orysa;KRP1 plays an important role in seed development of rice. *Plant Physiology* **142**: 1053–1064.

Bird DA, Buruiana MM, Zhou Y, Fowke LC, Wang H. 2007. Arabidopsis cyclin-dependent kinase inhibitors are nuclear-localized and show different localization patterns within the nucleoplasm. *Plant Cell Reports* **26**: 861–872.

Bisbis B, Delmas F, Joubes J, Sicard A, Hernould M, Inze D, Mouras A, Chevalier C. 2006. Cyclin-dependent kinase (CDK) inhibitors regulate the CDK–cyclin complex activities in endoreduplicating cells of developing tomato fruit. *Journal of Biological Chemistry* **281**: 7374–7383.

Churchman ML, Brown ML, Kato N, Kirik V, Hulskamp M, Inze D, De Veylder L, Walker JD, Zheng Z, Oppenheimer DG *et al.* 2006. SIAMESE, a plant-specific cell cycle regulator, controls endoreplication onset in *Arabidopsis thaliana*. *Plant Cell* **18**: 3145–3157.

De Clercq A, Inze D. 2006. Cyclin-dependent kinase inhibitors in yeast, animals, and plants: a functional comparison. *Critical Review in Biochemistry and Molecular Biology* **41**: 293–313.

De Veylder L, Beeckman T, Beemster GT, Krols L, Terras F, Landrieu I, Van Der Schueren E, Maes S, Naudts M, Inze D. 2001. Functional analysis of cyclin-dependent kinase inhibitors of Arabidopsis. *Plant Cell* **13**: 1653–1668.

Di Sansebastiano GP, Paris N, Marc-Martin S, Neuhaus JM. 1998. Specific accumulation of GFP in a non-acidic vacuolar compartment via a *C*-terminal propeptide-mediated sorting pathway. *Plant Journal* **15**: 449–457.

Genschik P, Criqui M. 2007. The UPS: an engine that drives the cell cycle. In: Inze D, ed. *Cell cycle control and plant development*. Oxford, UK: Blackwell Publishing, 87–113.

Inzé D, De Veylder L. 2006. Cell cycle regulation in plant development. *Annual Review in Genetics* **40**: 77–105.

Jakoby MJ, Weinl C, Pusch S, Kuijt SJ, Merkle T, Dissmeyer N, Schnittger A. 2006. Analysis of the subcellular localization, function, and proteolytic control of the Arabidopsis cyclin-dependent kinase inhibitor ICK1/KRP1. *Plant Physiology* **141**: 1293–1305.

Jasinski S, Perennes C, Bergounioux C, Glab N. 2002a. Comparative molecular and functional analyses of the tobacco cyclin-dependent kinase inhibitor NtKIS1a and its spliced variant NtKIS1b. *Plant Physiology* **130**: 1871–1882.

Jasinski S, Riou-Khamlichi C, Roche O, Perennes C, Bergounioux C, Glab N. 2002b. The CDK inhibitor NtKIS1a is involved in plant development, endoreduplication and restores normal development of cyclin D3; 1-overexpressing plants. *Journal of Cell Science* **115**: 973–982.

Joubès J, Chevalier C, Dudits D, Heberle-Bors E, Inzé D, Umeda M, Renaudin JP. 2000a. Cyclin-dependent kinases related protein kinases in plants. *Plant Molecular Biology* **43**: 607–621.

Joubès J, Lemaire-Chamley M, Delmas F, Walter J, Hernould M, Mouras A, Raymond P, Chevalier C. 2001. A new C-type cyclin-dependent kinase from tomato expressed in dividing tissues does not interact with mitotic and G1 cyclins. *Plant Physiology* **126**: 1403–1415.

Joubès J, Phan TH, Just D, Rothan C, Bergounioux C, Raymond P, Chevalier C. 1999. Molecular and biochemical characterization of the involvement of cyclin-dependent kinase A during the early development of tomato fruit. *Plant Physiology* **121**: 857–869.

Joubès J, Walsh D, Raymond P, Chevalier C. 2000b. Molecular characterization of the expression of distinct classes of cyclins during the early development of tomato fruit. *Planta* **211**: 430–439.

Kim HJ, Oh SA, Brownfield L, Hong SH, Ryu H, Hwang I, Twell D, Nam HG. 2008. Control of plant germline proliferation by SCF(FBL17) degradation of cell cycle inhibitors. *Nature* **455**: 1134–1137.

Kumar S, Tamura K, Nei M. 2004. MEGA3: integrated software for molecular evolutionary genetics analysis and sequence alignment. *Briefings in Bioinformatics* **5**: 150–163.

Labaer J, Garrett MD, Stevenson LF, Slingerland JM, Sandhu C, Chou HS, Fattaey A, Harlow E. 1997. New functional activities for the p21 family of CDK inhibitors. *Genes & Development* **11**: 847–862.

Le Foll M, Blanchet S, Millan L, Mathieu C, Bergounioux C, Glab N. 2008. The plant CDK inhibitor NtKIS1a interferes with

dedifferentiation, is specifically down regulated during development and interacts with a JAB1 homolog. *Plant Science* **175**: 513–523.

Liu J, Zhang Y, Qin G, Tsuge T, Sakaguchi N, Luo G, Sun K, Shi D, Aki S, Zheng N *et al.* 2008. Targeted degradation of the cyclin-dependent kinase inhibitor ICK4/KRP6 by RING-type E3 ligases is essential for mitotic cell cycle progression during Arabidopsis gametogenesis. *Plant Cell* **20**: 1538–1554.

Menges M, de Jager SM, Gruissem W, Murray JA. 2005. Global analysis of the core cell cycle regulators of Arabidopsis identifies novel genes, reveals multiple and highly specific profiles of expression and provides a coherent model for plant cell cycle control. *Plant Journal* **41**: 546–566.

Mironov V, De Veylder L, Van Montagu M, Inzé D. 1999. Cyclin-dependent kinases and cell division in plants – the nexus. *Plant Cell* **11**: 509–522.

Nakai T, Kato K, Shinmyo A, Sekine M. 2006. Arabidopsis KRPs have distinct inhibitory activity toward cyclin D2-associated kinases, including plant-specific B-type cyclin-dependent kinase. *FEBS Letters* **580**: 336–340.

Peres A, Churchman ML, Hariharan S, Himanen K, Verkest A, Vandepoele K, Magyar Z, Hatzfeld Y, Van Der Schueren E, Beemster GT *et al.* 2007. Novel plant-specific cyclin-dependent kinase inhibitors induced by biotic and abiotic stresses. *Journal of Biological Chemistry* **282**: 25588–25596.

Pettko-Szandtner A, Meszaros T, Horvath GY, Bako L, Csordas-Toth E, Blastyak A, Zhiponova M, Miskolczi P, Dudits D. 2006. Activation of an alfalfa cyclin-dependent kinase inhibitor by calmodulin-like domain protein kinase. *Plant Journal* **46**: 111–123.

Ren H, Santner A, Del Pozo JC, Murray JA, Estelle M. 2008. Degradation of the cyclin-dependent kinase inhibitor KRP1 is regulated by two different ubiquitin E3 ligases. *Plant Journal* **53**: 705–716.

Rontein D, Dieuaide-Noubhani M, Dufourc EJ, Raymond P, Rolin D. 2002. The metabolic architecture of plant cells. Stability of central metabolism and flexibility of anabolic pathways during the growth cycle of tomato cells. *Journal of Biological Chemistry* **277**: 43948–43960.

Schnittger A, Weinl C, Bouyer D, Schobinger U, Hulskamp M. 2003. Misexpression of the cyclin-dependent kinase inhibitor ICK1/KRP1 in single-celled Arabidopsis trichomes reduces endoreduplication and cell size and induces cell death. *Plant Cell* **15**: 303–315.

Schweichheimer K, Isono E. 2010. The COP9 signalsome and its role in plant development. *European Journal of Cell Biology* **89**: 157–162.

Sherr CJ, Roberts JM. 1999. CDK inhibitors: positive and negative regulators of G1-phase progression. *Genes & Development* **13**: 1501–1512.

Shimotohno A, Ohno R, Bisova K, Sakaguchi N, Huang J, Koncz C, Uchimiya H, Umeda M. 2006. Diverse phosphoregulatory mechanisms controlling cyclin-dependent kinase-activating kinases in Arabidopsis. *Plant Journal* **47**: 701–710.

Tomoda K, Kubota Y, Kato J. 1999. Degradation of the cyclin-dependent-kinase inhibitor p27Kip1 is instigated by Jab1. *Nature* **398**: 160–165.

Vandepoele K, Raes J, De Veylder L, Rouzé P, Rombauts S, Inzé D. 2002. Genome-wide analysis of core cell-cycle genes in Arabidopsis. *Plant Cell* **14**: 903–916.

Verkest A, Manes CL, Vercruysse S, Maes S, Van Der Schueren E, Beeckman T, Genschik P, Kuiper M, Inze D, De Veylder L. 2005. The cyclin-dependent kinase inhibitor KRP2 controls the onset of the endoreduplication cycle during Arabidopsis leaf development through inhibition of mitotic CDKA;1 kinase complexes. *Plant Cell* **17**: 1723–1736.

Vervoorts J, Luscher B. 2008. Post-translational regulation of the tumor suppressor p27(KIP1). *Cell Molecular Life Science* **65**: 3255–3264.

Wang H, Fowke LC, Crosby WL. 1997. A plant cyclin-dependent kinase inhibitor gene. *Nature* **386**: 451–452.

Wang G, Kong H, Sun Y, Zhang X, Zhang W, Altman N, DePamphilis CW, Ma H. 2004. Genome-wide analysis of the cyclin family in Arabidopsis and comparative phylogenetic analysis of plant cyclin-like proteins. *Plant Physiology* **135**: 1084–1099.

Wang H, Qi Q, Schorr P, Cutler AJ, Crosby WL, Fowke LC. 1998. ICK1, a cyclin-dependent protein kinase inhibitor from *Arabidopsis thaliana* interacts with both Cdc2a and CycD3, and its expression is induced by abscisic acid. *Plant Journal* **15**: 501–510.

Wang H, Zhou Y, Gilmer S, Whitwill S, Fowke LC. 2000. Expression of the plant cyclin-dependent kinase inhibitor ICK1 affects cell division, plant growth and morphology. *Plant Journal* **24**: 613–623.

Wang H, Zhou Y, Torres-Acosta L, Fowke LC. 2007. CDK inhibitors. In: Inze D, ed. *Cell cycle control and plant development*. Oxford, UK: Blackwell Publishing, 62–86.

Wei N, Serino G, Deng XW. 2008. The COP9 signalosome: more than a protease. *Trends in Biochemical Sciences* **33**: 592–600.

Yang X, Menon S, Lykke-Andersen K, Tsuge T, Xiao D, Wang X, Rodriguez-Suarez RJ, Zhang H, Wei N. 2002. The COP9 signalosome inhibits p27kip1 degradation and impedes G1-S phase progression via deneddylation of SCF Cul1. *Current Biology* **12**: 667–672.

Zhou Y, Niu H, Brandizzi F, Fowke LC, Wang H. 2006. Molecular control of nuclear and subnuclear targeting of the plant CDK inhibitor ICK1 and ICK1-mediated nuclear transport of CDKA. *Plant Molecular Biology* **62**: 261–278.

Zhou Y, Wang H, Gilmer S, Whitwill S, Fowke LC. 2003a. Effects of co-expressing the plant CDK inhibitor ICK1 and D-type cyclin genes on plant growth, cell size and ploidy in *Arabidopsis thaliana*. *Planta* **216**: 604–613.

Supporting Information

Additional supporting information may be found in the online version of this article.

Fig. S1 Multiple alignment of ICK/KRP primary sequences from subgroup 1 (a) and from subgroup 2 (b).

Fig. S2 Subcellular localization experiments using homologue model systems.

Fig. S3 Subcellular localization experiments and *in cellulo* interaction using homologue model systems.

Fig. S4 Colocalization experiments of YFP-tagged SlKRP1$^{\Delta 54–210}$ with CFP-tagged CyCD3;1 (a) or with CFP-tagged CDKA1 (b).

Table S1 *ICK/KRP* gene annotation and corresponding accession numbers, used for the construction of the phylogenetic tree

Please note: Wiley-Blackwell are not responsible for the content or functionality of any supporting information supplied by the authors. Any queries (other than missing material) should be directed to the *New Phytologist* Central Office.

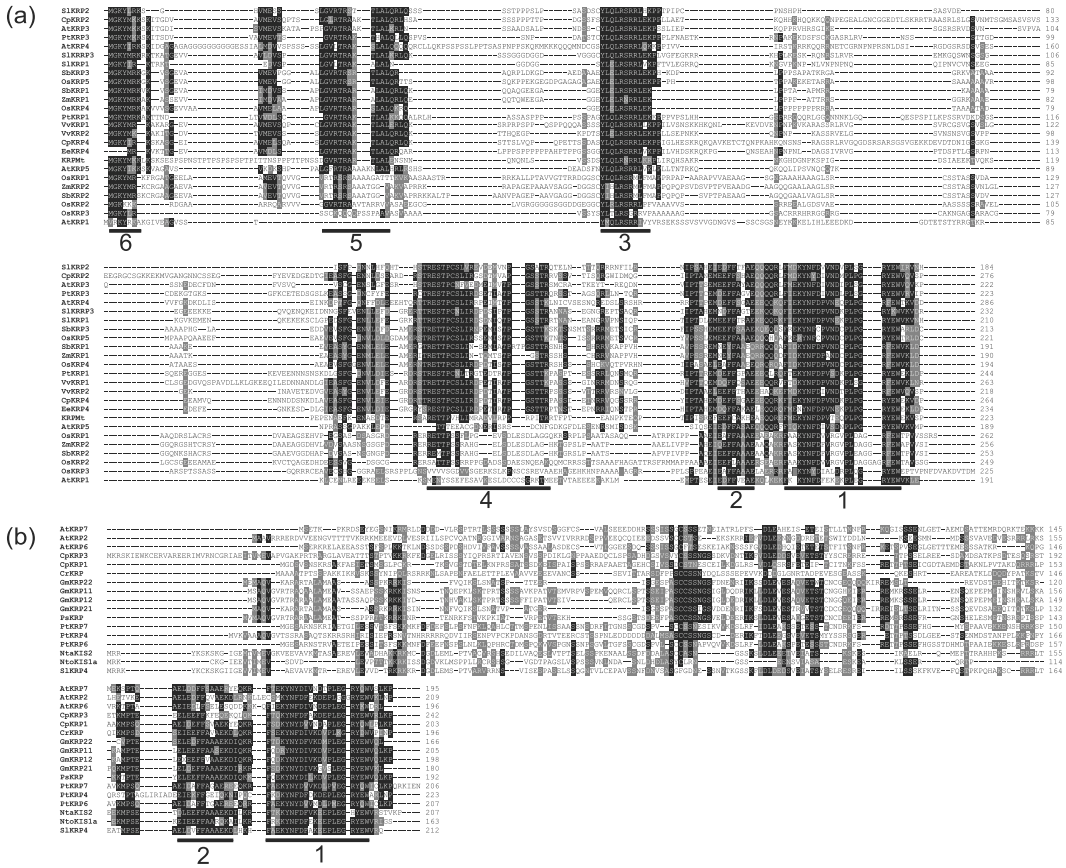

Fig. S1 Multiple alignment of ICK/KRP primary sequences from subgroup 1 (a) and from subgroup 2 (b). The regions numbered 1 to 6 denote conserved domains as referred to in the text. Accession numbers corresponding to the different *ICK/KRP* genes are given in Supporting Information Table S1. At, *Arabidopsis thaliana*; Cp, *Carica papaya*; Cr, *Chenopodium rubum*; Ee, *Euphorbia esula*; Gm, *Glycine max*; Mt, *Medicago truncatula*; Nta, *Nicotiana tabacum*; Nto, *Nicotiana tomentosiformis*; Os, *Oryza sativa*; Ps, *Pisum sativum*; Pt, *Populus trichocarpa*; Sl, *Solanum lycopersicum*; Sb, *Sorghum bicolor*; Vt, *Vitis vinifera*; Zm, *Zea mays*.Identical residues are highlighted in black, conservative amino acid substitutions are shaded in grey.

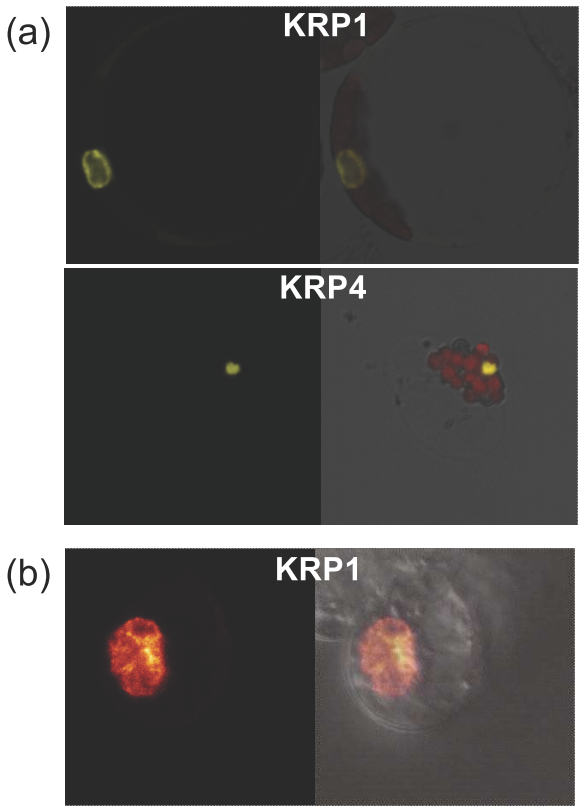

Fig. S2 Sub-cellular localization experiments using homolog model systems. (a) YFP-tagged protein transient expression in tomato leaf protoplasts after PEG transformation. (b) YFP-tagged protein transient expression in tomato SWEET100 cultured cells by biolistic transformation. The YFP signal is represented in yellow and chloroplast autofluorescence is shown in red.

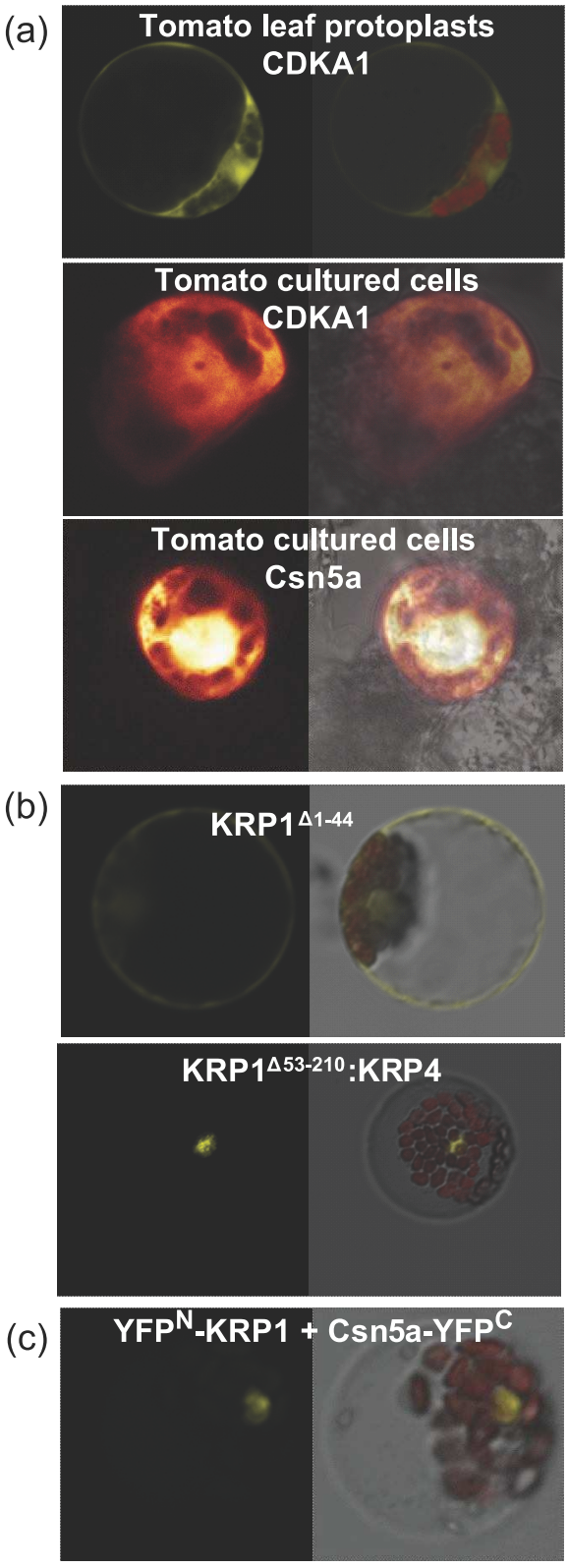

Fig. S3 Subcellular localization experiments and *In cellulo* interaction using homolog model systems. (a) of SlKRP1 and SlKRP4. (a) YFP-tagged CDKA1 and Csn5a were transiently expressed in Tomato leaf protoplast or in tomato SWEET100 cultured cells. (b) Sub-cellular localisation of YFP-KRP1$^{\Delta 1\text{-}44}$ and YFP-KRP1$^{\Delta 54\text{-}210}$:KRP4 chimeric protein comprising the N-terminal part of SlKRP1 (KRP1$^{\Delta 54\text{-}210}$) followed by full-length SlKRP4. (c) BiFC analyses in Tomato leaf protoplast of the SlKRP1- SlCSN5A interaction.

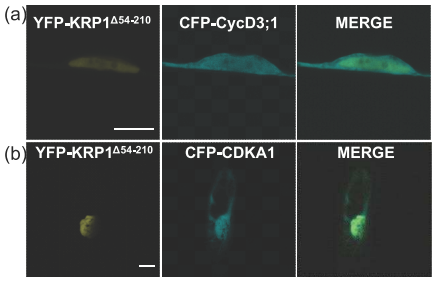

Fig. S4 Co-localization experiments of YFP-tagged SlKRP1$^{\Delta 54\text{-}210}$ with CFP-tagged CyCD3;1 (a) or with CFP-tagged CDKA1 (b). Scale bar = 20μm.

1.3 Searching for protein partners of SlKRP1

1.3.1 Global approach by two-hybrid screen

In order to specify a function for motifs 3 to 6 in SlKRP1, a two-hybrid screening approach has been performed using the truncated version SlKRP1$^{\Delta 165\text{-}210}$ as a bait against a cDNA library from young fruit at 4 days post-anthesis. Indeed, the absence of binding motifs for classical CDK/Cyc would simplify the analysis of potential interactions. However, after transformation of approximately 1 million clones, several thousands of colonies developed on a concentration of 20 mM 3-AT inhibitor. Several plasmids were sequenced to identify the incorporated cDNA, and it was found that the majority of them had been incorporated into the plasmid upside down or was composed of non-coding part of transcripts or out of reading frame. Therefore the interactions were non-specific. More problematic, the growth of yeasts was fairly uniform, preventing from selecting clones for priority consideration, and none of the transplanted yeast could grow on higher doses of the inhibitor. In this experiment, we drew the conclusion that the two-hybrid screen technique will certainly not allow in the future to detect new KRP interactors as it should only remain weak interactions, and their recognition will be swamped by false positives.

1.3.2 Targeted approach

Based on data from the literature, a candidate gene approach was undertaken to identify potential partners of tomato KRPs. The candidates dealt in this subpart have not been validated by two-hybrid. Informations from sub-cellular localization of various candidates were nevertheless obtained.

1.3.2.1 Degradation pathway candidates:

- Degradation of SlKRP1 by the proteasome

As a first approach, onion epidermis cells were bombarded with plasmids encoding SlKRP1 fused to YFP. They were then treated with 100 µM of the proteasome inhibitor MG132 for 24 hours post-bombardment. As seen in Figure 24, the addition of MG132 in the incubation medium of onion epidermis induces an increase in YFP

signal which becomes clearly visible in the cytoplasm. This result suggests that SlKRP1 is degraded by a proteasome dependent degradation pathway.

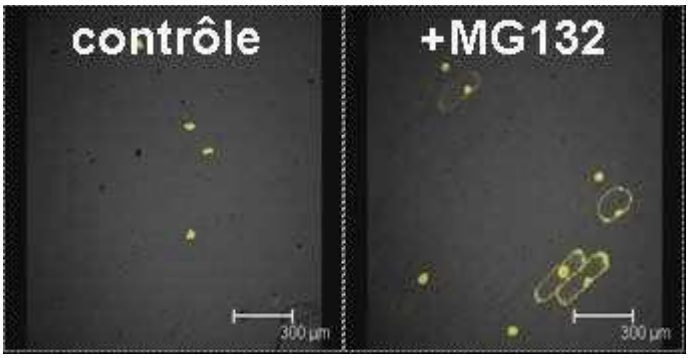

Figure 24 : Sub-cellular localization of YFP-SlKRP1 in the absence (left) or presence (right) of 100 µM MG132

- SKP2

In *Arabidopsis thaliana*, the mutation of the *SKP2b* gene increases the amount of KRP1 protein detectable in the plant (Ren *et al.*, 2008; see Introduction 3.3.3). The authors who made this discovery suggested that the F-box SKP2b protein binds AtKRP1 to the SCF complex. The SKP2b sequence found in tomato is excluded from the nucleus. Within the cytoplasm, it tends to form small aggregates (see Figure 25).

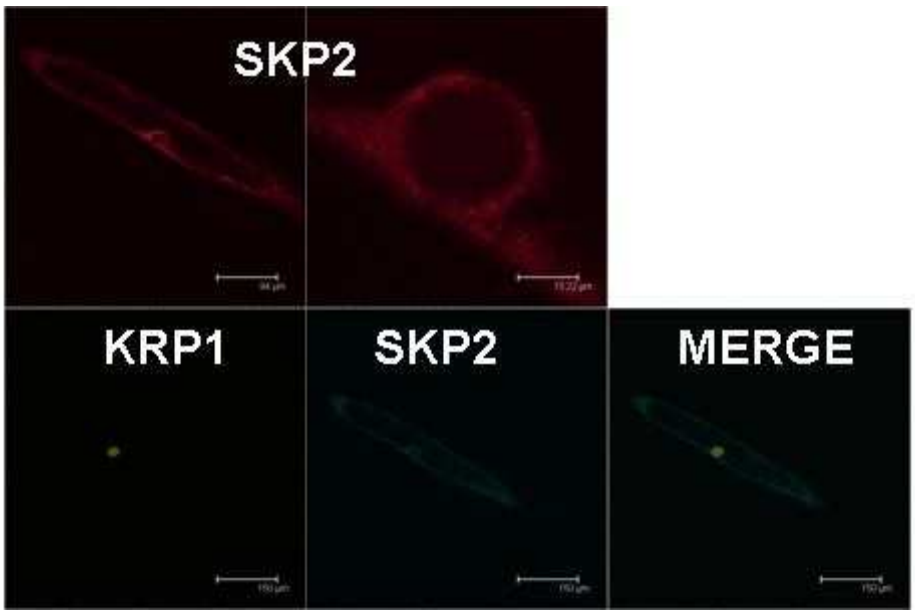

Figure 25 : Sub-cellular localization of YFP-SlSKP2 (pictures above), and co-localization SlSKP2-CFP and YFP-SlKRP1 (pictures below)

- KBR 1 and 2

A RING-type E3 ligase called KRP Binding Ring finger (KBR) has been identified by two hybrid approach using AtKRP5 as bait (Verkest, 2006). Two homologous sequences of AtKBR were found in tomato and named SlKBR1 and SlKBR2. These two proteins are localized in the nucleus in the form of hundreds of dots. Moreover KBR2 forms large aggregates in the cytoplasm (see Figure 26).

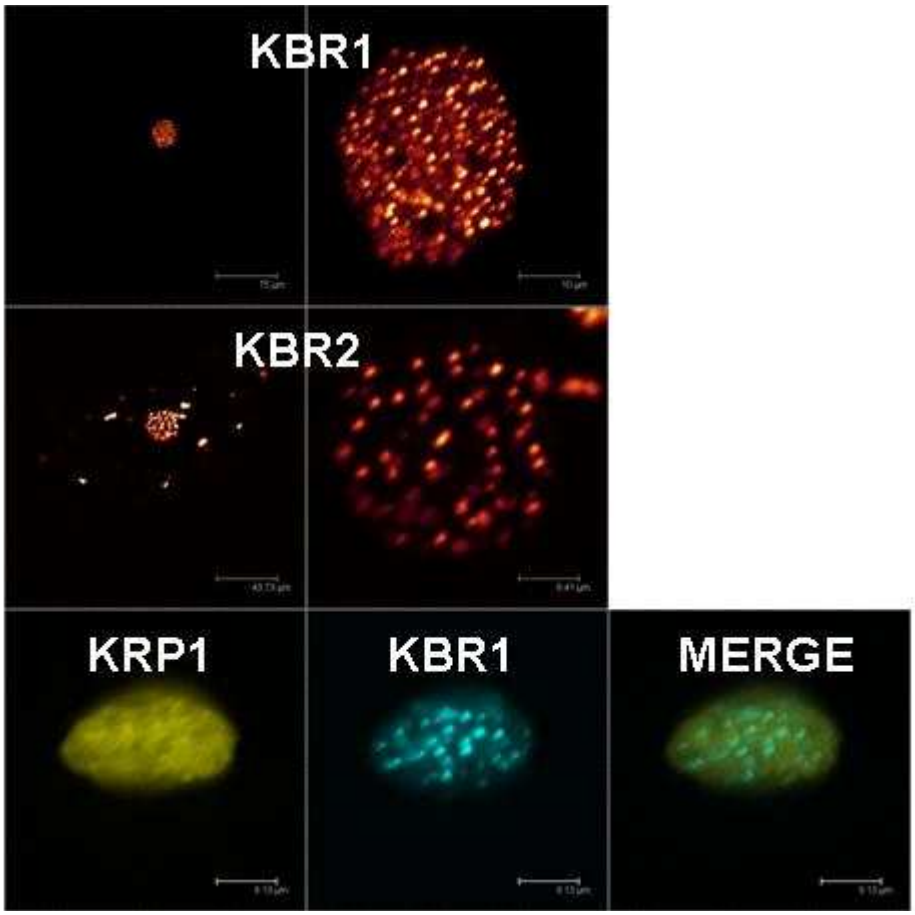

Figure 26 : Subcellular localization of YFP-SlKBR1 (upper images), YFP-SlKBR2 (central images) and co-localization YFP-SlKRP1 and CFP-SlKBR1 (pictures below)

1.3.2.2 Candidates for the S Phase

- RBR

The Retinoblastoma related protein (RBR) is responsible for the inhibition of E2F/DP complex. RBR is the target of the kinase activity of CDKA/CycD complexes, which leads to the lifting of the inhibition of E2F/DP complex (see Introduction 2.2.1). As KRP functions to prevent the CDK/Cyc kinase activity, the question was raised

whether the KRPs localize in the same areas as RBR. If SlRBR and SlKRP1 are both in the nucleus, RBR seems to be diffused while KRP1 is co-localized with DNA and form punctuations (see **Figure 27**)

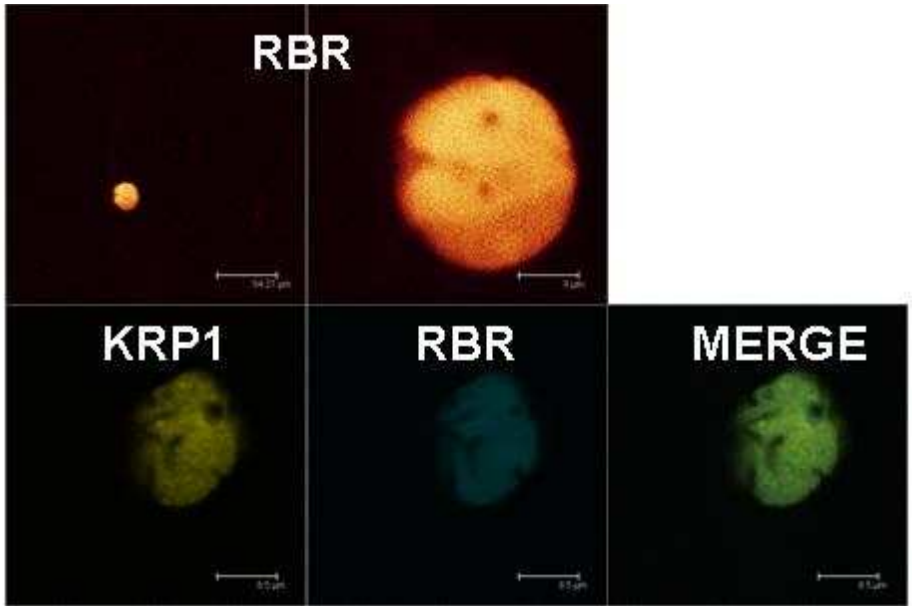

Figure 27 : Sub-cellular localization of YFP-SlRBR (pictures above), and co-localization YFP SlKRP1and CFP-SlRBR (pictures below)

- MCM7

The Mini-Chromosome Maintenance proteins form a complex involved in DNA replication. In humans, p27Kip1 binds to a subunit of the complex, MCM7. The question arose whether KRPs bind also to plant counterparts of MCM7. In the model studied, SlMCM7 is present throughout the cell, but in smaller amounts in the nucleus, whatever the position of the YFP fusion (see Figure 28).

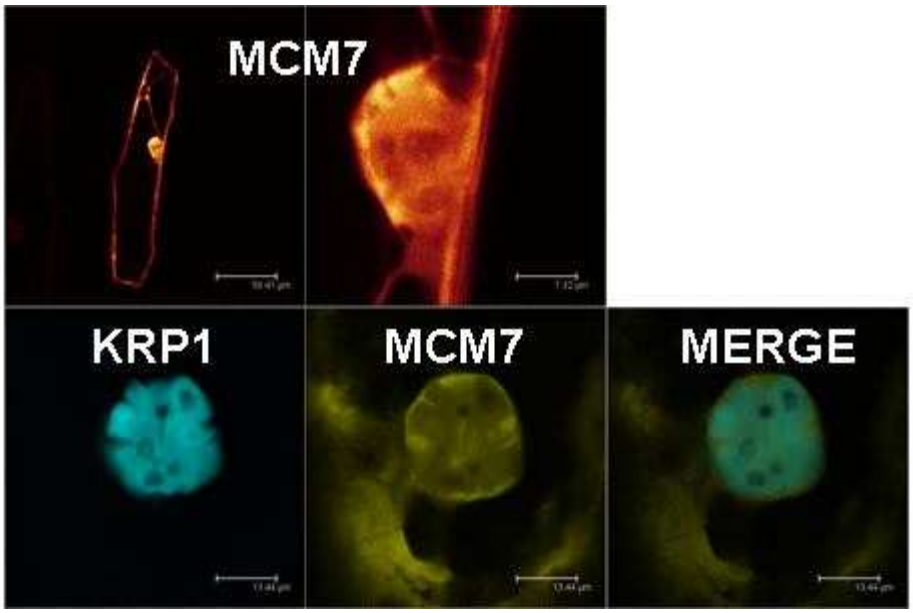

Figure 28 : Sub-cellular localization of YFP-MCM7 (upper images), and co-localization CFP-SlKRP1 and YFP-MCM7 (pictures below)

- PCNA

PCNA forms a homotrimer structure serving as docking point for the DNA replication machinery. The PCNA binding sites may be anchored by p21Cip1 but not by p27Kip1. Previous studies have shown thatPCNA does not interact with KRPs in two-hybrid (see Introduction 3.1.1). It may nevertheless be interesting to further analyze the protein, because the two hybrid method can lead to false negative results and other studies have shown that PCNA has a pattern of sub-nuclear localization similar to that observed punctuated for KRP (Leonhardt *et al.*, 2000).

When introduced into onion epidermis, YFP-PCNA is present all over within the cell. Adding a NLS to the sequence induces a PCNA fluorescence in the nucleus, but the signal remains widespread. Thus, in the model used for this study, PCNA does not form punctuation detectable in the nucleus.

1.3.2.3 Candidate from the tomato literature: CK2β

The regulatory β subunit of casein kinase 2 is the only known FW2.2 interactor, the major QTL for fruit size. The mutant phenotypes ck2β and fw2.2 are opposed, which suggests an antagonist role (Cong *et al.*, 2006). The SlKRP4 genomic sequence is located at close proximity to that of FW2.2. Moreover, the phenotypes KRP and FW2.2 are close and SlKRP4 and FW2.2 have similar temporal patterns of

expression in the fruit (Nesbitt *et al.*, 2001). Finally, in humans, p27Kip1 is regulated by casein kinase (Tapia *et al.*, 2004). The hypothesis of a regulatory pathway FW2.2/Casein kinase/KRP is open. In the onion model, CK2β is present predominantly in the cytoplasm (see Figure 29).

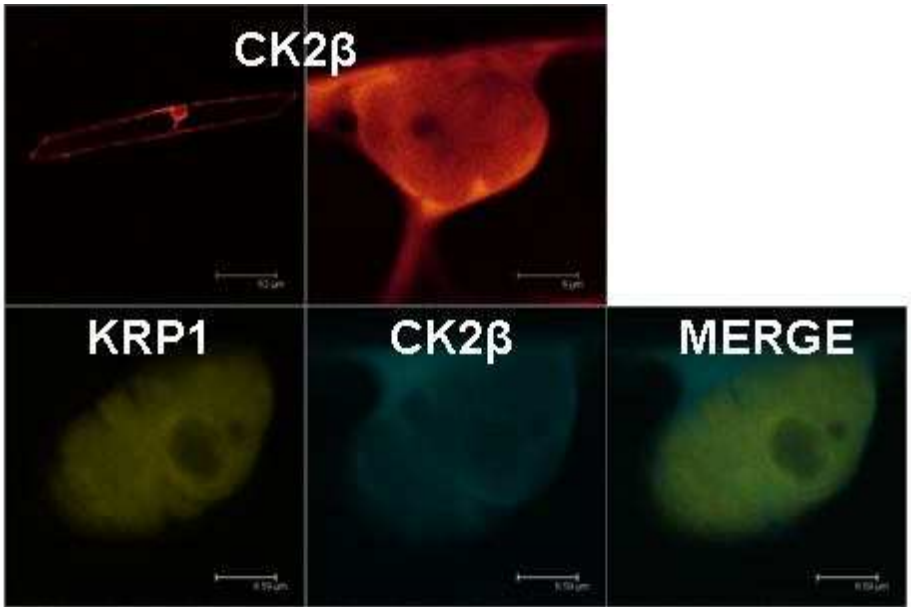

Figure 29 : Sub-cellular localization of YFP-CK2β (pictures above), and co-localization YFP-SlKRP1 and CFP-CK2β (pictures below)

1.3.2.4 Candidates for Cell cycle machinery

- CDKB1

CDKB1 interacts *in vitro* with KRPs (see Introduction 3.3.1). SlCDKB1 is detectable in both the nucleus and cytoplasm. Unlike CDKA (see 1.2), it does not vary in its location when it is colocalized with SlKRP1 (see Figure 30).

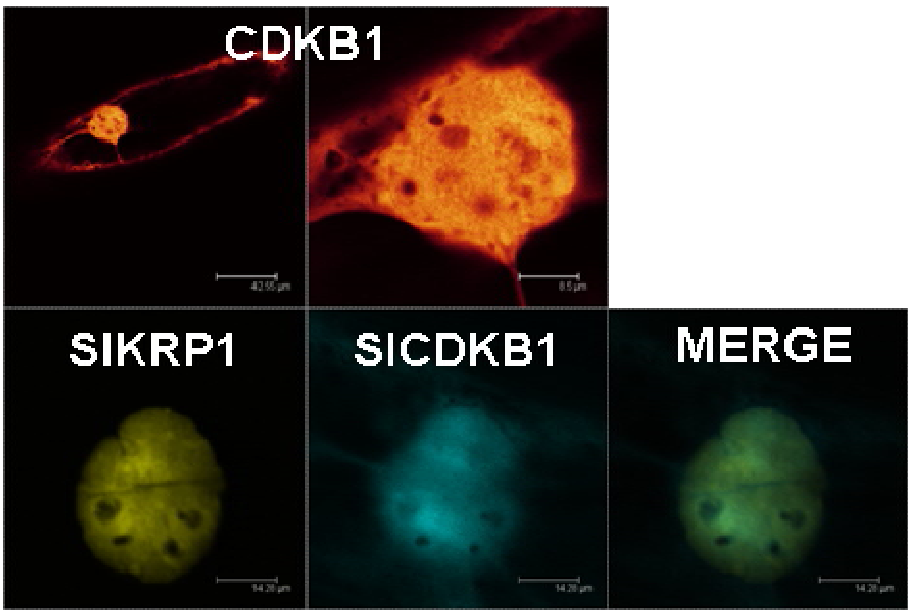

Figure 30 : Sub-cellular localization of YFP-CDKB1 (upper images), and co-localization YFP-SlKRP1 and CFP-CDKB1 (pictures below)

- CKS1

CDK complex subunit 1 (CKS1) is a CDK-associated protein that may play a role in CDK/Cyc structuration. It could interact with KRPs (Verkest, 2006). Within the model studied, SlCKS1 is present both in the cytoplasm and the nucleus, and its location does not change when it is colocalized with SlKRP1 (see Figure 31).

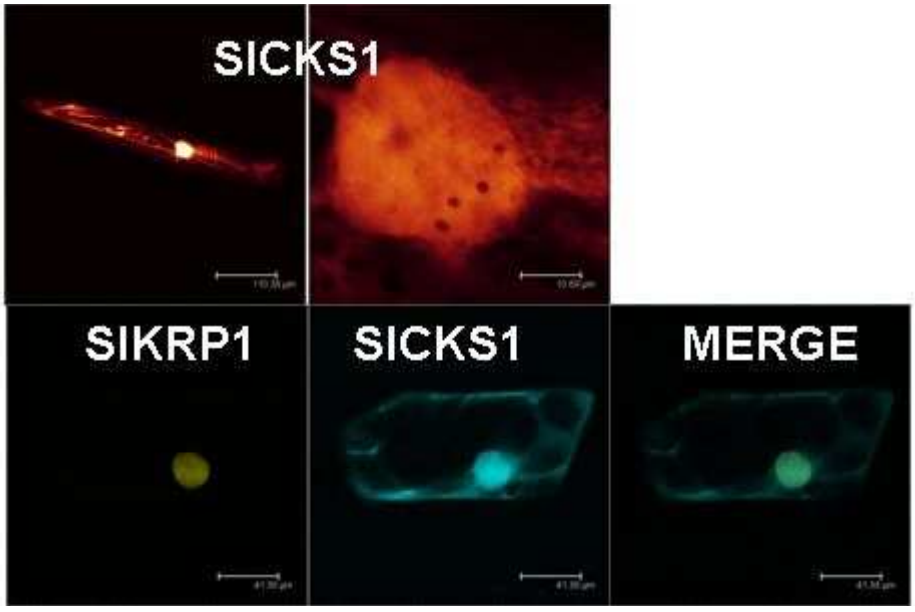

Figure 31 : Sub-cellular localization of YFP-SlCKS1 (pictures above), and co-localization YFP-SlKRP1 and CFP-SlCKS1 (pictures below)

2 Physiological role of KRPs during the phase of cell expansion of tomato fruit development

2.1 Development of an *in vivo* strategy to study tomato KRPs

At the beginning of this thesis, two tomato KRPs were already identified, namely SlKRP1 and SlKRP2. A previous work in the laboratory (Bisbis *et al.*, 2006) showed that:

- SlKRP1 has an inhibitory activity of CDKA/Cyc complexes;

- SlKRP1 and SlKRP2 have different expression patterns in tomato fruit: SlKRP1 being more highly expressed during the phase of fruit growth, and SlKRP2 being more specific to fruit ripening.

The lack of *in vivo* functional data on tomato KRPs has led to a prioritary axis to this thesis: the development and analysis of transgenic tomato lines altered in their KRP expression level.

Transgene expression by a constitutive promoter is the most frequently used method to study the *in vivo* function of a gene. However, when studying fruit development, it becomes difficult to separate the possible phenotypes associated with transgene expression in the fruit from those due to defects in development upstream in vegetative tissues and flowers. For example, the optimal fruit development requires the upstream proper pollination of the flower. Indeed, the seeds of the fruit will be responsible for the emission of different phytohormones that modulate the development of the different fruit tissues. Thus, if the transgene is expressed in the flower and disrupts the fertility of flowers, the fruit will contain fewer seeds will be less developed, or even parthenocarpic.

To study the effect of KRPs specifically in the fruit, the use of a fruit-specific promoter has been chosen. Two constructs were originally planned to allow:

- Overexpression of SlKRP1 during fruit growth, using the tomato *phosphoenolpyruvate carbolylase 2* promoter, previously studied in the laboratory

(Fernandez *et al.*, 2009). This promoter has an expression window from 6 to 25 days post-anthesis in fruit. .

- Downregulation of SlKRP2 by an antisense strategy specifically during fruit ripening, by using the E8 promoter. E8 is an ethylene response gene, which has an expression window extending from breaker stage to red ripe stage in fruit.

No phenotype could be associated with the under-expression of SlKRP2 during fruit ripening. This result seems consistent with the lack of phenotype observed in different *Arabidopsis* KRP mutants or even in double mutants, and it seems that some compensation phenomena are present due to gene redundancy within the KRP gene family. It will however be important to confirm the downregulation of SlKRP2 in these plants.

The effect of the SlKRP1overexpression during the growth phase of tomato fruit will be discussed in the next part.

2.2 **Article 2** Submitted to The Plant Journal

the plant journal

The specific overexpression of a Cyclin Dependent Kinase Inhibitor in tomato fruit mesocarp cells uncouples endoreduplication and cell growth

Journal:	*The Plant Journal*
Manuscript ID:	Draft
Manuscript Type:	Full Paper
Date Submitted by the Author:	n/a
Complete List of Authors:	Nafati, Mehdi; Institut National de la Recherche Agronomique, Fruit Biology Cheniclet, Catherine; Institut National de la Recherche Agronomique, Fruit Biology Hernould, Michel; Institut National de la Recherche Agronomique, Fruit Biology Do, Phuc Ti; Max Planck Institut, Molekulare Pflanzenphysiologie Fernie, Alisdair; Max Planck Institut, Molekulare Pflanzenphysiologie Chevalier, Christian; Institut National de la Recherche Agronomique, Fruit Biology Gévaudant, Frédéric; Institut National de la Recherche Agronomique, Fruit Biology
Key Words:	Cell cycle, Cyclin-Dependent Kinase (CDK), Cyclin-Dependent Kinase Inhibitor (CKI), Endoreduplication, Fruit growth, Kip-related protein (KRP), Tomato (Solanum lycopersicum)

The specific overexpression of a Cyclin Dependent Kinase Inhibitor in tomato fruit mesocarp cells uncouples endoreduplication and cell growth

Mehdi Nafati[1,2], Catherine Cheniclet[1], Michel Hernould[1,2], Phuc Thi Do[3], Alisdair R. Fernie[3], Christian Chevalier[1,*] and Frédéric Gévaudant[1,2]

[1] Institut National de la Recherche Agronomique (INRA), [2] Université de Bordeaux 2, Unité Mixte de Recherche 619 sur la Biologie du Fruit, BP 81, F-33883 Villenave d'Ornon Cedex, France ; [3] Max-Planck-Institut für Molekulare Pflanzenphysiologie, Am Mühlenberg 1, 14467 Potsdam-Golm, Germany

* Author for correspondence: Christian Chevalier
Institut National de la Recherche Agronomique (INRA), Université de Bordeaux, Unité Mixte de Recherche 619 sur la Biologie du Fruit, BP 81, F-33883 Villenave d'Ornon Cedex, France
Tel: +33 557122693; Fax: +33 557122541; e-mail: chevalie@bordeaux.inra.fr

Running title: uncoupling endoreduplication and cell growth in fruit

Key words: Cell cycle, Cyclin-Dependent Kinase (CDK), Cyclin-Dependent Kinase Inhibitor (CKI), Endoreduplication, Fruit growth, Kip-related protein (KRP), Tomato (*Solanum lycopersicum*).

Total word count = 6998

SUMMARY

Tomato fruit size results from the combination of cell number and cell size which are respectively determined by the cell division and cell expansion processes. As fruit growth is mainly sustained by cell expansion, the development of fleshy pericarp tissue is characterized by numerous rounds of endoreduplication inducing a spectacular increase in DNA ploidy and mean cell size. Although a clear relationship exists between endoreduplication and cell growth in plants, the exact role of endoreduplication has not been clearly elucidated. To decipher the molecular basis of the endoreduplication-associated cell growth in fruit, we investigated the putative involvement of the tomato Cyclin Dependent Kinase inhibitor SlKRP1. We studied the kinetics of pericarp development in tomato fruit at the morphological and cytological levels, and demonstrated that endoreduplication is directly proportional to cell- and fruit diameter. We established a mathematical model for tissue growth according to the number of divisions and endocycles. This model was tested in fruits where we managed to decrease the extent of endoreduplication by over-expressing Sl*KRP1* under the control of a fruit-specific promoter expressed during early development. Despite the fact that endoreduplication was impacted, we could not observe any morphological, cytological or metabolic phenotypes, indicating that cell- and fruit size determination can be, at least conditionally, uncoupled from endoreduplication.

Word count: 210

INTRODUCTION

Endoreduplication is an alternative cell cycle characterized by the absence of mitosis, consisting in repeated DNA replication rounds, thus leading to an exponential increase in the amount of genomic DNA. This process commonly associated with cell differentiation is widespread in plants and particularly in Angiosperms where it arises in most tissues (Nagl, 1976; D'Amato, 1984).

Several hypotheses have been proposed in attempt to decipher the physiological role of endoreduplication. Since endoreduplication leads to nuclear DNA amplification, and therefore a multiplication of the gene copy number, this process could support an increase in transcriptional and metabolic activities (Galitski *et al*., 1999; Kondorosi and Kondorosi, 2004). However, this theory has not yet been clearly demonstrated in plants (Leiva-Neto *et al*., 2004). The increase in gene copy number could additionally provide a means to protect the genome against DNA damage caused by adverse environmental factors (Hase *et al*. 2006; Ramirez-Parra and Gutierrez, 2007).

The frequently observed positive correlations between endoreduplication and cell size in many different plant species, organs and cell types (Joubès and Chevalier, 2000; Sugimoto-Shirasu and Roberts, 2003; Kondorosi and Kondorosi, 2004) are commonly interpreted as evidence that endoreduplication is the driver of cell expansion. It is believed that successive rounds of DNA synthesis during endoreduplication consequently induce hypertrophy of the nucleus, thus influencing the final size of the cell which may therefore adjust its cytoplasmic volume with respect to the DNA content of the nucleus (according to the "karyoplasmic ratio" theory; Sugimoto-Shirasu and Roberts, 2003). In tomato, evidence for such a positive

correlation between cell size and ploidy level has indeed been provided during fruit development (Cheniclet *et al*., 2005). In a recent survey (Bourdon *et al*., 2010), we showed that the ability to develop large cells in various fleshy fruit species is not restricted to endopolyploidizing fruits. Hence endoreduplication obviously does not appear to be a pre-requisite for cell expansion as previously reported (Beemster *et al*., 2002; De Veylder *et al*. 2001; Leiva-Neto *et al*., 2004). Nevertheless, it appears that endoreduplication participates clearly in modulating the rate of cell expansion and/or organ growth, such as in fruit development. Indeed when endopolyploidizing fruits are compared, it becomes apparent that the largest cells are present in fruits which undergo the highest number of endocycles (e.g. tomato, pepper, melon), and that endoreduplication occurs in fruit from species exhibiting rapid fruit development (in less than 10 weeks) while it is absent in fruit from species where fruit development lasts for a very long period of time (over 17 weeks) (Bourdon *et al*., 2010).

In fruits of Cucurbitaceae and Solanaceae, mesocarp cells commonly undergo six rounds of DNA duplication (endocycle), and the highest ploidy levels for these cells are reached in tomato fruits where eight endocycles (up to 512C) can be observed (Bourdon *et al*., 2010). This high level of endopolyploidy in tomato fruits and the numerous data reported on this process in this species (Chevalier, 2007) makes it an outstanding model for studying endoreduplication and its physiological role during fruit development.

Part of the molecular control existing for the classical cell cycle regulation is conserved in the endoreduplication cycle, especially those targeting the activity of Cyclin Dependent Kinase/Cyclin (CDK/CYC) complexes which phosphorylate various protein targets, allowing the transition from one phase of the cell cycle to the next. The commitment to endocycle and the consequent lack of mitosis has been proposed

to occur in the absence of a Mitosis Inducing Factor (MIF) which normally governs the passage through the G2-M transition (Inzé and De Veylder, 2006). Down-regulation of M-phase CDK activity is sufficient to drive cells into the endocycle (Vlieghe *et al.*, 2007), and given that the M-phase CDKB1;1 activity is required to prevent a premature entry in the endocycle (Boudolf *et al.* 2004), it was proposed as a likely candidate kinase to be a component of MIF. Various distinct mechanisms may account for the loss of CDK activity. The CDK phosphorylation status, the availability of the cyclin regulatory subunit and the involvement of specific CDK inhibitors represent just a few potential regulatory mechanisms. We could provide evidence of the direct implication of the two former mechanisms in the regulation of endoreduplication and its impact on tomato fruit development (Gonzalez *et al.*, 2007; Mathieu-Rivet *et al.*, 2010), and have previously hypothesized that CDK inhibitors could also play a part in the endoreduplication-driven fruit growth in tomato (Bisbis *et al.*, 2006).

In plants, most of the functional studies on CDK inhibitors have been focused on a particular class called Interactors of Cyclin dependent Kinase/Kip-Related Proteins (ICK/KRP) (Wang *et al.*, 2007). *ICK/KRP* genes belong to a multigene family, and so far no direct phenotypic effect induced by the down-expression or mutation of *ICK/KRP* genes has been reported, most probably because of gene functional redundancy. In addition, the simultaneous down-regulation of multiple ICK/KRPs shows a hyperplasic growth phenotype (Moulinier Anzola *et al.*, 2010). However, numerous studies have reported the effects of *ICK/KRP* over-expression in Arabidopsis (Wang *et al.*, 2000; Verkest *et al.*, 2005; Weinl *et al.*, 2005; Bemis *et al.*, 2007; Schnittger *et al.*, 2003), maize (Coelho *et al.*, 2005), tobacco (Jasinski *et al.*, 2002), rice (Barrôco *et al.*, 2006) and Brassica (Zhou *et al.*, 2002). A common

phenotype associated with an *ICK/KRP* over-expression is an impairment of the cell cycle resulting in plant dwarfism. At the cellular level, it appears that in all cases analysed, endoreduplication and cell size are affected. A low level of *ICK/KRP* over-expression appears to block cell division and induce nuclear endoreduplication, together with only a slight alteration in cell size and a slight decrease in final plant size (Verkest *et al*., 2005; Weinl *et al*., 2005). By contrast, a high level of *ICK/KRP* over-expression affects negatively both cell division and endoreduplication, generating cells of bigger size, and results in an overall plant dwarfism (De Veylder *et al*., 2001, Jasinski *et al*., 2002, Zhou *et al*., 2003).

In the present work, we aimed to perform a functional analysis of the tomato ICK/KRP gene *SlKRP1* during fruit development. As an initial step, we demonstrated that endoreduplication is directly proportional to cell diameter and fruit diameter, allowing us to establish a mathematical model for tissue growth according to the number of divisions and the number of endocycles. However, the over-expression of Sl*KRP1* under the control of a promoter specifically expressed during the phase of cell expansion of early fruit development revealed no general morphological, cytological or metabolic defects but did display a decreased level of endoreduplication. Thus in the conditions of study our data demonstrate that cell size and fruit size determination can be uncoupled from the endoreduplication process. The implications of these findings with respect to the relative role of both processes during fruit development will be discussed.

Word count = 1116

RESULTS

Fruit growth, cell enlargement and endoreduplication are linearly correlated during fruit development in tomato

Measurements of mean fruit diameter resulting from the geometric mean of the three diameters according to the X, Y and Z axis (Figure 1a), pericarp width and mesocarp cell area (Figure 1b), and endoreduplication levels were performed throughout fruit development (from anthesis to the onset of maturation) using fruits harvested from WT plants. As shown in Figure 2a, the mean fruit diameter increased at a relatively constant rate from anthesis to 20 days-post-anthesis (dpa). Interestingly, this indicates that no difference in growth rate occurred at the transition between the phase of cell division (0-6 dpa) and the phase of cell expansion (6-20 dpa) during the early development of tomato fruit. The mean fruit diameter is highly positively correlated and directly proportional to endoreduplication within pericarp cells during the entire period of fruit growth (Figure 2b). The correlation between endoreduplication in a particular tissue such as pericarp and fruit growth is due to the constant proportionality between pericarp thickness and fruit diameter (Figure 2c). At the cytological level, the same proportionality was observed between endoreduplication and the mean cell size in mesocarp (Figure 2d). From these observations, we conclude that fruit growth, pericarp thickness, mesocarp cell growth and pericarp cell endoreduplication all evolve according to a common proportionality law during fruit development. It is noteworthy that this relationship still occurred whatever the seasonal period of fruit growth (winter *vs* summer) (Figure S1).

Interestingly, the relative rates of fruit growth (Rf) and endoreduplication (Re) calculated across fruit development (see the "Experimental procedures" section for calculations) (Figure 3a) were quite similar from around 10 to 40 dpa. The observed discrepancy between anthesis and 10 dpa could be explained by active cell divisions which would be anticipated to contribute to the increased development of pericarp during this period (Figure 3b). This was confirmed when the relative rates of cell production (Rc) and endoreduplication (Re) were combined as it resulted in a perfect match with the relative rate for fruit growth (Rf) (Figure 3c). Hence, on the basis of the number of cell division cycles and the number of endocycles alone, we managed to represent the variations in fruit growth during the whole period of development. These data strongly support the existence of a linear quantitative relationship between the number of endocycles, cell growth and fruit growth, which could be expressed as follows: $L=(l_{ei} \times EI + l_0) \times 2^{DI_{in\ axis}}$, where L is the considered tissue size (*e.g.* pericarp thickness); EI, the endoreduplication index corresponding to the mean number of endoreduplication cycles per nucleus; $DI_{in\ axis}$, the division index corresponding to the mean number of successive cell divisions according to a considered axis; l_{ei}, a constant reflecting the mean gain in cell size resulting from each endoreduplication cycle; and l_0 being the mean size of 2C cells according to the axis considered.

In order to test the significance of the model, we retrieved the data published by Cheniclet *et al.* (2005) describing the cellular parameters of developing pericarp. Indeed, the resin-embedding method for tissue sample preparation offers a better accuracy for counting the number of sub-epidermal cell layers than toluidine blue-stained fresh tissues. We thus confirmed the existence of a linear correlation between endoreduplication and cell size (Figure 4a). In addition, we could also

demonstrate that such a linear correlation occurs when using data from fruits harvested from 20 different tomato varieties displaying a large range in fruit size (Figure S2). As shown in Figure 4b, on the basis of our model we could predict values for pericarp thickness (Table S2) which closely matched the experimentally measured pericarp thickness (Figure 3b) across the entire course of pericarp development.

The fruit-specific overexpression of Sl*KRP1* during the cell expansion phase induced a dramatic decrease in endoreduplication

The expression patterns of the four different genes encoding ICK/KRP identified so far in tomato (Bisbis *et al*., 2006; Nafati *et al*., 2010), were analysed in various vegetative organs and across the course of tomato fruit development, using real-time RT-qPCR (Figure 5). All tomato *KRP* genes were ubiquitously expressed. However, their level of expression displayed significant differences. *SlKRP1* and *SlKRP3* were indistinctly expressed in immature and mature leaves, while Sl*KRP2* and Sl*KRP4* showed a preferential expression in immature dividing leaves. Interestingly, the transcripts for *SlKRP2* and *SlKRP4* were more abundant in the very early development of tomato fruit, when cell divisions are maximal inside the young developing fruit (Cheniclet *et al*., 2005), while the transcripts for *SlKRP1* and *SlKRP3* accumulated during the course of fruit development to reach a maximum at 20 and 30 dpa respectively, when cell expansion accounts essentially for fruit growth.

We next initiated the functional analysis of *SlKRP1* during tomato development. For this purpose a gain-of-function strategy was applied using constructs referred to hereafter as *ProPEPC2:SlKRP1*^{OE}, in which *SlKRP1* was expressed in the sense orientation under the control of the tomato *PhosphoEnolPyruvate Carboxylase 2*

(*PEPC2*) promoter. The *PEPC2* promoter is a fruit-specific promoter leading to high levels of expression during the phase of cell expansion and more specifically within the expanding cells of fruit mesocarp (Fernandez *et al.*, 2009).

We ended up with 3 independent *ProPEPC2:SlKRP1*^{OE} T2 lines, namely lines 2, 5 and 30, and measured the expression level of Sl*KRP1* in leaves and fruits from 6 to 40 dpa (Figure 6). A negligible expression of the transgene could be detected in leaves and young fruits at 6 dpa. After 10 dpa, the expression of Sl*KRP1* was increased to a 30-fold level in fruits from line 30 and to a 20-fold level in those from line 5, in comparison to WT fruits. Fruits from line 2 showed only a 2-fold increase for Sl*KRP1* expression at 10 dpa. The over-expression level remained stable until 20 dpa in each transgenic line during early fruit development but decreased thereafter.

Ploidy levels in fruit pericarp tissues from anthesis to 40 dpa were determined by flow cytometry (Figure 7). Between anthesis (Figure 7a) and 6 dpa (Figure 7b), no significant differences could be detected between WT and any of the *ProPEPC2:SlKRP1*^{OE} plants. From 10 dpa to the end of fruit growth (40 dpa), endoreduplication was strikingly reduced in the strongest *ProPEPC2:SlKRP1*^{OE} lines 5 and 30 (Figures 7c to 7g). As shown by the evolution of EI during fruit growth (Figure 7h), the rate of endoreduplication was halved between 10 to 20 dpa in the strong *ProPEPC2:SlKRP1*^{OE} lines 5 and 30 in comparison to WT. After 20 dpa, the rate of endoreduplication in fruits from lines 5 and 30 matched that of WT. However, the endoreduplication level in fruits from lines 5 and 30 did not overcome its initial delay (Figure 7g).

We next compared WT and the representative *ProPEPC2:SlKRP1*^{OE} line 30 during the course of fruit development. In this analysis we documented the frequency of appearance of each DNA ploidy level referred to as EF and calculated as described

in Experimental Procedures (Figure 8). When compared to WT, the kinetics of appearance of each class of DNA ploidy levels was obviously lower in *ProPEPC2:SlKRP1*^{OE} line 30. Interestingly, a second wave of production of each ploidy level apparently occurs in the *ProPEPC2:SlKRP1*^{OE} line 30. This second wave of endoreduplication was confirmed by estimating the endoreduplication ratio between lines 5 and 30 and WT (as described in Experimental procedures). It was drastically decreased between 10 and 20 dpa in the *ProPEPC2:SlKRP1*^{OE} lines but thereafter increased in comparison to WT (Figure S3a). Intriguingly, the levels of the *SlCYCD3;1* transcript, used as a G1/S marker, and the *SlCYCA3;1* transcript, used as an S-phase and endoreduplication marker (Mathieu-Rivet *et al.*, 2010), decreased drastically at 10 dpa in *ProPEPC2:SlKRP1*^{OE} fruits and similarly increased at 20 dpa when compared to WT (Figure S3b).

The decrease in endoreduplication neither alters fruit morphology, cell division activity nor cell size determination in *ProPEPC2:SlKRP1*^{OE} fruits

We next intended to evaluate the model postulated above for fruit growth in developing fruits of the *ProPEPC2:SlKRP1*^{OE} lines (Figure 9). The EI in WT fruits at two developmental stages, namely 10 and 20 dpa, was experimentally determined by flow cytometry from fruits harvested at 2 independent seasonal periods. In parallel EI was predicted using linear regression of the data of mean fruit diameter (as described in Figure S1) (Figure 9a). Irrespective of the cultivation season, the predicted values for WT were found to perfectly match with the experimental values. When applied to fruits from *ProPEPC2:SlKRP1*^{OE} line 30, the model was, however, no longer valid since the experimentally determined EI values diverted significantly from the predicted values, experimentally determined EI being considerably smaller than

would be anticipated (Figure 9a). Whatever the growth conditions were, values obtained from *ProPEPC2:SlKRP1*^{OE} fruits deviated from the linear regression established with WT fruit values (Figure 9b), thus indicating that fruit growth as represented by the mean fruit diameter was no longer correlated to endoreduplication in *SlKRP1* over-expressing fruits.

To explain these unexpected results, we performed a careful analysis of morphological and cytological parameters during fruit development in three selected lines (Figure 10). Fruit size as expressed by the mean fruit diameter (Figure 10a), pericarp width on the equatorial plane (Figure 10b), the number of cell layers across pericarp (Figure 10c) and the mean mesocarp cell area (Figure 10d) were thus determined. For each of these parameters, no significant differences could be observed between the *ProPEPC2:SlKRP1*^{OE} lines and WT plants. Interestingly this was also the case when pericarp width and mean mesocarp cell area were determined on the antero-posterior axis (X, Z as shown in Figure 1) (data not shown). We next investigated whether the observed decrease in endoreduplication had impacted nuclear size. Nuclei were prepared from 10 and 20 dpa pericarp tissues from WT and *ProPEPC2:SlKRP1*^{OE} line 30 and the mean area of isolated nuclei was then measured by imaging and ploidy levels were determined by flow cytometry (Figures S4). As expected the size of nuclei correlated perfectly with the ploidy levels in both WT and *ProPEPC2:SlKRP1*^{OE} line 30 fruits. Therefore, the decrease in ploidy levels and consequent decrease in nuclear size in *ProPEPC2:SlKRP1*^{OE} fruit occurred while cell size was unaffected accordingly (Figure 9D), indicating that a disruption in the nuclear-to-cytoplasmic ratio was modified. Taken together, these results revealed that the *PEPC2*-driven over-expression of Sl*KRP1* during the phase of cell expansion induced neither morphological nor cytological effects on fruit

development. In addition, while the mathematical model for fruit growth is fully relevant for WT fruits, genetic modification can clearly induce a complete uncoupling of endoreduplication from cell size.

Fruits from ProPEPC2:SlKRP1^{OE} lines displayed no consistent changes in their metabolite content

Metabolite profiling using GC-MS was performed to compare the metabolite content in fruits from WT and *ProPEPC2:SlKRP1^{OE}* lines 5 and 30, at 15, 20, 30 and 40 dpa (Table S2). Globally no significant differences could be observed between the *ProPEPC2:SlKRP1^{OE}* lines and WT plants. In keeping with this statement line 5 was even more closely related to WT (Pearson coefficient = 0.9946) than to line 30 (Pearson coefficient = 0.9857), when evaluated on a global basis. That said when the data was assessed on a metabolite-by-metabolite basis, the majority of metabolites neither displayed dramatic, nor consistent, differences across the genotypes studied.

Word count = 1863

DISCUSSION

Establishing a model for mesocarp growth according to cell cycle and endocycle values

In early developmental stages, tomato fruit growth results from the combination of cell number and cell size which are respectively determined by cell division and cell expansion processes according to two successive developmental phases (Gillaspy *et*

al., 1993). In the course of fruit development, Cheniclet *et al.* (2005) demonstrated the existence of a clear correlation between endoreduplication and cell- and fruit size. We here confirm these data and reveal a linear relationship between endoreduplication, cell growth and fruit growth during the phase of cell expansion of tomato fruit development (Figures 2, 3 and 4). Interestingly, this indicates that fruit growth rate is constant throughout development, whatever the mode of growth according to cell proliferation or cell expansion associated to endoreduplication (Figure 2). This observation is consistent to that recently documented in the tomato cultivar MoneyMaker as well as the wild species tomato *S. pennellii* (Steinhauser *et al*., 2010), and is in full accordance with those obtained from *Arabidopsis* leaf and sepal epidermis (Horiguchi *et al*., 2006; Roeder *et al*., 2010).

This led us to propose the following formula to predict fruit growth from endoreduplication and cell division parameters: $L= (l_{ei} \times EI + l_0) \times 2^{DI}{}_{in\ axis}$. According to the established linear regression (Figure 2b), the value for l_{ei} (representing the mean gain in cell size resulting from each endoreduplication cycle) was estimated to be of 0.0271 mm and the value for l_0 (representing the mean cell size of a population solely composed of diploid cells with EI = 0), was estimated as a negative figure (-0.0048 mm) using the data provided by Cheniclet *et al*. (2005) (Figure 4a). One would have expected a positive figure for l_0 and we therefore postulate that the proposed formula applies only to cells under endoreduplication. This suggests that the cell size increase encountered at the end of the G2 phase which transiently reaches the 4C state in proliferating cells, is lower than the cell size increase induced by a round of endoreduplication (l_{ei}), found at a constant value.

In the present work our kinetic analysis allowed us to model tomato pericarp growth on the basis of the number of cell divisions and endocycles. To our

knowledge, this linkage has never been demonstrated before. It would be interesting to test this function in other types of fruit tissue such as the jelly-like locular tissue undergoing extended endoreduplication (Joubès *et al.*, 1999), as well as in other plant species in order to assess its generality.

Another intriguing aspect of the correlation between cell- and fruit size and the number of endocycles relies on the fact that endoreduplication is proportional to cell diameter rather than cell volume which better reflects the quantity of matter within a cell. A new hypothesis on intracellular protein gradients controlling mechanisms such as the cell cycle have emerged these last years (Moseley *et al.*, 2009). Such mechanisms are predicted to involve intracellular distances rather than cell volume since the diffusion of signal proteins would be omni-directional within the cytoplasm (Meyers *et al.*, 2006). While no such gradient has yet been proposed to control cell cycle and cell growth in plants, the existence of such a mechanism could explain the tight quantitative proportionality which was observed for the different parameters analysed across fruit development.

The regulation by the PEPC2 promoter restricts the effect of SlKRP1 over-expression to endoreduplicating cells in tomato mesocarp

Over the last decade, several reports have described the effects of ICK/KRPs on cell division and endoreduplication (for a review, see Wang *et al.*, 2007). With the exception of the specific over-expression of ICK/KRPs in Arabidopsis trichomes (Schnittger *et al.*, 2003), all these reports made use of promoters that are active in both dividing and endoreduplicating cells, precluding clear conclusions about the independent effect of ICK/KRPs on cell division or endoreduplication in a particular developing tissue context. To investigate the effect of endoreduplication on fruit

growth independently from cell divisions, we aimed at deregulating the expression of the tomato ICK/KRP gene *SlKRP1*, which was shown to be associated to DNA ploidy increase in fruit development (Bisbis *et al*., 2006). For this purpose we used the tomato *PEPC2* promoter (Fernandez *et al*., 2009) which it drives a high level of transgene expression in tomato fruit pericarp between 6 and 30 dpa, i.e. essentially during the cell expansion phase of fruit development (Figure 4).

The *PEPC2*-driven specific over-expression of SlKRP1 in fruit pericarp did not produce any apparent phenotype at the morphological and cytological levels (Figure 9). We could not detect any decrease in the number of pericarp cell layers between the transgenic and wild type lines), indicating that cell division was not affected. While most cell divisions have already been achieved prior to 6 dpa, some divisions continue to occur in the external cell layers of mesocarp until 15 dpa (Cheniclet *et al*., 2005). Given that the over-expression of SlKRP1 remains very high from 10 to 20 dpa in ProPEPC2:SlKRP1^{OE} fruits (Figure 4), we could expect an effect on these divisions in the external mesocarp. However, Fernandez *et al*. (2009) showed that the *PEPC2* promoter expression occurs preferentially in the largest cells of the central mesocarp of tomato fruits, thus explaining the absence of any effect on cell divisions within the mesocarp of ProPEPC2:SlKRP1^{OE} fruits.

The use of the *PEPC2* promoter to alter the endoreduplication process in tomato fruit mesocarp was fully relevant as DNA ploidy levels were clearly lowered (Figures 7 and 8). Thus the effect of *SlKRP1* over-expression on ploidy levels in the endoreduplicating cells of mesocarp was quite similar to that obtained in other plant models and organs such as Arabidopsis leaf mesophyl cells (De Veylder *et al*., 2001; Verkest *et al*., 2005; Weinl *et al*., 2005) or rice endosperm cells (Barrôco *et al*., 2006).

The fruit-specific over-expression of SlKRP1 results in an uncoupling of endoreduplication and cell growth

Numerous studies in plants have documented a clear numerical relationship between endoreduplication and cell growth suggesting a causal relationship between these two cellular processes. Nowadays, the function of an accelerator for organ growth, such as in fruit (Bourdon *et al.*, 2010), or for plant growth in response to environmental constraints (Barow and Meister, 2003), is a favoured role for endoreduplication. Indeed we have been able to demonstrate that the over-expression of the Anaphase Complex Activator CCS52A, required for proper destruction of cyclins, impacted fruit development in order to sustain and even enhance fruit growth via an induction of endoreduplication (Mathieu-Rivet *et al.*, 2010). Nevertheless the role of endoreduplication in modulating the rate or organ growth and/or cell expansion has been disputed (John and Qi, 2008), mainly because functional analyses aimed at deregulating target genes related to endoreduplication and/or cell size have also impacted the progress in the cell cycle and therefore also affected cell division. Four different situations have emerged from the literature. (i) Endoreduplication is induced while cell divisions are inhibited. This scenario was obtained when the progress into M phase is hampered by down-regulation of B-type CDKs (Boudolf *et al.*, 2009), A-type Cyclins (Cebolla *et al.*, 1999) or by a mild up-regulation of KRPs (De Veylder *et al.*, 2001; Jasinski *et al.*, 2002; Wang *et al.*, 2000; Zhou *et al.*, 2003). In such a situation the premature blockage of mitosis induces endoreduplication, generating plants with fewer cells of larger size (Cebolla *et al.*, 1999; Jasinski *et al.*, 2002; Wang *et al.*, 2000) or of approximately equal size (Zhou *et al.*, 2003, De Veylder *et al.*, 2001) to those of WT. (ii) Endoreduplication is decreased while cell divisions are promoted. This is the case

when D-type cyclins are up-regulated (Dewitte *et al.*, 2003; Qi and John, 2007). At the organ level no significant difference in size can be observed when compared to WT, however, tissues are composed of more cells of smaller size than those observed in WT. (iii) The dual decrease of endoreduplication and cell division can be achieved by targeting genes involved in S-phase or in both S and M phases (De Veylder *et al.*, 2001; Hemerly *et al.*, 1995; Jasinski *et al.*, 2002; Zhou *et al.*, 2003). In this extreme situation, plants are characterized by dwarfism; the plant organs are composed of very few cells which are generally diploid and far larger than WT. (iv) Endoreduplication is decreased independently from cell divisions which are not affected. This scenario was reported in plants over-expressing a dominant negative form of CDKA in the endoreduplicating cells of the maize endosperm using the 27 kD γ zein promoter (Leiva-Neto *et al.*, 2004). As such this represented the first report describing that cell size determination can be independent of endoreduplication level. As the case was unique and observed in a highly differentiated tissue, the authors proposed a specific role for endoreduplication in maize endosperm given the importance of this tissue as a source of mobilisable nitrogen reserves to fuel development.

Here we provide a second demonstration that cell size can be uncoupled from endoreduplication, this time in tomato fruit pericarp. Indeed, the use of the *PEPC2* promoter to drive the specific over-expression of *SlKRP1* in endoreduplicating cells within fruit pericarp provided data which are remarkably similar to those from Leiva-Neto *et al.* (2004). Although normal pericarp development is characterized by the close relationship between endoreduplication and cell growth (Figures 2, 3 and 4), in full agreement with the “karyoplasmic ratio” theory (Sugimoto-Shirasu and Roberts, 2003), the reduced levels of endoreduplication in *ProPEPC2:SlKRP1*^{OE} fruits

(Figures 7 and 9) do not result in any morphological and cytological defects (Figure 9a, 9b and 9c), any reduction in cell size (Figure 9d), or any consistent differences in biochemical composition (Table S2). Interestingly, Leiva-Neto *et al*. (2004) showed that lower levels of endoreduplication in maize endosperm have only minor effects on starch and storage protein contents, as well as on the associated transcribed genes. As far as maize endosperm and tomato fruit are concerned, these data thus suggest that endoreduplication is unlikely to contribute to the regulation of transcriptional activity and subsequent metabolic activity by increasing the availability of DNA templates for gene expression. It is noteworthy that the metabolic modifications observed for tomato fruits over-expressing the endoreduplicating-associated gene *SlCCS52A* were mostly secondary effects resulting from the observed alteration in fruit growth (Matthieu-Rivet *et al*., 2010).

Endoreduplication or cell growth: what comes first?

The mean level of endoreduplication in various plant organs has repeatedly been found to be correlated with organ size. From the literature two mechanisms accounting for organ growth are opposed: first the final size of an organ can result from a given balance of cell-based (autonomous) growth relying on division, expansion and endoreduplication; second growth itself is the dominant regulator of cell proliferation, and the determinant of final cell size and ultimate organ size, according to an organismal level of regulation (Mizukami, 2001; John and Qi, 2008). In view of the organismal control, the synthesis of cytoplasm is the primary process and cell division and endoreduplication-driven cell enlargement are secondary processes to maintain the karyoplasmic ratio (Cookson *et al*., 2006; John and Qi, 2008). Although the correlation between cell size and endoreduplication is obvious,

the direction of causality remains very much a matter of debate. Since endoreduplication corresponds to successive rounds of DNA duplication in the absence of mitosis, it would appear likely that a minimal cell size must be required to commit to a subsequent round of DNA replication thus implying cell growth. However once DNA synthesis is completed, the doubling of the DNA quantity can in turn promote cell growth, according to the "karyoplasmic ratio" theory (Sugimoto-Shirasu and Roberts 2003).

The strong proportionality between ploidy level and cell size during normal plant development reported in this work is obviously valid at the scale of a cell population within a tissue or an organ, and is thus experimentally determined according to means of parameters. At the cellular level, a high degree of variability occurs within each population studied which impairs the application of our model. Indeed, individual cells cannot be assigned to clearly defined subpopulations of a given size, since cell size shows a continuous distribution. Hence it is highly probable that for a given cell size, several distinct ploidy levels may occur. When referring to the mean number of endoreduplication cycles as the definition for EI (Figure 7h), the population of cells in ProPEPC2:SlKRP1^{OE} fruit mesocarp performed one endoreduplication round under WT cells. Nevertheless, the attained levels of endoreduplication were still sufficient to support the optimal cell size increase observed in WT (Figure 10d). These observations suggest that endoreduplication would likely support a range of cell size rather than a defined one. This assertion would infer that endoreduplication precedes cell growth, as reported during the elongation of hypocotyl in Arabidopsis (Traas *et al.*, 1998).

In conclusion, we here demonstrated that the fruit-specific overexpression of SlKRP1 under the control of the *PEPC2* promoter negatively impacts

endoreduplication within fruit pericarp in a similar manner to that previously observed for strong KRP overexpressors. However, final fruit size and mean pericarp cell size were not affected revealing that it was possible to uncouple endoreduplication and cell growth in *ProPEPC2:SlKRP1*^{OE} fruit. Although endoreduplication was not totally impaired in *ProPEPC2:SlKRP1*^{OE} fruit, it is likely that enough ploidy still occurred to support cell growth. This would thus infer that endoreduplication does not exert a direct control on cell growth but would rather be a limiting factor for cell growth, in accordance with the previous model from Schnittger *et al*. (2003). In the absence of such a direct control, we propose that endoreduplication and cell growth may be co-regulated by a common upstream factor, since both processes follow the very same dynamics during fruit development.

Word count = 2281

EXPERIMENTAL PROCEDURES

RNA Extraction, Reverse-Transcription and Real-time Quantitative PCR

Total RNA was extracted from vegetative organs and pericarp from fruits harvested at the following developmental stages: anthesis, 3, 5, 6, 10, 15, 20, 30 and 40 dpa, using TRI® Reagent (Sigma-Alldrich, Lille-Lezennes, France). After extraction, RNA samples were DNAse-treated using the TURBO DNA-free Kit (Applied Biosystems, Villebon sur Yvette, France). Complementary DNA was synthesized from 1 µg of total RNA using IScript cDNA Synthesis Kit (Biorad, Marnes-la-Coquette, France). Real-time quantitative PCR was performed with a CFX96 Real-Time PCR Detection System (Biorad) using a final volume of 25 µL of reaction mixture containing 12.5 µL

of iQ SYBR Green Supermix (Biorad), 0.2 mM of each primer and 1 µL of the template diluted to the tenth. For all real-time qPCR experiments, each reaction was performed in triplicate. To determine relative fold differences for each sample, the Ct value for each gene was normalized to the Ct value for internal references (cDNAs encoding actin and eiF4A).

Generation of *ProPEPC2:SlKRP1*^{OE} lines and plant growth conditions

The sequence encoding KRP1 from pET28-KRP1 vector (Bisbis *et al*., 2006) was amplified in a two-stage PCR reaction and inserted into the GATEWAY vector pDONR201 (Invitrogen, address) by attB recombination following the manufacturer's protocol. An error-free entry clone was confirmed by sequence analysis before recombination into pK2GW7 vector (www.vib.be) as to produce the pK2GW7-his-KRP1construct. A 2 Kb DNA fragment containing the *SlPEPC2* promoter (ProPECPC2) (Fernandez *et al*., 2009) was amplified using specific primers flanked by *Sac*I/*Spe*I restriction sites. pK2GW7-his-KRP1 and ProPECPC2 DNA fragment were both separately digested using *Sac*I and *Spe*I, and recombined by ligation. The ligation product, pK2GW7-pPEPC2-KRP1 vector, was introduced into the *Agrobacterium tumefaciens* strain GV3101 by transformation and subsequently into *Solanum lycopersicum* cv. WVA106 plants using the cotyledon transformation method as described previously (Gonzalez *et al*., 2007). Transgenic plants were selected on kanamycin-containing medium and later transferred to soil. Homozygosis was verified by real time qPCR on genomic DNA of T2 plants. For each transgenic line, 3 T2 plants were analysed and compared to 3 independent WT plants. Tomato plants were grown in a greenhouse under a thermoperiod of 25℃/20℃ and a photoperiod of 14/10 h (day/night).

Cytological methods

Fruits were harvested at various developmental stages determined according to dpas and weight. Fruit diameters according to the three X, Y, Z axes (as shown in Figure 1) were measured as to determine the Mean Fruit Diameter calculated as the geometric mean of the three diameters according to the formula: $MFD = \sqrt[3]{X \times Y \times Z}$. Morphometric analyses were performed by using a gauge of 2.5 x 10^3 μm^2. To visualize the size of mesocarp cells, the surface of a freshly sectioned fruit was incubated in 0.1% toluidin blue, washed in water and dried on a filter paper. Images of pericarp sections were taken using a microscope (Zeiss Axioplan) and then analysed with IMAGEPRO-PLUS software (Media Cybernetics, Silver Spring, MD). To evaluate the mean cell size in mesocarp, cell surface values were square rooted. Mean cell length in pericarp was directly measured according to Z-axis. Data from morphometric measurements were statistically analyzed and Student's test was used to evaluate the significance of the results.

Flow cytometry analysis

Ploidy profiles of isolated nuclei from tomato pericarp and ovaries at anthesis were determined as described (Cheniclet *et al.*, 2005).

Calculations for endoreduplication parameters

The endoreduplication index (EI) representing the mean number of endoreduplication cycles was calculated according to Barow and Meister (2002) using the formula:

$$EI = \frac{0xF_{2C} + 1xF_{4C} + 2xF_{8C} + 3xF_{16C} + 4xF_{32C} + 5xF_{64C} + 6xF_{128C}}{\sum_{n=2C}^{n=128C} Fx}$$, where F_x is the frequency of the peak x considered.

The frequency of appearance of each DNA ploidy level in a defined time interval (EF) was calculated according to the formula: $EF_x = \frac{\sum_{n=x}^{128C} F_n t_N - \sum_{n=x}^{128C} F_n t_{N-1}}{t_N - t_{N-1}}$ where x is the considered DNA ploidy level; F_n the frequency of the ploidy level n; t_N the developmental stage and t_{N-1} the preceding developmental stage. The calculated EF_x thus represents the number of nuclei reaching the following ploidy level.

The endoreduplication ratio (ER) between *ProPEPC2:SlKRP1*^{OE} and WT fruit was calculated for each developmental stage using EI according to the formula: $REt_N = \frac{EI_{transgenic} t_N - EI_{transgenic} t_{N-1}}{EI_{WT} t_N - EI_{WT} t_{N-1}}$ where t_N is the development stage (in DPA) and t_{N-1} the preceding stage.

Calculations of relative rates of fruit growth, endoreduplication and cell production

The relative rates of fruit growth (Rf), endoreduplication (Re) or cell production (Rc) per day were calculated according to the formula: $R_{Ft_N} = \frac{Ft_N - Ft_{N-1}}{(t_N - t_{N-1}) * Ft_N}$ where F is the considered factor (mean fruit diameter for Rf, EI for Re, or number of cell layers for Rc); t_N, the developmental stage (in DPA) and t_{N-1}, the preceding developmental stage.

Metabolite profiling

Metabolite extraction, derivatization and GC-MS analysis were performed as described previously (Lisec *et al.*, 2006) with modifications specific to tomato fruit (Schauer *et al.*, 2006). Data processing was performed using TagFinder software

(Luedemann *et al*., 2008), identifying metabolites by comparison with database entries for authentic standards (Schauer *et al*., 2005).

Word count = 793

ACKNOWLEDGMENTS

This research was supported by the 6th Framework Program of the European Commission, within the European Solanaceae Integrated project, EU-SOL (grant no. FOOD–CT–2006–016214), and by fundings from the Region Aquitaine; M.N. was supported by grant n°24220–2006 from the Ministère de l'Enseignement Supérieur et de la Recherche (France). We are indebted to Dr. Christophe Rothan for very stimulating scientific discussions within the EU-SOL project, and Mrs Patricia Ballias and Aurélie Honoré for excellent technical work in taking care of plants.

Word count = 83

LITERATURE CITED

Barow, M and Meister, A. (2002). Lack of correlation between AT frequency and genome size in higher plants and the effect of nonrandomness of base sequences on dye binding. *Cytometry* **47,** 1-7.

Barrôco, R.M., Peres, A., Droual, A.M., De Veylder, L., Nguyen Le, S.L., De Wolf, J., Mironov, V., Peerbolte, R., Beemster, G.T., Inzé, D., et al. (2006). The cyclin-dependent kinase inhibitor Orysa;KRP1 plays an important role in seed development of rice. *Plant Physiol*. **142,** 1053-1064.

Beemster, G.T., De Vusser, K., De Tavernier, E., De Bock, K. and Inzé, D. (2002). Variation in growth rate between Arabidopsis ecotypes is correlated with cell division and A-type cyclin-dependent kinase activity. *Plant Physiol*. **129,** 854-864.

Bemis, S.M. and Torii, K.U. (2007). Autonomy of cell proliferation and developmental programs during Arabidopsis aboveground organ morphogenesis. *Dev. Biol*. **304,**367-381.

Bisbis, B., Delmas, F., Joubès, J., Sicard, A., Hernould, M., Inzé, D., Mouras, A. and Chevalier, C. (2006). Cyclin-Dependent Kinase Inhibitors are involved in endoreduplication during tomato fruit development. *J. Biol. Chem*. **281,** 7374-7383.

Boudolf, V., Vlieghe, K., Beemster, G.T.S., Magyar, Z., Torres Acosta, J.A., Maes, S., Vand Der Schueren, E., Inzé, D. and De Veylder, L. (2004). The plant-specific Cyclin-Dependent Kinase CDKB1;1 and transcription factor E2Fa-DPa control the balance of mitotically dividing and endoreduplicating cells in Arabidopsis. *Plant Cell,* **16,** 2683-2692.

Boudolf, V., Lammens, T., Boruc, J., Van Leene, J., Van Den Daele, H., Maes, S., Van Isterdael, G., Russinova, E., Kondorosi, E., Witters, E., De Jaeger, G., Inzé D. and De Veylder, L. (2009). CDKB1;1 forms a functional complex with CYCA2;3 to suppress endocycle onset. *Plant Physiol*. **150,** 1482-1493.

Bourdon, M., Frangne, N., Mathieu-Rivet, E., Nafati, M., Cheniclet, C, Renaudin, J.P. and Chevalier, C. (2009) Endoreduplication and growth of fleshy fruits. In *Progress in Botany* (Lüttge, U. *et al*., eds). Heidelberg: Springer-Verlag. vol. 71, pp. 101-132.

Cebolla, A., Vinardell, J. M., Kiss, E., Olah, B., Roudier, F., Kondorosi A. and Kondorosi E. (1999). The mitotic inhibitor ccs52 is required for endoreduplication and ploidy-dependent cell enlargement in plants. *EMBO J*. **18,** 4476-4484.

Cheniclet, C., Rong, W.Y., Causse, M., Bolling, L., Frangne, N., Carde, J.P. and Renaudin, J.P. (2005). Cell expansion and endoreduplication show a large genetic variability in pericarp and contribute strongly to tomato fruit growth. *Plant Physiol.* **139,** 1984-1994.

Chevalier, C. (2007) Cell cycle control and fruit development. In *Cell cycle control and plant development* (Inzé, D., ed). Oxford: Blackwell Publishing Ltd. Annual Plant Reviews, vol 32, pp. 269-293.

Coelho, C.M., Dante, R.A., Sabelli, P.A., Sun, Y., Dilkes, B.P., Gordon-Kamm, W.J. and Larkins, B.A. (2005). Cyclin-dependent kinase inhibitors in maize endosperm and their potential role in endoreduplication. *Plant Physiol*. **138,** 2323-2336.

Cookson, S.J., Radziejwoski, A. and Granier, C. (2006). Cell and leaf size plasticity in Arabidopsis: what is the role of endoreduplication? *Plant Cell Environ*. **29,** 1273-1283.

D'Amato, F. (1984). Role of polyploidy in reproductive organs and tissues. In Embryology of Angiosperms, B.M. Johri, ed (New York: Springer-Verlag), pp. 519-566.

De Veylder, L., Beeckman, T., Beemster, G.T., Krols, L., Terras, F., Landrieu, .I, Van Der Schueren, E., Maes, S., Naudts, M. and Inzé, D. (2001). Functional analysis of cyclin-dependent kinase inhibitors of Arabidopsis. *Plant Cell*, **13,** 1653-1668.

Dewitte, W., Riou-Khamlichi, C., Scofield, S., Healy, J.M., Jacqmard, A., Kilby, N.J. and Murray, J.A. (2003). Altered cell cycle distribution, hyperplasia, and inhibited differentiation in Arabidopsis caused by the D-type cyclin CYCD3. *Plant Cell*, **15,** 79-92.

Fernandez, A.I., Viron, N., Alhagdow, M., Karimi, M., Jones, M., Amsellem, Z., Sicard, A., Czerednik, A., Angenent, G., Grierson, D., et al. (2009). Flexible tools for gene expression and silencing in tomato. *Plant Physiol*. **151,** 1729-1740.

Galitski, T., Saldanha, A.J., Styles, C.A., Lander, E.S. and Fink, G.R. (1999). Ploidy regulation of gene expression. *Science*, **285,** 251-254

Gillaspy, G., Ben-David, H. and Gruissem, W. (1993). Fruits: A developmental perspective. *Plant Cell,* **5,** 1439-1451.

Gonzalez, N., Gévaudant, F., Hernould, M., Chevalier, C. and Mouras, A. (2007). The cell cycle-associated protein kinase WEE1 regulates cell size in relation to endoreduplication in developing tomato fruit. *Plant J*. **51,** 642-655.

Guillet, C., Just, D., Bénard, N., Destrac-Irvine, A., Baldet, P., Hernould, M., Causse, M., Raymond, P. and Rothan, C. (2002). A fruit-specific phosphoenolpyruvate carboxylase is related to rapid growth of tomato fruit. *Planta,* **214,** 717-726.

Hase ,Y., Trung, K.H., Matsunaga, T. and Tanaka, A. (2006). A mutation in the uvi4 gene promotes progression of endoreduplication and confers increased tolerance towards ultraviolet B light. *Plant J.* **46,** 317-326

Hemerly, A., de Almeida Engler, J., Bergounioux, C., Van Montagu, M., Engler, G., Inzé, D. and Ferreira, P. (1995). Dominant negative mutants of the Cdc2 kinase uncouple cell division from iterative plant development. *EMBO J*. **14,** 3925-3936.

Horiguchi, G., Ferjani, A., Fujikura, U. and Tsukaya, H. (2006). Coordination of cell proliferation and cell expansion in the control of leaf size in Arabidopsis thaliana. *J. Plant Res.* **119,** 37-42.

Inzé, D. and De Veylder, L. (2006). Cell cycle regulation in plant development. *Annu. Rev. Genet*. **40,** 77-105.

Jasinski, S., Riou-Khamlichi, C., Roche, O., Perennes, C., Bergounioux, C. and Glab, N. (2002). The CDK inhibitor NtKIS1a is involved in plant development, endoreduplication and restores normal development of cyclin D3; 1-overexpressing plants. *J. Cell Sci*. **115,** 973-982.

John, P.C. and Qi, R. (2008). Cell division and endoreduplication: doubtful engines of vegetative growth. Trends Plant Sci. **13:** 121-127

Joubès, J. and Chevalier, C. (2000). Endoreduplication in higher plants. *Plant Mol. Biol.* **43,** 737-747.

Joubès, J., Phan, T.H., Just, D., Rothan, C., Bergounioux, C., Raymond, P. and Chevalier, C. (1999). Molecular and biochemical characterization of the involvement of cyclin-dependent kinase A during the early development of tomato fruit. *Plant Physiol*. **121,** 857-869.

Kondorosi, E. and Kondorosi, A. (2004). Endoreduplication and activation of the anaphase-promoting complex during symbiotic cell development. *FEBS Lett*. **567,** 152-157

Leiva-Neto, J.T., Grafi, G., Sabelli, P.A., Dante, R.A., Woo, Y.M., Maddock, S., Gordon-Kamm, W.J. and Larkins, B.A. (2004). A dominant negative mutant of cyclin-dependent kinase A reduces endoreduplication but not cell size or gene expression in maize endosperm. *Plant Cell*, **16,** 1854-1869.

Lisec, J., Schauer, N., Kopka, J., Willmitzer, L. and Fernie, A.R. (2006). Gas chromatography mass spectrometry-based metabolite profiling in plants. *Nat. Protoc*. **1,** 387-396.

Luedemann, A., Strassburg, K., Erban, A. and Kopka, J. (2008). TagFinder for the quantitative analysis of gas chromatography--mass spectrometry (GC-MS)-based metabolite profiling experiments. *Bioinformatics*, **24,** 732-737.

Mathieu-Rivet, E., Gevaudant, F., Sicard, A., Salar, S., Do, P.T., Mouras, A., Fernie, A.F., Gibon, Y., Rothan, C., Chevalier, C. and Hernould, M. (2010). The functional analysis of the Anaphase Promoting Complex activator CCS52A highlights the crucial role of endoreduplication for fruit growth in tomato. *Plant J.* **62,** 727-741.

Meyers, J., Craig, J. and Odde, D.J. (2006). Potential for control of signaling pathways via cell size and shape. *Curr Biol*. **16,** 1685-1693.

Mizukami, Y. (2001). A matter of size: developmental control of organ size in plants. *Curr. Op. Plant Biol*. **4,** 533-539.

Moseley, J.B, Mayeux, A., Paoletti, A. and Nurse, P. (2009). A spatial gradient coordinates cell size and mitotic entry in fission yeast. *Nature*, **459,** 857-860.

Moulinier Anzola, J., Sieberer, T., Ortbauer, M., Butt, H., Korbei, B., Wienhoffer, I., Müllner, A.E. and Luschnig, C. (2010). Putative *Arabidopsis* transcriptional adaptor protein (PROPORZ1) is required to modulate histone acetylation in response to auxin. *Proc. Natl. Acad. Sci. USA*. **107**, 10308-10313.

Nafati, M., Frangne, N. Hernould, M., Chevalier, C. and Gévaudant F. (2010). Functional characterization of the tomato Cyclin-Dependent Kinase inhibitor SlKRP1 domains involved in protein-protein interactions. *New Phytol*. In press.

Nagl, W. (1976). DNA endoreduplication and polyteny understood as evolutionary strategies. *Nature*, **261,** 614-645.

Qi, R. and John P.C.L. (2007). Expression of genomic *AtCycD2;1* in Arabidopsis induces cell division at smaller cell sizes: implications for the control of plant growth. *Plant Physiol*. **144,** 1587-1597.

Ramirez-Parra, E. and Gutierrez, C. (2007). The many faces of chromatin assembly factor 1. *Trends Plant Sci*. **12,** 570-576.

Roeder, A.H.K., Chickarmane, V., Cunha, A., Obara, B., Manjunath, B.S. and Meyerowitz, E.M. (2010). Variability in the control of cell division underlies sepal epidermal patterning in *Arabidopsis thaliana*. *PLOS Biology* **8,** e1000367.

Schauer, N., Semel, Y., Roessner, U., Gur, A., Balbo, I., Carrari, F., Pleban, T., Perez-Melis, A., Bruedigam, C., Kopka, J., Willmitzer, L., Zamir, D. and Fernie, A.R. (2006). Comprehensive metabolic profiling and phenotyping of interspecific introgression lines for tomato improvement. *Nat. Biotechnol*. **24,** 447-454.

Schauer, N., Steinhauser, D., Strelkov, S., Schomburg, D., Allison, G., Moritz, T., Lundgren, K., Roessner-Tunali, U., Forbes, M.G., Willmitzer, L., Fernie, A.R. and Kopka, J. (2005). GC-MS libraries for the rapid identification of metabolites in complex biological samples. *FEBS Lett*. **579,** 1332-1337.

Schnittger, A., Weinl, C., Bouyer, D., Schöbinger, U. and Hülskamp, M. (2003). Misexpression of the Cyclin-Dependent Kinase Inhibitor ICK1/KRP1 in single-celled Arabidopsis trichomes reduces endoreduplication and cell size and induces cell death. *Plant Cell*, **15,** 303-315.

Steinhauser, M.C., Steinhauser, D., Koehl, K., Carrari, F., Gibon, Y., Fernie, A.R. and Stitt M. (2010). Enzyme activity profiles during fruit development in tomato cultivars and *Solanum pennellii*. *Plant Physiol*. **153,** 80-98.

Sugimoto-Shirasu, K. and Roberts, K. (2003). "Big it up": endoreduplication and cell-size control in plants. *Curr. Opin. Plant Biol*. **6,** 544-553.

Traas, J., Hülskamp, M., Gendreau, E. and Hofte, H. (1998). Endoreduplication and development: rule without dividing? *Curr. Opin. Plant Biol*. **6,** 498-503.

Verkest, A., Manes, C.I., Vercruysse, S., Maes, S., Van Der Schueren, E., Beeckman , T., Genschik, P., Kuiper, M., Inzé, D. and De Veylder, L. (2005). The cyclin-dependent kinase inhibitor KRP2 controls the onset of the

endoreduplication cycle during Arabidopsis leaf development through inhibition of mitotic CDKA;1 kinase complexes. *Plant Cell*, **17,** 1723-1736.

Vlieghe, K., Inzé, D. and De Veylder, L. (2007). Physiological relevance and molecular control of the endocycle in plants. In Cell cycle control and plant development, Annual Plant Reviews, Vol 32, D. Inzé, ed (Oxford: Blackwell Publishing Ltd., UK) pp227-248.

Wang, H., Fowke, L.C. and Crosby, W.L. (1997). A plant cyclin-dependent kinase inhibitor gene. *Nature,* **386,** 451-452.

Wang, H., Zhou, Y., Gilmer, S., Whitwill, S. and Fowke, L.C. (2000). Expression of the plant cyclin-dependent kinase inhibitor ICK1 affects cell division, plant growth and morphology. *Plant J.* **24,** 613-623.

Wang, H., Zhou, Y., Torres-Acosta, L. and Fowke, L.C. (2007). CDK Inhibitors. In Cell cycle control and plant development, Annual Plant Reviews, Vol 32, D. Inzé, ed (Oxford: Blackwell Publishing Ltd., UK) 62-86.

Weinl, C., Marquardt, S. Kuijt, S.J.H., Nowack, M.K., Jakoby, M.J., Hülskamp, M. and Schnittger, A. (2005). Novel functions of plant Cyclin-Dependent Kinase inhibitors, ICK1/KRP1, can act non-cell-autonomously and inhibit entry into mitosis. *Plant Cell,* **17,** 1704-1722.

Zhou, Y., Wang, H., Gilmer, S., Whitwill, S., Keller, W. and Fowke, L.C. (2002). Control of petal and pollen development by the plant cyclin-dependent kinase inhibitor ICK1 in transgenic Brassica plants. *Planta,* **215,** 248-257.

Zhou, Y., Wang, H., Gilmer, S., Whitwill, S. and Fowke, L.C. (2003). Effects of co-expressing the plant CDK inhibitor ICK1 and D-type cyclin genes on plant growth, cell size and ploidy in Arabidopsis thaliana. *Planta*, **216,** 604-613.

Word count = 1803

Legends for supplementary material

Figure S1. Relationship between EI and Mean Fruit Diameter in wild type tomato (cv. Wva106) fruits harvested from 2 different cultures.

Fruits at 10 and 20 dpa were harvested from plants grown in the greenhouse during the summer period (July-August 2009) (♦) and during the winter period (December 2009-January 2010) (**x**). The linear regression corresponds to that calculated in Figure 2b.

Figure S2. Relationship between EI and mean cell size in mesocarp from the 20 different tomato lines differing in fruit weight described in Cheniclet *et al*. (2005).

Each point (△) represents one tomato line (fruit harvested at the breaker stage). Data obtained from developing Wva106 fruits (values from Figure 2d) (■) were compared.

Figure S3. Comparison of the effects of the SlKRP1 over-expression in *ProPEPC2:SlKRP1*^{OE} lines 5 and 30 relative to WT.

(a) Evolution of the Endoreduplication Ratio representing the relative increase or decrease of endoreduplication in *ProPEPC2:SlKRP1*^{OE} lines 5 and 30 relative to WT.

(b) Quantitative RT-PCR analysis of *SlCYCA3;1 and SlCYCD3;1* expression in pericarp during fruit development (at 10, 15, 20 and 30 dpa) from *ProPEPC2:SlKRP1*^{OE} T1 lines 5 and 30 compared with WT. Quantification and normalisation of expression were as in Figure 5.

Student's t-tests were performed for each dataset. Star symbols indicate statistical significance difference ($p<0.001$) between the considered transgenic line and the corresponding WT value.

Figure S4. Relationship between endoreduplication and nuclear size.

(a) Relationship between the mean nuclear area determined by imaging from the different classes of area and their associated C-value determined by flow cytometry using isolated nuclei from 10 and 20 dpa WT fruit pericarp.

(b) Relationship between the frequency of a given class of nuclear area (determined by imaging) and the frequency of a given ploidy level (determined by flow cytometry) from 10 and 20 dpa WT (■) and *ProPEPC2:SlKRP1*^{OE} (▲) fruits. The correlation line drawn has been calculated according to WT values.

(c) Comparison of the frequencies of the different classes of ploidy levels measured by flow cytometry (dark grey bars) and ploidy levels estimated from nuclear area measurements (light grey bars) in 20 dpa fruits from WT and line 30. Values for 2C nuclei were excluded deliberately as the percentage of 2C nuclei was very low and tended to be drowned in background generated by tissue and cell debris following chopping.

Table S1. Endoreduplication Index (EI) and Division index (DI) values used for predicting the pericarp thickness evolution during fruit development displayed in Figure 4b.

Table S2. Central metabolism of developing fruits from *ProPEPC2:SlKRP1*^{OE} lines and WT.

Word count = 419

FIGURE LEGENDS

Figure 1. Definition of measurement axes used for morphometrical analyses of fruit and cell size.

(a) Description of the axes used for Mean Fruit Diameter measurements.

(b) Median transverse section of a fruit and histological view of pericarp. The larger arrow encompasses pericarp as a whole; the smaller arrow encompasses mesocarp where cell size was measured.

Figure 2. Development of wild type tomato (cv. Wva106) fruits.

(a) Growth curve established by measuring the Mean Fruit Diameter in the course of fruit development (from anthesis to 40 dpa) (n=71).

(b) Relationship between the Endoreduplication Index (EI) and Mean Fruit Diameter (n=65).

(c) Relationship between the Endoreduplication Index (EI) and mesocarp cell size (n=23).

(d) Relationship between between mesocarp cell size and Mean Fruit Diameter (n=30).

Figure 3. Comparison of Relative Fruit Growth Rate (Rf) with Relative Endoreduplication Rate (Re) (a), Relative Cell Production rate (Rc) (b), and cumulated Re and Rc (c), in the course of wild type fruit development.

Figure 4. Modelling pericarp growth.

(a) Relationship between EI and mean cell size in pericarp. Data used to establish the linear regression were obtained from developing Wva106 fruits and extracted from Cheniclet *et al*. (2005).

(b) Evolution of pericarp thickness during fruit development. Experimentally determined values for pericarp thickness from Cheniclet *et al*. (2005) were compared to predicted values using the following equation: Predicted value = (EI x 0.0271 – 0.0048) x 2^{DI}.

Figure 5. Gene expression analysis of *ICK/KRP* gene in tomato.

Quantitative RT-PCR analysis of *SlKRP1* (a), *SlKRP2* (b), *SlKRP3* (c) and *SlKRP4* (d) expression in tomato vegetative organs and developing fruits were performed using total RNA isolated from roots (Ro), immature (IL) and mature (ML) leaves, flowers at 7 mm stage (FI), and fruits harvested at 3, 5, 8, 10, 15, 20, 25 and 30 dpa and Breaker (Br) and Red Ripe (RR) stage. All values were normalized to the Sl*Actin* and Sl*eiF4A* housekeeping genes. The ΔΔCt method was used for relative quantification of mRNA abundance. Data are mean ± standard deviation (n=3).

Figure 6. Quantitative RT-PCR analysis of *SlKRP1* expression in leaf and pericarp from developing fruits (at 6, 10, 15, 20, 30 and 40 dpa) from *ProPEPC2:SlKRP1*^{OE} T1 lines 2, 5 and 30 compared with WT. Quantification and normalisation of expression were as in Figure 5.

Figure 7. Effects on endoreduplication of SlKRP1 overexpression during fruit development. (a) to (g) Ploidy level distribution in *ProPEPC2:SlKRP1*^{OE} fruit pericarp

as measured by flow cytometry during fruit development at Anthesis (a), 6 (b), 10 (c), 15 (d), 20 (e), 30 (f) and 40 dpa (g).

(h) Evolution of Endoreduplication index during fruit development. Values are mean ± standard error (n>4).

Figure 8. Kinetics of endoreduplication in the representative *ProPEPC2:SlKRP1*^{OE} line 30 compared to WT, in the course of fruit development. The frequency of appearance of each DNA ploidy level referred to as EF was calculated as described in Methods.

Figure 9. Phenotypical analysis of *ProPEPC2:SlKRP1*^{OE} lines compared to WT.

(a) Comparison between experimentally determined EI and predicted EI. EI were determined experimentally by flow cytometry using nuclei preparations from 10 and 20 dpa pericarp from WT and *ProPEPC2:SlKRP1*^{OE} fruits harvested from plants cultivated in summer (July-August 2009) and winter (December 2009-January 2010). The predicted EI were obtained using the linear regression obtained from data of mean fruit diameter (as described in Figure S1). Star symbols above bars indicate that Student's tests are significantly different (P≤0.001) from WT.

(b) Absence of relationship between the Mean fruit diameter of *ProPEPC2:SlKRP1*^{OE} fruits and EI. Data were obtained from 10 and 20 dpa fruits harvested from plants cultivated in summer (July-August 2009) and winter (December 2009-January 2010).

Figure 10. Morphological and cytological analysis of *ProPEPC2:SlKRP1*^{OE} fruits compared to WT in the course of fruit development.

(a) Evolution of Mean Fruit Diameter.

(b) Evolution of pericarp thickness.

(c) Number of cell layers in the Z-axis of the pericarp.

(d) Mean cell size in the Z-axis in pericarp.

Word count = 652

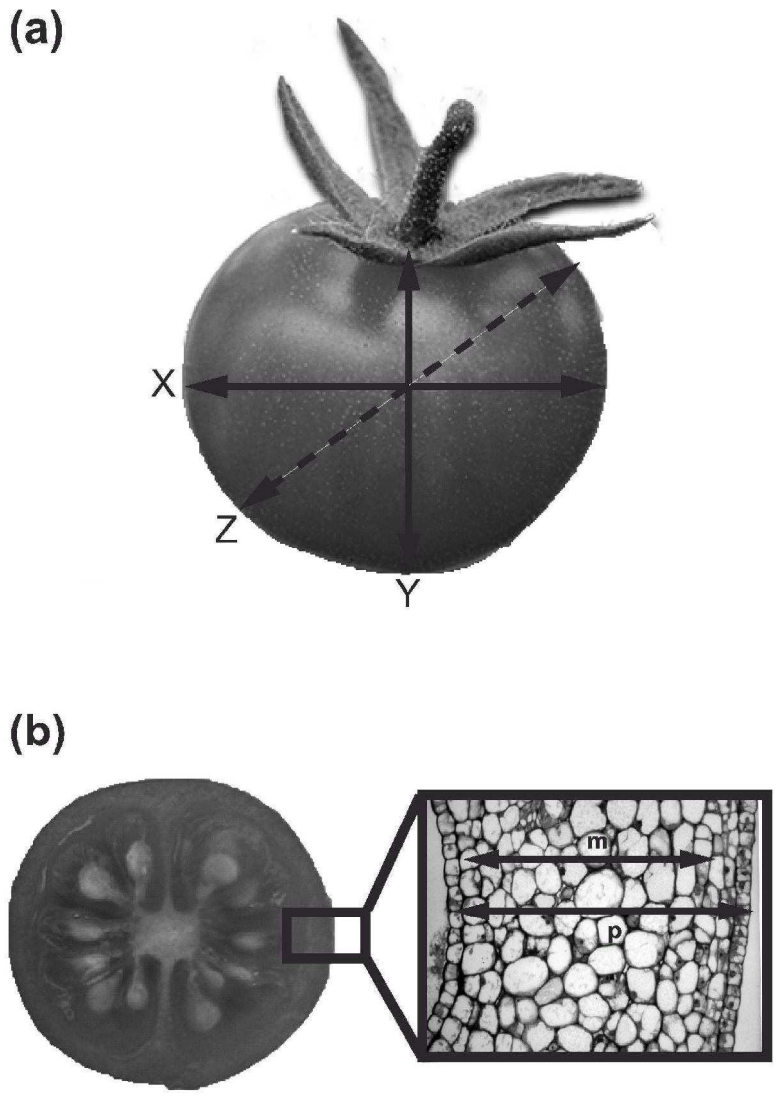

Figure 1. Definition of measurement axes used for morphometrical analyses of fruit and cell size.
(a) Description of the axes used for Mean Fruit Diameter measurements.
(b) Median transverse section of a fruit and histological view of pericarp. The larger arrow encompasses pericarp as a whole; the smaller arrow encompasses mesocarp where cell size was measured.

85x127mm (600 x 600 DPI)

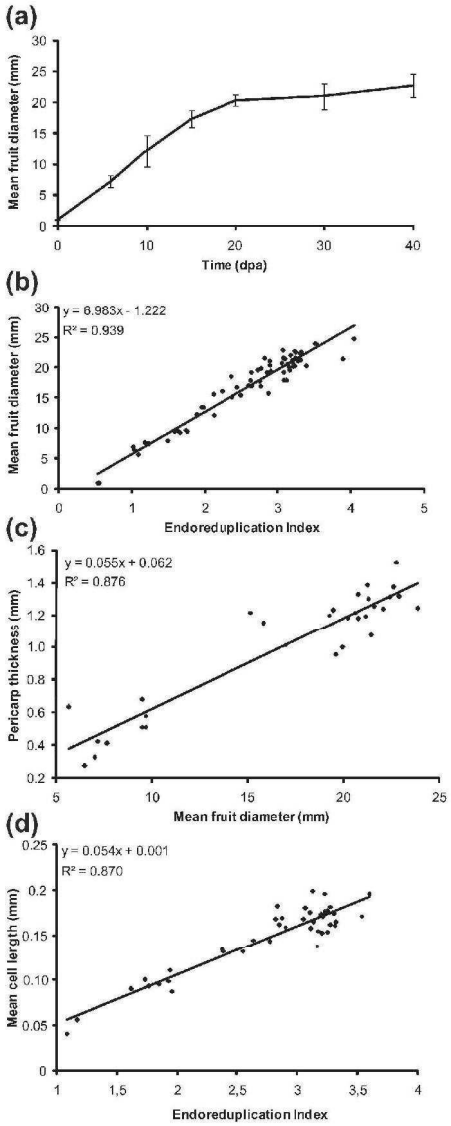

Figure 2. Development of wild type tomato (cv. Wva106) fruits.
(a) Growth curve established by measuring the Mean Fruit Diameter in the course of fruit development (from anthesis to 40 dpa) (n=71).
(b) Relationship between the Endoreduplication Index (EI) and Mean Fruit Diameter (n=65).
(c) Relationship between the Endoreduplication Index (EI) and mesocarp cell size (n=23).
(d) Relationship between between mesocarp cell size and Mean Fruit Diameter (n=30).

85x220mm (600 x 600 DPI)

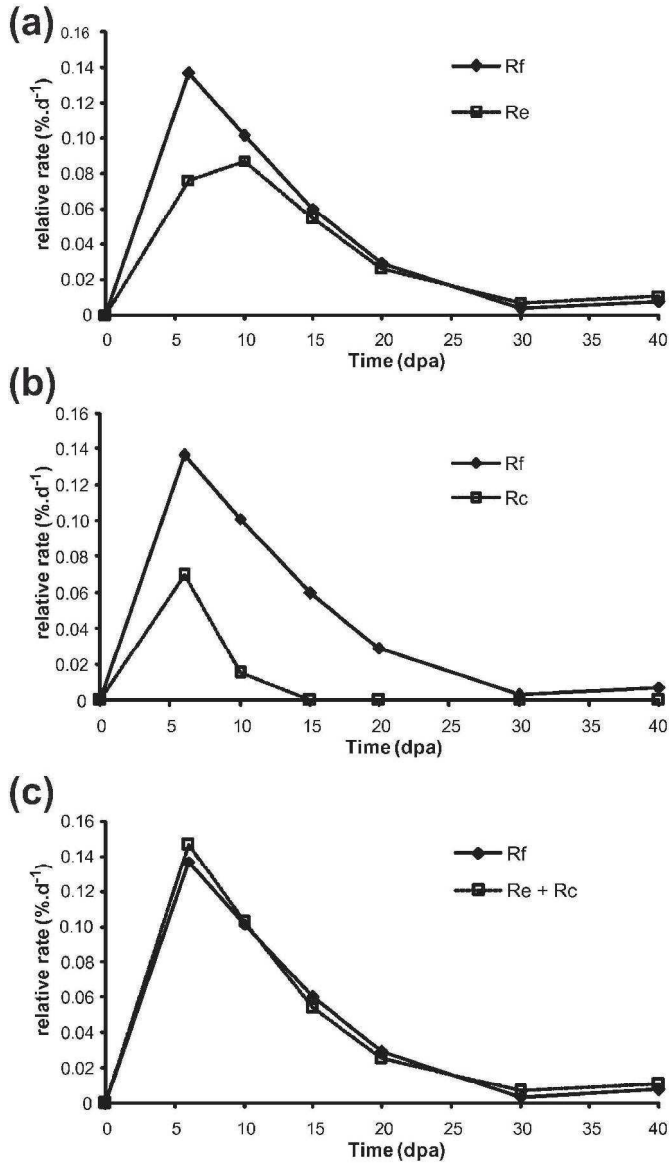

Figure 3. Comparison of Relative Fruit Growth Rate (Rf) with Relative Endoreduplication Rate (Re) (a), Relative Cell Production rate (Rc) (b), and cumulated Re and Rc (c), in the course of wild type fruit development.
85x149mm (600 x 600 DPI)

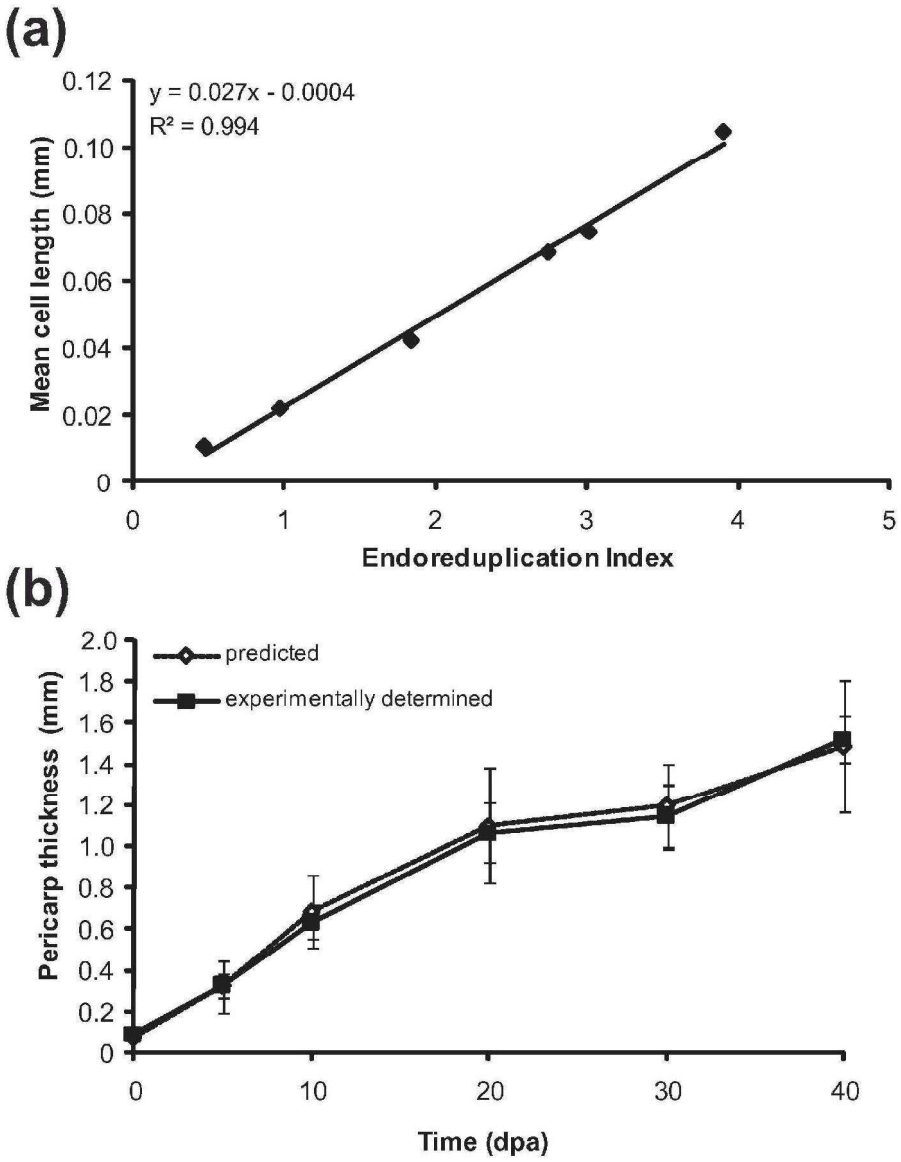

Figure 4. Modelling pericarp growth.
(a) Relationship between EI and mean cell size in pericarp. Data used to establish the linear regression were obtained from developing Wva106 fruits and extracted from Cheniclet et al. (2005).
(b) Evolution of pericarp thickness during fruit development. Experimentally determined values for pericarp thickness from Cheniclet et al. (2005) were compared to predicted values using the following equation: Predicted value = (EI x 0.0271 – 0.0048) x 2DI.

85x109mm (600 x 600 DPI)

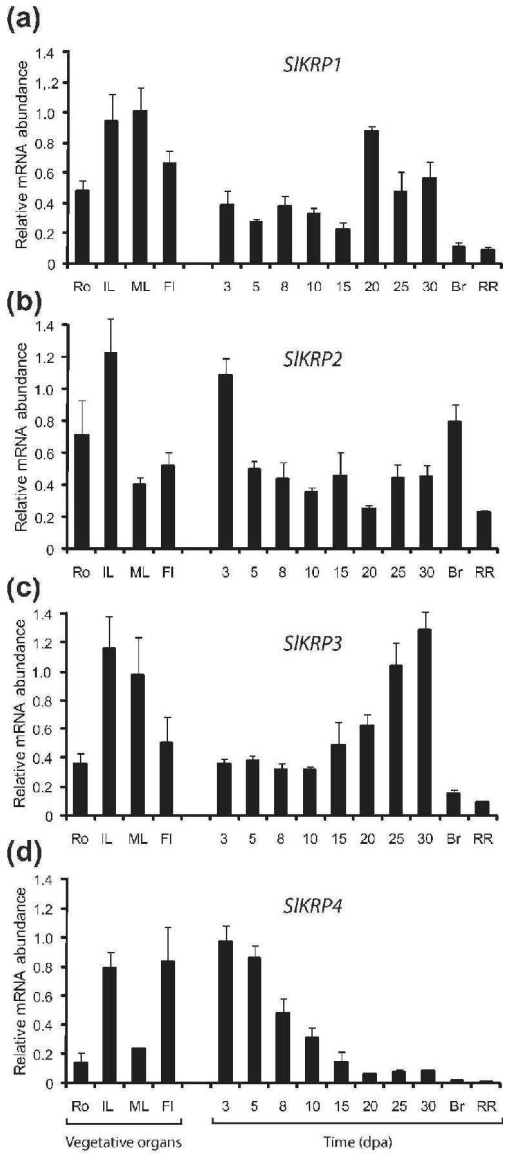

Figure 5. Gene expression analysis of ICK/KRP gene in tomato.
Quantitative RT-PCR analysis of SlKRP1 (a), SlKRP2 (b), SlKRP3 (c) and SlKRP4 (d) expression in tomato vegetative organs and developing fruits were performed using total RNA isolated from roots (Ro), immature (IL) and mature (ML) leaves, flowers at 7 mm stage (Fl), and fruits harvested at 3, 5, 8, 10, 15, 20, 25 and 30 dpa and Breaker (Br) and Red Ripe (RR) stage. All values were normalized to the SlActin and SleiF4A housekeeping genes. The ΔΔCt method was used for relative quantification of mRNA abundance. Data are mean ± standard deviation (n=3).

85x199mm (600 x 600 DPI)

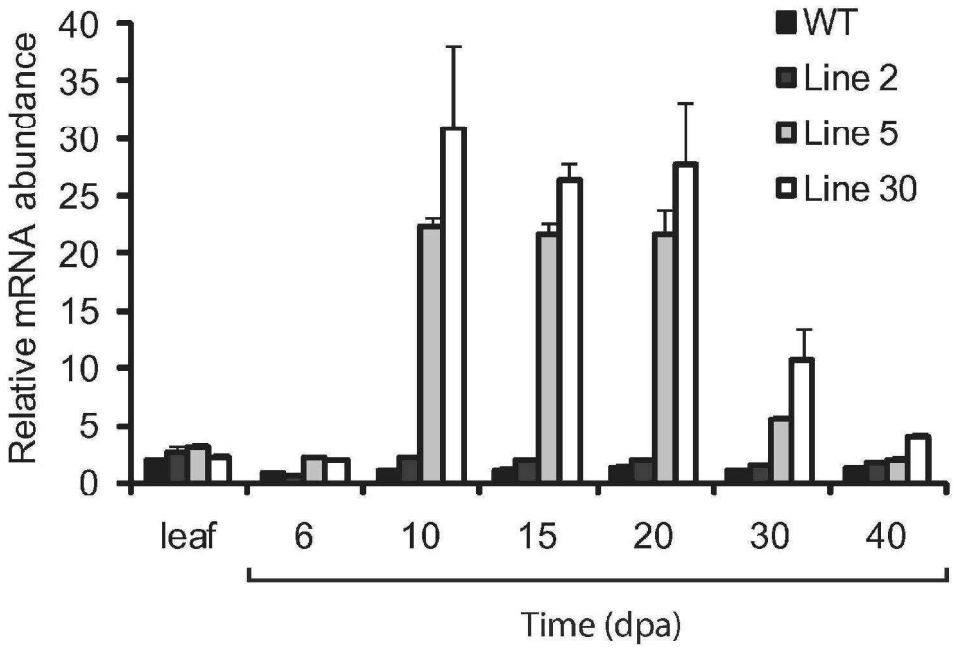

Figure 6. Quantitative RT-PCR analysis of SlKRP1 expression in leaf and pericarp from developing fruits (at 6, 10, 15, 20, 30 and 40 dpa) from ProPEPC2:SlKRP1OE T1 lines 2, 5 and 30 compared with WT. Quantification and normalisation of expression were as in Figure 5.
85x59mm (600 x 600 DPI)

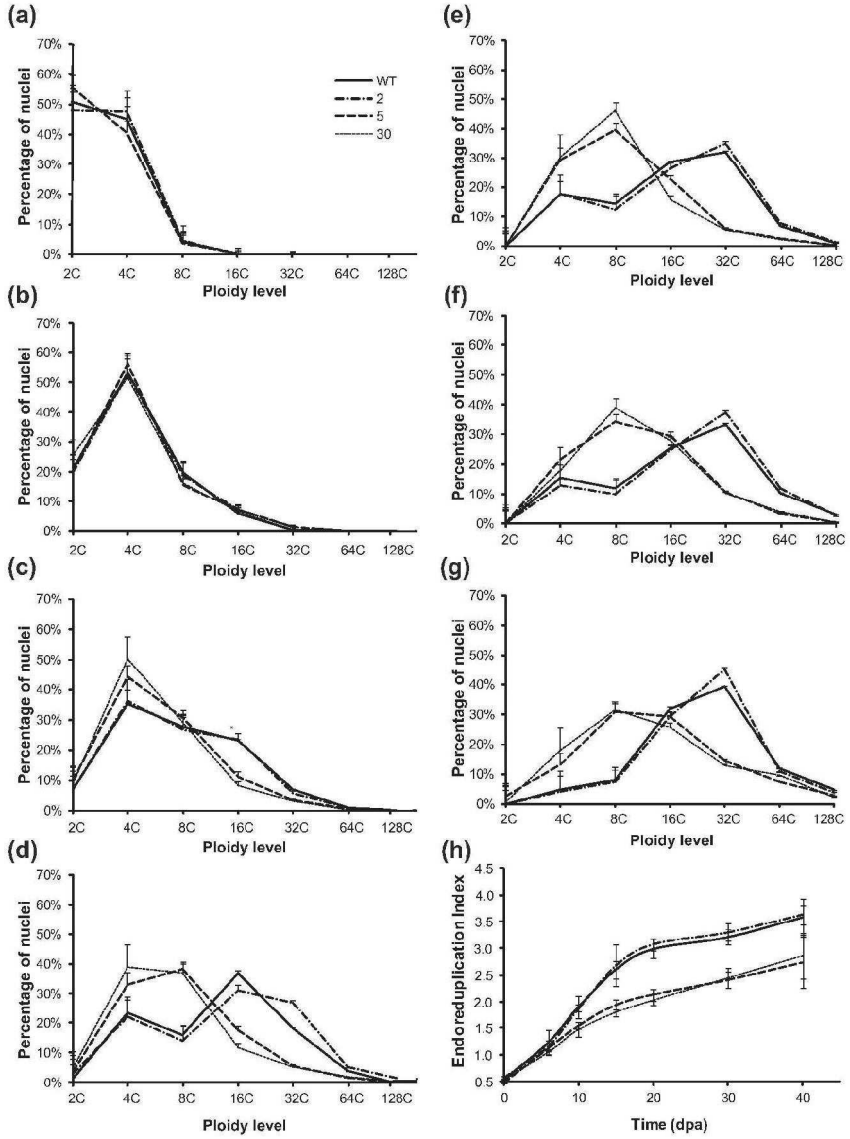

Figure 7. Effects on endoreduplication of SlKRP1 overexpression during fruit development. (a) to (g) Ploidy level distribution in ProPEPC2:SlKRP1OE fruit pericarp as measured by flow cytometry during fruit development at Anthesis (a), 6 (b), 10 (c), 15 (d), 20 (e), 30 (f) and 40 dpa (g).
(h) Evolution of Endoreduplication index during fruit development. Values are mean ± standard error (n>4).

175x239mm (600 x 600 DPI)

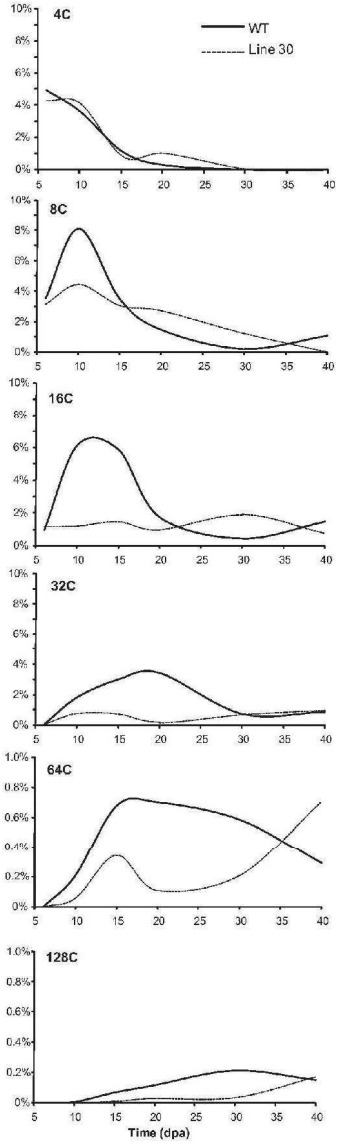

Figure 8. Kinetics of endoreduplication in the representative ProPEPC2:SlKRP1OE line 30 compared to WT, in the course of fruit development. The frequency of appearance of each DNA ploidy level referred to as EF was calculated as described in Experimental Procedures.
85x297mm (600 x 600 DPI)

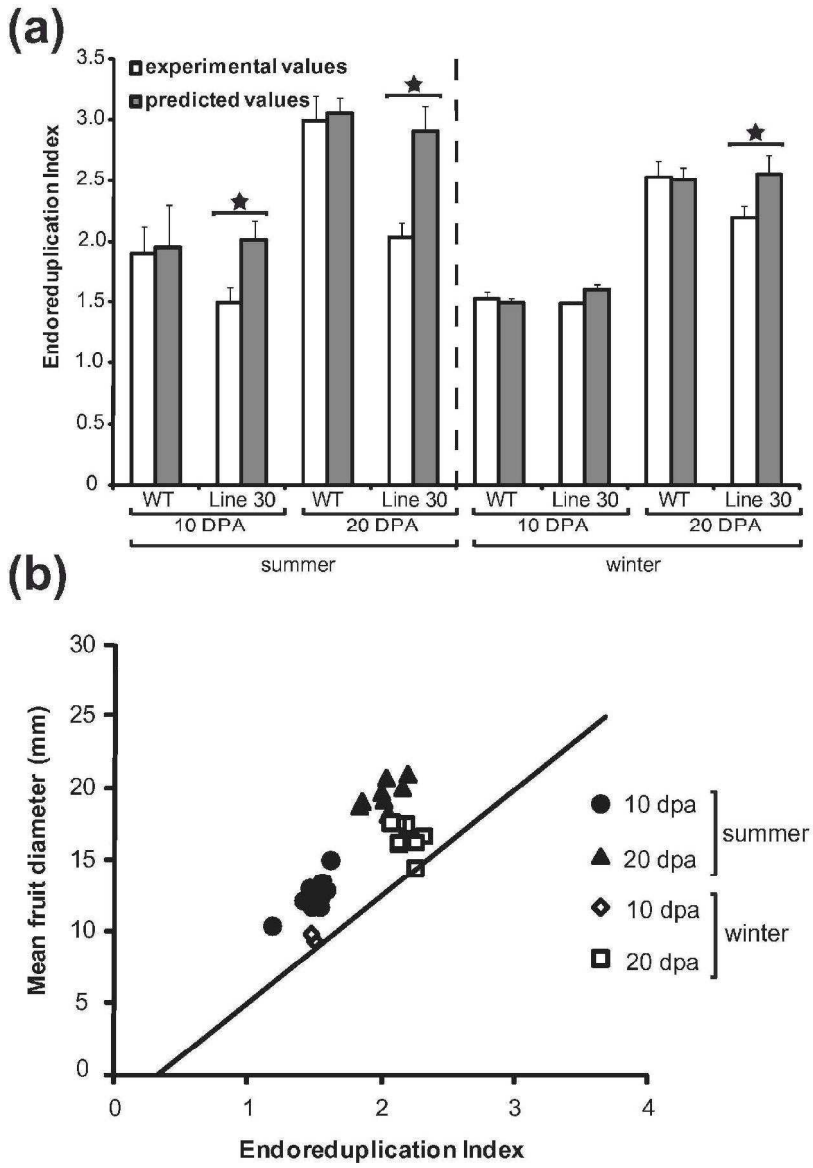

Figure 9. Phenotypical analysis of ProPEPC2:SlKRP1OE lines compared to WT.
(a) Comparison between experimentally determined EI and predicted EI. EI were determined experimentally by flow cytometry using nuclei preparations from 10 and 20 dpa pericarp from WT and ProPEPC2:SlKRP1OE fruits harvested from plants cultivated in summer (July-August 2009) and winter (December 2009-January 2010). The predicted EI were obtained using the linear regression obtained from data of mean fruit diameter (as described in Figure S1). Star symbols above bars indicate that Student's tests are significantly different ($P \leq 0.001$) from WT.
(b) Absence of relationship between the Mean fruit diameter of ProPEPC2:SlKRP1OE fruits and EI. Data were obtained from 10 and 20 dpa fruits harvested from plants cultivated in summer (July-August 2009) and winter (December 2009-January 2010).

85x120mm (600 x 600 DPI)

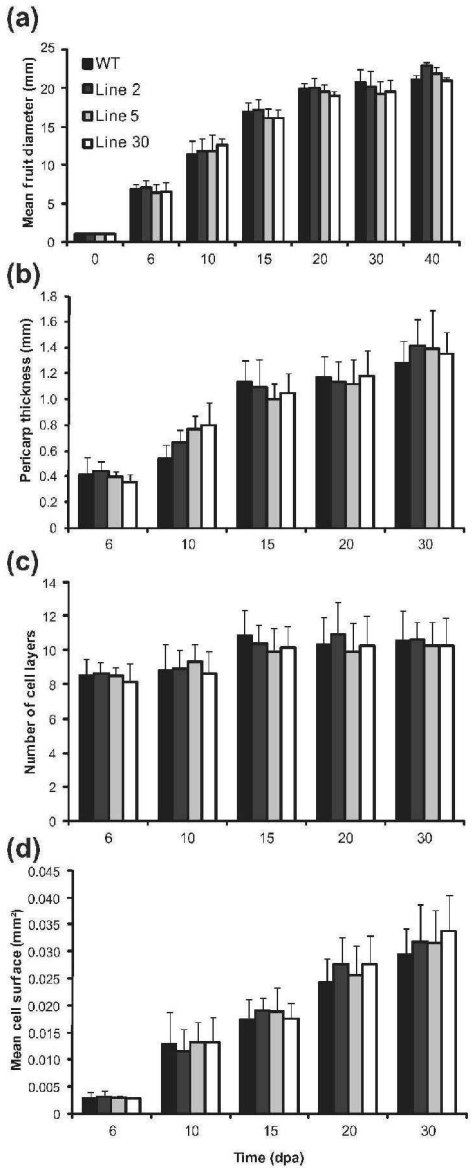

Figure 10. Morphological and cytological analysis of ProPEPC2:SlKRP1OE fruits compared to WT in the course of fruit development.
(a) Evolution of Mean Fruit Diameter.
(b) Evolution of pericarp thickness.
(c) Number of cell layers in the Z-axis of the pericarp.
(d) Mean cell size in the Z-axis in pericarp.

85x210mm (600 x 600 DPI)

Supplementary figure legends

Supplemental Figure S1. Relationship between EI and Mean Fruit Diameter in wild type tomato (cv. Wva106) fruits harvested from 2 different cultures. Fruits at 10 and 20 dpa were harvested from plants grown in the greenhouse during the summer period (July-August 2009) (♦) and during the winter period (December 2009-January 2010) (**x**). The linear regression corresponds to that calculated in Figure 2b.

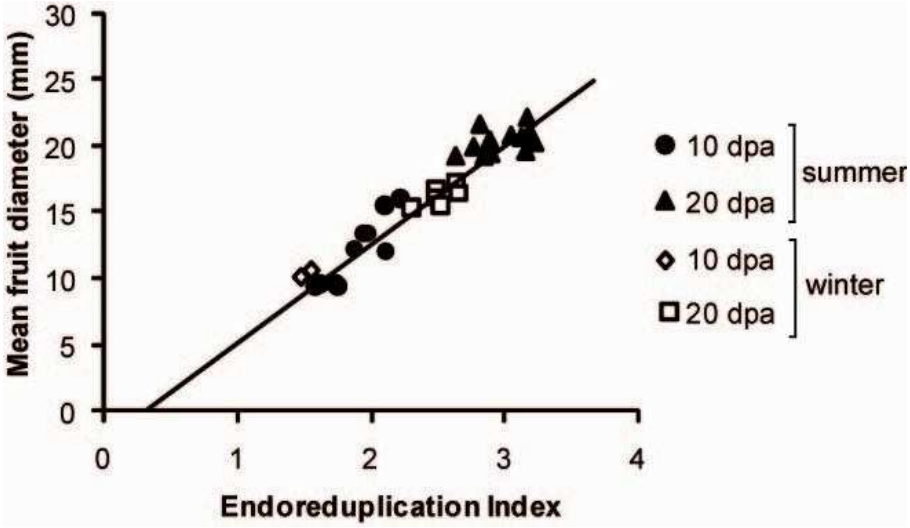

Supplemental Figure S2. Relationship between EI and mean cell size in pericarp from the 20 different tomato lines differing in fruit weight described in Cheniclet *et al*. (2005). Each point (△) represents one tomato line (fruit harvested at the breaker stage). Data obtained from developing Wva106 fruits (values from Figure 2d) (■) were compared.

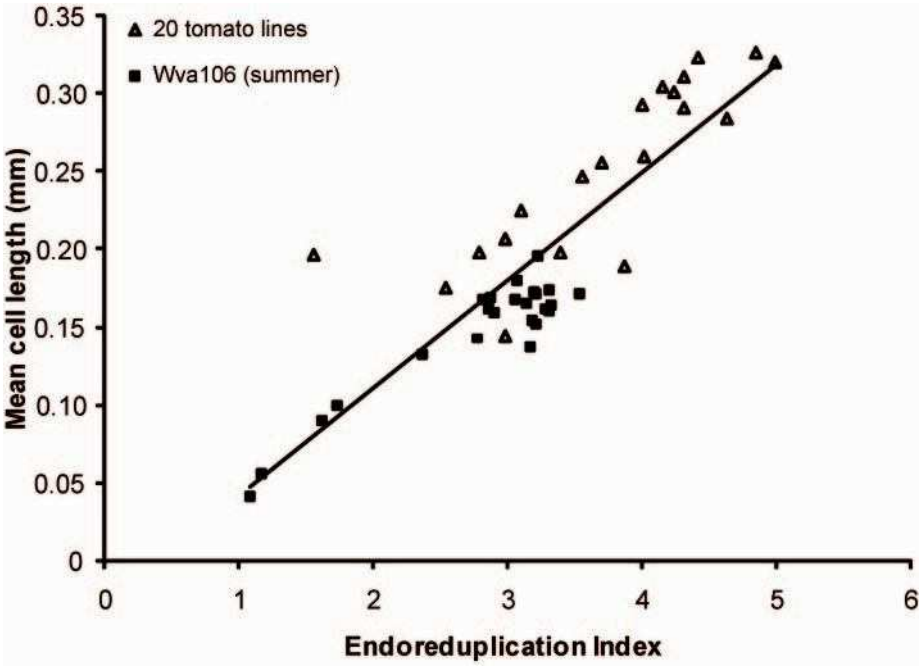

Supplemental Figure S3. Comparison of the effects of the SlKRP1 over-expression in *ProPEPC2:SlKRP1*^{OE} lines 5 and 30 relative to WT.

(a) Evolution of the Endoreduplication Ratio representing the relative increase or decrease of endoreduplication in *ProPEPC2:SlKRP1*^{OE} lines 5 and 30 relative to WT. (b) Quantitative RT-PCR analysis of *SlCYCA3;1 and SlCYCD3;1* expression in pericarp during fruit development (at 10, 15, 20 and 30 dpa) from *ProPEPC2:SlKRP1*^{OE} T1 lines 5 and 30 compared with WT. Quantification and normalisation of expression were as in Figure 5.

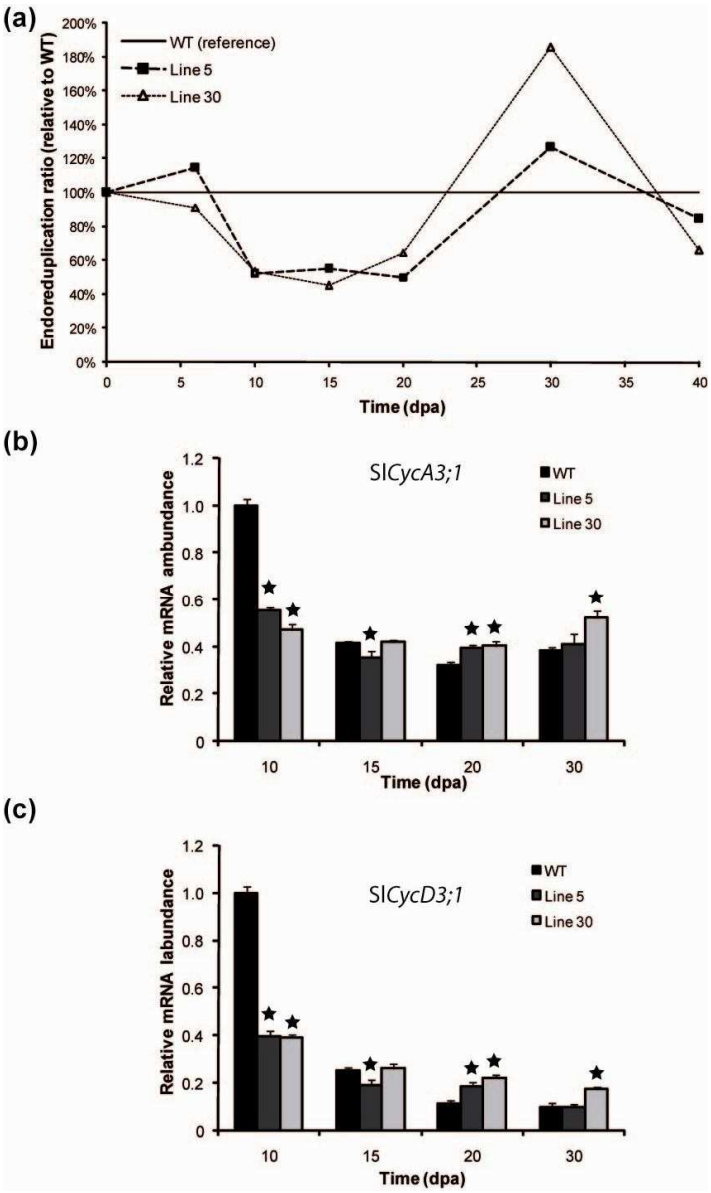

Supplemental Figure S4. Relationship between endoreduplication and nuclear size. (a) Relationship between the mean nuclear area determined by imaging from the different classes of area and their associated C-value determined by flow cytometry using isolated nuclei from 10 and 20 dpa WT fruit pericarp; (b) Relationship between the frequency of a given class of nuclear area (determined by imaging) and the frequency of a given ploidy level (determined by flow cytometry) from 10 and 20 dpa WT (■) and *ProPEPC2:SlKRP1*^{OE} (▲) fruits. The correlation line drawn has been calculated according to WT values; (c) Comparison of the frequencies of the different classes of ploidy levels measured by flow cytometry (dark grey bars) and ploidy levels estimated from nuclear area measurements (light grey bars) in 20 dpa fruits from WT and line 30. Values for 2C nuclei were excluded deliberately as the percentage of 2C nuclei was very low and tended to be drowned in background generated by tissue and cell debris following chopping.

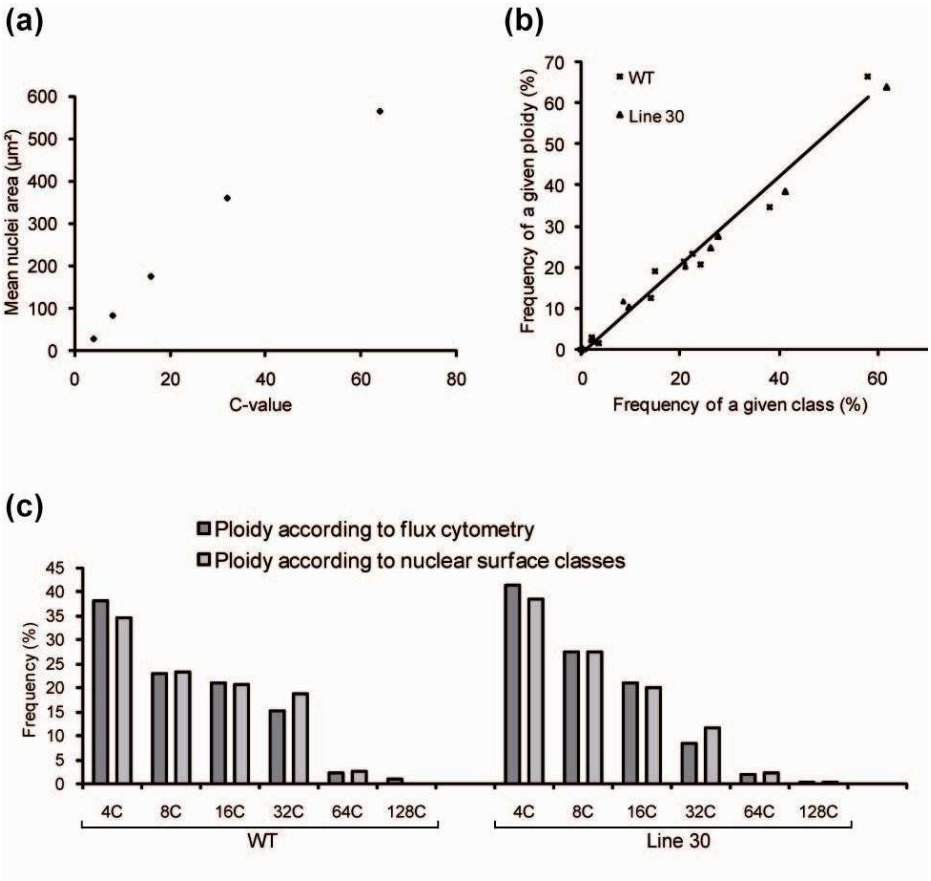

Supplemental Table S1. Endoreduplication Index (EI) and Division index (DI) values used for predicting the pericarp thickness evolution during fruit development.

Time (DPA)	EI value	DI value
0	0,48	3,11824897
5	0,98	3,87883431
10	1,84679416	3,90902634
20	2,75	3,98117613
30	3,02	3,95729555
40	3,9068906	3,87446912

Supplemental Table S2. Metabolomic data from GC-MS profiling of tomato pericarp from WT and transgenic lines 2, 5 and 30 at 15, 20, 30 and 40 days post-anthesis

Sample	Lactate	Alanine	Valine	Glycerol	Leucine	Isoleucine	Glycine	Phosphate
Line2.1-15-1	0,207942058	0,520531395	0,621239466	0,035634254	0,189787791	0,300897895	0,054778251	1,411040743
Line2.1-15-2	0,159232034	0,465317443	0,578570374	0,028760538	0,173095274	0,272682337	0,05027409	1,220771776
Line2.1-15-3	0,269991546	0,484815595	0,586621676	0,028527625	0,173837976	0,280290005	0,051094681	1,320996676
Line2.1-15-3	0,217262989	0,459277946	0,566664785	0,032288336	0,174102094	0,274773781	0,111535691	1,289279366
Line2.2-15-1	0,127644387	0,45740309	0,641869047	0,027681362	0,228557037	0,317468619	0,077516073	1,471277719
Line2.2-15-2	0,184295116	0,511735253	0,66184858	0,033865579	0,238003777	0,337398764	0,084201346	1,621038898
Line30.1-15-1	0,298478719	0,569911213	0,931705263	0,039875515	0,297962471	0,438440275	0,100836613	1,415644851
Line30.1-15-2	0,204037704	0,539024378	0,918272264	0,030187425	0,288255108	0,409873859	0,085114618	1,363278283
Line30.2-15-1	0,172912969	0,536209858	0,996895306	0,029541329	0,295893344	0,469471838	0,0782447	1,62569321
Line30.2-15-2	0,268109226	0,519513953	1,001670002	0,029366071	0,301679404	0,471186866	0,075360528	1,537704889
Line30.3-15-1	0,172761069	0,425620743	0,663896667	0,027325416	0,212984623	0,340483081	0,042076305	1,244640001
Line30.3-15-2	0,163791973	0,432150787	0,663649435	0,028524282	0,21721986	0,338287836	0,043240049	1,280325778
Line5.1-15-1	0,186439255	0,426842949	0,772584707	0,031593407	0,24508547	0,390876832	0,052594628	1,435061813
Line5.1-15-2	0,153483879	0,37896889	0,745624591	0,027158139	0,237977256	0,369112509	0,051980229	1,296253576
Line5.2-15-1	0,198335262	0,318221873	0,50296036	0,032693131	0,180969469	0,29002679	0,039052685	1,611026765
Line5.2-15-2	0,191810085	0,302992927	0,503480697	0,032961208	0,176895313	0,277532843	0,044836165	1,507319173
Line5.3-15-1	0,183866967	0,411924139	0,46357111	0,032122394	0,119874951	0,201471295	0,038054375	1,08094566
Line5.3-15-2	0,123742881	0,338465438	0,418615719	0,022412105	0,112287717	0,186933619	0,03447311	0,943464737
WT1-15-1	0,215778584	0,39701761	0,548658258	0,03736416	0,130969359	0,258274978	0,047104165	1,065908744
WT1-15-2	0,213418008	0,368925942	0,486315968	0,05450942	0,126166051	0,241275479	0,043947601	0,978358168
WT2-15-1	0,155075444	0,416688068	0,497332133	0,035474627	0,136784842	0,234307019	0,064936733	1,56485289
WT5-15-1	0,157725865	0,463476837	0,558417237	0,037694376	0,142312438	0,255926798	0,047618406	1,232007884
WT5-15-2	0,214501412	0,408401405	0,535225815	0,042932827	0,138471855	0,239911685	0,045463577	1,121160839
WT5-15-2	0,137912058	0,404235846	0,533943647	0,026126953	0,13906552	0,231124336	0,049389127	1,144917555
Line2.1-20-1	0,124587076	0,284771131	0,389543511	0,030123409	0,152748262	0,250915743	0,045797721	1,210654026
Line2.1-20-2	0,212159059	0,287721363	0,398595426	0,03240391	0,156484768	0,259831071	0,046852045	1,289775078
Line2.2-20-1	0,246803659	0,369768353	0,604020955	0,027263317	0,238109893	0,361434786	0,068340141	1,457895031
Line2.2-20-2	0,153502354	0,371278241	0,53720635	0,035679075	0,220418781	0,322391612	0,066681196	1,245917178
Line2.3-20-1	0,168250366	0,43348048	0,64460711	0,062508313	0,252390097	0,365501962	0,072338887	1,472416201
Line2.3-20-2	0,197525817	0,392465473	0,624877802	0,027310215	0,245067631	0,348740691	0,069808571	1,367563676
Line30.1-20-1	0,188569259	0,282814013	0,25737017	0,03347954	0,098543625	0,149803475	0,022603247	1,182967815
Line30.1-20-2	0,107577152	0,305108684	0,262742184	0,025801784	0,100943392	0,150386559	0,03710083	1,150475141
Line30.2-20-1	0,151422987	0,287109348	0,492136338	0,025522819	0,2309112	0,349079024	0,058523934	1,374117364
Line30.2-20-2	0,160950245	0,289838941	0,528811958	0,02817489	0,242371016	0,360744465	0,059833747	1,393347161
Line30.3-20-1	0,140739008	0,275414842	0,320623251	0,034070293	0,12416777	0,20493961	0,029068714	1,407795732
Line30.3-20-2	0,121372435	0,257280631	0,311371276	0,03207604	0,119707894	0,200973687	0,025158224	1,30853831
Line5.1-20-1	0,156512771	0,208319876	0,235513501	0,024327621	0,102582151	0,16483235	0,02780989	1,468886409
Line5.1-20-2	0,104644701	0,205394178	0,236482744	0,028401731	0,10226454	0,162871683	0,023819921	1,307903142
Line5.2-20-1	0,154305217	0,256810381	0,273611133	0,026697936	0,118839983	0,183367761	0,037868669	1,577286564
Line5.2-20-2	0,114907367	0,241004643	0,26104564	0,026362597	0,110297513	0,167891018	0,037480478	1,416826472
Line5.3-20-1	0,152549927	0,22504541	0,252046851	0,025558586	0,066748108	0,11995742	0,024175849	1,13941513
Line5.3-20-2	0,129144422	0,205001395	0,24543237	0,025844908	0,063335105	0,112946583	0,023747719	1,046737622
WT1-20-1	0,141603977	0,30392183	0,379597045	0,023436211	0,140649208	0,250287939	0,051816635	1,242307276
WT1-20-2	0,116723583	0,305275922	0,377074981	0,037955951	0,148393962	0,256421678	0,04264291	1,128458302
WT2-20-1	0,1109703	0,187093444	0,124533254	0,022931105	0,053254814	0,082762456	0,01870676	1,09011001
WT2-20-2	0,157454889	0,196680257	0,12242588	0,034730644	0,053118588	0,079442077	0,016188705	0,981596657
WT5-20-1	0,137910196	0,256404312	0,311422335	0,047305686	0,119367356	0,189759824	0,037371608	1,481027688
WT5-20-2	0,129645852	0,24450594	0,313889937	0,031628073	0,122519903	0,193756183	0,035861862	1,399295018
Line2.1-30-1	0,293837825	0,252423132	0,163518468	0,036615623	0,124700501	0,15661011	0,0336511	1,331070724
Line2.1-30-2	0,129068047	0,228255947	0,151547971	0,025264914	0,11299209	0,151993268	0,019204353	1,352621966
Line2.1-30-3	0,120823778	0,23750134	0,161460493	0,029009282	0,122773544	0,159487008	0,019915121	1,363208545
Line2.3-30-1	0,137440545	0,243041128	0,098750879	0,026646876	0,149173943	0,166683964	0,020521698	1,382473139
Line2.3-30-2	0,182295159	0,235670636	0,099929807	0,032119307	0,151364944	0,162702797	0,019804371	1,361159927
Line2.3-30-3	0,186779669	0,275587347	0,103370146	0,031583759	0,151836672	0,173745307	0,020908656	1,482601227
Line30.1-30-1	0,156951001	0,317293186	0,070965883	0,035417726	0,090198408	0,078756123	0,016746446	1,722666673
Line30.1-30-2	0,171764889	0,292747633	0,067822549	0,024087498	0,087451775	0,073513375	0,014575296	1,615420214
Line30.2-30-1	0,20594421	0,267930594	0,085841276	0,025519103	0,140480426	0,130487897	0,02035569	1,725909647
Line30.2-30-2	0,144524817	0,257721259	0,085874341	0,028103709	0,14082179	0,127589983	0,018993494	1,621601074
Line30.3-30-1	0,212694463	0,214752333	0,021391767	0,031292565	0,044172236	0,028982859	0,011055651	1,401171546
Line30.3-30-2	0,17830434	0,250079862	0,023419204	0,037524673	0,046563385	0,029496138	0,009551735	1,310216654
Line5.1-30-1	0,274378208	0,202181208	0,018958087	0,031912094	0,023699664	0,016120542	0,009882057	1,645524905
Line5.1-30-2	0,171816603	0,214312622	0,021837201	0,029677624	0,027845099	0,017337077	0,010461629	1,66666512
Line5.2-30-1	0,24392006	0,263625732	0,047282437	0,032478237	0,053884257	0,049393902	0,015219309	1,626965279
Line5.2-30-2	0,28664164	0,258952181	0,049820404	0,041934383	0,058914371	0,052604572	0,020903357	1,62282625
Line5.3-30-1	0,178687409	0,214660718	0,057278941	0,03134955	0,038432097	0,044335509	0,014226951	1,55344385
Line5.3-30-2	0,135546109	0,202868474	0,058971005	0,024198823	0,039874394	0,044159078	0,013793161	1,485288692
WT1-30-1	0,154994574	0,229703169	0,123568162	0,035280016	0,092298805	0,123223406	0,020486159	1,280626291
WT1-30-2	0,187442157	0,230115719	0,118738494	0,037696418	0,088303439	0,112930312	0,021116533	1,152195257
WT2-30-1	0,184690148	0,200972715	0,093318574	0,033974351	0,067469804	0,085138037	0,025526887	0,914842336
WT2-30-2	0,190937791	0,214348985	0,096980734	0,046113558	0,071844557	0,086487087	0,022167025	0,869907024
WT5-30-1	0,142980715	0,232510583	0,137615301	0,033687307	0,099766409	0,122834501	0,020493012	1,546694251
WT5-30-2	0,124653049	0,215462151	0,131956522	0,031538606	0,098180379	0,119795367	0,019227314	1,453415415
Line2.1-40-1	0,259341638	0,357173602	0,031656507	0,036206732	0,046842301	0,047253644	0,026699178	1,439427511
Line2.1-40-2	0,224889569	0,32000491	0,032549049	0,030923515	0,045912956	0,047504925	0,024234368	1,313920904
Line2.1-40-3	0,148373222	0,363329545	0,031131863	0,028708698	0,044782913	0,048450855	0,022675681	1,49065318
Line2.3-40-1	0,187880188	0,401057828	0,056687367	0,030336229	0,075779783	0,077585458	0,040422789	1,431670087
Line2.3-40-2	0,161949949	0,463472093	0,058083154	0,028313845	0,074342884	0,082910657	0,038675562	1,610165906
Line2.3-40-3	0,12832119	0,389131008	0,050390662	0,038118315	0,064777578	0,070521126	0,03272252	1,3286667
Line30.1-40-1	0,231772698	0,458689888	0,039088107	0,034472428	0,044057219	0,038823031	0,032162485	1,372274457
Line30.1-40-2	0,103971741	0,413358322	0,036629298	0,027282446	0,043860154	0,038294267	0,030602786	1,309557397
Line30.2-40-1	0,136261724	0,419275077	0,028542587	0,031910225	0,040922157	0,038876049	0,026899937	1,540126356
Line30.2-40-2	0,142780982	0,385176135	0,027804902	0,035362981	0,040057315	0,037730209	0,02514177	1,439069198
Line30.3-40-1	0,154148929	0,456577569	0,038999024	0,032874436	0,04381272	0,039118196	0,034785444	1,345574847
Line30.3-40-2	0,11737012	0,426071867	0,037082861	0,035030727	0,041804762	0,035832653	0,029870506	1,255766646
Line5.1-40-1	0,211938564	0,830896677	0,086874064	0,028992394	0,090045945	0,079519755	0,057312464	1,686760058
Line5.1-40-2	0,106463409	0,710824729	0,083753384	0,029514419	0,083628972	0,07171889	0,051262641	1,44994368
Line5.2-40-1	0,215008918	0,694625286	0,050615764	0,037298503	0,050912457	0,041367431	0,045343112	1,502307421
Line5.2-40-2	0,151573551	0,611136166	0,046474981	0,03077793	0,049467702	0,039225146	0,036983335	1,398816079
Line5.3-40-1	0,179046285	0,558829238	0,037620516	0,034324472	0,042204566	0,037602627	0,032929132	1,35719186
Line5.3-40-2	0,159672437	0,534577723	0,041149385	0,02998776	0,047589905	0,03897826	0,051397875	1,241310641
WT1-40-1	0,174079657	0,310578046	0,02199423	0,026413404	0,034706977	0,034271971	0,018672736	1,56248882
WT1-40-2	0,117773479	0,286025044	0,020256138	0,037015868	0,030452251	0,030017817	0,015770476	1,24671034
WT2-40-1	0,205574239	0,359380152	0,020745137	0,032293659	0,026482031	0,025646774	0,016542477	1,349014177
WT2-40-2	0,101479074	0,318661246	0,017998988	0,027253737	0,022996366	0,023108771	0,01425681	1,101357301
WT5-40-1	0,189878486	0,523940656	0,063976895	0,032726739	0,070675741	0,066813268	0,041010616	1,614271628

Sample	Proline	Benzoate	Serine	Succinate	Threonine	Fumarate	Nonanoate	Nicotinate
Line2.1-15-1	0,108113309	0,00856058	0,194393392	0,00150234	0,058749004	0,001474738	0,00417974	0,007700974
Line2.1-15-2	0,100977249	0,007418614	0,179127993	0,001360151	0,054247275	0,002849022	0,003925987	0,008847416
Line2.1-15-3	0,100040119	0,007210712	0,17375917	0,00121074	0,055382422	0,001157009	0,004846544	0,008328318
Line2.1-15-3	0,098533103	0,007848602	0,183144026	0,001407188	0,05576143	0,002814376	0,00472627	0,008327645
Line2.2-15-1	0,083314754	0,008766835	0,169666475	0,001935952	0,060454921	0,003101193	0,004156333	0,009376981
Line2.2-15-2	0,083978829	0,009131019	0,178630683	0,001944099	0,061188368	NA	0,004930516	0,008252661
Line30.1-15-1	0,164463158	0,008915332	0,235057208	0,001658581	0,098310297	0,001080092	0,00593135	0,008150114
Line30.1-15-2	0,16599664	0,006920215	0,221382498	0,001553025	0,096195008	0,003464131	0,003664116	0,008545661
Line30.2-15-1	0,261562414	0,008469993	0,229293521	0,001545619	0,111797366	0,001371055	0,005909721	0,008997322
Line30.2-15-2	0,271767113	0,006988937	0,225418956	0,001495391	0,109602289	0,003666841	0,002919146	0,010463258
Line30.3-15-1	0,239630815	0,007667048	0,152661739	0,001518474	0,072118616	0,0012731	0,005323549	0,01008167
Line30.3-15-2	0,248245324	0,006180122	0,159517909	0,001394169	0,071260766	0,003229478	0,002463726	0,009068341
Line5.1-15-1	0,175553266	0,008402015	0,189064408	0,001095085	0,074526862	0,001346917	0,005074786	0,006929182
Line5.1-15-2	0,155486802	0,009777263	0,18256166	0,001378311	0,070248054	0,002727473	0,005013554	0,007524495
Line5.2-15-1	0,068033422	0,007952096	0,143212052	0,001737641	0,062024228	0,001305885	0,005248313	0,007300923
Line5.2-15-2	0,066753444	0,008017236	0,145508686	0,001701421	0,060778787	0,003302244	0,004373833	0,008082844
Line5.3-15-1	0,337886486	0,008696163	0,157766248	0,001488092	0,043130195	0,000958086	0,005777057	0,008932627
Line5.3-15-2	0,288690875	0,007270084	0,145955697	0,001076164	0,039650653	0,002347631	0,003790488	0,008099128
WT1-15-1	0,129073804	0,008170366	0,147317584	0,002232709	0,060582834	0,001187531	0,00452161	0,006780542
WT1-15-2	0,124785098	0,006486432	0,139035456	0,001956725	0,052728125	0,00414286	0,002667444	0,008339698
WT2-15-1	0,086014545	0,007107766	0,184409141	0,001669305	0,04800197	0,001559781	0,003731388	0,007836671
WT5-15-1	0,203126955	0,008103213	0,164050606	0,001605245	0,044892955	0,001381973	0,004253706	0,008380378
WT5-15-2	0,201265289	0,006470327	0,159826933	0,001370288	0,043202602	0,002864758	0,003061737	0,008101826
WT5-15-2	0,202552044	0,006241276	0,166442406	0,001363182	0,043412099	0,004148267	0,00285639	0,009080888
Line2.1-20-1	0,045732001	0,007149439	0,15283276	0,001281548	0,06840084	0,003055998	0,004107524	0,007872363
Line2.1-20-2	0,042759799	0,007322767	0,150638702	0,001442536	0,068562209	0,001503274	0,004145392	0,007531555
Line2.2-20-1	0,053820222	0,007749552	0,14175456	0,001370859	0,062660866	0,001304415	0,003878273	0,007455797
Line2.2-20-2	0,051017549	0,011851514	0,123122905	0,001639702	0,053010098	0,003736029	0,008357635	0,012377325
Line2.3-20-1	0,056086226	0,008259344	0,16427657	0,001550446	0,079450984	0,001575386	0,00575286	0,008961825
Line2.3-20-2	0,052727467	0,007634063	0,158249054	0,001324185	0,080761984	0,003239367	0,005807753	0,008229502
Line30.1-20-1	0,117626507	0,006862242	0,106294503	0,001310168	0,043793791	0,001355739	0,003167189	0,008396468
Line30.1-20-2	0,136065905	0,007470362	0,124072971	0,001299193	0,044669616	0,0030659	0,004059979	0,009050063
Line30.2-20-1	0,071068867	0,007485453	0,165753408	0,001331065	0,101457946	0,00187852	0,002479646	0,007850423
Line30.2-20-2	0,080692305	0,006275666	0,174573915	0,001597195	0,106437467	0,004578929	0,003185342	0,010592166
Line30.3-20-1	0,069732979	0,007418218	0,141446738	0,001303259	0,057162141	0,001825425	0,00252884	0,009541408
Line30.3-20-2	0,072400603	0,006426336	0,140248058	0,001432711	0,054563579	0,004270314	0,002276574	0,008396893
Line5.1-20-1	0,104226762	0,006507908	0,135648857	0,001228818	0,042756175	0,001637186	0,003912912	0,007443443
Line5.1-20-2	0,099902688	0,008513653	0,125356681	0,001473869	0,041053203	0,002837884	0,0042019	0,007103866
Line5.2-20-1	0,038027863	0,007054996	0,117034495	0,001549226	0,051590383	0,001603585	0,003506143	0,008231475
Line5.2-20-2	0,03562891	0,007363901	0,115322592	0,001550741	0,049250857	0,002847262	0,004991183	0,007902
Line5.3-20-1	0,201695195	0,007037929	0,133564351	0,001226427	0,030600565	0,0016673	0,002817577	0,007747334
Line5.3-20-2	0,186008875	0,007328379	0,127777715	0,001192334	0,028762121	0,003176416	0,003765514	0,008308638
WT1-20-1	0,087554815	0,008582274	0,161284999	0,001419731	0,070929764	0,00142328	0,004922917	0,010477615
WT1-20-2	0,084444444	0,007349666	0,155520911	0,001747092	0,070744865	0,003989112	0,002558773	0,008913635
WT2-20-1	0,055082655	0,007263363	0,090287994	0,00125918	0,024854954	0,001321954	0,004383127	0,009545395
WT2-20-2	0,060361156	0,006963453	0,087998414	0,001539948	0,022810482	0,002617912	0,003113583	0,010447586
WT5-20-1	0,099248047	0,007542326	0,146306443	0,0012094	0,048117104	0,001379411	0,004559398	0,008639673
WT5-20-2	0,099781858	0,006698856	0,149208555	0,00118379	0,047871523	0,002957153	0,003504946	0,008764685
Line2.1-30-1	0,040843059	0,007010277	0,22870695	0,00111225	0,04571303	0,003802034	0,004050185	0,008698592
Line2.1-30-2	0,036438836	0,00701908	0,20719116	0,001007578	0,042337127	0,001686843	0,004018989	0,008453085
Line2.1-30-3	0,037681231	0,008235505	0,213212293	0,00120022	0,043905299	0,003671821	0,004639588	0,008562838
Line2.3-30-1	0,026466724	0,007049438	0,208980593	0,000889012	0,048927017	0,001903348	0,004260994	0,007601644
Line2.3-30-2	0,025920359	0,008365123	0,209879326	0,001119959	0,048563803	0,003687107	0,004295479	0,008452692
Line2.3-30-3	0,026943163	0,008986826	0,222268109	0,001082229	0,048665655	0,002216404	0,006233637	0,007978189
Line30.1-30-1	0,092344578	0,008517487	0,197973273	0,001221301	0,023841059	0,001375446	0,007584713	0,008074815
Line30.1-30-2	0,094311007	0,006575149	0,19179733	NA	0,023372708	0,003404415	0,003528129	0,008925708
Line30.2-30-1	0,058806943	0,008084865	0,185486778	0,001184569	0,051990221	0,001795022	0,006842157	0,009149523
Line30.2-30-2	0,059987323	0,006248591	0,189366889	0,00126424	0,051415265	0,00482205	0,002716407	0,008742901
Line30.3-30-1	1,126726614	0,008177512	0,065531625	0,001845607	0,011077237	0,001194428	0,005680727	0,01108803
Line30.3-30-2	1,215148861	0,006500045	0,065963033	0,002015067	0,011233602	0,003871467	0,003501245	0,009345468
Line5.1-30-1	0,402104718	0,007735393	0,080746644	0,001850572	0,006892354	0,001299513	0,005124029	0,00748565
Line5.1-30-2	0,439648229	0,008777562	0,088921529	0,001939229	0,007636293	0,002922761	0,004295995	0,0075899
Line5.2-30-1	0,039662804	0,010481486	0,14021881	0,001309188	0,013806344	0,001728288	0,005200829	0,007587702
Line5.2-30-2	0,048597727	0,007723979	0,157636944	0,001487836	0,015241724	0,003810431	0,006643703	0,009069415
Line5.3-30-1	0,420773668	0,008346736	0,199590975	0,001237126	0,01196533	0,001561872	0,00595367	0,00893437
Line5.3-30-2	0,428946353	0,007039124	0,196743305	0,001391893	0,012246147	0,003706126	0,003328805	0,008162701
WT1-30-1	0,054793198	0,007178583	0,191883451	0,001620353	0,035463886	0,001942125	0,004313279	0,008588252
WT1-30-2	0,048799627	0,007343104	0,178073682	0,001457722	0,032692026	0,004037118	0,002783749	0,00831946
WT2-30-1	0,04613132	0,006335598	0,219685104	0,001181546	0,025126496	0,001962701	0,003670251	0,008631958
WT2-30-2	0,055635664	0,006433989	0,226032276	0,001268953	0,025795438	0,004079486	0,004069572	0,01091498
WT5-30-1	0,046419204	0,007713281	0,280237258	0,001327402	0,030043928	0,001981137	0,0035796	0,008610174
WT5-30-2	0,046378024	0,007414866	0,274350037	0,001239847	0,029272011	0,003424109	0,00393264	0,009298852
Line2.1-40-1	0,353815001	0,007459316	0,052736814	0,00309992	0,029769414	NA	0,00502942	0,008816327
Line2.1-40-2	0,35287523	0,00748513	0,048957836	0,003121601	0,0295713	0,001606354	0,004425865	0,008655132
Line2.1-40-3	0,360391872	0,007385675	0,048998556	0,00284224	0,032057147	NA	0,004033076	0,00824872
Line2.3-40-1	0,506345302	0,008343926	0,086974064	0,00241357	0,046182034	0,001395908	0,004448893	0,008758196
Line2.3-40-2	0,540983995	0,008136211	0,089324851	0,002420131	0,049925788	NA	0,005030658	0,008284296
Line2.3-40-3	0,463920533	0,01057284	0,073594822	0,002568892	0,041253709	0,001592937	0,004857337	0,009484707
Line30.1-40-1	0,825937168	0,006854093	0,072529686	0,003016811	0,036471013	NA	0,00315566	0,009105131
Line30.1-40-2	0,912695214	0,006237633	0,075312218	0,002835724	0,035679259	0,001281114	0,003190789	0,009759496
Line30.2-40-1	0,864840786	0,006615886	0,066352354	0,003034168	0,049168342	NA	0,002881842	0,008909009
Line30.2-40-2	0,905384592	0,006941195	0,065459882	0,003209801	0,048041695	0,00175536	0,00302925	0,01092837
Line30.3-40-1	0,855241821	0,0066183	0,074805941	0,002813309	0,037479581	NA	0,002885664	0,008635711
Line30.3-40-2	0,831482926	0,005364438	0,069727734	0,003103106	0,03400466	0,001847917	0,002231447	0,008019262
Line5.1-40-1	1,424929334	0,007449177	0,142165434	0,002280949	0,049409572	NA	0,00473926	0,008212243
Line5.1-40-2	1,328828333	0,00846482	0,135221784	0,002153289	0,046453628	0,001449881	0,004411851	0,009072526
Line5.2-40-1	0,553310581	0,006773069	0,116066161	0,002225195	0,033081229	NA	0,004314759	0,008434548
Line5.2-40-2	0,562585434	0,007468335	0,108161942	0,002062641	0,03049825	0,001494541	0,004081583	0,009714516
Line5.3-40-1	0,942713239	0,007754871	0,090214104	0,002330039	0,031408569	NA	0,003161876	0,008309429
Line5.3-40-2	0,988736376	0,006974801	0,111203396	0,002501409	0,034087156	0,001466845	0,004002254	0,008849643
WT1-40-1	0,553282954	0,008732644	0,044813752	0,003354018	0,025945874	NA	0,005281055	0,011419925
WT1-40-2	0,491302946	0,007442953	0,038266828	0,003444067	0,021815913	0,001685394	0,002658945	0,008599699
WT2-40-1	0,217039235	0,008607539	0,040892406	0,003785031	0,016252335	NA	0,005240136	0,010502253
WT2-40-2	0,193562891	0,006243209	0,033520364	0,003662558	0,014448837	0,001807861	0,002927236	0,010308554
WT5-40-1	1,084407957	0,017139201	0,091994421	0,002798833	0,035187709	NA	0,005989752	0,011032657

Sample	beta-Alanine	Erythritol	Malate	Aspartate	Threonate	Methionine	Asparagine	Glutamine
Line2.1-15-1	0,065491792	NA	1,568478926	0,340723718	0,015654309	0,022373438	0,01721974	0,024384445
Line2.1-15-2	0,06241676	NA	1,595272339	0,318279568	0,01552374	0,021114517	0,011061415	0,016527763
Line2.1-15-3	0,061919704	0,000816713	1,466926725	0,324019945	0,016373653	0,019934233	0,015958133	0,029458964
Line2.1-15-3	0,06160404	NA	1,556183159	0,325479599	0,015273764	0,020979506	0,011526966	0,020158289
Line2.2-15-1	0,06051456	NA	2,106141556	0,352852502	0,016960225	0,026438133	0,011913904	0,022818544
Line2.2-15-2	0,06088387	NA	1,895609694	0,371479053	0,014654915	0,025761263	0,015560599	0,030445839
Line30.1-15-1	0,075225629	0,000794508	1,716049428	0,493052633	0,014938215	0,033219222	0,023846224	0,04700778
Line30.1-15-2	0,079123804	0,001122523	1,826321117	0,490598969	0,016085476	0,031052452	0,017682758	0,03884574
Line30.2-15-1	0,089624094	0,000898278	1,537403803	0,567693212	0,015681671	0,029934098	0,023504322	0,053471152
Line30.2-15-2	0,094352885	0,001096918	1,732611606	0,534499201	0,016865679	0,034407418	0,025838023	0,044333409
Line30.3-15-1	0,074622142	0,000768127	1,355001398	0,530157174	0,016941474	0,01764559	0,016148453	0,03954433
Line30.3-15-2	0,075243511	NA	1,505111606	0,535219415	0,017999347	0,016983892	0,015081996	0,028927967
Line5.1-15-1	0,071794872	0,000923382	1,341514042	0,405364774	0,016479701	0,024412393	0,020550977	0,037065018
Line5.1-15-2	0,068540781	0,00092859	1,417340901	0,387209607	0,017618229	0,022323641	0,008457249	0,02697492
Line5.2-15-1	0,08036678	NA	1,484348845	0,37359989	0,015022986	0,017093291	0,014463826	0,022486702
Line5.2-15-2	0,079822457	0,001167813	1,569650671	0,364624611	0,015636454	0,01630565	0,010002957	0,017447221
Line5.3-15-1	0,066601272	NA	1,016407331	0,359045925	0,017555404	0,01228389	0,008741009	0,021130901
Line5.3-15-2	0,063182766	NA	0,951500092	0,330258694	0,01823101	0,010032237	0,006484883	0,01414956
WT1-15-1	0,067348392	0,000899077	1,317710364	0,322997314	0,015861224	0,014340285	0,009406598	0,017614425
WT1-15-2	0,063195481	NA	1,286949497	0,29269912	0,016463482	0,013670088	0,003836981	0,007494033
WT2-15-1	0,07242217	0,000974391	1,651075153	0,225099403	0,013558385	0,015284341	0,008739304	0,015680895
WT5-15-1	0,062107952	NA	1,209515212	0,281749293	0,016795401	0,014012207	0,007864544	0,019959696
WT5-15-2	0,059847316	NA	1,175552697	0,26773709	0,017317011	0,014113963	0,008101826	0,015557048
WT5-15-2	0,059577338	NA	1,244257859	0,281843089	0,017654253	0,014093203	0,010318238	0,02138308
Line2.1-20-1	0,059767998	0,001215827	2,072201356	0,347027115	0,015406736	0,017523872	0,015786976	0,020246574
Line2.1-20-2	0,060427067	0,000952833	1,835816646	0,366612888	0,012603208	0,01623612	0,023627218	0,033933757
Line2.2-20-1	0,06205587	NA	1,823372454	0,498122062	0,016439822	0,033900795	0,023318599	0,038412041
Line2.2-20-2	0,059444369	NA	2,323138818	0,410395846	0,010855239	0,027681206	0,010149545	0,022374661
Line2.3-20-1	0,078910615	0,000993449	2,075938581	0,442205374	0,010524741	0,025189545	0,021307196	0,036117485
Line2.3-20-2	0,080904179	0,001137555	2,161821688	0,438714207	0,010789001	0,026648122	0,020240486	0,03805478
Line30.1-20-1	0,050147157	NA	1,408104054	0,310376911	0,016272667	0,007560999	0,011757334	0,020924713
Line30.1-20-2	0,04982702	0,001023607	1,532939966	0,313445176	0,017376712	0,008449678	0,007844372	0,012032303
Line30.2-20-1	0,07759538	0,00091958	1,830311362	0,552528058	0,015493314	0,021790827	0,032725599	0,055507569
Line30.2-20-2	0,080529418	0,001275947	2,201224909	0,550883118	0,01522539	0,027527867	0,02398508	0,03507948
Line30.3-20-1	0,057986387	0,001048649	1,918319331	0,420318237	0,015095362	0,012065933	0,02357086	0,029918853
Line30.3-20-2	0,054864959	0,001344616	2,009073838	0,399378695	0,015092153	0,012449287	0,012110815	0,014150922
Line5.1-20-1	0,051168565	0,001020921	1,888262229	0,273417517	0,012496074	0,012837619	0,01805731	0,021086661
Line5.1-20-2	0,048349312	0,001125999	2,05987387	0,235146192	0,011900806	0,011850456	0,008362605	0,009337555
Line5.2-20-1	0,055170298	0,000947396	1,957207977	0,272151211	0,014172115	0,013426623	0,019371146	0,026402845
Line5.2-20-2	0,051640523	0,001173648	2,024335618	0,25091498	0,012965212	0,013240617	0,010007788	0,015261664
Line5.3-20-1	0,049153284	NA	1,75313781	0,248832489	0,015927524	0,00714614	0,008721261	0,011715187
Line5.3-20-2	0,048555814	0,001074515	1,811089935	0,246511597	0,015467357	0,0076677	0,008775204	0,010127773
WT1-20-1	0,052970166	0,001103841	1,813269871	0,353864419	0,018236446	0,01562769	0,013803335	0,021196585
WT1-20-2	0,055144766	0,001197723	2,18332096	0,335887157	0,016916605	0,013338283	0,009047266	0,013402623
WT2-20-1	0,046261011	0,000864071	1,54896474	0,137287527	0,015918839	0,004973945	0,004855781	0,008884418
WT2-20-2	0,042184955	NA	1,60824007	0,130626104	0,014980808	0,004408102	0,002155927	0,003325326
WT5-20-1	0,062003948	0,000799827	1,777121946	0,236891634	0,014493476	0,013415449	0,009555416	0,01584584
WT5-20-2	0,063868931	NA	1,907038627	0,228146432	0,01525928	0,010644822	0,010398779	0,01748759
Line2.1-30-1	0,028807717	0,001440164	2,477295256	0,319565806	0,007143215	0,016431167	0,014685244	0,012301219
Line2.1-30-2	0,026974399	0,001181168	2,205059021	0,303280854	0,007543624	0,014917431	0,016642012	0,018279797
Line2.1-30-3	0,028890683	0,001560761	2,54107553	0,315373354	0,008150114	0,015460548	0,015674026	0,012656871
Line2.3-30-1	0,038298031	0,001527378	2,341776341	0,421728718	0,006614723	0,019675765	0,038157042	0,042911496
Line2.3-30-2	0,038719228	0,001543976	2,593607571	0,40626845	0,006175904	0,019454096	0,018306484	0,019278959
Line2.3-30-3	0,039548962	0,001541094	2,468004994	0,428164263	0,006999855	0,024492998	0,03700356	0,032432227
Line30.1-30-1	0,02533903	0,001628401	2,143256621	0,35782931	0,006402937	0,015497479	0,015371001	0,018442039
Line30.1-30-2	0,023661373	0,001599113	2,335712911	0,348093436	0,006442272	0,016389762	0,012472164	0,012719592
Line30.2-30-1	0,038302273	0,00150433	2,316119294	0,51907374	0,008073964	0,025678983	0,043938059	0,045845724
Line30.2-30-2	0,037568423	0,001823751	2,529423472	0,500357062	0,007337716	0,020629318	0,032622512	0,027006041
Line30.3-30-1	0,009267607	0,001759262	1,746404305	0,395092917	0,007598287	0,017301212	0,015718236	0,021255056
Line30.3-30-2	0,009911379	0,002454045	2,029204191	0,382693483	0,007166446	0,01452858	0,008605024	0,009044001
Line5.1-30-1	0,007023951	0,001702527	1,993374951	0,19447049	0,004721016	0,013110278	0,005161041	0,00687792
Line5.1-30-2	0,00719556	0,0019949	2,20062111	0,191709936	0,004857351	0,014530298	0,00339597	0,00346556
Line5.2-30-1	0,018149016	0,001740262	2,16456252	0,176660533	0,004957352	0,015450812	0,008709292	0,012600933
Line5.2-30-2	0,018654417	0,001983781	2,479382671	0,183288608	0,004763039	0,016700098	0,006702627	0,005980805
Line5.3-30-1	0,015394489	0,00161213	2,08712461	0,21432824	0,00519593	0,011489809	0,008748802	0,011203724
Line5.3-30-2	0,014711308	0,001756637	2,172481595	0,207404706	0,005257333	0,010594322	0,005865238	0,006146132
WT1-30-1	0,022646629	0,001628014	2,140435917	0,238494443	0,00660399	0,01654062	0,00907474	0,00758846
WT1-30-2	0,020648791	0,00171657	2,306997156	0,208327089	0,005740064	0,012247589	0,007188704	0,006162395
WT2-30-1	0,012290433	0,001161919	2,13334982	0,256964644	0,007807624	0,005758564	0,007309098	0,009004871
WT2-30-2	0,012253329	0,001323478	2,466854796	0,24563661	0,007479884	0,006409205	0,00419845	0,004803186
WT5-30-1	0,022932562	0,001546642	2,050556871	0,247921201	0,005891592	0,014071257	0,009550916	0,009806032
WT5-30-2	0,02261752	0,001632142	2,325042341	0,231032885	0,005550252	0,012306449	0,006785256	0,006436549
Line2.1-40-1	0,004410284	0,003736019	0,100266101	0,992326531	0,013875431	0,009927379	0,01793798	0,011475219
Line2.1-40-2	0,003869635	0,004047053	0,091619723	0,93097089	0,012572717	0,009614149	0,013349522	0,008981198
Line2.1-40-3	0,004244688	0,003879554	0,106245833	1,040472975	0,015020304	0,009456153	0,016277529	0,016144753
Line2.3-40-1	0,007065095	0,004683046	0,077270253	0,849779154	0,01127083	0,017088614	0,011689602	0,008231353
Line2.3-40-2	0,007653877	0,00427754	0,088872134	0,940644161	0,013196486	0,01630627	0,023977071	0,015866246
Line2.3-40-3	0,006618542	0,004279617	0,067795184	0,752236562	0,009989511	0,012749107	0,009815634	0,008250742
Line30.1-40-1	0,003879358	0,004851301	0,07578212	0,81187134	0,011995715	0,009025187	0,0124333	0,014705375
Line30.1-40-2	0,003896121	0,00524441	0,074237425	0,841792523	0,012576027	0,009270082	0,013765976	0,010224919
Line30.2-40-1	0,00586249	0,00460683	0,117962027	1,569611717	0,02196787	0,009271297	0,050028777	0,033643447
Line30.2-40-2	0,005918071	0,005145712	0,112849586	1,507142058	0,020342115	0,009298393	0,028988516	0,021209764
Line30.3-40-1	0,003834783	0,00494138	0,075614608	0,828615401	0,012559873	0,008584637	0,014815628	0,010248788
Line30.3-40-2	0,003775528	0,004911175	0,070449965	0,766835719	0,011291719	0,007869835	0,010245728	0,006405448
Line5.1-40-1	0,003167756	0,004648517	0,075522938	0,51967288	0,009053678	0,011817216	0,009053678	0,00611278
Line5.1-40-2	0,00326343	0,00493821	0,066560565	0,459363603	0,007790122	0,00960367	0,004608039	0,003971623
Line5.2-40-1	0,003098319	0,004963244	0,113370496	0,567204274	0,008667664	0,008803294	0,009362772	0,006349222
Line5.2-40-2	0,003299352	0,004505473	0,106960191	0,560750032	0,008587056	0,008420996	0,006515674	0,005292074
Line5.3-40-1	0,004101048	0,004342549	0,094977044	0,818630831	0,0113595	0,009266489	0,015125129	0,00934699
Line5.3-40-2	0,004079967	0,004832818	0,089545569	0,811413223	0,01177362	0,009447067	0,013420178	0,007951079
WT1-40-1	0,00404515	0,003817483	0,121744773	0,833008095	0,012025681	0,006773085	0,009379055	0,008240722
WT1-40-2	0,003826159	0,004182081	0,1017727	0,65515783	0,009625591	0,005480149	0,005888412	0,00434434
WT2-40-1	0,001586988	0,004061985	0,153594901	0,546684251	0,008264644	0,003947687	0,002189252	0,002738763
WT2-40-2	0,001643936	0,003751546	0,127594702	0,484946982	0,007381318	0,003339391	0,002243434	0,00248698
WT5-40-1	0,005326542	0,005447505	0,08806521	0,573047449	0,013105712	0,011616616	0,007403768	0,005910501

Sample	Xylose	Ribose	Pyroglutamate	Rhamnose	Putrescine	Fucose	2-oxo-Glutarate	Phenylalanine
Line2.1-15-1	0,007377635	0,001261808	1,757931549	0,011131515	0,079900065	0,027728236	NA	0,141247605
Line2.1-15-2	0,007688928	0,001270046	1,632313921	0,011790834	0,077867558	0,028962201	NA	0,124357254
Line2.1-15-3	0,006401163	0,001096114	1,718792985	0,011294274	0,074435465	0,025862563	NA	0,128299089
Line2.1-15-3	0,007600526	0,001355862	1,650712833	0,011424314	0,07822939	0,029302873	NA	0,126386016
Line2.2-15-1	0,008482406	0,00141297	2,117183823	0,013904907	0,123203625	0,03354427	NA	0,192842849
Line2.2-15-2	0,008631331	0,00149516	2,045555157	0,012593701	0,12398901	0,030176476	NA	0,20681231
Line30.1-15-1	0,008534554	0,001581693	3,506138215	0,014085126	0,089589016	0,031275057	0,000816476	0,186907094
Line30.1-15-2	0,008404842	0,001496698	3,4026535	0,014017458	0,098355564	0,034383811	NA	0,180352062
Line30.2-15-1	0,007549895	0,001440153	3,657386041	0,012063103	0,090947872	0,029344945	0,000763718	0,20113052
Line30.2-15-2	0,008085855	0,001499868	3,539052531	0,013427176	0,10129705	0,032804574	NA	0,189265423
Line30.3-15-1	0,00642951	0,001454463	2,34397237	0,011692604	0,04274486	0,024373816	0,000753903	0,179980043
Line30.3-15-2	0,007241356	0,001473241	2,2260385	0,012867972	0,0485587	0,028669942	NA	0,173343072
Line5.1-15-1	0,00731456	0,001251526	2,608363858	0,011942918	0,100812729	0,027663309	NA	0,189186508
Line5.1-15-2	0,007745192	0,00131585	2,356095591	0,012063344	0,108320251	0,029485861	NA	0,171335296
Line5.2-15-1	0,007261995	0,001727024	1,570523097	0,011367216	0,073536542	0,026807801	NA	0,159788652
Line5.2-15-2	0,008240302	0,001377757	1,475761965	0,011756864	0,080985897	0,029519001	0,000949122	0,15205194
Line5.3-15-1	0,006396755	0,001300551	1,528702229	0,009519709	0,034629726	0,024266085	NA	0,151838344
Line5.3-15-2	0,006241749	0,001167837	1,316267769	0,009553942	0,034951405	0,023978521	NA	0,14196592
WT1-15-1	0,005712888	0,001112608	1,379855346	0,011463237	0,065243052	0,024533575	0,000801677	0,108159015
WT1-15-2	0,00596014	0,001416939	1,197264003	0,011358003	0,063856719	0,024416334	NA	0,090576141
WT2-15-1	0,009120752	0,001223654	1,214412072	0,013142947	0,069710493	0,030296759	NA	0,151230754
WT5-15-1	0,006682745	0,001343478	1,373719798	0,010751674	0,041836446	0,02562617	NA	0,166737562
WT5-15-2	0,006491738	0,000984894	1,296810313	0,011493288	0,041117196	0,026904743	NA	0,160212326
WT5-15-2	0,006723632	0,001178628	1,369112732	0,010918038	0,044024482	0,026017898	NA	0,157567043
Line2.1-20-1	0,006543873	0,001182967	1,715959304	0,012890584	0,109584051	0,030306487	NA	0,140890427
Line2.1-20-2	0,006605296	0,001176806	1,710141406	0,012238778	0,106815982	0,027077916	0,000865521	0,14853184
Line2.2-20-1	0,00659901	0,001147046	2,390604017	0,013673624	0,111064095	0,029455993	0,000902249	0,259032985
Line2.2-20-2	0,006399679	0,001563597	2,05038104	0,014030864	0,099572086	0,029908986	NA	0,205626875
Line2.3-20-1	0,007556864	0,001309358	2,558389033	0,014673118	0,080577447	0,031054636	NA	0,247052906
Line2.3-20-2	0,007798475	0,001373065	2,61928334	0,015490304	0,089573594	0,033384583	NA	0,249973339
Line30.1-20-1	0,005453337	0,00108611	1,057214469	0,009592709	0,048791417	0,022132346	NA	0,128931928
Line30.1-20-2	0,006210538	0,001235218	1,044886148	0,010078591	0,053852551	0,024601015	NA	0,126981393
Line30.2-20-1	0,007109749	0,001374003	3,16698357	0,0135647	0,125506574	0,028753872	0,000844439	0,203144892
Line30.2-20-2	0,007845714	0,001425259	3,118503758	0,013795606	0,127314124	0,032722146	NA	0,199631333
Line30.3-20-1	0,007629674	0,001592392	1,6394305 71	0,011962363	0,096281483	0,029444156	NA	0,123964945
Line30.3-20-2	0,007112554	0,001534717	1,50702214	0,012268459	0,093891272	0,030773154	NA	0,112576794
Line5.1-20-1	0,00743973	0,001403302	1,223007775	0,012923005	0,164227222	0,028459567	NA	0,089618309
Line5.1-20-2	0,007639402	0,00162034	1,021107452	0,012436342	0,16047779	0,0304386	NA	0,078252376
Line5.2-20-1	0,008010157	0,001308494	1,282894839	0,012013295	0,123973007	0,029369283	0,000842561	0,161169957
Line5.2-20-2	0,00798674	0,001398209	1,234864386	0,01196528	0,118229172	0,030502143	NA	0,137545643
Line5.3-20-1	0,006801461	0,00129857	0,872995833	0,010416617	0,099108155	0,025430332	NA	0,069561676
Line5.3-20-2	0,006866526	0,001206473	0,885494428	0,010537785	0,110269722	0,026740337	NA	0,064211683
WT1-20-1	0,006814709	0,001504915	1,447848841	0,012490084	0,11239301	0,025413186	NA	0,118490755
WT1-20-2	0,00711705	0,001464984	1,308522643	0,013041326	0,12196486	0,031759465	NA	0,112491957
WT2-20-1	0,006089113	0,001214869	0,452477593	0,01071226	0,046563805	0,024024117	NA	0,0795425
WT2-20-2	0,006097232	0,001405203	0,38143554	0,011934598	0,046280255	0,026145433	NA	0,068816434
WT5-20-1	0,006046998	0,001178488	1,174052698	0,011162797	0,083699727	0,024825535	NA	0,144189028
WT5-20-2	0,006810272	0,00128592	1,101694955	0,012158216	0,092744113	0,029845425	NA	0,13755171
Line2.1-30-1	0,008747336	0,00128507	1,118653141	0,013892046	0,171924596	0,032534419	NA	0,148784479
Line2.1-30-2	0,007283239	0,00113211	1,105863573	0,011736203	0,157212293	0,025921537	0,000864177	0,143087338
Line2.1-30-3	0,008728876	0,001432674	1,106133649	0,013937738	0,175682869	0,032652639	NA	0,145819675
Line2.3-30-1	0,007934534	0,001323728	2,203078646	0,014478763	0,238502073	0,029012354	0,000951674	0,182224059
Line2.3-30-2	0,008549478	0,001378056	1,957881259	0,016066567	0,249474242	0,03272768	NA	0,176584753
Line2.3-30-3	0,008181648	0,001454515	2,254632804	0,0131599	0,241994972	0,028687716	NA	0,194372584
Line30.1-30-1	0,009782265	0,001640259	1,394678211	0,012548966	0,132758176	0,026714475	0,00112249	0,095557903
Line30.1-30-2	0,009585514	0,001704499	1,246813229	0,012994511	0,135571786	0,029957021	0,001768646	0,089623636
Line30.2-30-1	0,010185113	0,001558835	2,88978858	0,013964105	0,196097027	0,030097498	0,001300846	0,159687884
Line30.2-30-2	0,010929695	0,001635824	2,457630883	0,014325203	0,197370894	0,034600022	0,001080583	0,147100278
Line30.3-30-1	0,012253676	0,001780848	1,699609365	0,016027636	0,132383595	0,028738217	0,002547153	0,026378143
Line30.3-30-2	0,012524091	0,001406845	1,239821532	0,018050981	0,137786155	0,033684939	0,001935734	0,022990804
Line5.1-30-1	0,01220553	0,001702527	0,583239912	0,013554415	0,192726839	0,028502928	0,001792999	0,009565403
Line5.1-30-2	0,013328719	0,001605199	0,58091038	0,01564837	0,20766914	0,031881293	0,001605199	0,009974502
Line5.2-30-1	0,011351617	0,001840048	0,618335815	0,013427158	0,229375302	0,028562647	0,001141548	0,065064242
Line5.2-30-2	0,012570494	0,001816829	0,586015816	0,014505172	0,244235864	0,033581879	NA	0,067261965
Line5.3-30-1	0,00973077	0,001585068	0,701879659	0,010198559	0,185781554	0,025469335	0,001391767	0,044470819
Line5.3-30-2	0,009521054	0,001479935	0,63835505	0,01137831	0,180225051	0,027720481	0,000993611	0,043458939
WT1-30-1	0,009411835	0,001612691	0,780906501	0,015460385	0,201789436	0,031204236	0,000900196	0,097408853
WT1-30-2	0,008941603	0,001562169	0,612738219	0,015803341	0,20749151	0,03186553	NA	0,086273527
WT2-30-1	0,006543645	0,001452399	0,545823176	0,011768354	0,163123992	0,026520014	0,0009735	0,064368737
WT2-30-2	0,006389377	0,001199557	0,483327393	0,01275397	0,154172848	0,027341974	NA	0,059026148
WT5-30-1	0,006896112	0,001351319	0,792020441	0,012129982	0,194645747	0,027038339	NA	0,117927499
WT5-30-2	0,00766671	0,001365769	0,710979571	0,012926373	0,201063459	0,030463427	NA	0,1111794
Line2.1-40-1	0,016530082	0,00187013	2,865102571	0,042211503	0,12406467	0,047648025	0,00677233	0,090186059
Line2.1-40-2	0,017765796	0,002047502	2,957681441	0,045601275	0,133749355	0,051820503	0,005077997	0,082868689
Line2.1-40-3	0,018352156	0,00183812	3,274629669	0,044546405	0,132415186	0,051081483	0,006808928	0,09232923
Line2.3-40-1	0,018142299	0,002120879	4,09276573	0,049937477	0,218207411	0,052805842	0,005907842	0,112834382
Line2.3-40-2	0,01867563	0,002174733	3,875709327	0,04751835	0,203494128	0,048978044	0,008030436	0,126853812
Line2.3-40-3	0,016877282	0,002024825	3,624543573	0,043968433	0,194467348	0,04787786	0,004442276	0,101134687
Line30.1-40-1	0,014385601	0,002697037	2,729944519	0,044246559	0,085732967	0,043245163	0,005049056	0,076918157
Line30.1-40-2	0,01522942	0,002682182	2,771687289	0,048629544	0,097700521	0,046811034	0,005709833	0,079011614
Line30.2-40-1	0,013491138	0,002375461	6,099752079	0,043577568	0,132091287	0,047492756	0,007126384	0,08721689
Line30.2-40-2	0,014398967	0,002587902	6,225599869	0,04779093	0,13915491	0,050459077	0,006008346	0,07708538
Line30.3-40-1	0,014070803	0,00259199	2,449741354	0,042693354	0,0842716	0,043927635	0,005852194	0,081892417
Line30.3-40-2	0,016377226	0,002839118	2,193054024	0,047687215	0,088565528	0,047871509	0,004457913	0,074280284
Line5.1-40-1	0,014951974	0,002087089	2,017353364	0,048225788	0,110681732	0,042946195	0,005650815	0,117598824
Line5.1-40-2	0,016503766	0,002354263	2,122090547	0,051286566	0,109635922	0,045429619	0,004794658	0,101496488
Line5.2-40-1	0,014817678	0,002360826	1,908276199	0,041871808	0,138144332	0,042995002	0,00467079	0,090567548
Line5.2-40-2	0,015880591	0,002512752	2,020868512	0,046195301	0,145197716	0,048664352	0,004522953	0,086630938
Line5.3-40-1	0,014208319	0,001976732	2,610578467	0,043394183	0,138415949	0,045017607	0,005769195	0,061994245
Line5.3-40-2	0,015086165	0,002229411	3,03916283	0,049115036	0,148816809	0,050096171	0,00477939	0,060359231
WT1-40-1	0,015318717	0,001935167	2,712254486	0,038475674	0,151975659	0,043370508	0,007378841	0,071275942
WT1-40-2	0,014467175	0,001962804	NA	0,039146165	0,140777543	0,044888021	0,004899159	0,058967869
WT2-40-1	0,015153314	0,001780415	1,709862622	0,036623805	0,09226948	0,043996044	0,006334762	0,058586658
WT2-40-2	0,014542508	0,001789127	NA	0,03593709	0,090393046	0,045032598	0,005133201	0,051753531
WT5-40-1	0,016571926	0,001593374	2,458847565	0,053373866	0,148079525	0,044931485	0,007791683	0,092903728

Sample	1-6-anhydro-Glucose	Glycerol-3-P	Lysine	1-4-lactone-Galactonate	Galacturonate	Dehydroascorbate	Tyramine	Ascorbate
Line2.1-15-1	0,009014043	0,003229441	0,12846391	0,079557011	0,021241753	0,011214321	0,01404156	0,006186804
Line2.1-15-2	0,008984718	0,002904801	0,110180793	0,018046669	NA	0,009615451	0,012880671	0,006041301
Line2.1-15-3	0,010670994	0,003080582	0,121518226	0,077777539	0,019139013	0,008339065	0,01346501	0,006225642
Line2.1-15-3	0,010402071	0,002600518	0,111291893	0,017925608	NA	0,008947834	0,012959817	0,00774595
Line2.2-15-1	0,010386245	0,002587386	0,117721485	0,017203366	NA	0,009230179	0,013803981	0,005321574
Line2.2-15-2	0,011008753	0,002338384	0,119772892	0,081488196	0,023473629	0,011098541	0,01491647	0,006839481
Line30.1-15-1	0,010313959	0,002555606	0,179606407	0,060627918	0,01293913	0,008296568	0,014008238	0,005426087
Line30.1-15-2	0,009004326	0,003307219	0,171347736	0,017039017	NA	0,007781218	0,014785924	0,005749411
Line30.2-15-1	0,010961168	0,003153063	0,191394938	0,060984679	0,010091984	0,009775587	0,012990475	0,00701893
Line30.2-15-2	0,008475373	0,003416117	0,188884859	0,022354748	NA	0,009688699	0,014443504	0,006868052
Line30.3-15-1	0,009740281	0,002940932	0,114621658	0,040397805	0,006265927	0,011009824	0,008502742	0,0054978
Line30.3-15-2	0,008539806	0,00281747	0,114738031	0,013413155	NA	0,01085371	0,008885227	0,00546431
Line5.1-15-1	0,008791209	0,002575549	0,131417888	0,057482448	0,009348291	0,011458333	0,009649725	0,00795177
Line5.1-15-2	0,015444578	0,002198635	0,116860782	0,022660931	NA	0,010964027	0,010422696	0,008219897
Line5.2-15-1	0,009381846	0,002873655	0,097283122	0,060283048	0,013083623	0,011951148	0,013111935	0,00647634
Line5.2-15-2	0,011245125	0,002637421	0,089519246	0,018409464	NA	0,010829611	0,012701612	0,006219591
Line5.3-15-1	0,010286178	0,002866105	0,074192578	0,047406929	0,009262861	0,010547104	0,00839039	0,00503505
Line5.3-15-2	0,008681054	0,002399446	0,065570255	0,014763272	NA	0,008772727	0,00803137	0,005584094
WT1-15-1	0,010065921	0,001966732	0,087184288	0,050419513	0,01080766	0,009919821	0,009792452	0,004592787
WT1-15-2	0,010467356	0,001862263	0,075048288	0,013053832	NA	0,010269434	0,010143484	0,00550582
WT2-15-1	0,008433391	0,002571939	0,088144609	0,085383834	0,022018213	0,010533241	0,018173523	0,008051943
WT5-15-1	0,009723856	0,00257532	0,069926301	0,050717259	0,009539079	0,010089559	0,007976179	0,005273825
WT5-15-2	0,008393012	0,002487929	0,063966743	0,016366374	NA	0,009626271	0,007814922	0,007129778
WT5-15-2	0,007650596	0,002726364	0,067957761	0,016769234	NA	0,00934933	0,007495403	0,00638808
Line2.1-20-1	0,009459041	0,002192244	0,116771045	0,022617202	NA	0,010191354	0,01390925	0,008374655
Line2.1-20-2	0,009953497	0,002418146	0,138475847	0,055275695	0,005352567	0,013119484	0,015051723	0,010021828
Line2.2-20-1	0,018615012	0,002021318	0,218145003	0,056677344	0,005207168	0,011092771	0,017702272	0,006557045
Line2.2-20-2	0,012896218	0,002013304	0,170224542	0,013228309	NA	0,010128789	0,015566787	0,005590206
Line2.3-20-1	0,010404197	0,002144852	0,207314944	0,052873105	0,006035515	0,011069267	0,014315642	0,006729682
Line2.3-20-2	0,011988767	0,002115142	0,202458186	0,022035691	NA	0,010309095	0,013926166	0,00899824
Line30.1-20-1	0,009516757	0,002263363	0,073175733	0,038796164	NA	0,010773759	0,0118105	0,007800247
Line30.1-20-2	0,009729187	0,002057056	0,06972338	0,018513506	NA	0,010964405	0,011180937	0,014822616
Line30.2-20-1	0,008841565	0,001917879	0,222391667	0,057321682	NA	0,009399754	0,012806136	0,009335348
Line30.2-20-2	0,008800411	0,001927494	0,20016524	0,025034794	NA	0,01060574	0,011691652	0,014080658
Line30.3-20-1	0,010253454	0,0023217	0,096406631	0,056873007	0,003327194	0,013835258	0,013593594	0,013934513
Line30.3-20-2	0,008610177	0,001873189	0,087905413	0,024393184	NA	0,013307059	0,01225455	0,017901936
Line5.1-20-1	0,009945628	0,002398236	0,082371626	0,072062179	0,005913917	0,018395142	0,013910514	0,013364785
Line5.1-20-2	0,014903471	0,00183547	0,066832179	0,029774901	NA	0,016372763	0,012147976	0,013351789
Line5.2-20-1	0,010922236	0,002248125	0,08359995	0,054424806	0,003805116	0,010763042	0,015216581	0,008829422
Line5.2-20-2	0,009537481	0,001838857	0,068029229	0,022752675	NA	0,008609578	0,012994871	0,007291872
Line5.3-20-1	0,008677174	0,002240434	0,045401859	0,055125104	0,005442772	0,013410542	0,014877445	0,010176141
Line5.3-20-2	0,009270046	0,002050061	0,041698714	0,020090599	NA	0,012682102	0,012677389	0,014213757
WT1-20-1	0,011098748	0,001888242	0,103427408	0,057098034	0,00411722	0,012376506	0,011251369	0,010502461
WT1-20-2	0,009675823	0,001524375	0,096278149	0,023860431	NA	0,012853254	0,011150705	0,010225192
WT2-20-1	0,009390306	0,002485126	0,035497055	0,046264704	0,003530135	0,011055673	0,011690802	0,007281826
WT2-20-2	0,008681458	0,001843125	0,027338893	0,017800839	NA	0,010341715	0,010279154	0,00810879
WT5-20-1	0,009992037	0,002461302	0,063758157	0,058140052	0,00477964	0,01069913	0,014640304	0,009729292
WT5-20-2	0,007905858	0,002776103	0,062884761	0,028011712	NA	0,013063466	0,014042994	0,010830514
Line2.1-30-1	0,009961506	0,001976349	0,109448054	0,040266993	NA	0,019776779	0,014326311	0,02325533
Line2.1-30-2	0,010321066	0,001977418	0,107622117	0,074032424	NA	0,016804281	0,013438142	0,018770378
Line2.1-30-3	0,010716593	0,002006693	0,109101467	0,038919403	NA	0,019113393	0,0146351	0,020166551
Line2.3-30-1	0,011901801	0,002122664	0,186414558	0,087052728	NA	0,018195383	0,01697348	0,014666748
Line2.3-30-2	0,014001787	0,001949558	0,164062417	0,038078593	0,001152221	0,016080394	0,015066439	0,013047748
Line2.3-30-3	0,011337427	0,001991301	0,177320991	0,078448586	NA	0,020618619	0,015796209	0,036077172
Line30.1-30-1	0,011165615	0,001833928	0,101589312	0,083530658	NA	0,020331301	0,012837493	0,078400404
Line30.1-30-2	0,008142188	0,002217681	0,094288097	0,050530136	0,001044693	0,018951092	0,012307213	0,079460792
Line30.2-30-1	0,009687303	0,002289198	0,180922917	0,08252739	0,001002887	0,018437125	0,017572317	0,038102422
Line30.2-30-2	0,009836298	0,001776769	0,171402725	0,04510688	0,00098662	0,017584038	0,015217859	0,04147219
Line30.3-30-1	0,010638321	0,002007502	0,089672014	0,109246957	NA	0,02616588	0,014401487	0,08895248
Line30.3-30-2	0,011376402	0,001554934	0,077439924	0,062519966	0,031913161	0,020801203	0,01252938	0,019219825
Line5.1-30-1	0,011033524	0,002187788	0,042423345	0,102155711	NA	0,031990229	0,013439268	0,071826885
Line5.1-30-2	0,013426144	0,001902114	0,040547512	0,067705994	0,02027839	0,032247798	0,0131849	0,06227337
Line5.2-30-1	0,013802353	0,002219233	0,073589929	0,093594958	0,001716313	0,024387615	0,018248802	0,062797112
Line5.2-30-2	0,010856782	0,001983781	0,069874271	0,059086233	0,001723533	0,023638422	0,017092926	0,045224317
Line5.3-30-1	0,009989794	0,002346674	0,048363901	0,091377231	0,001878885	0,022662605	0,016279807	0,078317818
Line5.3-30-2	0,009147926	0,00208784	0,043546981	0,054032299	0,00210461	0,022467341	0,014551995	0,04866177
WT1-30-1	0,008726154	0,001723779	0,094616331	0,081385367	NA	0,021022446	0,013112215	0,015111799
WT1-30-2	0,009241322	0,001466804	0,082254574	0,03652025	NA	0,023750423	0,012320248	0,013423758
WT2-30-1	0,008934214	0,002080463	0,051112655	0,062272572	NA	0,024443476	0,012545584	0,015230558
WT2-30-2	0,009422968	0,001754724	0,046807517	0,028754676	NA	0,019455629	0,010939764	0,029116526
WT5-30-1	0,009523012	0,002076806	0,079269411	0,076602648	NA	0,022446246	0,01533488	0,043696635
WT5-30-2	0,010369189	0,002208477	0,070981237	0,041912638	NA	0,021702165	0,014214651	0,034982088
Line2.1-40-1	0,012942486	0,002756427	0,1157445	0,146285714	NA	0,0332934	0,016004241	0,031393586
Line2.1-40-2	0,012313783	0,002344797	0,102135348	0,145933671	0,206649059	0,033954009	0,014351695	0,032155852
Line2.1-40-3	0,016281678	0,002622329	0,120925898	0,165961916	NA	0,034077834	0,016464245	0,03493673
Line2.3-40-1	0,016255572	0,002454096	0,160038581	0,14362991	0,198583649	0,035658691	0,015436039	0,027787572
Line2.3-40-2	0,015240058	0,003570963	0,178438152	0,163485802	NA	0,035515006	0,017093236	0,037055089
Line2.3-40-3	0,021459781	0,00236697	0,134962168	0,118354114	0,168391414	0,028212938	0,013360481	0,034393983
Line30.1-40-1	0,015307054	0,002107981	0,097951682	0,167052218	NA	0,025098015	0,016018129	0,03664773
Line30.1-40-2	0,012561633	0,002461466	0,099211947	0,146661139	0,155585752	0,028861047	0,015901165	0,037176291
Line30.2-40-1	0,014454496	0,002251954	0,150576245	0,152165375	NA	0,029510062	0,01276656	0,046080654
Line30.2-40-2	0,013872359	0,00215157	0,130879641	0,124053798	0,138111724	0,024715469	0,011515162	0,029570293
Line30.3-40-1	0,014109109	0,00205146	0,096078136	0,164418998	NA	0,023766294	0,015049716	0,035257875
Line30.3-40-2	0,013911677	0,001733356	0,084052826	0,132138513	0,138768102	0,025402632	0,014957667	0,034931109
Line5.1-40-1	0,014300274	0,002223204	0,135029733	0,177823314	NA	0,030320541	0,013170111	0,039118489
Line5.1-40-2	0,016025258	0,002148504	0,107817589	0,147012239	0,172779935	0,027686516	0,012101486	0,032141432
Line5.2-40-1	0,013965746	0,002331156	0,097789894	0,152025309	NA	0,030546627	0,01600021	0,034768139
Line5.2-40-2	0,012769148	0,002521492	0,09063386	0,139918753	0,163084138	0,0293839	0,016103461	0,031966571
Line5.3-40-1	0,013559844	0,002652041	0,096967193	0,153719968	NA	0,024185895	0,017790586	0,03465989
Line5.3-40-2	0,013327893	0,002467409	0,102188611	0,137995182	0,156622176	0,029060053	0,017713858	0,034912864
WT1-40-1	0,014107205	0,002931209	0,084911551	0,178946033	NA	0,035581054	0,016115551	0,051505527
WT1-40-2	0,013310429	0,002161702	0,066505036	0,130523854	0,159337818	0,028452808	0,012640458	0,073963692
WT2-40-1	0,014744477	0,002571711	0,053377294	0,162052973	NA	0,033823497	0,012256292	0,036188592
WT2-40-2	0,010519315	0,002590018	0,045515006	0,134905766	0,176200869	0,031497059	0,010720709	0,027867286
WT5-40-1	0,015324756	0,003462043	0,108407844	0,156071423	NA	0,033740325	0,015504115	0,042887628

Sample	Inositol	Tyrosine	1-4-lactone-Glucarate	Fructose-6-P	Octadecanoate	Glucose-6-P	Inositol-1-P	Tryptophan
Line2.1-15-1	0,739727205	0,108381443	0,01007475	0,004416329	0,067234664	0,003099317	0,002511787	0,006987263
Line2.1-15-2	0,714066276	0,098857645	0,009748462	0,003303836	0,046399591	0,002673104	0,002364174	0,005513545
Line2.1-15-3	0,728027568	0,106645461	0,009789804	0,003879384	0,060325682	0,003026851	0,002331929	0,008328318
Line2.1-15-3	0,711968712	0,09153138	0,009850316	0,00366981	0,053836705	0,002651844	0,002365274	0,006899071
Line2.2-15-1	0,30989455	0,108518831	0,008564982	0,004032469	0,041494518	0,002954391	0,002624087	0,009147603
Line2.2-15-2	0,314768359	0,115240565	0,009010001	0,004329329	0,054110754	0,002994225	0,002861495	0,00878358
Line30.1-15-1	0,312307551	0,163855378	0,009233867	0,00427643	0,050449428	0,003258581	0,002797254	0,012917162
Line30.1-15-2	0,323117702	0,159985709	0,008968116	0,003351476	0,038206023	0,002747969	0,002361724	0,008159416
Line30.2-15-1	0,480192981	0,1451391	0,010753873	0,003811315	0,05024899	0,002785751	0,002920311	0,012972291
Line30.2-15-2	0,51258322	0,138095302	0,01169897	0,003514616	0,041365014	0,002851988	0,002807215	0,009536474
Line30.3-15-1	0,447540819	0,140617076	0,007560364	0,003861973	0,052396237	0,002898258	0,002229703	0,014256584
Line30.3-15-2	0,472261238	0,131692792	0,008681303	0,003004746	0,042798909	0,002409624	0,002151598	0,006409016
Line5.1-15-1	0,609214744	0,151713217	0,010878358	0,003731685	0,052384768	0,003067766	0,002606074	0,01204594
Line5.1-15-2	0,634422796	0,130802127	0,012479752	0,002835739	0,069577637	0,002331886	0,002215291	0,01074333
Line5.2-15-1	0,416863965	0,122685947	0,010117954	0,003857492	0,046169581	0,00299398	0,002728556	0,010924843
Line5.2-15-2	0,427625306	0,110386804	0,009639929	0,00335473	0,05315957	0,002440599	0,002746767	0,0095612
Line5.3-15-1	0,574464511	0,092962917	0,008961165	0,003693729	0,056184631	0,002841643	0,002205637	0,007391534
Line5.3-15-2	0,582216515	0,084598424	0,008653153	0,003092974	0,053138572	0,002044711	0,001893251	0,004468072
WT1-15-1	0,661155322	0,097628571	0,00956019	0,002768409	0,058076656	0,002262678	0,001944255	0,005312049
WT1-15-2	0,588812389	0,081872087	0,008924467	0,002118661	0,096284381	0,001574377	0,001524896	0,003139757
WT2-15-1	0,745986869	0,109588762	0,012036371	0,003727612	0,052296088	0,002813648	0,002745667	0,006858503
WT5-15-1	0,849235969	0,122572164	0,009350453	0,003256683	0,054135622	0,002359748	0,002159574	0,00624775
WT5-15-2	0,787547168	0,115969162	0,010024511	0,002667779	0,055359623	0,002380875	0,002299514	0,005596769
WT5-15-2	0,810224954	0,122791226	0,009437413	0,003166776	0,03337908	0,002546004	0,001992343	0,007294071
Line2.1-20-1	0,62476147	0,134825374	0,012735672	0,003300102	0,034414011	0,002412877	0,002074887	0,006942889
Line2.1-20-2	0,646844453	0,157020025	0,013506691	0,003169783	0,05813799	0,002733226	0,002110658	0,009190472
Line2.2-20-1	0,265082951	0,226450593	0,010417832	0,003507582	0,053211728	0,00296903	0,002717239	0,015967715
Line2.2-20-2	0,203668919	0,176444338	0,007029269	0,003217136	0,057652459	0,002310803	0,001944119	0,011042041
Line2.3-20-1	0,506555101	0,225820531	0,012278864	0,003711925	0,059981045	0,003138301	0,002340217	0,012715317
Line2.3-20-2	0,55340289	0,218512824	0,012801941	0,003381561	0,056544498	0,003146051	0,002350651	0,01327296
Line30.1-20-1	0,571183898	0,077675876	0,011043387	0,002396278	0,065816007	0,001951961	0,001860818	0,005666002
Line30.1-20-2	0,580158757	0,071618037	0,01102838	0,002175165	0,035092986	0,001761785	0,001673204	0,005093429
Line30.2-20-1	0,386645837	0,182119786	0,013435887	0,002715803	0,067218796	0,002193395	0,001946504	0,008501643
Line30.2-20-2	0,366707931	0,172972195	0,01288163	0,003198916	0,03495279	0,0024614	0,001922969	0,009836552
Line30.3-20-1	0,544589577	0,099185765	0,013727372	0,002451162	0,061054656	0,001890157	0,002162029	0,006451563
Line30.3-20-2	0,498792164	0,087886867	0,012393648	0,002156022	0,036197983	0,00181755	0,001882462	0,004423322
Line5.1-20-1	0,628594106	0,092747896	0,016223364	0,002888279	0,054268452	0,002502185	0,002112379	0,010379983
Line5.1-20-2	0,559383648	0,071107315	0,014271813	0,002320657	0,035574255	0,001840048	0,001789698	0,006939085
Line5.2-20-1	0,417467812	0,126225014	0,013100471	0,003079038	0,06312998	0,002799478	0,002450029	0,009598211
Line5.2-20-2	0,354594303	0,108560345	0,0117958	0,002910817	0,033086712	0,002364244	0,001991389	0,009118018
Line5.3-20-1	0,677957814	0,046435708	0,012436615	0,003042021	0,067689972	0,002529005	0,00199595	0,002977894
Line5.3-20-2	0,67012962	0,042702537	0,011715981	0,002855947	0,03728758	0,002375243	0,001762581	0,002832383
WT1-20-1	0,602310257	0,13145649	0,015340194	0,003389608	0,051333926	0,002825265	0,002289316	0,015883241
WT1-20-2	0,56125711 5	0,121756991	0,014174709	0,002152932	0,040732492	0,001920317	0,001618411	0,005538233
WT2-20-1	0,779391694	0,072238519	0,013249083	0,0032975	0,052394436	0,00277315	0,002230336	0,012170841
WT2-20-2	0,68863114	0,05674709	0,012074156	0,002324359	0,034254222	0,001660257	0,001568822	0,005028893
WT5-20-1	0,941774556	0,126465334	0,014404606	0,003276584	0,055218946	0,002573355	0,002322202	0,014319601
WT5-20-2	0,985223985	0,123388015	0,013434851	0,002827168	0,03862868	0,002390791	0,002446499	0,009266055
Line2.1-30-1	0,299806752	0,098108422	0,019617253	0,002649902	0,089090778	0,002175756	0,002038386	0,012057498
Line2.1-30-2	0,291374834	0,102135159	0,019106237	0,002528378	0,058273457	0,002158556	0,002622721	0,013373989
Line2.1-30-3	0,306274449	0,098569887	0,018681693	0,002613919	0,036248557	0,002224915	0,00224389	0,011850398
Line2.3-30-1	0,265403512	0,136202977	0,020639188	0,002729699	0,069863848	0,002318482	0,002236238	0,016730666
Line2.3-30-2	0,255046381	0,116254471	0,019749065	0,00218922	0,037299692	0,001640762	0,002000255	0,011706563
Line2.3-30-3	0,254267444	0,143620392	0,019324274	0,002839768	0,056561595	0,002298654	0,002116839	0,015480198
Line30.1-30-1	0,31228941	0,034405904	0,020410349	0,002331934	0,058914924	0,001995977	0,00224498	0,005541307
Line30.1-30-2	0,311414642	0,030625991	0,019949965	0,002602568	0,041017934	0,001690753	0,002336813	0,003949671
Line30.2-30-1	0,241528515	0,084126195	0,021910891	0,002881482	0,049711924	0,002347336	0,002761572	0,015072368
Line30.2-30-2	0,232278433	0,070917018	0,018664621	0,002259402	0,057762091	0,002024492	0,002434516	0,007388969
Line30.3-30-1	0,39343439	0,016524115	0,02843961	0,002701853	0,049568747	0,00197872	0,002586727	0,002403246
Line30.3-30-2	0,364610769	0,012947202	0,023937515	0,001777067	0,055961742	0,0013328	0,002020356	NA
Line5.1-30-1	0,325832346	0,010605836	0,027750362	0,002130215	0,056158705	0,001616167	0,002788196	0,001735426
Line5.1-30-2	0,328963728	0,010526579	0,024783159	0,001925311	0,054961828	0,001363955	0,002379963	0,001744378
Line5.2-30-1	0,225316021	0,034901033	0,023361819	0,002530564	0,058937402	0,002394856	0,002598419	0,007507873
Line5.2-30-2	0,213811339	0,031701215	0,024090174	0,002356968	0,064482707	0,002170374	0,002563202	0,007110186
Line5.3-30-1	0,373001268	0,023416479	0,023401014	0,002601831	0,0539387	0,001960072	0,002493582	0,002744874
Line5.3-30-2	0,363108115	0,01871929	0,022282873	0,002251346	0,041635223	0,001396086	0,001995606	0,002029146
WT1-30-1	0,297757976	0,063588303	0,019045846	0,002359662	0,061619364	0,001804222	0,002225591	0,006393306
WT1-30-2	0,267221782	0,053767689	0,018132971	0,001666617	0,072382027	0,001693864	0,00160304	0,004613849
WT2-30-1	0,286597501	0,042378636	0,02018049	0,002767408	0,056203901	0,002127568	0,002072612	0,00649654
WT2-30-2	0,251322115	0,035540601	0,016392297	0,002190927	0,059130242	0,001789422	0,001596105	0,005685505
WT5-30-1	0,367056516	0,069371696	0,021194582	0,002200378	0,052155334	0,001865538	0,002846141	0,008614161
WT5-30-2	0,356562544	0,061682385	0,019711629	0,001995379	0,036711093	0,001535279	0,002310184	0,007947613
Line2.1-40-1	0,370154254	0,020694408	0,038204082	0,00290485	0,061650676	0,001700504	0,003078717	0,00735754
Line2.1-40-2	0,360091836	0,018931003	0,036097413	0,002517421	0,098203377	0,001606354	0,002718814	0,00606099
Line2.1-40-3	0,394266393	0,023223382	0,04240124	0,00273021	0,073977074	0,001813225	0,0030663	0,007958272
Line2.3-40-1	0,36603405	0,026697863	0,036406177	0,002589184	0,089500206	0,001819183	0,002319008	0,013409721
Line2.3-40-2	0,414210572	0,030327801	0,041620337	0,003583656	0,066109359	0,002360897	0,003562501	0,015557383
Line2.3-40-3	0,32446	0,021964585	0,032285024	0,002237965	0,045993258	0,001570501	0,002254791	0,008660194
Line30.1-40-1	0,32514657	0,023831543	0,041499031	0,002019622	0,06806548	0,00154417	0,00246983	0,004817641
Line30.1-40-2	0,320647908	0,022954488	0,041595414	0,002447071	0,036917189	0,001569005	0,002667788	0,006242431
Line30.2-40-1	0,34596925	0,019999984	0,040662791	0,002342526	0,064409169	0,001683819	0,003388223	0,004615064
Line30.2-40-2	0,322595044	0,016901609	0,035989895	0,002196708	0,035739129	0,001534686	0,002964051	0,003726378
Line30.3-40-1	0,329421088	0,022463914	0,0411654	0,001991874	0,07011993	0,001332172	0,002230218	0,004817952
Line30.3-40-2	0,312920575	0,020695673	0,037650685	0,001733356	0,041809743	0,001160552	0,001922631	0,002824175
Line5.1-40-1	0,343421069	0,087298906	0,042929696	0,00273054	0,062769419	0,001975723	0,003423487	0,014960224
Line5.1-40-2	0,306771951	0,070259438	0,038433822	0,002038447	0,037572506	0,001287189	0,002426039	0,011106188
Line5.2-40-1	0,319995728	0,034636746	0,039782245	0,002941496	0,062436847	0,001750487	0,003161896	0,00754447
Line5.2-40-2	0,306158033	0,032648292	0,037870445	0,002407872	0,043638849	0,001664971	0,003364902	0,007861635
Line5.3-40-1	0,340910209	0,027660829	0,04016075	0,002643096	0,070173979	0,002173511	0,002991931	0,006927506
Line5.3-40-2	0,329316508	0,02691807	0,039323114	0,002554837	0,033688873	0,001529988	0,002613122	0,007227371
WT1-40-1	0,407433969	0,019286623	0,045817925	0,002996257	0,070568549	0,002036804	0,003423132	0,007561787
WT1-40-2	0,362098096	0,013347068	0,035398517	0,001769141	0,040527979	0,001141043	0,002318726	0,002214043
WT2-40-1	0,307796461	0,017144741	0,041543027	0,002866249	0,074526871	0,002074953	0,003433344	0,004857677
WT2-40-2	0,287744951	0,01445352	0,037890142	0,002515081	0,037894826	0,001667354	0,002819514	0,003091161
WT5-40-1	0,430423771	0,034929099	0,038228468	0,003829104	0,070750821	0,002319152	0,003724825	0,011483139

Sample	Maltose	Trehalose	Maltitol	Melibiose	3-caffeoyl-Quinate	Raffinose	GABA	Glutamate
Line2.1-15-1	0,00274049	0,001265751	0,002531503	NA	0,097316962	0,001912428	1,476743514	0,00157123
Line2.1-15-2	0,002432825	0,001089837	0,001222848	NA	0,104778806	0,002334139	1,884151404	0,000819889
Line2.1-15-3	0,00259342	0,001293128	0,002901479	NA	0,094305221	0,002138497	1,640055594	0,001841191
Line2.1-15-3	0,002339611	0,001133449	0,00176647	NA	0,097587849	0,002634735	1,947185388	NA
Line2.2-15-1	0,002137805	0,001477196	0,001605647	NA	0,082424766	0,005037146	1,608885868	0,004480003
Line2.2-15-2	0,001577141	0,000925204	0,001908965	NA	0,071092342	0,003743757	1,403160809	0,00297398
Line30.1-15-1	0,003463616	0,001204577	0,002361556	NA	0,062319451	0,003441648	1,749273612	0,00195456
Line30.1-15-2	0,003548622	0,001058149	0,001878919	NA	0,067194481	0,004373415	2,200730407	0,002559469
Line30.2-15-1	0,003785858	0,001534709	0,00316761	NA	0,052041908	0,002578457	1,545079314	0,007533651
Line30.2-15-2	0,003295232	0,00122228	0,002063997	NA	0,056856187	0,002449038	2,116490031	0,000590291
Line30.3-15-1	0,004310047	0,001650051	0,00279513	NA	0,069405277	0,00229727	1,914272543	0,002521891
Line30.3-15-2	0,004007716	0,001002969	0,001381684	NA	0,0661502	0,001856118	1,943951186	0,000298232
Line5.1-15-1	0,003968254	0,001262973	0,002083333	NA	0,109561966	0,002125305	1,439118036	0,001345759
Line5.1-15-2	0,00378515	0,001332506	NA	NA	0,078447131	0,001982103	1,721259441	0,004807468
Line5.2-15-1	0,003291255	0,001489912	0,002509139	NA	0,108675111	0,002916123	1,853769937	0,001486216
Line5.2-15-2	0,003315366	0,001500225	NA	NA	0,100453829	0,003477197	2,104199887	NA
Line5.3-15-1	0,003648882	0,001219012	0,002120021	NA	0,0975495	0,00343688	1,50738626	0,001279053
Line5.3-15-2	0,003698814	0,001104064	0,001271467	NA	0,090405722	0,003415823	1,753025613	NA
WT1-15-1	0,00197797	0,000929047	0,001558401	NA	0,041653508	0,002839586	1,535572627	0,001411528
WT1-15-2	0,002316583	NA	NA	NA	0,039791247	0,003904454	1,842808936	NA
WT2-15-1	0,002020539	0,001276528	0,001722179	NA	0,074827933	0,002700347	1,37042669	0,001962609
WT5-15-1	0,002806291	0,00085844	NA	NA	0,060991595	0,002313554	0,950028848	0,001693682
WT5-15-2	0,002226718	0,001177591	0,001130487	NA	0,061538765	0,002565007	1,710901248	0,000702182
WT5-15-2	0,002613115	0,000977297	0,001321238	NA	0,067244712	0,002676031	1,695236882	NA
Line2.1-20-1	0,004337546	0,001581984	0,001746285	NA	0,066626389	0,006163633	1,727239257	NA
Line2.1-20-2	0,004517415	0,001772801	0,002232134	NA	0,061152131	0,00397077	1,594396297	0,002224449
Line2.2-20-1	0,004207	0,001049127	0,002654292	NA	0,10213952	0,006812332	1,77071638	0,00254657
Line2.2-20-2	0,003701436	NA	NA	NA	0,077951549	0,007001595	0,520919027	0,005655699
Line2.3-20-1	0,003973796	0,001280261	0,002053405	NA	0,05328046	0,005486832	1,549029597	0,002227492
Line2.3-20-2	0,003870354	0,001328629	0,001501929	NA	0,05524253	0,00709639	1,792364442	0,001117664
Line30.1-20-1	0,007971138	0,001659546	0,002950726	NA	0,034816292	0,002248172	1,195300017	0,001378506
Line30.1-20-2	0,007603234	0,002017687	0,00207182	NA	0,039246468	0,004163324	1,488146636	0,000633364
Line30.2-20-1	0,008905972	0,001645941	0,002393771	NA	0,02841395	0,002690756	1,691876366	0,003521532
Line30.2-20-2	0,00875969	0,001556474	0,001990839	NA	0,036581658	0,005330018	2,116931069	0,002506954
Line30.3-20-1	0,007340541	0,00146293	0,002131821	NA	0,053243734	0,001303259	1,549271693	0,001635853
Line30.3-20-2	0,007066188	0,00151617	0,001984467	NA	0,060957459	0,001942738	1,714324823	NA
Line5.1-20-1	0,006095827	0,00187107	0,00279918	NA	0,091381718	0,002134653	1,2046177	0,000881021
Line5.1-20-2	0,004755745	0,00145556	0,000965796	NA	0,068145845	0,002595291	1,370070106	NA
Line5.2-20-1	0,006425987	0,001626881	0,002294718	NA	0,056024508	0,00340519	1,553397854	0,001653439
Line5.2-20-2	0,005923322	0,001499897	0,000995694	NA	0,047458607	0,004669171	1,798254983	0,00141678
Line5.3-20-1	0,004841582	0,001695355	0,002737418	NA	0,080290912	0,003514957	1,488210728	0,001726455
Line5.3-20-2	0,005113371	0,00154108	0,001762581	NA	0,074782458	0,004656231	1,748503149	0,001171292
WT1-20-1	0,004983256	0,001543958	0,002576812	NA	0,038251104	0,006885696	1,10513065	0,001903216
WT1-20-2	0,004617669	0,001177926	0,001138332	NA	0,039312051	0,0051519	1,518395581	NA
WT2-20-1	0,002828539	0,001643211	0,002082632	NA	0,035194261	0,006299592	1,072691495	0,000622671
WT2-20-2	0,002935526	0,00156401	0,001318581	NA	0,02980281	0,005909551	1,35269365	0,000764057
WT5-20-1	0,002998384	0,001541695	0,002283563	NA	0,061609831	0,002673816	1,524862153	0,001411571
WT5-20-2	0,002859664	0,001346271	0,00190799	NA	0,065837271	0,002455783	1,884979668	0,001203061
Line2.1-30-1	0,009482928	0,002463789	0,003141774	NA	0,056764629	0,005064947	1,005639206	0,001035297
Line2.1-30-2	0,008785171	0,002328372	0,003951063	NA	0,045627793	0,004064274	0,903643654	0,00125068
Line2.1-30-3	0,008430007	0,002262866	0,002884324	NA	0,047671999	0,005403364	0,96483644	0,000823804
Line2.3-30-1	0,008306588	0,002357645	0,003838027	NA	0,050184167	0,006704799	1,296558452	0,003547023
Line2.3-30-2	0,007669182	0,002332095	0,002663935	NA	0,04259069	0,00912098	1,24900062	0,00207258
Line2.3-30-3	0,007467377	0,001870091	0,003939312	NA	0,05187771	0,00661891	NA	NA
Line30.1-30-1	0,012675443	0,002557222	0,004616438	NA	0,04100251	0,003308184	0,88440559	0,004062097
Line30.1-30-2	0,01322361	0,002918725	0,003780138	NA	0,042566645	0,003587695	0,964383737	0,002616243
Line30.2-30-1	0,006893028	0,002365504	0,004287703	NA	0,025468232	0,004058784	1,092667373	0,004655668
Line30.2-30-2	0,006240048	0,001828022	0,002763389	NA	0,024131604	0,004198472	1,145493081	0,002851939
Line30.3-30-1	0,006231171	0,002115432	0,004101348	NA	0,046730182	0,00228812	0,468478734	0,01483428
Line30.3-30-2	0,006690446	0,001914578	0,002797823	NA	0,043866051	0,001898711	0,50728767	0,008203066
Line5.1-30-1	0,003766943	0,001904033	0,003927326	NA	0,082424497	0,002882781	0,401291906	0,007087331
Line5.1-30-2	0,00359546	0,001897475	0,002472749	NA	0,065813159	0,003623296	0,578967619	0,011744209
Line5.2-30-1	0,006549931	0,002402839	0,003855718	NA	0,056774049	0,004175032	0,731888173	0,014479442
Line5.2-30-2	0,006491482	0,002563202	0,003412693	NA	0,056272603	0,006810654	1,101273878	0,001009593
Line5.3-30-1	0,007666316	0,002137909	0,004364736	NA	0,060781554	0,002501314	0,673381269	0,001672315
Line5.3-30-2	0,007299056	0,001848871	0,003094028	NA	0,06276098	0,0031653	0,91581723	0,001175676
WT1-30-1	0,006565684	0,0019766	0,002957239	NA	0,045634184	0,003489695	0,712718992	NA
WT1-30-2	0,006380372	0,001952712	0,002161606	NA	0,045648041	0,004554814	1,008763526	0,001436574
WT2-30-1	0,010268851	0,001950925	0,003795863	NA	0,043411017	0,003348368	0,561287764	0,007992944
WT2-30-2	0,009115644	0,002071963	0,003212038	NA	0,04288665	0,004966762	0,625010218	0,000675906
WT5-30-1	0,00657323	0,001853579	0,003910454	NA	0,049396889	0,002431577	0,821393326	0,002328426
WT5-30-2	0,005831155	0,0018743	0,002455478	NA	0,04720136	0,004058561	1,006332615	0,000621233
Line2.1-40-1	NA	0,002849722	0,005394116	0,001785317	0,0545815	NA	0,439868811	0,079070541
Line2.1-40-2	0,006665171	0,00246947	0,005336932	0,002085863	0,055723703	NA	0,567463909	0,08177367
Line2.1-40-3	0,005941734	0,00317418	0,005634689	0,001975046	0,057487933	0,001087105	0,477144835	0,256339249
Line2.3-40-1	0,007650475	0,002242458	0,004908192	0,002472108	0,054764616	NA	0,709712747	0,045094699
Line2.3-40-2	NA	0,002470903	0,006422656	0,002217043	0,074727904	0,001400461	0,782932106	0,210139769
Line2.3-40-3	0,00718504	0,002518411	0,004245963	0,00236697	0,04140515	NA	0,766573384	0,024842993
Line30.1-40-1	0,00677415	0,002259452	0,005490848	0,002772773	0,034703843	NA	0,455192227	0,061005058
Line30.1-40-2	0,006770231	0,002744558	0,005465126	0,003118816	0,048567168	NA	0,56024282	0,043405614
Line30.2-40-1	0,006257714	0,002289006	0,004960885	0,002280772	0,0257472	NA	0,607100013	0,116931458
Line30.2-40-2	0,005647244	0,001875728	0,003786562	0,001750345	0,028953409	NA	0,695808139	0,196976888
Line30.3-40-1	0,006345907	0,001979106	0,006167149	0,002379183	0,035062093	NA	0,523248603	0,150206713
Line30.3-40-2	0,005937243	0,001892745	0,004602359	0,002336046	0,036171355	NA	0,489758808	0,035164876
Line5.1-40-1	0,004495904	0,002247952	0,004314418	0,002462435	0,067735537	0,001035295	0,237885554	0,033436287
Line5.1-40-2	0,006603421	0,001981026	0,004631965	0,002847127	0,051568887	NA	0,375640026	0,036637731
Line5.2-40-1	0,007243539	0,003034742	0,004641121	0,002093802	0,060042113	NA	0,33641119	0,042045145
Line5.2-40-2	0,007193025	0,003229432	0,004396223	0,002691922	0,052894515	NA	0,374918377	0,036777349
Line5.3-40-1	0,008076873	0,002625207	0,00601964	0,002884597	0,068733917	0,001140422	0,480840453	0,093719585
Line5.3-40-2	0,005158244	0,002656836	0,004036253	0,002501409	0,076275961	NA	0,556981801	0,055204548
WT1-40-1	NA	0,002398631	0,005959989	0,002073393	0,042463907	0,000882208	0,309699938	0,044787419
WT1-40-2	0,005040481	0,001889526	0,003627262	0,001659224	0,033493289	NA	0,378034702	0,07174415
WT2-40-1	0,008638312	0,002611276	0,005459941	0,0020222	0,049020772	0,000958347	0,263107436	0,08348205
WT2-40-2	0,007203342	0,002252801	0,004332309	0,001779759	0,048329836	NA	0,276196307	0,023090569
WT5-40-1	0,009610299	0,002836373	0,006060662	0,002673699	0,063976895	0,00132225	0,466485652	0,088992454

Word count = 146

2.3 Use of a SWEET100 cell culture to study cell cycle in tomato

2.3.1 Synchronization of tomato SWEET100 cultured cells

To understand the molecular mechanisms governing the cell cycle, it is necessary to be able to study separately each phase of the cycle, in order to identify and analyze molecular complexes which are active during each phase.

Considering a single cell over time raises the problem of quantity of material in molecular biology, and one must therefore work on a set of cells. However, at the scale of the plant or organ, cells are involved in various phases of the cycle. Thus, studying the mechanisms of the cycle on such a scale leads to study the mechanisms of the cycle regardless of a specific phase. For example, as mitosis represents a relatively short time during cell cycle, mitosis-specific genes appear lowly expressed. For this reason, plant cell cultures are often used as models to study cell cycle.

Indeed, it is possible to "synchronize" the cells to pass through each phase of the cycle simultaneously. The validity of such approach in plant biology was shown for example by the work of Menges *et al.* (2005), where the levels of expression of 62 cell cycle genes were monitored during a complete mitotic cycle.

The synchronization of cultured cells can be achieved by restricting cell-state progression at a given phase. Cells become arrested at that point and are subsequently released from the arrest to get one or more rounds of synchronized cell division. Thus, during the first hours after the inhibition release, the cells will progress in the cell cycle at an approximatly equal speed, and culture samples may be taken as representative of a specific phase of the cell cycle.

A secondary objective of the thesis was to develop a synchronization method for cultured tomato SWEET100 cells, in order to first study the expression patterns of different tomato KRPs during the cycle.

Obtention of synchronized cells is achieved after 4 steps:

1- From a mother culture, transplantation of cells in a conventional culture medium: the cells will multiply until reaching the desired biomass.

2- After a preset culture time, resuspension of cells in the "blocking" medium, cells will progress in the cycle to the phase of the cycle affected by inhibition.

3- After a preset culture time, the washed cells of resuspensed in conventional culture medium. This is the T0 time: cells blocked in the same phase of the cycle will be able to resume their cycle simultaneously.

4- Periodic sampling of culture: for several hours, the cultured cells progress simultaneously through the same phases of the cycle.

The first step is to choose the age of the start culture for synchronization (step 1).

Blocking cells 4 days after transplanting seems adequate, since older cell cultures turn brown, are slowed in the cycle and start to endoreduplicate (see Figure 32), and younger cultures represent a low biomass towards the material requirements for subsequent experiments.

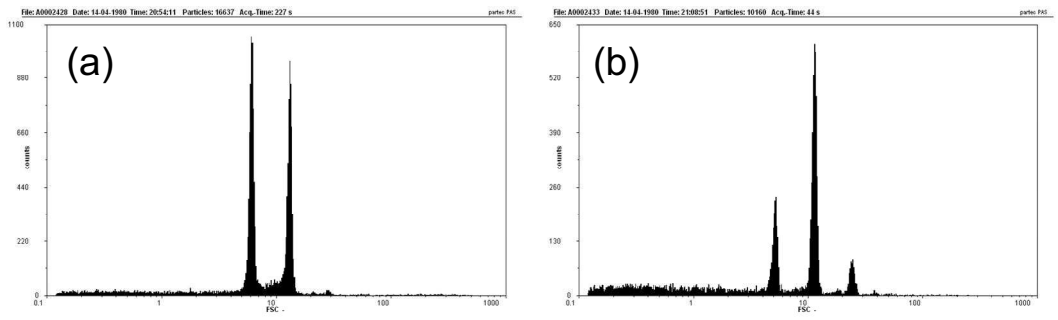

Figure 32 : Comparison of ploidy profiles using SWEET100 cells culture at 4 days after subculture (a) and 7 days after subculture (b)

The second stage of development is to find a suitable medium to block cells (step 2). There are various methods to synchronize cultured cells (see Table 5).

Table 5 : Different chemical inhibitors used to synchronize cultured cells, from Planchais *et al.* (2000)

Name	Target/mechanism	Block	Reversibility[a]
HU	ribonucleotide reductase	G1/S progression	+/−
Aphidicolin	DNA polymerase α and δ	G1/S progression	+
Colchicine	microtubule depolymerisation	metaphase	+/−
Oryzalin	microtubule depolymerisation	metaphase	+/−
Propyzamide	microtubule depolymerisation	metaphase	+/−
APM	microtubule depolymerisation	metaphase	+/−
Mimosine	ribonucleotide reductase	G1, before initiation of replication	+/−
Olomoucine	CDK activity	G1/S and G2/M	+
Roscovitine	CDK activity	G1/S and G2/M	+
MG132	proteasome	metaphase/anaphase	−

[a] + reversible arrest; − irreversible arrest; +/− reversibility dependent on the duration of the treatment.

Two methods are commonly used: a block with aphidicolin, arresting cells in S phase, and sugar starvation, arresting cells in G1 phase.

The use of a medium deficient in sugar for 24 hours had no blocking effect.

Addition of aphidicolin induced a blocking effect of the cell cycle depending on the inhibitor concentration used. A minimum concentration of 40 µg/mL aphidicolin for 24 hours seemed sufficient during the first tests for effectively blocking the cycle (see Figure 33).

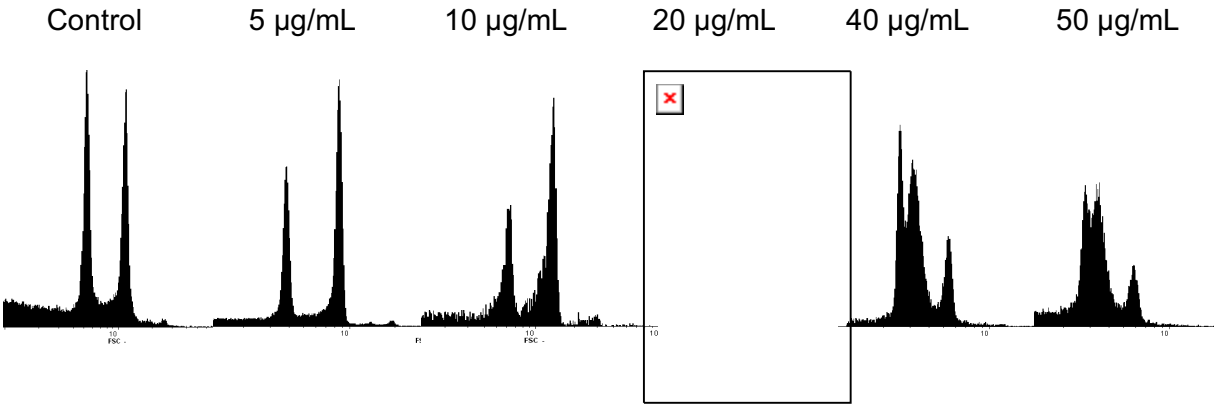

Figure 33 : Ploidy level of SWEET100 cultured cells after a block of 24 hours. The different tested concentrations of aphidicolin are indicated above the graphs.

These first tests have established the conditions for synchronization. Several tests were then conducted in the pre-established conditions. Figure 34 is representative of the obtained results:

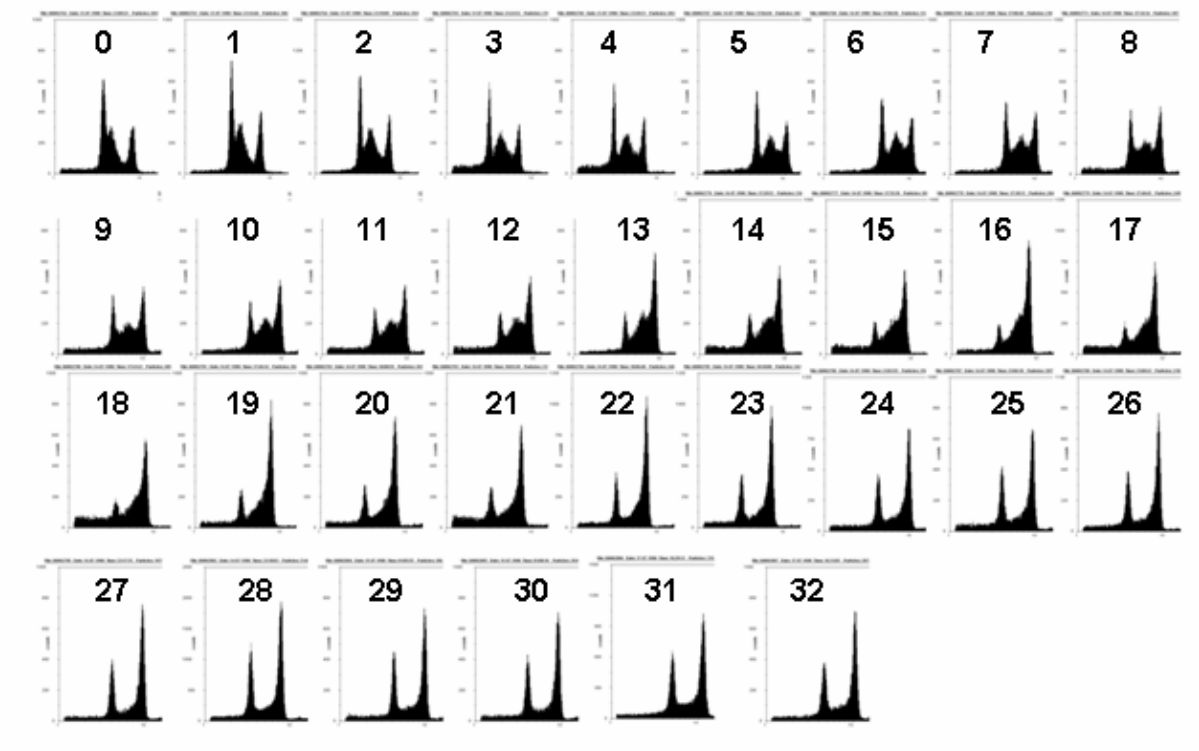

Figure 34 : Evolution of ploidy in a SWEET100 cell culture after synchronization with 40 µg/mL aphidicolin. The numbers indicate the sampling time after depletion of aphidicolin (h).

On the above figure, the ploidy was represented as the frequency (number of nuclei) on ordinate and the amount of DNA (DAPI signal intensity) on abscissa. It can be extracted from these data the relative amount (in percentage) of cells in G1 phase (2C), S (intermediate 2C/4C) and G2 (4C). The M phase can not be viewed as the nucleus is not found during this period (Figure 35).

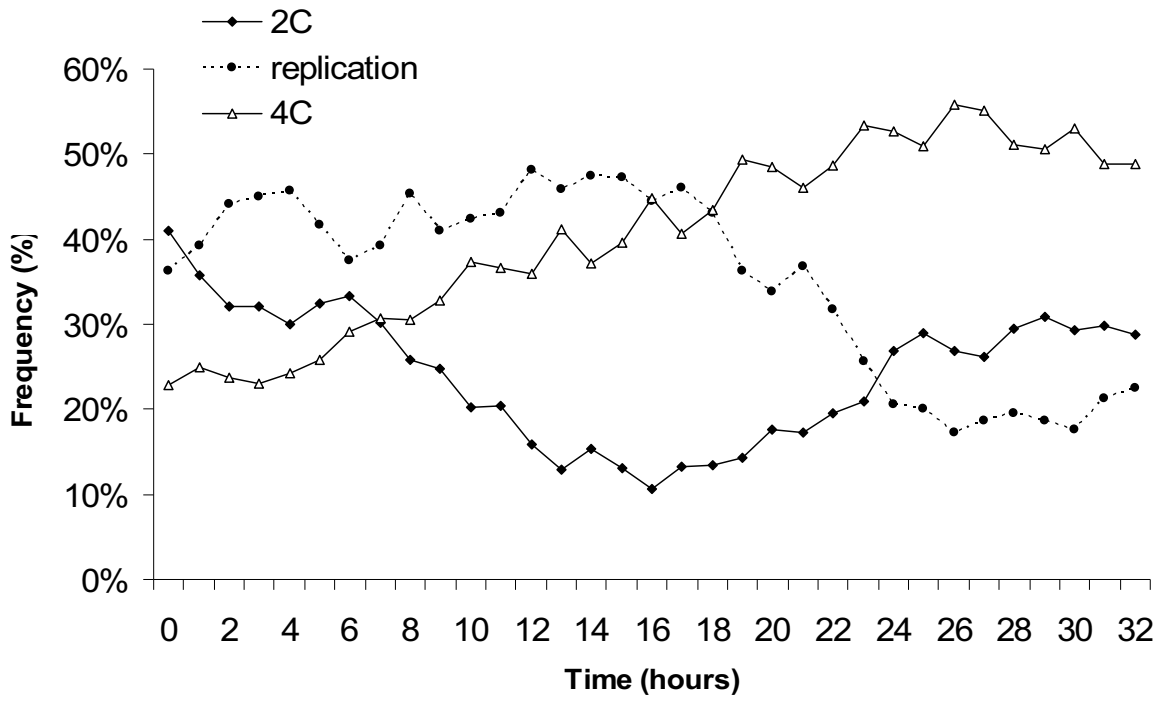

Figure 35 : Evolution of the average ploidy in a SWEET100 cell culture synchronized after release of aphidicolin block

The frequencies of the different classes of ploidy evolve during time, meaning that the cells have been able to resume cell cycle progression.

Thus, in the early hours, the proportion of 4C cells increases as the proportion of 2C cells decreases. 2C cells are present in minimum relative amount at 16 hours, and rose again from 16 to 24 hours. Meanwhile, the 4C cells have increased steadily up to 24 hours.

The curve of cells undergoing replication remains stable until about 16 hours, and then drops to a minimum at about 24 hours.

A plateau is reached for each class of cells at 24 hours and stretches until the end of the experiment.

The graph can be interpreted as follows: between 0 to 16 hours, 2C cells enter significantly in replication, and at the same time, cells complete replication and integrate 4C class. These two movements are done at the same speed, so the rate of cell replication remains unchanged.

From 16 to 24 hours, there are few cells ready to go to replication, and the pool of replicating cells falls progressively as the cells enter G2. At the same time, early G2 cells enter mitosis, and the pool of 2C cells increases.

It becomes difficult to analyze the results after 24 hours. There are two possibilities:

- The level of synchronization is too low at 24 hours and the culture is returned to an asynchronous state

- The experiment was not followed on a long enough time: indeed, during BY-2 synchronization, the transition time of the majority block of G2 cells into mitosis may represent 8 hours of time, whereas arrival of cells in G2 takes only 6 hours. By keeping these proportions of time, and given that in this experiment, the minimum frequency of 2C class happens after 16 hours, mitosis should have been achieved at around 40 hours.

In all cases, the cells appear to have progressed through the cell cycle much more slowly than in the case of synchronization of BY-2 or *Arabidopsis* mm2d cell cultures (Menges *et al.*, 2006).

It does not seem that SWEET100 cells show an inherent slow development, because just like BY-2 cells cultures, SWEET100 cultures saturate after a week starting at 1:25 dilution of previous culture. However, tracking parallel developments in the biomass of the two cultures over time might allow concluding on this point.

The most likely hypothesis is that concentration of inhibitor used is too strong to allow cells that have been targeted to restart the cycle at a normal speed. A SWEET100 specific feature is that cells produced during culture form cell aggregates, in contrast to BY-2 cells that form cell chains. Thus, cells in the centre of the aggregates are less wetted with the culture medium than the cells on the surface of the aggregate. It is therefore possible that concentration of inhibitor, inhibition time or wash quality are heterogeneous according to the position of cells, leading to a low synchronization level over time.

This study may nevertheless serve as a basis for further development of synchronization in SWEET100 cell culture.

It will then be necessary to:

- Ensure the speed of multiplication of SWEET100 cells during exponential growth;

- Try different washing tests;

- Search a possible alternative to aphidicolin;

- Facilitate the entry or disposal of drugs, for example by use of low concentrations of detergent.

2.3.2 Transformation of SWEET100 cells

The transient transformation of tomato leaf protoplasts is a useful tool for studying the molecular biology in tomato. This protocol allows expressing a transgene in a homologous system, without having to go through a protocol of stable expression, with more varied possibilities, but longer to implement. The main technical limitation of the transformation of tomato leaf protoplasts is that it is necessary to have sterile tomato plants, and therefore *in vitro* cultures. This brings a problem of time and logistics, as it is space consuming to germinate seeds in a sterile environment in a quantity sufficient to occupy the space in corresponding culture chamber. To transiently transform cultured cells is an attractive alternative, because liquid culture of cells allows obtaining a greater quantity of biomass more rapidly and in a shorter time.

Several processing methods were considered:

- Transformation of SWEET100 protoplasts by use of chemicals;

- Transformation of SWEET100 cells by biolistic.

The “chemical” transformation of SWEET100 cell protoplasts was first proposed because the protocol was adapted to tomato leaves where it gives very good transformation efficiency, of about 80% of the cells transformed. The first step requires degrading cell walls to obtain protoplasts. Once the protoplasts released from the walls, a series of differential centrifugation is used to isolate protoplasts from remaining debris. The conventional protocol of wall degradation seems to work, since

it allows the release of protoplasts without walls. However, during the following centrifugation, the protoplasts form aggregates and did not dispose themselves at the interface but all along the wall of the centrifuge tube.

This behaviour, incompatible with the continuation of the transformation protocol, might originate from the SWEET100 cells: isolated from mesocarps, it is possible that they have, or produce, pectins leading to their adhesion to each other.

The other direction considered was the transformation of SWEET100 cells by biolistic. This protocol was tested using different constructs for the expression of genes fused to the YFP sequence under the 35S promoter dependence. The sample (500 µL of cultured cells) is deposited on a Petri dish containing solid MS medium and is subjected to biolistic bombardment. After 24 hours of incubation in the dark at 25°C, the Petri dish is viewed under epifluorescence microscope to identify transformed cells. The areas containing these cells were diluted in PBS, transferred between slide and coverslip, and observed by confocal microscopy (see Figure 36).

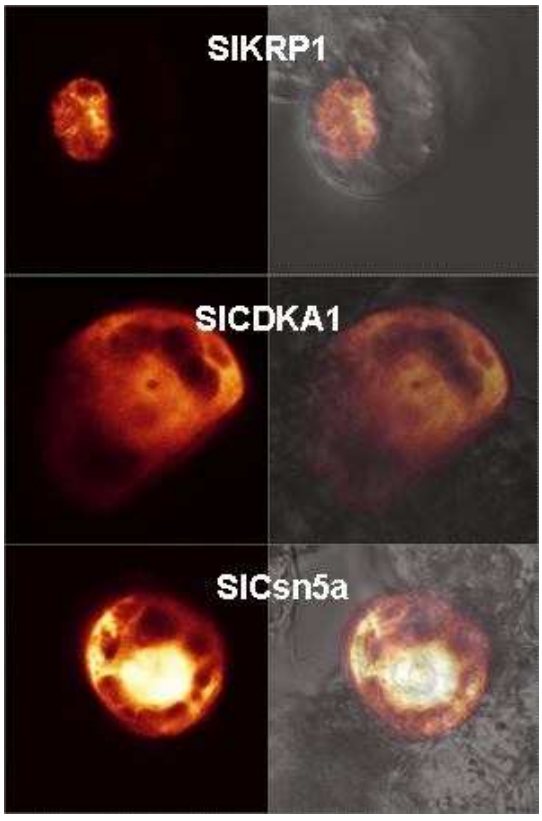

Figure 36 : Examples of SWEET100 cells transformed by biolistic with different constructs expressing proteins fused to YFP

As can be seen in Figure 36, such a protocol is operational. However, this method has some drawbacks: first, the transformation rate is extremely low, and only few cells can be recovered by shoot. In addition, the expression level is relatively low compared with the onion epidermis model frequently used with this protocol, and the signal decreases after a few seconds of visualization. Finally, SWEET100 cells are arranged in clusters, and it may be difficult to obtain a clear picture of an isolated cell.

A possible alternative to these methods is the cell transformation by agrotransfection. The agrotransfection is widely used to transform leaf cells by injecting a solution of *Agrobacterium* containing a construct for plant stable transformation. This technique, used on cultured cells, could combine readily available biomass, good level of processing and no need to degrade the cell walls. However, it is possible with such a protocol that cells could be subject to necrosis, as is often seen on infected leaves.

CHAPTER 3 : CONCLUSIONS/PERSPECTIVES

1 A common biochemical activity but different roles for KRPs?

The alignment of KRP primary sequences from various plant species allowed the classification of KRPs into two subgroups. KRPs of each of these 2 subgroups share common structural motifs. KRPs from the first subgroup have 4 specific motifs, ranked from 3 to 6 (see Article 1 Suppl. Fig. S1). In addition, all KRPs from the first subgroup, each having the motif 3 and/or 5, are putatively localized in the nucleus in the vicinity to the genomic DNA, and furthermore form proteinaceous islets. These results imply a specific functional role for KRPs from the first group. It is interesting to note that in *Arabidopsis thaliana*, KRPs which share all the motifs from 3 to 6 are expressed preferentially around the S phase. This could argue for a role of these SlKRPs in the regulation of S phase. Interestingly the increase in SlKRP3 expression during fruit development parallels the slowdown of endoreduplication from 15 to 30 days post-anthesis. Hence, SlKRP3 function *in vivo* could be to downregulate the entry rate into S phase. The roles of SlKRP1 and SlKRP2 during fruit development can be addressed less easily because of their heterogeneous pattern of expression during fruit development. However, the increase in SlKRP2 expression at Breaker stage could argue for a role of cell cycle cessation at this time of development.

The homologies between proteins of the second subgroup are less clear, even if some of them share two highly conserved motifs (see Article 1 Suppl. Fig. S1). Nonetheless, it is possible that there are different functions, and thus different subclasses, between KRPs of this subgroup. Interestingly SlKRP4 is expressed mostly in dividing tissues, and between 10 to 20 days post-anthesis during fruit growth; the SlKRP4 expression decreases while the endoreduplication index remains constant. The high expression of SlKRP4 during divisions and the uncoupling between SlKRP4 expression and endoreduplication rate are a strong argument for the involvement of SlKRP4 in a specific M-phase regulation.

An interesting point is that we could not find any Monocotyledone member of the second subgroup. This could argue for a fundamental difference of function between the KRPs of these two subgroups: for instance we may think of a role for KRP

members of the subgroup 1 in the control of secondary meristems which are absent in monocotyledonous species.

2 The over-expression of SlKRP1 inhibits endoreduplication in fruit

In Article 1, we have shown using two-hybrid and BiFC experiements that SlKRP1 interacts with SlCDKA1 and SlCycD3;1 which is consistent with its CDK/Cyc inhibitor activity (Bisbis *et al.*, 2006). This interaction is also confirmed by translocation into the nucleus of CDKA1 and CycD3;1 proteins when co-expressed with SlKRP1. Indeed, when over-expressed in tomato fruit, SlKRP1 effectively blocks the cell cycle (Article 2). The expression of the transgene in the fruit between 10 and 20 DPA led to a slowdown in the rate of endoreduplication by a factor 2.

The reason for the import of CDKA1 and CycD3;1 in the nucleus under the influence of KRP1 is not clear at present. Several hypotheses may be put forward to explain this phenomenon. KRP1 could sequester CDK/Cyc complexes in specific areas of the nucleus until release. Alternatively, as co-expression of CDKA1 and CycD3;1 leads to their translocation to the nucleus, the associated movement of both proteins when co-expressed with SlKRP1 could be due to the promotion by SlKRP1 of CDK/Cyc complex formation. Such a phenomenon has indeed been observed in animals, and could be glimpsed during the experiments of *in vitro* CDK/Cyc inhibition achieved by Jasinski *et al.* (2002b) using NtKIS1b, a sliced variant of NtKIS1a which does not have the CDK/Cyc inhibition motif or by Verkest (2006) who used different versions of AtKRP2 mutated on the same motif. Indeed, in both cases, the phosphorylation activity of CDK/Cyc complexes was higher when the modified KRP was added.

The expression profiles of the different tomato KRPs studied (Article 2) suggest a specific role for each of them. Thus, SlKRP4 would be highly active during the fruit division phase, while SlKRP1 and SlKRP3 could take over the control of the cell cycle during the cell expansion phase of fruit development. Finally, SlKRP2 is relatively highly expressed during fruit ripening, where endoreduplication stops. With the sequencing of the tomato genome completed in 2010, it would be interesting to investigate the existence of other putative KRPs and study their expression profiles.

3 Endoreduplication and Fruit Development

Studying at the same time the evolution of endoreduplication, cell size, pericarp size and fruit size, we have shown that these three factors operate in parallel during normal fruit development. This observation allowed us to develop a simple mathematical model of pericarp growth by taking into account the number of mitosis rounds and the number of endoreduplication rounds. A striking point from this study is the linear trend between endoreduplication and cell size in the pericarp. The relationship between endoreduplication and cell size has been the subject of numerous reports, but no one can yet understand the exact mechanism by which this relationship is forged.

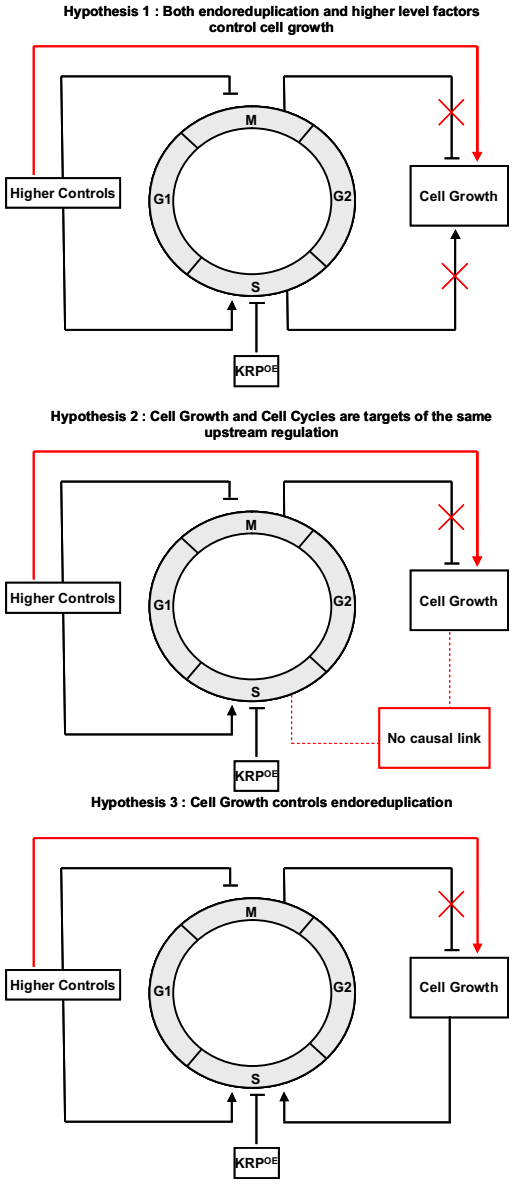

Figure 37 : Different hypotheses addressing the link between cell size and endoreduplication

The loss of linear relationship between endoreduplication and cell size in plants over-expressing SlKRP1 suggests that endoreduplication does not drive directly cell size.

It is however possible that a compensatory mechanism takes place at the organ scale leading to an increase in cell size in the absence of an "endoreduplication" signal in order to reach the expected size for the organ (Hypothesis 1). It would be interesting to grow pPEPC2::KRP1 plants under abiotic and biotic stresses in order to verify a possible growth speed difference with control fruits. If this is the case, endoreduplication could allow optimal growth of the organ in adverse conditions, and allow the biological system to respond more flexibly to environmental difficulties.

Alternatively, the possibility remains that endoreduplication and cell growth are not linked. However, in the pericarp of tomato fruit, endoreduplication speed and cell growth speed slow down in a parallell manner, which suggests at least a common control of both processes (Hypothesis 2).

Finally, it is possible that endoreduplication does not control cell size but is on the contrary under cell size regulation (Hypothesis 3). This hypothesis is in accordance with our results, as endoreduplication could be blocked downstream of a hypothetic cell size control, but is discarded by data from literature. Indeed, Ramirez-Parra *et al.* (2004) have shown that modulating the expression level of the transcription factor AtE2FF modify cell length but do not affect endoreduplication level. Meanwhile, Gendreau *et al.* (1998) have shown that in different mutants affected in light sensitivity, cell length could be uncoupled from endoreduplication.

Nevertheless, in each hypothesis proposed here appears the notion of higher level controls of cell growth and cell cycle. We propose three possibilities to explain their nature. First, cell cycle and cell growth could be co-regulated by a common factor (Hypothesis A). Our results as well as data from literature could support such a mechanism as a disruption of endoreduplication or cell size could be due to factors downstream of this control. The second possibility is an independent regulation between the two processes (Hypothesis B). However, as we could find a parallel evolution between endoreduplication and cell size at any time of development, and a common increase and decrease of each of theses phenomenons, this implies that the two ways of regulation are themselves co-controlled, which only displaces the question. The third possibility is a control of cell growth by cell cycle, independently of

cell cycle speed (Hypothesis C). In this case, factors induced during the gap phases would promote cell growth. Indeed, during classical cell cycle, cell growth is promoted prior to mitosis, to maintain the mean size of cells stable. S and M phases representing a relatively low part of cell cycle duration, the delay at the checkpoints would not change globally the duration of the gap phases. However, a control of cell size by gap phase factors as well as a co-regulation of endoreduplication and cell size would imply a common cell size evolution between tissues or plants of different species endoreduplicating during time, and it appears that endoreduplication can occur before cell size increases, like in *Arabidopsis* hypocotyls (Gendreau *et al.*, 1998).

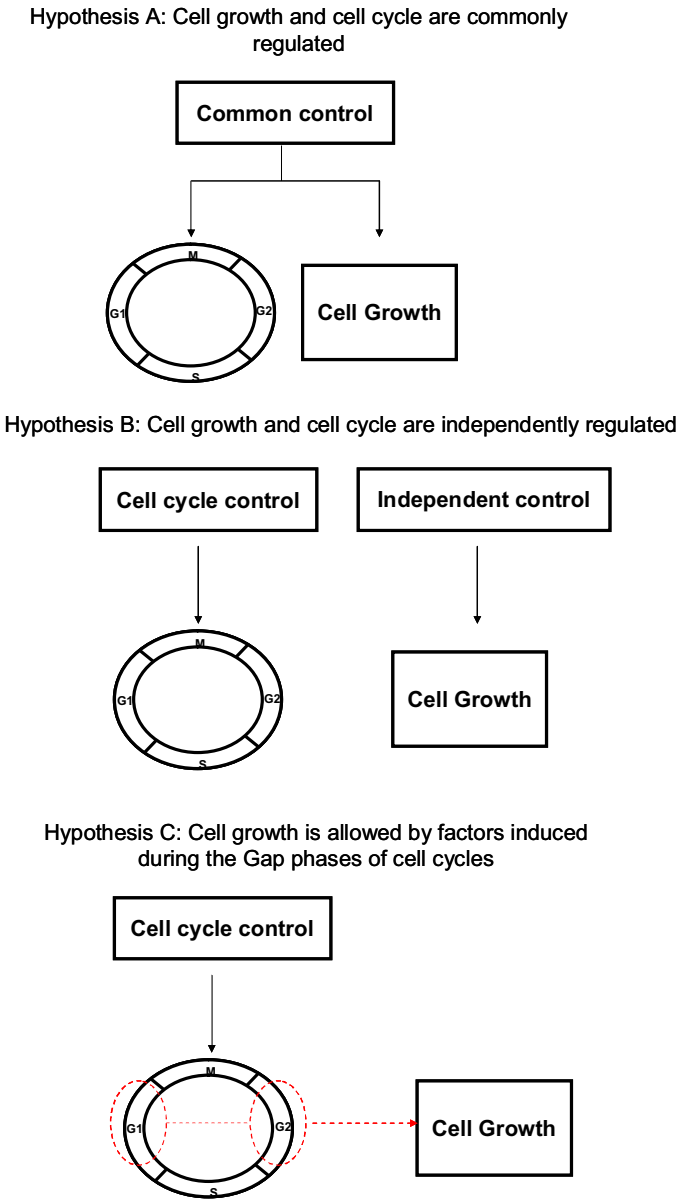

Figure 38 : Nature of the cell growth control

The metabolomics study by GC-MS performed on fruits SlKRP1 overexpressing did not reveal significant differences between normal fruits and fruits lowered in their endoreduplication level. It does not seem that optimal endoreduplication, through a hypothetic increase in the number of transcripts in cells, is necessary for the metabolism of the fruit. Again, the cultivation of plants has been made in controlled conditions in the greenhouse, hence it is possible that under adverse conditions differences in the metabolic profile could have been noticeable.

The reduced level of endoreduplication did not affect the final size of the organ: it might be interesting to restore the mitotic cycle during the cell expansion phase of fruit growth to study the effect of forced divisions on fruit size, for example by over-expressing candidates such as mitotic CDK/cyclins.

4 Post-Translational Regulation of SlKRP1

We have shown that SlKRP1 is a potential SlCSN5a target through its structural motif 2 (Article 1). Based on data in animal cells, we can assume that CSN5a is part of the SlKRP1 degradation pathway. SlKRP1 degradation depends on proteasome activity, as shown in the literature, and Figure 24.

While it would be interesting to compare the *in vivo* stability of SlKRP1 variant SlKRP1$^{\Delta 169\text{-}174}$ (deleted for the CSN5A interaction motif), it is likely that SlKRP1$^{\Delta 169\text{-}174}$ has no inhibitory activity on CDK/Cyc complexes, given the weakness of the interaction between SlKRP1$^{\Delta 169\text{-}174}$ and CycD3;1 or CDKA;1 in two-hybrid, and the proximity of the motif 2 to CDK/Cyc inhibition motif. The close proximity between the interaction sites of CSN5A and CDK/Cyc in KRP allow to hypothesize a competition between CDK/Cyc and CSN5A for KRP accessibility, or alternatively cooperation between CDK/Cyc and CSN5A for KRPs degradation. Competition co-immunoprecipitation, multicolour BiFC techniques, use of simultaneous BiFC and FRET, or triple-hybrid could help in answering the question of competition between CDK/Cyc and CSN5A for KRP accessibility. Nevertheless, the assumption of collaboration between CSN5 and CDK/Cyc is to be put into perspective with the necessity, in animals, of p27 phosphorylation by CDK/Cyc before the protein can be targeted by CSN5A. Such KRPs phosphorylation by CDK/Cyc was shown moreover in *Arabidopsis* (Verkest *et al.*, 2005).

To mitigate the possible effects that disrupting motif 2 would entail KRP ability to bind CDK/Cyc, using modified versions of SlKRP1 mutated on a single amino acid within motif 2 could possibly prevent the CSN5A binding while allowing CDK/Cyc binding.

CHAPTER 4 : MATERIAL ET METHODS

1 Biological Material

1.1 Plant Material

1.1.1 Tomato lines

Plants of cherry tomato (*Solanum lycopersicum* Mill. var. cerasiformae. cv. West Virginia 106) (Wva106) were grown either in greenhouses or in axenic conditions in MS medium (Murashige and Skoog, 1962) under a thermoperiod 25°C/20°C and a photoperiod of 14h/10h (day/night). After seed surface decontamination for 20 min with calcium hypochlorite 4% (w/v) and wash three times with water, tomato seeds were sown on MS ¼ germination medium.

1.1.2 SWEET100 tomato cells

A suspension of Tomato SWEET100 cells (*Solanum lycopersicum* L. cv. SWEET100) was also used. The cells were grown in the dark at 26°C in modified MS medium. The liquid cultures were kept under constant agitation (100 rpm) and subcultured every 7 days by transferring 2 mL of stationary phase cells in 50 mL NT medium (MS 4.4 g/L, sucrose 30 g/L, 2,4-D 10 µg/mL, pH 5.7). The cells were grown on solid media (NT added with 7 g/L agar) and subcultured every three weeks. Tomato cells were synchronized according to the protocol described by Porceddu *et al*. (2001), with aphidicolin (a specific inhibitor of DNA polymerase α). Ten mL of a 4 d-culture were diluted in 50 mL of fresh medium supplemented with 40 mg/mL of aphidicolin (ALEXIS Biochemicals). After 24h of culture, aphidicolin was rinsed with 6 successive washes of 5 min in 200 mL of medium without vitamins. The cells were then brought back into cultivation in 50 mL of fresh medium (corresponding to time zero, T0). Samples were then taken every hour. 200 µL of culture were taken for measurements of mitotic index, 500 µL for analysis by flow cytometry and 2 mL to achieve extraction of RNA or proteins.

1.2 Bacterial and Yeast Strains and Plasmids

1.2.1 Bacterial strains and culture mediums

Escherichia coli strain TOP10 (F- mcrA D(mrr-hsdRMS-mcrBC) f80lacZDM15 DlacX74 deoR recA1 araD139 D(ara-leu)7697 galU galK rpsL (StrR) endA1 nupGest) was used for cloning recombined plasmids of Gateway Technology.

Escherichia coli strain DB3.1 (F- gyrA462 endA1 glnV44 Δ(sr1-recA) mcrB mrr hsdS20(r_B^-, m_B^-) ara14 galK2 lacY1 proA2 rpsL20(Sm^r) xyl5 Δleu mtl1) was used for the propagation of Gateway plasmids containing the ccdB operon.

Escherichia coli strain XL1-Blue (*res*A1, *end*A1, *gyr*A96, *thi*, *hsd*R17 (rk^-, mk^+), *sup*E44, *rel*A1, *l*-, *lac*-, [F', *pro*AB, *lac*I^qZΔM15, Tn10 (Tetr)]) was used for plasmid cloning and propagation. Using this strain to clone plasmid with Gateway technology induced false positives, probably because of the gyrA96 mutation.

Agrobacterium tumefaciens strain GV3101 was used as a transformation vector to generate transgenic plants. It harbours a Ti plasmid (Tumour inducing) containing disarmed virulence gene *Vir* allowing the transfer of Transfer-DNA (T-DNA) in the nucleus of plant cells.

All bacterial strains were grown in LB medium (1% (w/v) Bactotryptone, 0.5% yeast extract (w/v), 1% (w/v) NaCl) in presence or absence of antibiotics. *E. coli* cells were grown at 37°C for about 16h and *A. tumefaciens* cells at 28°C for 48h. For solid media, 15 g/L bacteriological agar was added.

1.2.2 Yeast Strains and culture mediums

The *Saccharomyces cerevisiae* MAV203 strain (*MAT*α, *leu*2-3, 112, *trp*1-901, *his*3Δ 200, *ade*2-101, *gal*4Δ, *gal*80Δ, *SPAL*10::*URA*3, *GAL*1::*lac*Z, $HIS3_{UAS}$ *GAL*1::*HIS*3@*LYS*2, *can*1^R, *cyh*2^R) was used as a transformation vehicle for the two-hybrid. It contains endogenous Gal80 and Gal4 deletions for this purpose. Furthermore, it possesses *leu2* and *tpr1* mutations for the selection of positive co-transformation clones. Yeasts were cultured in YPAD medium and co-transformed

yeasts were grown in medium SD-L-T, 30°C for 72h. For solid media, 15 g/L bacteriological agar was added.

1.2.3 Plasmids

1.2.3.1 Entry vectors

The pGEM-T Easy plasmid (Promega) was used for cloning sequences amplified by PCR, at the multiple cloning site located between promoters T7 and SP6 of corresponding bacteriophages. This multisite is located in the DNA fragment encoding the α subunit of the β-galactosidase, allowing a selection of recombinant colonies by the white/blue system. It contains a selection cassette conferring ampicillin resistance.

The pDONR201 plasmid (Invitrogen) was used for cloning DNA fragments attB1/attB2-flanked by Gateway recombination. It contains the bacterial selection cassette conferring kanamycin resistance.

1.2.3.2 Expression vectors used for plant stable transformation

The vector pK2GW7 and pK2WG7 are binary vectors for *Agrobacterium tumefaciens* plant transformation. They contain between LB and RB of the T-DNA sequences, the strong constitutive 35S promoter and the terminator of the CaMV gene VI between which is a site of recombination R Gateway. The vector pK2GW7 has two sites attR1 and attR2 in the normal direction, while pK2WG7 vector has attR1 and attR2 sites inverted to allow the recombination of the DNA fragment in antisense orientation. They also contain the transformed plant selection cassette conferring kanamycin resistance.

1.2.3.3 Expression vectors used for plant transient transformation

All vectors of this subpart use the Gateway technology.

pBS-35S-YFP-attR and pBS-35S-attR-YFP vectors:

These vectors were used for transient expression of eYFP fused proteins, upstream or downstream of the protein according to the eYFP sequence orientation relative to the attR site.

p2CGW7 and p2GWC7 vectors:

These vectors were used for transient expression of proteins fused to eCFP, upstream (p2CGW7) or downstream (p2GWC7) of protein according to the orientation of the eCFP sequence from the attR site.

nEYFP/pUGW2, cEYFP/pUGW2, and nEYFP/pUGW0 cEYFP/pUGW0 vectors:

These vectors were used for transient expression of proteins fused to half-eYFP, for BiFC experiments. YFP (239 amino acids) is separated from nEYFP (1-174) and cEYFP (175-239), upstream (vector names ending with 0) or downstream (vector names ending with 2) protein sequence of interest.

1.2.3.4 Expression vectors used for two-hybrid experiments:

The vectors used are from the ProQuest Two-Hybrid System with Gateway Technology system (Invitrogen).

The plasmid pDEST32 was used to express the gene of interest, also known as "bait" in yeast. It carries the sequence encoding the binding domain of the GAL4 protein followed attR1 and attR2 DNA recombination sites. Furthermore, it has the leucine synthesis selection cassette for the yeast and the gene for gentamycin resistance for bacteria.

The plasmid pDEST22 allows overexpressing "target" proteins in yeast fused to activation domain of GAL4 protein transcription. It also differs in the plasmid selection markers harbouring the tryptophan supplementation cassette for yeast selection and the gene for ampicillin resistance for bacteria.

2 Methods for manipulating and analyzing nucleic acids

2.1 Nucleic acids extraction

2.1.1 Tomato genomic DNA Extraction

For the extraction and manipulation of genomic DNA, powdered samples were homogenized in Plant DNAzol®.(Invitrogen) in a polytron (0.3 mL per 50-100 mg of tissue). To ensure complete dissociation of nucleoprotein complexes, samples stand

for 5 minutes at room temperature. 0.3 mL of chloroform are added per mL of Plant DNAzol® used. The sample is shaked vigorously for 15 seconds, and is incubated for 5 minutes at room temperature. The sample is then centrigugated at 12000 *g* for 10 min. Centrifugation separates the mixture into 3 phases. The upper aqueous phase is transferred into a new tube, and 0.225 mL of 100% Ethanol per 1 mL of Plant DNAzol® are added. The samples are mixed by inversion and incubated for 5 minutes at room temperature. The tubes are then centrifugated at 5000 *g* for 4 minutes at 4°C. The supernantant is removed and the DNA pellet is washed in 0.3mL DNAzol® - ethanol wash mixture (0.75 volume of Ethanol 100% and 1 volume of Plant DNAzol®). The tubes are then centrifugated at 5000 *g* for 4 minutes, and the supernant removed. The DNA is resuspended in 75% ethanol (1.5-2 mL for each mL Plant DNAzol®). The DNA pellets are dried for 5-10 minutes under a vacuum and dissolved in 8 mM NaOH by repeated slow pipetting with a micropipette. Eight mM NaOH are added to the sample to reach a DNA concentration of 0.2-0.3 µg/µL. The samples are centrifugated at 12000 *g* for 10 minutes to remove any insoluble material and the supernatant is transferred to a new tube.

2.1.2 Plasmid DNA Extraction

Plasmid DNA is extracted using the kit "NucleoSpin ® Plasmid" of Macherey Nagel, according to the protocol described by the supplier. The plasmid DNA is eluted in 50 µL of sterile mQ water and quantified by spectrometry at 260 nm.

2.1.3 Total RNA Extraction

For the extraction and manipulation of RNA, tissue samples were powdered by grinding in frozen mill in liquid nitrogen. Powders were homogenized in TRI REAGENT™ (SIGMA) by vortexing (1 mL per 50-100 mg of tissue). To ensure complete dissociation of nucleoprotein complexes, samples stand for 5 minutes at room temperature. 0.2 mL of chloroform is added per mL of TRI REAGENT used, the sample is shaked vigorously for 15 seconds, and is incubated for 2-15 minutes at room temperature. The sample is then centrifuged at 12000 *g* for 15 minutes at 4°C. Centrifugation separates the mixture into 3 phases. The upper aqueous phase is transferred to a fresh tube and 0.5mL of isopropanol per mL of TRI REAGENT is added. The sample is incubated for 5-10 minutes at room temperature and

centrifuged at 12000 *g* for 10 minutes at 4°C. The RNA precipitate forms a pellet on the side and bottom of the tube. The supernatant is discarded and the RNA pellet is washed by adding 1 mL of 75% Ethanol per 1mL of TRI REAGENT. The sample is then vortexed and centrifuged at 7500 *g* for 5 minutes at 4°C. The ethanol is removed and the RNA pellet is briefly dried by 5-10 minutes air-drying. The RNA is finally dissolved with an appropriate volume of water (50µL).

DNA contamination is removed from RNA extract by using TURBO DNA-free™ Kit (Applied Biosystems): 0.1 volume of 10x TURBO Dnase Buffer and 1 µL TURBO Dnase are added to the sample for 10µg of RNA. After mixing, the sample is incubated at 37°C for 20-30 min. 0.1 volume Dnase Inactivation Reagent is added to the solution. After mixing, the solution is incubated for 2 minutes at room temperature. The sample is then centrifuged at 10000 *g* for 1.5 min and the RNA is transferred to a new tube.

2.2 Molecular Cloning

2.2.1 Cloning according to digest/ligation method

2.2.1.1 Enzymatic digestion of DNA

Hydrolysis of DNA by restriction endonucleases is done for analytical purposes or for cloning fragments of interest. This hydrolysis is performed in the presence of one unit of enzyme per mg of plasmid DNA. This digestion is done in the buffer recommended by the supplier (Promega). The reactions proceed at the optimum temperature for the enzyme used. The enzymes are inactivated by heat or by extraction with phenol/chloroform/isoamyl alcohol (25:24:1, v/v/v) followed by precipitation with 0.5 volume of 7 M ammonium acetate (DNA larger than 400 bp) or 0.1 volume of 3 M sodium acetate (DNA smaller than 400 bp) and 3 volumes of absolute ethanol.

2.2.1.2 Ligation in cloning vectors

For cloning into the vector pGEM-T Easy (Promega), the amplification products obtained by PCR were purified on a column (Wizard ® SV Gel and PCR Clean-Up System, Promega) and mixed with the cloning vector in a ratio 3/1. The ligation was performed overnight at 4°C by T4 DNA ligase (Promega) with 3U per 10 µL of reaction mixture according to the supplier's protocol. For cloning in other vectors,

DNA fragments are digested with restriction enzymes to generate ends compatible with restriction sites of cloning vector. The purification of these products and ligation performed in the conditions listed above. The mixture was then precipitated with ethanol before being resuspended in water. A fraction of this ligation mixture is used for electroporation of competent bacteria.

2.2.2 Cloning by recombination using GATEWAY technology

The cloning of the tomato sequences of interest is done with the Gateway® technology developed by Invitrogen. This technology is based on the use of the capacity of bacteriophage lambda to recognize specific sites on the chromosome of *Escherichia coli* to induce the phenomena of recombinant DNA (Landy, 1989). Recombination occurs between specific DNA sequences called "att": site-specific attachment, attB on the chromosome of *E. coli* and attP on the lambda phage. Recombination is an exchange followed by ligation of two strands of DNA to give a new DNA. This technology therefore provides an efficient means to integrate a DNA sequence with attB sites in an intermediate "entry" vector with the attP sites. Integration into the first vector can transfer quickly, once more by recombination, the sequence of interest in different "destination" vectors based on the desired applications.

2.2.2.1 Insert preparation

The sequence of the gene of interest to be inserted in the destination vector is obtained from tomato cDNA by PCR using Taq DNA Polymerase High Fidelity Isis ® (Eurogentec) as recommended by the supplier. To add the attB sites in the sequence of interest, a second PCR is performed on the amplicons (10-100 ng) previous column purification (Wizard ® SV Gel and PCR Clean-Up System, Promega) in the presence of a pair of primers containing specific sequences of the gene of interest flanked by attB sites (Table 6 and Table 8).

The PCR amplification reaction is performed with the Isis polymerase as recommended by the supplier. The conditions of this second PCR differ from the usual conditions: denaturation at 94°C for 3 minutes, the first step consists of 5 cycles of 15 seconds at 94°C, 30 seconds at 50°C and 1 min/kbp of target gene at 72°C, followed by a second phase of 25 cycles of 15 seconds at 94°C, 30 seconds

(Tm -2°C) and 1 minute/kb of target gene at 72°C. A step of DNA synthesis by primer extension performed at 72°C for 5 minutes ended the reaction. The attB-PCR fragments were purified on a column (Wizard ® SV Gel and PCR Clean-Up System, Promega).

2.2.2.2 Cloning into entry vector:

Cloning purified attB-flanked PCR fragment in the entry vector pDONR™ 201 is achieved through the reaction of "BP recombination" according to the supplier's protocol (Invitrogen). The recombination reaction is carried out from 50 to 150 ng of attB-flanked PCR product in 5 µL of reaction mixture consisting of 75 ng pDONR™ vector (entry vector), 1 µL BP clonase enzyme qsp H2O. The reaction is incubated for 24 h at 25°C. One µL of this reaction is used to transform 40 µL of TOP10 electrocompetents cells.

2.2.2.3 Cloning into destination vector :

Cloning also occurs by recombination called "LR recombination" that transfers the sequence of interest in different destination vectors. This reaction is done on the product of the "BP recombination" after selection and amplification of recombinant clones. At 75 ng of recombined entry vector are added 75 ng of destination vector, and 1 µl of LR clonase enzyme (Invitrogen), qsp H2O. The reaction is incubated overnight at 25°C. One µL of reaction is used to transform 40 µL of electrocompetent TOP10 cells as shown below.

2.2.3 Preparation and transformation of electrocompetent bacteria

E. coli bacteria were plated on solid LB medium and incubated overnight to 37°C. A colony is inoculated in 10 mL of LB medium. The preculture was held in liquid medium under agitation (200 rpm) overnight at 37°C. Two hundred mL of LB medium were inoculated with 2 mL of the preculture. Incubation is performed under the same conditions as before until a DO600nm = 0.5. All subsequent steps consist of cycles of centrifugation and resuspension of the bacterial pellet in a solution of glycerol 10% (v/v) and are performed at 4°C to avoid thermal shock. The pellets are taken successively in decreasing volumes of 60 mL, 20 mL, 10 mL and 400 µL. Aliquots of 40µL of this mixture were immediately frozen in liquid nitrogen and stored at -80°C.

The transformation is performed by electroporation using MicropulserTM (BioRad). 40 µL of electrocompetent bacteria were thawed in ice and added to a fraction of the ligation or recombination mixture. The mixture, placed in an electroporation tank (1 mm gap), is subjected to an electric pulse of 1800 volts in a few milliseconds provided by the generator. The bacteria are then immediately incubated in 1 mL of LB medium with stirring (200 rpm) for 45 minutes at 37°C. A fraction of the culture is spread on solid LB medium supplemented with the appropriate selection antibiotic, according to the plasmid used for cloning.

The preparation of electrocompetent *Agrobacterium tumefaciens* bacteria and transformation are performed using the same protocol, but the incubations are longer and take place at 28°C.

2.2.4 Preparation and transformation of thermocompetent yeasts

The following protocol allows ten independent co-transformations.

MAV203 yeasts are plated on solid YPAD medium and incubated for 3 days at 30°C. A colony is inoculated in 10 mL of liquid YPAD medium. The preculture was held in liquid medium under agitation (200 rpm) overnight at 30°C. The concentration of cells in the medium is counted using a Malassez cell, and a volume of preculture equivalent to 2.5 x 10^8 cells is used to inoculate 50 mL of liquid YPAD medium. Yeasts are incubated for 3-4 hours at 30°C under agitation (200 rpm), until yeasts reach a concentration of 2 x 10^7 cells per mL. The culture is then centrifuged (5 min, 10000 *g*), the pellet is solubilized in 25 mL sterile water, centrifuged (5 min, 10000 *g*), and the pellet is then solubilized in 3 mL 0.1M Lithium Acetate, and incubated for 15 minutes at 30°C under agitation (200 rpm). After incubation, the mix is centrifuged (5 min, 10000 *g*), and the pellet is resuspended in the transformation mix (2.4mL of 50%PEG 3350, 360 µL of 1M Lithium Acetate, 280 µL H2O, 500 µL of salmon sperm DNA at 2 mg/mL). The mix is dispatched between ten tubes containing 6 µL of the two tested plasmids (354 µL of transformation mix per tube). The tubes are incubated 30 min at 30°C under agitation (200 rpm) and then incubated in a water bath at 42°C for 20 minutes. The tubes are then centrifuged on a tabletop centrifuge (5 min, 7000 rpm), and the pellet is solubilized in 500 µL H2O. Each mix is then spread on solid SD-L-T medium, and incubated for 3 days at 30°C.

2.3 Retro-Transcription Reaction (RT)

The synthesis of complementary DNA (cDNA) was performed according to the protocol provided by the supplier (Biorad). One µg of total RNA is denatured for 10 min at 70°C in a thermal cycler (PTC-100; MJResearch) and then quickly placed on ice. Four µL of 5x iScript Reaction Mix, 1 µL of iScript Reverse Transcriptase and water (qsp 20 µL) were added to the samples. After homogenization, the stabilization of hybrid primer / template is made for 5 min at 25°C. The synthesis of cDNA is carried out for 1 h at 42°C. The reaction was stopped by inactivation of the enzyme at 70°C for 15 min.

2.4 Polymerase Chain Reaction (PCR)

PCR reactions were performed either in the presence of genomic DNA (0.1 µg) or plasmid DNA (0.1 ng) or cDNA, or directly on bacterial or yeast colonies.

2.4.1 Reaction Mix

The PCR reactions are performed in a reaction mixture of 50 µL containing 10 µL of 5X reaction buffer, 50 pmol of each primer, 0.5 µL of dNTP (20 mM), 1.25 units GoTaq ® DNA Polymerase (Promega). To achieve the different clonings, the Isis DNA Polymerase (Ifremer) was used as recommended by the supplier. The primers used in PCR are presented in Table 6, Table 7 and Table 8 according to the given combinations shown Table 9.

2.4.2 PCR conditions

The amplification reactions are performed in a thermal cycler (PTC-100; MJResearch). The samples undergo an initial step of denaturation of 5 min at 94°C, then the reaction mixtures are subjected to amplification cycles comprising a denaturation step of 30 s at 94°C, a hybridization step of 30 s at a temperature suitable for primers and a DNA synthesis step at 72°C whose duration varies with the size of the DNA molecule to be amplified. PCR reactions were completed by a step of 10 min at 72°C. The amount of transcript obtained was estimated by visualization following electrophoresis.

Table 6 : List of primers used for cloning of candidate genes

Primer name	Sequence
MCM7GATFOR	GGGGACAAGTTTGTACAAAAAAGCAGGCTTCATGAATGATCTTGACTTCAACCGC
MCM7GATREV	GGGGACCACTTTGTACAAGAAAGCTGGGTCTCATGCATCAATGAATCTGATGTT
MCM7GATREVNS	GGGGACCACTTTGTACAAGAAAGCTGGGTCTGCATCAATGAATCTGATGTTAAA
BZIPGATFOR	GGGGACAAGTTTGTACAAAAAAGCAGGCTTCATGGCTAGCGAGAAAGTTTTCAGCG
BZIPGATREV	GGGGACCACTTTGTACAAGAAAGCTGGGTCTCAGCCATTTTCACCTGCCAAAAAC
BZIPGATREVNOSTP	GGGGACCACTTTGTACAAGAAAGCTGGGTCGCCATTTTCACCTGCCAAAAACAAA
SKP2GATFOR	GGGGACAAGTTTGTACAAAAAAGCAGGCTTCATGATAGGGGTAGAAGATTTGAGCT
SKP2GATREV	GGGGACCACTTTGTACAAGAAAGCTGGGTCTCAGTGAGCTGGATGGAGAACTCGT
SKP2GATREVNS	GGGGACCACTTTGTACAAGAAAGCTGGGTCGTGAGCTGGATGGAGAACTCGTGCA
KRB2GATFOR	GGGGACAAGTTTGTACAAAAAAGCAGGCTTCATGGCTAGTGTTGAAGCAAGACATC
KRB2GATREV	GGGGACCACTTTGTACAAGAAAGCTGGGTCTCAAGAAGTCATGTTGACGTGAACT
KRB2GATREVNS	GGGGACCACTTTGTACAAGAAAGCTGGGTCAGAAGTCATGTTGACGTGAACTGTT
GATEKBR5	GGGGACAAGTTTGTACAAAAAAGCAGGCTACATGGCAGTTGAGGCAAGACATCTC
GATEKBR3	GGGGACCACTTTGTACAAGAAAGCTGGGTCTCAAGAAGACATGTTAACATGCAC
GATEKBRNS3	GGGGACCACTTTGTACAAGAAAGCTGGGTCAGAAGACATGTTAACATGCACAGT
CKS1GATFOR	GGGGACAAGTTTGTACAAAAAAGCAGGCTTCATGGGACAGATCCAGTATTCTGAG
CKS1GATREV	GGGGACCACTTTGTACAAGAAAGCTGGGTCTCACTTGGCAAGCAGAACTTGCTGA
CKS1GATREVNS	GGGGACCACTTTGTACAAGAAAGCTGGGTCCTTGGCAAGCAGAACTTGCTGAGTC
CDKA1GATF	GGGGACAAGTTTGTACAAAAAAGCAGGCTTCATGGGACCAGTATGAAAAA
CDKA1GATR	GGGGACCACTTTGTACAAGAAAGCTGGGTCTCACGGCACATACCCAAT
CDKA1GATRNOSTOP	GGGGACCACTTTGTACAAGAAAGCTGGGTCCGGCACATACCCAATATC
CYCD3GATF	GGGGACAAGTTTGTACAAAAAAGCAGGCTTCATGGTTTTCCCTTTAGAT
CYCD3GATR	GGGGACCACTTTGTACAAGAAAGCTGGGTCTCAGTGAAGATTACTACC
CYCD3GATRNOSTOP	GGGGACCACTTTGTACAAGAAAGCTGGGTCGTGAAGATTACTACCCAG
JABGATF	GGGGACAAGTTTGTACAAAAAAGCAGGCTTCATGGACGCTCTGAATTCT
JABGATR	GGGGACCACTTTGTACAAGAAAGCTGGGTCTCAGGTTTCGACCATCGG
JABGATRNOSTOP	GGGGCACACTTTGTACAAGAAAGCTGGGTCGGTTTCGACCATCGGCTC
GATERB5	GGGGACAAGTTTGTACAAAAAAGCAGGCTACATGGAGGAGCTGAAGAATCATTCG
GATERB3	GGGGACCACTTTGTACAAGAAAGCTGGGTCTTAGGGCTCGGGCTGCTCAGTCTTC
GATERBNS3	GGGGACCACTTTGTACAAGAAAGCTGGGTCGGGCTCGGGCTGCTCAGTCTTCAC
CKB2gatfor	GGGGACAAGTTTGTACAAAAAAGCAGGCTTCATGTATAGAGATCGAGGAGGTG
CKB2gatrev	GGGGACCACTTTGTACAAGAAAGCTGGGTCCTACCATAACCAATTGTACATC
CK2gatrevns	GGGGACCACTTTGTACAAGAAAGCTGGGTCCCATAACCAATTGTACATCAAAGC
PCNAgatfor	GGGGACAAGTTTGTACAAAAAAGCAGGCTTCATGTTGGAACTACGTCTTGTTCAG
PCNAgatrev	GGGGACCACTTTGTACAAGAAAGCTGGGTCTCAAGGCTTGGTTTCCTCTTCATCCTC
PCNAgatrevnostop	GGGGACCACTTTGTACAAGAAAGCTGGGTCAGGCTTGGTTTCCTCTTCATCCTC
5LINKERPCNA	GGTGGGCGGAGAAGGTCAAGGACAAGGTCAGGGACCTGGTAGAGGAATGTTGGAACTACGTCTTGTTC
ATTB1NLSLINK	GGGGACAAGTTTGTACAAAAAAGCAGGCTTCCCAAAGAAGAAGCGTAAGGTGGGCGGAGAAGGTCAAG
GATECDKB1.15	GGGGACAAGTTTGTACAAAAAAGCAGGCTACATGGAGAAATACGAGAAATTGGAG
GATECDKB1.13	GGGGACCACTTTGTACAAGAAAGCTGGGTCTCAGAATTGAGACTTGTCCAAGCTG
GATECDKB1.13NS	GGGACCACTTTGTACAAGAAAGCTGGGTCGAATTGAGACTTGTCCAAGCTGTC

Table 7 : List of the different primers used for plasmid constructions for tomato plant transformation

primer name	sequence
NTKRP2ATTB5	GGGGACAAGTTTGTACAAAAAAGCAGGCTGGTGGGGCTGATGAAATTGC
NTKRP2ATTB3	GGGGACCACTTTGTACAAGAAAGCTGGGTGCTATGTCACCTTGCAAG
KRP2NTas5	GCTATGTCACCTTGCAAG
KRP2NTas3	GCTGGTGGGGCTGATG
E85	CTGAGCTCCATTCATTTTTGACATCCC
E83	CTACTAGTGTCTTTTGCACTGTGAATG
Sac1PEPC2b	CTCGAGCTCCATTCTACTTTGAAGTTGTTTAATG
Xba1PEPC2b	CTCAATCTAGAAAATCAAAATCCTGCAAAAAA
KRP1pet28ATTB5	GGGGACAAGTTTGTACAAAAAAGCAGGCTTCATGGGCAGCAGCCATCATCAT
KRP1pet28ATTB3	GGGGACCACTTTGTACAAGAAAGCTGGGTCTAATGGTTTACTTTCACC

Table 8 : List of primers used to obtain the different KRPs and their variants

KRP1GATF	GGGGACAAGTTTGTACAAAAAAGCAGGCTTCATGGGGAAGTACATAAGG
KRP1GATR	GGGGACCACTTTGTACAAGAAAGCTGGGTCCTAATGGTTTACTTTCAC
KRP1GATRNOSTOP	GGGGACCACTTTGTACAAGAAAGCTGGGTCATGGTTTACTTTCACCCA
KRP2GATF	GGGGACAAGTTTGTACAAAAAAGCAGGCTTCATGGGAAAATACTTGAGA
KRP2GATR	GGGGACCACTTTGTACAAGAAAGCTGGGTCTTAGTGATTCACCCTAAT
KRP2GATRNOSTOP	GGGGACCACTTTGTACAAGAAAGCTGGGTCGTGATTCACCCTAATCCA
KRP3GATFOR	GGGGACAAGTTTGTACAAAAAAGCAGGCTTCATGGGTAAGTATATGAGG
KRP3GATR	GGGGACCACTTTGTACAAGAAAGCTGGGTCCTAACGATCTACTTTCAC
KRP3GATRNOSTOP	GGGGACCACTTTGTACAAGAAAGCTGGGTCACGATCTACTTTCACCCA
KRP4GATFOR	GGGGACAAGTTTGTACAAAAAAGCAGGCTTCATGAGAAGAAAGTATAAG
KRP4GATR	GGGGACCACTTTGTACAAGAAAGCTGGGTCTCATTGTCGAACCCATTC
KRP4GATRNOSTOP	GGGGACCACTTTGTACAAGAAAGCTGGGTCTTGTCGAACCCATTCGTA
KRP15no456	GGGGACAAGTTTGTACAAAAAAGCAGGCTTCATGGTCAAACCCTTTACGGTTCTTGAA
KRP15no56	GGGGACAAGTTTGTACAAAAAAGCAGGCTTCATGCTTAACGGCGGTGATGGTGGGTCG
KRP13no123	GGGGACCACTTTGTACAAGAAAGCTGGGTCCTAGATAGTTGGTTGAATCGAGTTTGG
KRP1NO123NS	GGGGACCACTTTGTACAAGAAAGCTGGGTCGATAGTTGGTTGAATCGAGTTTGGT
KRP1motif1235	GGGGACAAGTTTGTACAAAAAAGCAGGCTTCATGCGTACTAATGCAAATGAGGCCAAC
krp1M456gatrev	GGGGACCACTTTGTACAAGAAAGCTGGGTCCCCTTCAAGAACCGTAAAGGGTTTG
KRP1NO6GATFOR	GGGGACAAGTTTGTACAAAAAAGCAGGCTTCATGATAAGGAAGACAAGAAAAACAGAG
KRP1NO5	ATGGGGAAGTACATAAGGAAGACAAGAAAAACAGAGGATGTATCACCTCTTAACGGCGGTGATGGTGGG
KRP15no4	CTTAACGGCGGTGATGGTGGGTCGGTCAAACCCTTTACGGTTCTTGAA
KRP13no4	TTCAAGAACCGTAAAGGGTTTGACCGACCCACCATCACCGCCGTTAAG
KRP1NO353	ATCCCAACAGATCTTACCCGTGCAGAAAAGGAGCAGCAGAGAAAATTCATCGAG
KRP1NO335	CTTTTCTGCACGGGTAAGATCTGTTGGGATAGTTGGTTGAATCGAGTTTGGTAC
KRP15noTRESTPC	GAATTTGAAGGTAGAAAAAGGACCAGTTTGATAAGGGATTCAGACAAC
KRP13noTRESTPC	GTTGTCTGAATCCCTTATCAAACTGGTCCTTTTTCTACCTTCAAATTC
KRP1dom3gatrev	GGGGACCACTTTGTACAAGAAAGCTGGGTCTCACTCGATGAATTTTCTCTGCTGCTC
KRP15after4KRP4	GTCAAACCCTTTACGGTTCTTGAAAGAAGAAAGTATAAGTGCAAGTCG
KRP13after4KRP4	CGACTTGCACTTATACTTTCTTCTTTCAAGAACCGTAAAGGGTTTGAC
KRP1A4GATFOR	GGGGACAAGTTTGTACAAAAAAGCAGGCTTCATGGGGAAGGCCATAAGGAAGACAAGAAAAAC
KRP1A21	GTATCACCTCTTGGTGTTCTTGCAAGGGCTAAAGCTTTAGCTCTT
KRP1A21REV	GAACACCAAGAGGTGATAC
KRP1A125	GAAAAAGGACCACCAGGGAGGCCACACCTTGCAGTTTGATAAG
KRP1A125REV	CTCCCTGGTGGTCCTTTTTC
KRP136A	CTTAACGGCGGTGATGGTGGGTCGGCTCTAGAGCTTAGGAGTAGGAGGCTGGTC
KRP1A36REV	CGACCCACCATCACCGCCGTTAAG
KRP141A	CTTAACGGCGGTGATGGTGGGTCGTATCTAGAGCTTAGGGCTAGGAGGCTGGTC
KRP1A142	CAACATTCAGACCCCTGGTGCCAGTACTAGGCGTACTAATG
KRP1A142REV	CCAGGGGTCTGAATGTTG
KRP143A	CTTAACGGCGGTGATGGTGGGTCGTATCTAGAGCTTAGGAGTAGGGCGCTGGTC

Table 9 : List of the different couples of primers used and the corresponding matrix from previous PCR reactions, used to obtain PCR products of different candidate genes and modified sequences of SlKRP1

PCR product name	Primer 1	Primer 2	Matrix 1	Matrix 2
attB-CDKB1;1 attB-CDKB1;1 without STOP codon	GATECDKB1.15 GATECDKB1.15	GATECDKB1.13 GATECDKB1.13NS		
attB-MCM7 attB-MCM7 without STOP codon	GATEMCM75 GATEMCM75	GATEMCM73 GATEMCM73NS		
attB-BZIP attB-BZIP without STOP codon	BZIPGATFOR BZIPGATFOR	BZIPGATREV BZIPGATREVNOSTP		
attB-SKP2 attB-SKP2 without STOP codon	SKP2GATFOR SKP2GATFOR	SKP2GATREV SKP2GATREVNS		
attB-KBR2 attB-KBR2 without STOP codon	KRB2GATFOR KRB2GATFOR	KRB2GATREV KRB2GATREVNS		
attB-KBR1 attB-KBR1 without STOP codon	GATEKBR5 GATEKBR6	GATEKBR3 GATEKBRNS3		
attB-CKS1 attbB-CKS1 without STOP codon	CKS1GATFOR CKS1GATFOR	CKS1GATREV CKS1GATREVNS		
attB-CDKA;1 attB-CDKA;1 without STOP codon	CDKA1GATF CDKA1GATF	CDKA1GATR CDKA1GATRNOSTOP		
attB-CycD3;1 attB-CycD3;1 without STOP codon	CYCD3GATF CYCD3GATF	CYCD3GATR CYCD3GATRNOSTOP		
attB-CSN5 attB-CSN5 without STOP codon	JABGATF JABGATF	JABGATR JABGATRNOSTOP		
attB-RB attB-RB without STOP codon	GATERB5 GATERB5	GATERB3 GATERBNS3		
attB-CK2B attB-CK2B without STOP codon	CKB2gatfor CKB2gatfor	CKB2gatrev CK2gatrevns		
attB-PCNA attB-PCNA without STOP codon	PCNAgatfor PCNAgatfor	PCNAgatrev PCNAgatrevnostop		
LINKER-PCNA attB-NLS-LINKER-PCNA	5LINKERPCNA ATTB1NLSLINK	PCNAgatrev PCNAgatrev	attB-PCNA LINKER-PCNA	
attB-KRP1 attB-KRP1 without STOP codon	KRP1GATF KRP1GATF	KRP1GATR KRP1GATRNOSTOP		
attB-KRP2 attB-KRP2 without STOP codon	KRP2GATF KRP2GATF	KRP2GATR KRP2GATRNOSTOP		
attB-KRP3 attB-KRP3 without STOP codon	KRP3GATFOR KRP3GATFOR	KRP3GATR KRP3GATRNOSTOP		
attB-KRP4 attB-KRP4 without STOP codon	KRP4GATFOR KRP4GATFOR	KRP4GATR KRP4GATRNOSTOP		
attB-KRP1Δ1-44 attB-KRP1Δ1-44 without STOP codon	KRP15no456 KRP15no456	KRP1GATR KRP1GATRNOSTOP		
attB-KRP1Δ1-28 attB-KRP1Δ1-28 without STOP codon	KRP15no56 KRP15no56	KRP1GATR KRP1GATRNOSTOP		
attB-KRP1Δ165-210 attB-KRP1Δ165-210 without STOP codon	KRP1GATF KRP1GATF	KRP13no123 KRP1NO123NS		
attB-KRP1Δ1-4 attB-KRP1Δ1-4 without STOP codon	KRP1NO6GATFOR KRP1NO6GATFOR	KRP1GATR KRP1GATRNOSTOP		
KRP1Δ18-28 KRP1Δ18-28 without STOP codon	KRP1NO5 KRP1NO5	KRP1GATR KRP1GATRNOSTOP		
attB-KRP1Δ18-28 attB-KRP1Δ18-28 without STOP codon	KRP1GATF KRP1GATF	KRP1GATR KRP1GATRNOSTOP	KRP1Δ18-28 KRP1Δ18-28 without STOP codon	
KRP1Δ36-44 5' side KRP1Δ36-45 3' side KRP1Δ36-44 3' side without STOP codon attB-KRP1Δ36-44 attB-KRP1Δ36-44 without STOP codon	KRP1GATF KRP15no4 KRP15no4 KRP1GATF KRP1GATF	KRP13no4 KRP1GATR KRP1GATRNOSTOP KRP1GATR KRP1GATRNOSTOP	KRP1Δ36-44 5' side KRP1Δ36-44 5' side	KRP1Δ36-45 3' side KRP1Δ36-44 3' side without STOP codon
KRP1Δ122-128 5' side KRP1Δ122-128 3' side KRP1Δ122-128 3' side without STOP codon attB-KRP1Δ122-128 attB-KRP1Δ122-128 without STOP codon	KRP1GATF KRP15noTRESTPC KRP15noTRESTPC KRP1GATF KRP1GATF	KRP13noTRESTPC KRP1GATR KRP1GATRNOSTOP KRP1GATR KRP1GATRNOSTOP	KRP1Δ122-128 5' side KRP1Δ122-128 5' side	KRP1Δ122-128 3' side KRP1Δ122-128 3' side without STOP codon
attB-KRP1Δ53-210:KRP4 5' side attB-KRP1Δ53-210:KRP4 3' side attB-KRP1Δ53-210:KRP4 3' side without STOP codon attB-KRP1Δ53-210:KRP4 attB-KRP1Δ53-210:KRP4 without STOP codon	KRP1GATF KRP15after4KRP4 KRP15after4KRP4 KRP1GATF KRP1GATF	KRP13after4KRP4 KRP4GATR KRP4GATRNOSTOP KRP4GATR KRP4GATRNOSTOP	attB-KRP1Δ53-210:KRP4 5' side attB-KRP1Δ53-210:KRP4 5' side	attB-KRP1Δ53-210:KRP4 3' side attB-KRP1Δ53-210:KRP4 3' side without STOP codon
attB-KRP1Y4A attB-KRP1Y4A without STOP codon	KRP1A4GATFOR KRP1A4GATFOR	KRP1GATR KRP1GATRNOSTOP		
attB-KRP1T21A 5' side attB-KRP1T21A 3' side attB-KRP1T21A side without STOP codon attB-KRP1T21A attB-KRP1T21A without STOP codon	KRP1GATF KRP1A21 KRP1A21 KRP1GATF KRP1GATF	KRP1A21REV KRP1GATR KRP1GATRNOSTOP KRP1GATR KRP1GATRNOSTOP	attB-KRP1T21A 5' side attB-KRP1T21A 5' side	attB-KRP1T21A 3' side attB-KRP1T21A side without STOP codon
attB-KRP1Y36A 5' side attB-KRP1Y36A 3' side attB-KRP1Y36A side without STOP codon attB-KRP1Y36A attB-KRP1Y36A without STOP codon	KRP1GATF KRP136A KRP136A KRP1GATF KRP1GATF	KRP1A36REV KRP1GATR KRP1GATRNOSTOP KRP1GATR KRP1GATRNOSTOP	attB-KRP1Y36A 5' side attB-KRP1Y36A 5' side	attB-KRP1Y36A 3' side attB-KRP1Y36A side without STOP codon
attB-KRP1T125A 5' side attB-KRP1T125A 3' side attB-KRP1T125A side without STOP codon attB-KRP1T125A attB-KRP1T125A without STOP codon	KRP1GATF KRP1A125 KRP1A125 KRP1GATF KRP1GATF	KRP1A125REV KRP1GATR KRP1GATRNOSTOP KRP1GATR KRP1GATRNOSTOP	attB-KRP1T125A 5' side attB-KRP1T125A 5' side	attB-KRP1T125A 3' side attB-KRP1T125A side without STOP codon
attB-KRP1T142A 5' side attB-KRP1T142A 3' side attB-KRP1T142A side without STOP codon attB-KRP1T142A attB-KRP1T142A without STOP codon	KRP1GATF KRP1A142 KRP1A142 KRP1GATF KRP1GATF	KRP1A142REV KRP1GATR KRP1GATRNOSTOP KRP1GATR KRP1GATRNOSTOP	attB-KRP1T142A 5' side attB-KRP1T142A 5' side	attB-KRP1T142A 3' side attB-KRP1T142A side without STOP codon
attB-KRP1Δ1-145 attB-KRP1Δ1-145 without STOP codon	KRP1motif1235 KRP1motif1235	KRP1GATR KRP1GATRNOSTOP		
attB-KRP1Δ54-210	KRP1GATF	krp1M456gatrev		
attB-KRP1Δ188-210	KRP1GATF	KRP1dom3gatrev		
attB-KRP1Δ169-174 5' side attB-KRP1Δ169-174 3' side attB-KRP1Δ169-174 3' side without STOP codon attB-KRP1Δ169-174 attB-KRP1Δ169-174 without STOP codon	KRP1GATF KRP1NO353 KRP1NO353 KRP1GATF KRP1GATF	KRP1NO335 KRP1GATR KRP1GATRNOSTOP KRP1GATR KRP1GATRNOSTOP	attB-KRP1Δ169-174 5' side attB-KRP1Δ169-174 5' side	attB-KRP1Δ169-174 3' side attB-KRP1Δ169-174 3' side without STOP codon
attB-KRP1Δ18-28Δ36-44 5' side attB-KRP1Δ18-28Δ36-44 3' side KRP1Δ18-28Δ36-44 3' side without STOP codon attB-KRP1Δ18-28Δ36-44 attB-KRP1Δ18-28Δ36-44 without STOP codon	KRP1GATF KRP15no4 KRP15no4 KRP1GATF KRP1GATF	KRP13no4 KRP1GATR KRP1GATRNOSTOP KRP1GATR KRP1GATRNOSTOP	KRP1Δ18-28 attB-KRP1Δ18-28Δ36-44 5' side attB-KRP1Δ18-28Δ36-44 5' side	attB-KRP1Δ18-28Δ36-44 3' side KRP1Δ18-28Δ36-44 3' side without STOP codon
attB-KRP1Δ1-4Δ18-28 KRP1Δ1-4Δ18-28 without STOP codon	KRP1NO6GATFOR KRP1NO6GATFOR	KRP1GATR KRP1GATRNOSTOP	KRP1Δ18-28 KRP1Δ18-28 without STOP codon	
attB-KRP1Δ1-4Δ36-44 attB-KRP1Δ1-4Δ36-44 without STOP codon	KRP1NO6GATFOR KRP1NO6GATFOR	KRP1GATR KRP1GATRNOSTOP	attB-KRP1Δ36-44 attB-KRP1Δ36-44 without STOP codon	
attB-KRP1Δ1-44Δ165-210 attB-KRP1Δ1-44Δ165-210 without STOP codon	KRP15no456 KRP15no456	KRP13no123 KRP1NO123NS		
KRP1Δ18-28 Y36A KRP1Δ18-28 Y36A without STOP codon attB-KRP1Δ18-28 Y36A attB-KRP1Δ18-28 Y36A without STOP codon	KRP1NO5 KRP1NO5 KRP1GATF KRP1GATF	KRP1GATR KRP1GATRNOSTOP KRP1GATR KRP1GATRNOSTOP	attB-KRP1Y36A attB-KRP1Y36A KRP1Δ18-28 Y36A KRP1Δ18-28 Y36A without STOP codon	
attB-KRP1Δ122-128Δ165-210 attB-KRP1Δ122-128Δ165-210 without STOP codon	KRP1GATF KRP1GATF	KRP13no123 KRP1NO123NS	attB-KRP1Δ18-28Δ36-44 attB-KRP1Δ18-28Δ36-44 without STOP codon	
attB-KRP1Δ1-44Δ122-128Δ165-210 attB-KRP1Δ1-44Δ122-128Δ165-210 without STOP codon	KRP15no456 KRP15no456	KRP13no123 KRP1NO123NS	attB-KRP1Δ122-128Δ165-210 attB-KRP1Δ122-128Δ165-210 without STOP codon	

2.5 Real Time PCR

2.5.1 Real Time RT-PCR

The PCR amplification was performed in the presence of SYBR® Green, a fluorescent DNA intercalating agent, which allows the detection of the accumulation of double-stranded DNA in the reaction at each PCR cycle (wavelength of maximum excitation 497 nm, wavelength maximum emission 520 nm). The real-time recording of the fluorescence emitted allow detecting the exponential phase of PCR, during which the signal is proportional to the amount of DNA initially present.

Each PCR reaction was performed from 2 µL cDNA diluted to the tenth in a total reaction volume of 25 µL containing 12.5 mL of pre-mix iQ^{TM} SYBR® Green Supermix (Biorad) and 0.4 µM of oligonucleotides. The amplifications were performed in 96 well plates in the Biorad thermocycler iCycle Optical System. For each sample cDNA, 3 amplification reactions are performed. The amplification reactions include an initial denaturation step of 3 min at 95°C, followed by a series of 40 cycles comprising a denaturation step of 15 s at 95°C and 25 s step at 60°C for both hybridization of oligonucleotides and DNA synthesis. Finally, in a final step, each PCR product formed is subject to a gradual increase in temperature from 65°C to 95°C by 0.5°C steps every 5 s, which allows to establish a melting curve to determine for each PCR product formed its dissociation temperature. The completion of melting curves thereby allows verifying the synthesis of a unique PCR product per reaction.

The efficiency of each primer pair was previously verified by performing PCR from a standard series. For each pair of primers, the corresponding PCR product was first cloned into the vector pGEM-T easy and then purified on a column (Plasmid Miniprep PureYieldTM System, Promega). Each plasmid is then successively diluted to obtain a standard series ranging from 10^2 to 10^6 plasmid copies. The efficiency of each primer pair is then determined by performing a series of PCR from the reference range.

The levels of expression of the gene of interest are normalized with respect to the expression of *SlActin* and *SleiF4A* reference genes. Thus, the values represented correspond to values of relative expression.

2.5.2 Real Time Genomic PCR

Real time genomic PCR allows determining the number of insertions of a transgene in a transgenic plant. For this, we compare the level of amplification of the transgene, using primers specific to NPT2 (neomycin phosphotransferase), the resistance gene associated with the transgene and primers specific to APX (ascorbate peroxidase), an endogenous monocopy gene in tomato. The comparison of different reports NPT2/APX between plants allow to find the value NPT2/APX for which the transgene would be in monocopy, and allows afterwards to predict of the number of inserts present in the different genomes studied. The Real-Time PCR Genomics was conducted according to Mason *et al.* (2002). Each reaction was performed in a total volume of 25 µL containing 12.5 µL of iQ SuperMix, 150 mM of oligonucleotides and 100 mM of probe. The amplification reactions include an initial denaturation step of 5 min at 95°C, followed by a series of 40 cycles comprising a denaturation step of 15 s at 95°C and 1min step at 60°C for both hybridization of oligonucleotides and DNA synthesis. Finally, in a final step, each PCR product formed is subject to a gradual increase in temperature from 65°C to 95°C by 0.5°C steps every 5 s, which allows to establish a melting curve to determine for each PCR product formed its dissociation temperature. The completion of melting curves thereby allows verifying the synthesis of a unique PCR product per reaction.

2.6 DNA Electrophoresis

The plasmid DNA or PCR products were analyzed by electrophoresis in non denaturing agarose gel (1.5% (w/v)) in TAE buffer 0.5 X (20 mM Tris-HCl pH=8, 0.5 mM Na_2EDTA, 2.5 mM sodium acetate pH=8) The samples were added to 0.2 volume of loading buffer (glycerol 50% (v/v) bromophenol blue 0.25% (w/v), xylene cyanol 0.25% (w/v), EDTA 20 mM). DNA is visualized under UV light with Gel Green (Interchim, France) 1/50000 (v/v) after staining the gel for 15 min.

3 Protein analysis methods

3.1 Protein Extraction

Pericarps of tomato crushed in a mortar in the presence of liquid nitrogen are used for the extraction of proteins. One hundred milligrams of powder are placed in the presence of 1 mL of extraction buffer (50 mM Tris-HCl pH=7.2, 10 mM DTT, 5% PVPP, 1 mM PMSF, protease inhibitor cocktail 3% (v/v)) and agitated by vortexing until completely thawed. The cellular debris are removed by centrifugation (18000 *g*, 15 min) at 4°C. The supernatant is used directly for determination of protein quantity. The protein quantification is made by the method of Bradford (1976). A solution of BSA is used as standard.

3.2 Analysis by monodimentional electrophoresis in denaturing conditions

The proteins were analyzed by electrophoresis in denaturing conditions by one-dimensional system described by Laemmli (1970). The gel consists of two parts differing in their concentration of acrylamide and pH:

- Gel concentration (stacking gel): 5% (w/v) acrylamide, 0.13% (w/v) bisacrylamide, 125 mM Tris-HCl pH=6.8, 2 mM EDTA, 0.1 % (w/v) SDS and catalysts 0.05% (w/v) PSA and 0.05% (w/v) TEMED.
- Gel separation (Resolving gel): acrylamide from 10 to 15% (w/v), bisacrylamide 0.26 to 0.39% (w/v), 400 mM Tris-HCl pH=8.8, 2 mM EDTA, 0.1% (w/v) SDS and catalysts 0.05% (w/v) PSA and 0.05% (w/v) TEMED.

The samples were diluted in loading buffer [80 mM Tris-HCl pH=6.8, 15% (v/v) glycerol, 2% (w/v) SDS, 0.05% (w/v) bromophenol blue, 1% DTT] and denatured at 100°C for 5 min. The samples are then placed on gel and migration occurs in the electrophoresis buffer (25 mM Tris, 1mM EDTA, 192 mM glycine, 0.1% SDS).

3.3 Coomassie Blue protein revelation

After electrophoresis, proteins were found and fixed by immersion of the gel for 30 min in staining solution: 45% methanol, 10% acetic acid, 0.25% (w/v) Coomassie blue R250. The gel is then bleached in a solution of 45% methanol, 10% acetic acid.

3.4 western-blot analysis

3.4.1 Protein Electrotransfer on nitrocellulose membrane

After electrophoresis under denaturing conditions, proteins were transferred onto a nitrocellulose membrane (Hybond-C extra, Amersham) previously incubated in transfer buffer (25 mM Tris, 192 mM glycine, 20% methanol). The electrotransfer was performed for 1h at 350mA amperage, using the system Mini Trans-Blot cell (Bio-Rad).

The effectiveness and quality of the transfer are verified by membrane staining in Ponceau Red [0.1% (w/v) Ponceau Red, 1% (v/v) acetic acid]. The membrane is then bleached with water before performing the immunodetection.

3.4.2 Protein Immunodetection on nitrocellulose membranes

The membrane is saturated for 1h with gentle shaking in a solution of TBS (20 mM Tris-HCl, 135 mM NaCl, pH=7.6, 0.2% (v/v) Tween20 supplemented with 3% (w/v) skim milk powder). The membrane was washed briefly with TBS-0.2% Tween 20 supplemented with 0.5% (w/v) skim milk powder, and then incubated for 2h at room temperature or overnight at 4°C with primary antibodies diluted in this solution 1: 1000. Three successive washes of 5 min were then performed in TBS-0.2% Tween 20 supplemented with 0.5% (w/v) skim milk powder to remove unbound primary antibodies. The membrane is then incubated for 1h with a secondary antibody coupled to peroxidase (dilution 1:2000), then washed as before. The revelation is made using the system "BM Chemiluminescence Western Blotting Substrate" (Roche) according to the protocol described by the supplier.

3.5 Protein-protein interaction analysis by two-hybrid

3.5.1 Protein auto-activation verification

Proteins studied have been checked for their auto-activation in two-hybrid experiment. This verification is done by co-transforming yeast with the candidate construct and the complementary empty construct (pDEST22 + pDEST32-candidate, or pDEST32 + pDEST22-candidate).

Meanwhile, yeasts are transformed with control proteins known to interact with each other or not to be respectively positive and negative controls.

The yeasts are then grown at 30°C for 2 to 3 days on different 3-AT testing concentrations (ranging from 0 to 100 mM), and suitable 3-AT concentration for interaction experiment was chosen according to the minimum 3-AT concentration leading to an absence of growth of the tested constructs.

3.5.2 Protein-Protein interaction screening

After transformation, yeasts were plated on cotransformation selection medium (SD-Leu-Trp). Clones positive for co-transformation are selected on PCR. Three colonies from different transformation events are then delivered by culture on co-transformation selection (SD-L-T) and interaction selection (SD-L-T-H) medium with addition of 3-AT, ranging from minimal concentration (see 3.5.1) to 100 mM.

3.5.3 Verification of interaction specificity

When a positive clone was isolated by two-hybrid screening, the phagemids were isolated. For this, the isolated colony is used to inoculate a liquid culture of 3 mL of selective co-transformation medium (SD-L-T). After 2 to 3 days of incubation at 30°C, 2 mL of YPAD liquid are added to the culture before incubation under the same conditions for 6h. 1.5 ml is then centrifuged at 14,000 *g* for 10s. The pellet is then solubilized in 0.2 mL of yeast lysis buffer (2% (v/v) Triton X-100, 1% (w/v) SDS, 100 mM NaCl, 10mM Tris-HCl pH=8, 0,1mM EDTA). An equal volume of phenol/chloroform/isoamyl alcohol (25:24:1 (v/v/v)) and 0.3 g of glass beads (0.5 mm) are washed with acid then added to the mixture. The cells are then broken by vigorous shaking or vortex for 8 cycles of 1 min followed by a min cooling in ice. The DNA was centrifugation for 5 min at 14,000 *g*, and extracted with chloroform/isoamyl alcohol (24:1 (v/v)) then precipited by addition of 1/10th volume of 3M sodium acetate (pH=5.2) and 2.5 volumes of 100% ethanol. After centrifugation, the pellet is washed in 2.5 volumes of 70% ethanol, centrifuged, dried and finally solubilized in 50 µL of water. 5-20 µL of this solution are then used to transform TOP10 bacteria. After selection of positive clones by PCR, clones are amplified and the phagemid DNA is extracted.

The phagemids extracted are cotransformed with the construct coding for the bait plasmids and with controls to verify that the target protein is not able to auto-activate.

3.6 Sub-cellular localization, co-localization, and protein-protein interaction by BiFC

Images of sub-cellular localization, proteins colocalization and BiFC assays were obtained by using a Leica TCS SP2 AOBS confocal scanning microscope. CFP was excited using an argon laser at 458 nm and emissions were collected from 465–500 nm. YFP was excited by an argon laser at 514 nm and the emission collected from 525–600 nm. DAPI was excited by a 406nm Hg lamp and emissions were collected from 465-500 nm. Images of DAPI colocalization were obtained by using a Nikon Eclipse E800 epifluorescence microscope. YFP was visualized using a GFP filter (Ex: 460-500 nm, DM:505 nm, BA:510 nm), DAPI was visualized using a DAPI filter (Ex: 340-380 nm, DM:400 nm, BA:435-485 nm) and images were recorded using a camera Spot RTke. All images were processed using Photoshop Software (version CS3, Adobe Systems).

4 Methods for transgenesis and transgenic plants analysis

4.1 Construction of transformation vectors

4.1.1 Stable transformation vectors

The coding sequence of tomato histidine tagged-SlKRP1 was amplified by PCR from the plasmid-pet28 krp1 (Bisbis *et al.*, 2006) using primers KRP1pet28ATTB5 and KRP1pet28ATTB3 (Table 7) and introduced by BP reaction into pDONR201 plasmid. pDONR201-his-KRP1 vector was then recombined by LR with the destination vector pK2GW7. The promoter sequence of tomato PEPC2 was amplified by PCR using primers Sac1-PEPC2 and Spe1-PEPC2 (Table 7), and inserted by ligation into pK2GW7-his-krp1 vector digested Sac1/Xba1.

4.1.2 Transient transformation vectors

The various candidates tested in two-hybrid and transient transformation by microprojectile bombardment and chemical transformation were first transferred into

pDONR201 vector by BP-reaction and the corresponding destination vectors by LR-reaction.

4.2 Transformation and plant selection

4.2.1 Tomato cotyledon transformation

The transformation of tomato cotyledons is performed according to the amended protocol from Hamza *et al.* (1993).

The cotyledons of tomato were cut into 3 explants to induce a better response to the injury necessary for infection by *A. tumefaciens*. The preculture, co-culture and regeneration media used in the transformation of tomato cotyledons are described in Table 10. After 2 days of preculture, the explants were immersed for 30 minutes in an exponential growth phase culture of *A. tumefaciens* transformed with the recombinant plasmids containing the construct. The excess bacterial cells are eliminated between two sheets of absorbent sterile paper. The plant material is then co-cultivated with agrobacteria for 48h on agar. Then, the explants were rinsed twice for 3 min in water supplemented with 0.05% Tween20 (v/v) and cultured on selection medium [regeneration medium + 300 mg/mL kanamycin (Duchefa) + 250 mg/mL Timentin (Duchefa)] until the formation of callus. The regenerated plantlets growing from callus were subcultured on regeneration medium without hormone. The resistant regenerants were subcultured 3 times on the selection medium and rooted plants were transferred into a greenhouse.

Table 10 : *in vitro* culture and transformation media

Culture medium	Composition
MS	MS 5 g.L^{-1} sucrose 30 g.L^{-1} agar 5 g.L^{-1} pH 5,7
Germination	MS 1,25 g.L^{-1} sucrose 30 g.L^{-1} pH 5,7
Preculture	MS medium AIA 0,1 mg.L^{-1} BAP 2 mg.L^{-1}
Co-culture	MS medium AIA 0,1 mg.L^{-1} BAP 2 mg.L^{-1}
Regeneration	MS medium AIA 0,1 mg.L^{-1} BAP 2 mg.L^{-1} Timentin 250 mg.L^{-1} Kanamycine 300 mg.L^{-1}

4.2.2 Transient transformation by chemical method

The solutions used for isolation and transformation of protoplasts are detailed in Table 11. During the different steps that follow, all centrifugations are carried out for 5 minutes at 80 *g*.

Table 11 : Solutions used for protoplasts isolation and transformation

Solution	Composition
K3	Gamborg B5 3.19 g.L-1 sucrose 0.3 M pH 5.7
K4	macroelements 3.19g.L-1 sucrose 0.4 M pH 5.7
W5	NaCl 154 mM $CaCl_2$ 125 mM KCl 5 mM glucose 5mM pH 5.7
Mannitol/Mg	Mannitol 0.5 M MES 1% $MgCl_2$ 15 mM

4.2.2.1 Protoplast isolation

Protoplasts were obtained under sterile conditions from the mesophyll of leaves from tomato 6 week-old seedlings grown under axenic conditions, according to Paszkowski *et al.* (1984). Leaflets were placed in a Petri dish containing 15 mL of enzymatic digestion [K4 medium + 1.2% (w/v) cellulase Onozuka R10 (Duchefa Biochemie BV), 0.6 % (w/v) Macerozyme® R10 (Yakult Pharmaceutical], the lower epidermis in contact with the digestion solution. The leaflets are then coarsely shredded with a scalpel. The Petri dishes are placed at 28°C for 18 hours without agitation. The Petri dishes are then agitated very gently for 30 minutes at room temperature. The digestion medium was then filtered (pore size 140 µm), and each Petri dish was rinsed with 5 mL K4 environment. The filtrate is divided into several tubes so that the volume of filtrate in each tube does not exceed 2/3 of the tube volume. In each tube, 1 ml of W5 solution is then placed very gently at the surface of the filtrate. The tubes are then centrifuged driving the protoplasts at the interface of the filtrate and the W5 solution. Protoplasts are gently removed and transferred into new tubes. Two successive washes are then carried with 5 volumes of W5 solution. After the final wash, the supernatant is removed and 5 volumes of W5 are added to each tube. Protoplasts are incubated for two hours at 4°C in the dark. Protoplasts are counted by depositing 20 µL of the suspension in a Malassez cell.

4.2.2.2 Protoplast transformation

The transformation of protoplasts was performed according to the protocol adapted from Liu *et al.* (1994). The tubes containing the suspension of protoplasts are centrifuged. After removal of supernatant, the entire protoplast is resuspended in medium MMM in order to obtain a final concentration 2.5 x 10^6 protoplasts/mL. For transformation, 300 µL of protoplasts are placed in the presence of 10 µg of plasmid DNA and 300 µL of the transformation solution (40% (w/v) PEG6000, 0.4 M mannitol, 0.1 M $Ca(NO_3)_2$ pH=8). This preparation is incubated for 5 minutes at room temperature. Two mL of K3 are then added very slowly to above mixture. The protoplast suspension is incubated for two hours at 26°C in the dark and then rinced with 5 volumes of W5 medium. After centrifugation, the supernatant is removed and the protoplasts are resuspended in 3 mL of K3.

4.2.3 Biolistic transient transformation

This transformation protocol was adapted from the method described by Varagona *et al.* (1992). Five µL of plasmid DNA solution (100 ng/µL to 2 µg/µL) is mixed with 25 µL of 50% ethanol solution containing gold microparticles (diameter 1 or 1.6 µm) to 0.125 mg/µL. Then 25µL of 2.5 M $CaCl_2$ and 10 µL of 0.1 M spermidine are added. The mixture is then vortexed for 3 minutes and centrifuged a few seconds at room temperature. The pellet is then washed successively with 200 µL 70% ethanol, then 200 µL of 100% ethanol before being resuspended in 30 µL of 100% ethanol. Eight µL of this solution is deposited on a macrocarrier disk which will be used after evaporation of ethanol to transform the plant material.

The transformation of the cells was performed by a biolistic particle gun PDE-1000HE (Biorad) at a depressure of 710 mm Hg using a rupture disk corresponding to a helium pressure of 1100 psi and at a distance of 6 cm. After transformation, cells were incubated at 28°C in the dark for 2 to 24 hours.

4.3 Methods for transgenic plants analysis

4.3.1 Molecular Analysis

The transformed plants are analyzed by PCR and RT-PCR in order to verify the integration of T-DNA into the genomic DNA of the plant and whether the transcription of mRNAs corresponding respectively (see 2.4). The transgene copy number was estimated by real-time genomic PCR (see 2.5.2).

4.3.2 Morphometric analysis

The fruits are collected at different stages (anthesis, 3, 5, 6, 8, 10, 15, 20, 25, 30 and 40 days after anthesis), weighed and subjected to measurements of ploidy and pericarp cell size.

4.3.3 Trangene segregation analysis

To study the segregation of the transgene via the selection marker, the seeds of transgenic plants were sown on sterilized MS¼ medium supplemented with 300 mg/mL kanamycin. The ratio between the number of resistant plants and the number

of susceptible plants was used to determine the number of integration loci of the selection marker present on the T-DNA.

5 Methods for histological and cytological analysis

5.1 Measurement of cell surface

5.1.1 Pericarp cells

Sections of the pericarp of approximately 1 to 2 mm in thickness are made with razor blade from a fruit cut in the equatorial plane and placed on the surface of a drop of 0.04% toluidine solution. After 2 minutes of staining, the sections were briefly rinsed in water and placed in a Petri dish, flushed face upwards. The pericarp fragments are observed with a binocular Olympus and images are taken with a digital camera (Sony DKC-CM30). For each plant, at least three fruits were analyzed and for each fruit at least three servings of pericarp are removed. The number of epidermal cell layers external to the internal skin is counted. The cell surface of each layer was measured using the ImagePro-Plus software (Media Cybernetics). The average area of cells in the central area of the pericarp was measured by counting the number of cells in a given area.

5.2 Mitotic Index Measurement

To determine the mitotic index of cells synchronized SWEET100 tomato, 200 µL of cell suspension were fixed in a solution of one volume of acetic acid and two volumes of 100% ethanol. After 10 minutes, nuclei were stained with DAPI (4 ',6-diamino-2-phenylindole, 5 mg/mL) and mitotic figures are observed between slide and coverslip in epifluorescence at 471 nm when excited with UV (357 nm) using objectives of 20x or 40x Zeiss Axioplan microscope. The mitotic index corresponds to the percentage of mitotic figures observed (metaphase/anaphase/telophase). For each measurement, the counting is done on 500 nuclei.

5.3 Flow cytometry

The core preparations were analyzed with a Partec Pas-II cytometer (Münster, Germany). The computer system associated cytometer (DPAC, Partec) can process

the signals to represent the form of histograms of populations of nuclei. Measurements of flow cytometry were performed on 20000 nuclei.

5.3.1 Nuclei preparation from leaf or tomato pericarp

Nuclei were prepared from leaves or pericarp of tomato fruits are placed in a Petri dish and are sliced with a razor blade in 1mL of buffer Cystain UV ploidy (Partec) containing DAPI. The samples are then filtered through a nylon film (pore size, 100 µm).

5.3.2 Nuclei preparation from tomato SWEET100 cells culture

To follow the evolution of 2C and 4C peaks in synchronized cells of tomato, 500 µL of cells are taken every hour. After sedimentation of cells, the cell pellet was frozen in liquid nitrogen, thawed and resuspended in 1mL of buffer Cystain UV ploidy (Partec). The samples are then filtered through a nylon film (pore size, 20 µm).

CHAPTER 5: BIBLIOGRAPHIC REFERENCES

Achard P, Gusti A, Cheminant S, Alioua M, Dhondt S, Coppens F, Beemster Gt, Genschik P. 2009. Gibberellin signaling controls cell proliferation rate in Arabidopsis, *Curr Biol*, Vol. 19, pp. 1188-1193.

Adams Pd, Sellers Wr, Sharma Sk, Wu Ad, Nalin Cm, Kaelin Wg, Jr. 1996. Identification of a cyclin-cdk2 recognition motif present in substrates and p21-like cyclin-dependent kinase inhibitors, *Mol Cell Biol*, Vol. 16, pp. 6623-6633.

Akoulitchev S, Chuikov S, Reinberg D. 2000. TFIIH is negatively regulated by cdk8-containing mediator complexes, *Nature*, Vol. 407, pp. 102-106.

Andersen Su, Buechel S, Zhao Z, Ljung K, Novak O, Busch W, Schuster C, Lohmann Ju. 2008. Requirement of B2-type cyclin-dependent kinases for meristem integrity in Arabidopsis thaliana, *Plant Cell*, Vol. 20, pp. 88-100.

Ayala Fj, Fitch Wm, Clegg Mt. 2000. Variation and evolution in plants and microorganisms: toward a new synthesis 50 years after Stebbins, *Proc Natl Acad Sci U S A*, Vol. 97, pp. 6941-6944.

Barroco Rm, Peres A, Droual Am, De Veylder L, Nguyen Le Sl, De Wolf J, Mironov V, Peerbolte R, Beemster Gt, Inze D*, et al.* 2006. The cyclin-dependent kinase inhibitor Orysa;KRP1 plays an important role in seed development of rice, *Plant Physiology*, Vol. 142, pp. 1053-1064.

Beemster Gt, De Vusser K, De Tavernier E, De Bock K, Inze D. 2002. Variation in growth rate between Arabidopsis ecotypes is correlated with cell division and A-type cyclin-dependent kinase activity, *Plant Physiol*, Vol. 129, pp. 854-864.

Bemis Sm, Torii Ku. 2007. Autonomy of cell proliferation and developmental programs during Arabidopsis aboveground organ morphogenesis, *Developmental Biology*, Vol. 304, pp. 367-381.

Besson A, Dowdy Sf, Roberts Jm. 2008. CDK inhibitors: cell cycle regulators and beyond, *Dev Cell*, Vol. 14, pp. 159-169.

Bird Da, Buruiana Mm, Zhou Y, Fowke Lc, Wang H. 2007. Arabidopsis cyclin-dependent kinase inhibitors are nuclear-localized and show different localization patterns within the nucleoplasm, *Plant Cell Reports*, Vol. 26, pp. 861-872.

Bisbis B, Delmas F, Joubes J, Sicard A, Hernould M, Inze D, Mouras A, Chevalier C. 2006. Cyclin-dependent kinase (CDK) inhibitors regulate the CDK-cyclin complex activities in endoreduplicating cells of developing tomato fruit, *Journal of Biological Chemistry*, Vol. 281, pp. 7374-7383.

Boniotti Mb, Gutierrez C. 2001. A cell-cycle-regulated kinase activity phosphorylates plant retinoblastoma protein and contains, in Arabidopsis, a CDKA/cyclin D complex, *Plant J*, Vol. 28, pp. 341-350.

Boudolf V, Barroco R, Engler Jde A, Verkest A, Beeckman T, Naudts M, Inze D, De Veylder L. 2004. B1-type cyclin-dependent kinases are essential for the formation of stomatal complexes in Arabidopsis thaliana, *Plant Cell*, Vol. 16, pp. 945-955.

Boudolf V, Lammens T, Boruc J, Van Leene J, Van Den Daele H, Maes S, Van Isterdael G, Russinova E, Kondorosi E, Witters E*, et al.* 2009. CDKB1;1 forms a functional complex with CYCA2;3 to suppress endocycle onset, *Plant Physiol*, Vol. 150, pp. 1482-1493.

Boudolf V, Vlieghe K, Beemster Gt, Magyar Z, Torres Acosta Ja, Maes S, Van Der Schueren E, Inze D, De Veylder L. 2004. The plant-specific cyclin-dependent kinase CDKB1;1 and transcription factor E2Fa-DPa control the balance of mitotically dividing and endoreduplicating cells in Arabidopsis, *Plant Cell*, Vol. 16, pp. 2683-2692.

Canepa Et, Scassa Me, Ceruti Jm, Marazita Mc, Carcagno Al, Sirkin Pf, Ogara Mf. 2007. INK4 proteins, a family of mammalian CDK inhibitors with novel biological functions, *IUBMB Life*, Vol. 59, pp. 419-426.

Cebolla A, Vinardell Jm, Kiss E, Olah B, Roudier F, Kondorosi A, Kondorosi E. 1999. The mitotic inhibitor ccs52 is required for endoreduplication and ploidy-dependent cell enlargement in plants, *Embo J*, Vol. 18, pp. 4476-4484.

Chao Ws, Serpe Md, Jia Y, Shelver Wl, Anderson Jv, Umeda M. 2007. Potential roles for autophosphorylation, kinase activity, and abundance of a CDK-activating kinase (Ee;CDKF;1) during growth in leafy spurge, *Plant Mol Biol*, Vol. 63, pp. 365-379.

Chen J, Saha P, Kornbluth S, Dynlacht Bd, Dutta A. 1996. Cyclin-binding motifs are essential for the function of p21CIP1, *Mol Cell Biol*, Vol. 16, pp. 4673-4682.

Cheniclet C, Rong Wy, Causse M, Frangne N, Bolling L, Carde Jp, Renaudin Jp. 2005. Cell expansion and endoreduplication show a large genetic variability in pericarp and contribute strongly to tomato fruit growth, *Plant Physiol*, Vol. 139, pp. 1984-1994.

Churchman Ml, Brown Ml, Kato N, Kirik V, Hulskamp M, Inze D, De Veylder L, Walker Jd, Zheng Z, Oppenheimer Dg*, et al.* 2006. SIAMESE, a plant-specific cell cycle regulator, controls endoreplication onset in Arabidopsis thaliana, *Plant Cell*, Vol. 18, pp. 3145-3157.

Coelho Cm, Dante Ra, Sabelli Pa, Sun Y, Dilkes Bp, Gordon-Kamm Wj, Larkins Ba. 2005. Cyclin-dependent kinase inhibitors in maize endosperm and their potential role in endoreduplication, *Plant Physiol*, Vol. 138, pp. 2323-2336.

Colasanti J, Cho So, Wick S, Sundaresan V. 1993. Localization of the Functional p34cdc2 Homolog of Maize in Root Tip and Stomatal Complex Cells: Association with Predicted Division Sites, *Plant Cell*, Vol. 5, pp. 1101-1111.

Cong B, Tanksley Sd. 2006. FW2.2 and cell cycle control in developing tomato fruit: a possible example of gene co-option in the evolution of a novel organ, *Plant Mol Biol*, Vol. 62, pp. 867-880.

Cookson Sj, Radziejwoski A, Granier C. 2006. Cell and leaf size plasticity in Arabidopsis: what is the role of endoreduplication?, *Plant Cell Environ*, Vol. 29, pp. 1273-1283.

Cui X, Fan B, Scholz J, Chen Z. 2007. Roles of Arabidopsis cyclin-dependent kinase C complexes in cauliflower mosaic virus infection, plant growth, and development, *Plant Cell*, Vol. 19, pp. 1388-1402.

De Clercq A, Inze D. 2006. Cyclin-dependent kinase inhibitors in yeast, animals, and plants: a functional comparison, *Crit Rev Biochem Mol Biol*, Vol. 41, pp. 293-313.

De Schutter K, Joubes J, Cools T, Verkest A, Corellou F, Babiychuk E, Van Der Schueren E, Beeckman T, Kushnir S, Inze D*, et al.* 2007. Arabidopsis WEE1 kinase controls cell cycle arrest in response to activation of the DNA integrity checkpoint, *Plant Cell*, Vol. 19, pp. 211-225.

De Veylder L, Beeckman T, Beemster Gt, De Almeida Engler J, Ormenese S, Maes S, Naudts M, Van Der Schueren E, Jacqmard A, Engler G*, et al.* 2002. Control of proliferation, endoreduplication and differentiation by the Arabidopsis E2Fa-DPa transcription factor, *Embo J*, Vol. 21, pp. 1360-1368.

De Veylder L, Beeckman T, Beemster Gt, Krols L, Terras F, Landrieu I, Van Der Schueren E, Maes S, Naudts M, Inze D. 2001. Functional analysis of cyclin-dependent kinase inhibitors of Arabidopsis, *Plant Cell*, Vol. 13, pp. 1653-1668.

Deane Cm, Salwinski L, Xenarios I, Eisenberg D. 2002. Protein interactions: two methods for assessment of the reliability of high throughput observations, *Mol Cell Proteomics*, Vol. 1, pp. 349-356.

Del Pozo Jc, Diaz-Trivino S, Cisneros N, Gutierrez C. 2006. The balance between cell division and endoreplication depends on E2FC-DPB, transcription factors regulated by the ubiquitin-SCFSKP2A pathway in Arabidopsis, *Plant Cell*, Vol. 18, pp. 2224-2235.

Dewitte W, Riou-Khamlichi C, Scofield S, Healy Jm, Jacqmard A, Kilby Nj, Murray Ja. 2003. Altered cell cycle distribution, hyperplasia, and inhibited differentiation in Arabidopsis caused by the D-type cyclin CYCD3, *Plant Cell*, Vol. 15, pp. 79-92.

Di Sansebastiano Gp, Paris N, Marc-Martin S, Neuhaus Jm. 1998. Specific accumulation of GFP in a non-acidic vacuolar compartment via a C-terminal propeptide-mediated sorting pathway, *Plant J*, Vol. 15, pp. 449-457.

Dissmeyer N, Nowack Mk, Pusch S, Stals H, Inze D, Grini Pe, Schnittger A. 2007. T-loop phosphorylation of Arabidopsis CDKA;1 is required for its function and can be partially substituted by an aspartate residue, *Plant Cell*, Vol. 19, pp. 972-985.

Engler Jde A, De Veylder L, De Groodt R, Rombauts S, Boudolf V, De Meyer B, Hemerly A, Ferreira P, Beeckman T, Karimi M*, et al.* 2009. Systematic analysis of cell-cycle gene expression during Arabidopsis development, *Plant J*, Vol. 59, pp. 645-660.

Evans Rb, Gottlieb Pd, Bose Hr, Jr. 1993. Identification of a rel-related protein in the nucleus during the S phase of the cell cycle, *Mol Cell Biol*, Vol. 13, pp. 6147-6156.

Fabian-Marwedel T, Umeda M, Sauter M. 2002. The rice cyclin-dependent kinase-activating kinase R2 regulates S-phase progression, *Plant Cell*, Vol. 14, pp. 197-210.

Fang G, Yu H, Kirschner Mw. 1998. Direct binding of CDC20 protein family members activates the anaphase-promoting complex in mitosis and G1, *Mol Cell*, Vol. 2, pp. 163-171.

Ferjani A, Horiguchi G, Yano S, Tsukaya H. 2007. Analysis of leaf development in fugu mutants of Arabidopsis reveals three compensation modes that modulate cell expansion in determinate organs, *Plant Physiol*, Vol. 144, pp. 988-999.

Fernandez Ai, Viron N, Alhagdow M, Karimi M, Jones M, Amsellem Z, Sicard A, Czerednik A, Angenent G, Grierson D*, et al.* 2009. Flexible tools for gene expression and silencing in tomato, *Plant Physiol*, Vol. 151, pp. 1729-1740.

Ferreira Pc, Hemerly As, Villarroel R, Van Montagu M, Inze D. 1991. The Arabidopsis functional homolog of the p34cdc2 protein kinase, *Plant Cell*, Vol. 3, pp. 531-540.

Fisher Rp, Morgan Do. 1994. A novel cyclin associates with MO15/CDK7 to form the CDK-activating kinase, *Cell*, Vol. 78, pp. 713-724.

Fulop K, Pettko-Szandtner A, Magyar Z, Miskolczi P, Kondorosi E, Dudits D, Bako L. 2005. The Medicago CDKC;1-CYCLINT;1 kinase complex phosphorylates the carboxy-terminal domain of RNA polymerase II and promotes transcription, *Plant J*, Vol. 42, pp. 810-820.

Gendreau E, Hofte H, Grandjean O, Brown S, Traas J. 1998. Phytochrome controls the number of endoreduplication cycles in the Arabidopsis thaliana hypocotyl, *Plant J*, Vol. 13, pp. 221-230.

Genschik P, Criqui M. 2007. The UPS: an engine that drives the cell cycle. In D Inzé (Ed.), *Cell cycle control and plant development*, Vol. 32. Oxford: Blackwell Publishing.

Gonzalez N, Gevaudant F, Hernould M, Chevalier C, Mouras A. 2007. The cell cycle-associated protein kinase WEE1 regulates cell size in relation to endoreduplication in developing tomato fruit, *Plant J*, Vol. 51, pp. 642-655.

Gonzalez N, Hernould M, Delmas F, Gevaudant F, Duffe P, Causse M, Mouras A, Chevalier C. 2004. Molecular characterization of a WEE1 gene homologue in tomato (Lycopersicon esculentum Mill.), *Plant Mol Biol*, Vol. 56, pp. 849-861.

Guo J, Song J, Wang F, Zhang Xs. 2007. Genome-wide identification and expression analysis of rice cell cycle genes, *Plant Mol Biol*, Vol. 64, pp. 349-360.

Healy Jm, Menges M, Doonan Jh, Murray Ja. 2001. The Arabidopsis D-type cyclins CycD2 and CycD3 both interact in vivo with the PSTAIRE cyclin-dependent kinase Cdc2a but are differentially controlled, *J Biol Chem*, Vol. 276, pp. 7041-7047.

Hemerly A, Engler Jde A, Bergounioux C, Van Montagu M, Engler G, Inze D, Ferreira P. 1995. Dominant negative mutants of the Cdc2 kinase uncouple cell division from iterative plant development, *Embo J*, Vol. 14, pp. 3925-3936.

Hermand D, Westerling T, Pihlak A, Thuret Jy, Vallenius T, Tiainen M, Vandenhaute J, Cottarel G, Mann C, Makela Tp. 2001. Specificity of Cdk activation in vivo by the two Caks Mcs6 and Csk1 in fission yeast, *Embo J*, Vol. 20, pp. 82-90.

Himanen K, Boucheron E, Vanneste S, De Almeida Engler J, Inze D, Beeckman T. 2002. Auxin-mediated cell cycle activation during early lateral root initiation, *Plant Cell*, Vol. 14, pp. 2339-2351.

Hirt H. 1996. In and out of the plant cell cycle, *Plant Mol Biol*, Vol. 31, pp. 459-464.

Hutchins Ap, Roberts Gr, Lloyd Cw, Doonan Jh. 2004. In vivo interaction between CDKA and eIF4A: a possible mechanism linking translation and cell proliferation, *FEBS Lett*, Vol. 556, pp. 91-94.

Ito M, Araki S, Matsunaga S, Itoh T, Nishihama R, Machida Y, Doonan Jh, Watanabe A. 2001. G2/M-phase-specific transcription during the plant cell cycle is mediated by c-Myb-like transcription factors, *Plant Cell*, Vol. 13, pp. 1891-1905.

Ivanov A, Cragg Ms, Erenpreisa J, Emzinsh D, Lukman H, Illidge Tm. 2003. Endopolyploid cells produced after severe genotoxic damage have the potential to repair DNA double strand breaks, *J Cell Sci*, Vol. 116, pp. 4095-4106.

Iwakawa H, Shinmyo A, Sekine M. 2006. Arabidopsis CDKA;1, a cdc2 homologue, controls proliferation of generative cells in male gametogenesis, *Plant J*, Vol. 45, pp. 819-831.

Jakoby Mj, Weinl C, Pusch S, Kuijt Sj, Merkle T, Dissmeyer N, Schnittger A. 2006. Analysis of the subcellular localization, function, and proteolytic control of the Arabidopsis cyclin-dependent kinase inhibitor ICK1/KRP1, *Plant Physiology*, Vol. 141, pp. 1293-1305.

Jasinski S, Perennes C, Bergounioux C, Glab N. 2002. Comparative molecular and functional analyses of the tobacco cyclin-dependent kinase inhibitor NtKIS1a and its spliced variant NtKIS1b, *Plant Physiology*, Vol. 130, pp. 1871-1882.

Jasinski S, Riou-Khamlichi C, Roche O, Perennes C, Bergounioux C, Glab N. 2002. The CDK inhibitor NtKIS1a is involved in plant development, endoreduplication and restores normal development of cyclin D3; 1-overexpressing plants, *J Cell Sci*, Vol. 115, pp. 973-982.

Joubes J, Lemaire-Chamley M, Delmas F, Walter J, Hernould M, Mouras A, Raymond P, Chevalier C. 2001. A new C-type cyclin-dependent kinase from tomato expressed in dividing tissues does not interact with mitotic and G1 cyclins, *Plant Physiol*, Vol. 126, pp. 1403-1415.

Joubes J, Phan Th, Just D, Rothan C, Bergounioux C, Raymond P, Chevalier C. 1999. Molecular and biochemical characterization of the involvement of cyclin-dependent kinase A during the early development of tomato fruit, *Plant Physiol*, Vol. 121, pp. 857-869.

Joubes J, Walsh D, Raymond P, Chevalier C. 2000. Molecular characterization of the expression of distinct classes of cyclins during the early development of tomato fruit, *Planta*, Vol. 211, pp. 430-439.

Kasili R, Walker Jd, Simmons La, Zhou J, De Veylder L, Larkin Jc. SIAMESE Cooperates with the CDH1-like Protein CCS52A1 to Establish Endoreplication in Arabidopsis thaliana Trichomes, *Genetics*.

Kawamura K, Murray Ja, Shinmyo A, Sekine M. 2006. Cell cycle regulated D3-type cyclins form active complexes with plant-specific B-type cyclin-dependent kinase in vitro, *Plant Mol Biol*, Vol. 61, pp. 311-327.

Kim Hj, Oh Sa, Brownfield L, Hong Sh, Ryu H, Hwang I, Twell D, Nam Hg. 2008. Control of plant germline proliferation by SCF(FBL17) degradation of cell cycle inhibitors, *Nature*, Vol. 455, pp. 1134-1137.

Kono A, Umeda-Hara C, Lee J, Ito M, Uchimiya H, Umeda M. 2003. Arabidopsis D-type cyclin CYCD4;1 is a novel cyclin partner of B2-type cyclin-dependent kinase, *Plant Physiol*, Vol. 132, pp. 1315-1321.

Koroleva Oa, Tomlinson M, Parinyapong P, Sakvarelidze L, Leader D, Shaw P, Doonan Jh. 2004. CycD1, a putative G1 cyclin from Antirrhinum majus, accelerates the cell cycle in cultured tobacco BY-2 cells by enhancing both G1/S entry and progression through S and G2 phases, *Plant Cell*, Vol. 16, pp. 2364-2379.

Labaer J, Garrett Md, Stevenson Lf, Slingerland Jm, Sandhu C, Chou Hs, Fattaey A, Harlow E. 1997. New functional activities for the p21 family of CDK inhibitors, *Genes & Development*, Vol. 11, pp. 847-862.

Lammens T, Boudolf V, Kheibarshekan L, Zalmas Lp, Gaamouche T, Maes S, Vanstraelen M, Kondorosi E, La Thangue Nb, Govaerts W*, et al.* 2008. Atypical E2F activity restrains APC/CCCS52A2 function obligatory for endocycle onset, *Proc Natl Acad Sci U S A*, Vol. 105, pp. 14721-14726.

Le Foll M, Blanchet S, Millan L, Mathieu C, Bergounioux C, Glab N. 2008. The plant CDK inhibitor NtKIS1a interferes with dedifferentiation, is specifically down regulated during development and interacts with a JAB1 homolog, *Plant Science*, Vol. 175, pp. 513-523.

Leiva-Neto Jt, Grafi G, Sabelli Pa, Dante Ra, Woo Ym, Maddock S, Gordon-Kamm Wj, Larkins Ba. 2004. A dominant negative mutant of cyclin-dependent kinase A reduces endoreduplication but not cell size or gene expression in maize endosperm, *Plant Cell*, Vol. 16, pp. 1854-1869.

Lisec J, Schauer N, Kopka J, Willmitzer L, Fernie Ar. 2006. Gas chromatography mass spectrometry-based metabolite profiling in plants, *Nat Protoc*, Vol. 1, pp. 387-396.

Liu J, Zhang Y, Qin G, Tsuge T, Sakaguchi N, Luo G, Sun K, Shi D, Aki S, Zheng N*, et al.* 2008. Targeted degradation of the cyclin-dependent kinase inhibitor ICK4/KRP6 by RING-type E3 ligases is essential for mitotic cell cycle progression during Arabidopsis gametogenesis, *Plant Cell*, Vol. 20, pp. 1538-1554.

Lorca T, Castro A, Martinez Am, Vigneron S, Morin N, Sigrist S, Lehner C, Doree M, Labbe Jc. 1998. Fizzy is required for activation of the APC/cyclosome in Xenopus egg extracts, *Embo J*, Vol. 17, pp. 3565-3575.

Luedemann A, Strassburg K, Erban A, Kopka J. 2008. TagFinder for the quantitative analysis of gas chromatography--mass spectrometry (GC-MS)-based metabolite profiling experiments, *Bioinformatics*, Vol. 24, pp. 732-737.

Lui H, Wang H, Delong C, Fowke Lc, Crosby Wl, Fobert Pr. 2000. The Arabidopsis Cdc2a-interacting protein ICK2 is structurally related to ICK1 and is a potent inhibitor of cyclin-dependent kinase activity in vitro, *Plant Journal*, Vol. 21, pp. 379-385.

Lyapina S, Cope G, Shevchenko A, Serino G, Tsuge T, Zhou C, Wolf Da, Wei N, Deshaies Rj. 2001. Promotion of NEDD-CUL1 conjugate cleavage by COP9 signalosome, *Science*, Vol. 292, pp. 1382-1385.

Mariconti L, Pellegrini B, Cantoni R, Stevens R, Bergounioux C, Cella R, Albani D. 2002. The E2F family of transcription factors from Arabidopsis thaliana. Novel and conserved components of the retinoblastoma/E2F pathway in plants, *J Biol Chem*, Vol. 277, pp. 9911-9919.

Marshall Nf, Price Dh. 1995. Purification of P-TEFb, a transcription factor required for the transition into productive elongation, *J Biol Chem*, Vol. 270, pp. 12335-12338.

Mathieu-Rivet E, Gevaudant F, Sicard A, Salar S, Do Pt, Mouras A, Fernie Ar, Gibon Y, Rothan C, Chevalier C*, et al.* 2010. The functional analysis of the Anaphase Promoting Complex activator CCS52A highlights the crucial role of endoreduplication for fruit growth in tomato, *Plant J*.

Menges M, De Jager Sm, Gruissem W, Murray Ja. 2005. Global analysis of the core cell cycle regulators of Arabidopsis identifies novel genes, reveals multiple and highly specific profiles of expression and provides a coherent model for plant cell cycle control, *Plant J*, Vol. 41, pp. 546-566.

Menges M, Samland Ak, Planchais S, Murray Ja. 2006. The D-type cyclin CYCD3;1 is limiting for the G1-to-S-phase transition in Arabidopsis, *Plant Cell*, Vol. 18, pp. 893-906.

Meyers J, Craig J, Odde Dj. 2006. Potential for control of signaling pathways via cell size and shape, *Curr Biol*, Vol. 16, pp. 1685-1693.

Moseley Jb, Mayeux A, Paoletti A, Nurse P. 2009. A spatial gradient coordinates cell size and mitotic entry in fission yeast, *Nature*, Vol. 459, pp. 857-860.

Murray A. 1994. Cell cycle checkpoints, *Curr Opin Cell Biol*, Vol. 6, pp. 872-876.

Nakagami H, Sekine M, Murakami H, Shinmyo A. 1999. Tobacco retinoblastoma-related protein phosphorylated by a distinct cyclin-dependent kinase complex with Cdc2/cyclin D in vitro, *Plant J*, Vol. 18, pp. 243-252.

Nakai T, Kato K, Shinmyo A, Sekine M. 2006. Arabidopsis KRPs have distinct inhibitory activity toward cyclin D2-associated kinases, including plant-specific B-type cyclin-dependent kinase, *FEBS Letters*, Vol. 580, pp. 336-340.

Nesbitt Tc, Tanksley Sd. 2001. fw2.2 directly affects the size of developing tomato fruit, with secondary effects on fruit number and photosynthate distribution, *Plant Physiol*, Vol. 127, pp. 575-583.

Nigg Ea, Blangy A, Lane Ha. 1996. Dynamic changes in nuclear architecture during mitosis: on the role of protein phosphorylation in spindle assembly and chromosome segregation, *Exp Cell Res*, Vol. 229, pp. 174-180.

Nowack Mk, Grini Pe, Jakoby Mj, Lafos M, Koncz C, Schnittger A. 2006. A positive signal from the fertilization of the egg cell sets off endosperm proliferation in angiosperm embryogenesis, *Nat Genet*, Vol. 38, pp. 63-67.

Ormenese S, De Almeida Engler J, De Groodt R, De Veylder L, Inze D, Jacqmard A. 2004. Analysis of the spatial expression pattern of seven Kip related proteins (KRPs) in the shoot apex of Arabidopsis thaliana, *Annals of Botanny (London)*, Vol. 93, pp. 575-580.

Pardee Ab. 1974. A restriction point for control of normal animal cell proliferation, *Proc Natl Acad Sci U S A*, Vol. 71, pp. 1286-1290.

Peres A, Churchman Ml, Hariharan S, Himanen K, Verkest A, Vandepoele K, Magyar Z, Hatzfeld Y, Van Der Schueren E, Beemster Gt*, et al.* 2007. Novel plant-specific cyclin-dependent kinase inhibitors induced by biotic and abiotic stresses, *Journal of Biological Chemistry*, Vol. 282, pp. 25588-25596.

Pettko-Szandtner A, Meszaros T, Horvath Gv, Bako L, Csordas-Toth E, Blastyak A, Zhiponova M, Miskolczi P, Dudits D. 2006. Activation of an alfalfa cyclin-dependent kinase inhibitor by calmodulin-like domain protein kinase, *Plant Journal*, Vol. 46, pp. 111-123.

Planchais S, Glab N, Inze D, Bergounioux C. 2000. Chemical inhibitors: a tool for plant cell cycle studies, *FEBS Lett*, Vol. 476, pp. 78-83.

Porceddu A, Stals H, Reichheld Jp, Segers G, De Veylder L, Barroco Rp, Casteels P, Van Montagu M, Inze D, Mironov V. 2001. A plant-specific cyclin-dependent kinase is involved in the control of G2/M progression in plants, *J Biol Chem*, Vol. 276, pp. 36354-36360.

Qi R, John Pc. 2007. Expression of genomic AtCYCD2;1 in Arabidopsis induces cell division at smaller cell sizes: implications for the control of plant growth, *Plant Physiol*, Vol. 144, pp. 1587-1597.

Ramirez-Parra E, Lopez-Matas Ma, Frundt C, Gutierrez C. 2004. Role of an atypical E2F transcription factor in the control of Arabidopsis cell growth and differentiation, *Plant Cell*, Vol. 16, pp. 2350-2363.

Ren H, Santner A, Del Pozo Jc, Murray Ja, Estelle M. 2008. Degradation of the cyclin-dependent kinase inhibitor KRP1 is regulated by two different ubiquitin E3 ligases, *Plant Journal*, Vol. 53, pp. 705-716.

Rontein D, Dieuaide-Noubhani M, Dufourc Ej, Raymond P, Rolin D. 2002. The metabolic architecture of plant cells. Stability of central metabolism and flexibility of anabolic pathways during the growth cycle of tomato cells, *J Biol Chem*, Vol. 277, pp. 43948-43960.

Roudier F, Fedorova E, Gyorgyey J, Feher A, Brown S, Kondorosi A, Kondorosi E. 2000. Cell cycle function of a Medicago sativa A2-type cyclin interacting with a PSTAIRE-type cyclin-dependent kinase and a retinoblastoma protein, *Plant J*, Vol. 23, pp. 73-83.

Ruggiero B, Koiwa H, Manabe Y, Quist Tm, Inan G, Saccardo F, Joly Rj, Hasegawa Pm, Bressan Ra, Maggio A. 2004. Uncoupling the effects of abscisic acid on plant growth and water relations. Analysis of sto1/nced3, an abscisic acid-deficient but salt stress-tolerant mutant in Arabidopsis, *Plant Physiol*, Vol. 136, pp. 3134-3147.

Russo Aa, Jeffrey Pd, Patten Ak, Massague J, Pavletich Np. 1996. Crystal structure of the p27Kip1 cyclin-dependent-kinase inhibitor bound to the cyclin A-Cdk2 complex, *Nature*, Vol. 382, pp. 325-331.

Saiz Je, Fisher Rp. 2002. A CDK-activating kinase network is required in cell cycle control and transcription in fission yeast, *Curr Biol*, Vol. 12, pp. 1100-1105.

Schauer N, Semel Y, Roessner U, Gur A, Balbo I, Carrari F, Pleban T, Perez-Melis A, Bruedigam C, Kopka J*, et al.* 2006. Comprehensive metabolic profiling and phenotyping of interspecific introgression lines for tomato improvement, *Nat Biotechnol*, Vol. 24, pp. 447-454.

Schauer N, Steinhauser D, Strelkov S, Schomburg D, Allison G, Moritz T, Lundgren K, Roessner-Tunali U, Forbes Mg, Willmitzer L*, et al.* 2005. GC-MS libraries for the rapid identification of metabolites in complex biological samples, *FEBS Lett*, Vol. 579, pp. 1332-1337.

Schnittger A, Weinl C, Bouyer D, Schobinger U, Hulskamp M. 2003. Misexpression of the cyclin-dependent kinase inhibitor ICK1/KRP1 in single-celled Arabidopsis trichomes reduces endoreduplication and cell size and induces cell death, *Plant Cell*, Vol. 15, pp. 303-315.

Schwechheimer C, Isono E. The COP9 signalosome and its role in plant development, *Eur J Cell Biol*, Vol. 89, pp. 157-162.

Sherr Cj, Roberts Jm. 1999. CDK inhibitors: positive and negative regulators of G1-phase progression, *Genes & Development*, Vol. 13, pp. 1501-1512.

Shimotohno A, Matsubayashi S, Yamaguchi M, Uchimiya H, Umeda M. 2003. Differential phosphorylation activities of CDK-activating kinases in Arabidopsis thaliana, *FEBS Lett*, Vol. 534, pp. 69-74.

Shimotohno A, Ohno R, Bisova K, Sakaguchi N, Huang J, Koncz C, Uchimiya H, Umeda M. 2006. Diverse phosphoregulatory mechanisms controlling cyclin-dependent kinase-activating kinases in Arabidopsis, *Plant J*, Vol. 47, pp. 701-710.

Shimotohno A, Umeda-Hara C, Bisova K, Uchimiya H, Umeda M. 2004. The plant-specific kinase CDKF;1 is involved in activating phosphorylation of cyclin-dependent kinase-activating kinases in Arabidopsis, *Plant Cell*, Vol. 16, pp. 2954-2966.

Shirayama M, Zachariae W, Ciosk R, Nasmyth K. 1998. The Polo-like kinase Cdc5p and the WD-repeat protein Cdc20p/fizzy are regulators and substrates of the anaphase promoting complex in Saccharomyces cerevisiae, *Embo J*, Vol. 17, pp. 1336-1349.

Sims Rj, 3rd, Mandal Ss, Reinberg D. 2004. Recent highlights of RNA-polymerase-II-mediated transcription, *Curr Opin Cell Biol*, Vol. 16, pp. 263-271.

Sorrell Da, Marchbank A, Mcmahon K, Dickinson Jr, Rogers Hj, Francis D. 2002. A WEE1 homologue from Arabidopsis thaliana, *Planta*, Vol. 215, pp. 518-522.

Sozzani R, Maggio C, Giordo R, Umana E, Ascencio-Ibanez Jt, Hanley-Bowdoin L, Bergounioux C, Cella R, Albani D. The E2FD/DEL2 factor is a component of a regulatory network controlling cell proliferation and development in Arabidopsis, *Plant Mol Biol*, Vol. 72, pp. 381-395.

Stals H, Bauwens S, Traas J, Van Montagu M, Engler G, Inze D. 1997. Plant CDC2 is not only targeted to the pre-prophase band, but also co-localizes with the spindle, phragmoplast, and chromosomes, *FEBS Lett*, Vol. 418, pp. 229-234.

Sugimoto-Shirasu K, Roberts K. 2003. "Big it up": endoreduplication and cell-size control in plants, *Curr Opin Plant Biol*, Vol. 6, pp. 544-553.

Sun Y, Dilkes Bp, Zhang C, Dante Ra, Carneiro Np, Lowe Ks, Jung R, Gordon-Kamm Wj, Larkins Ba. 1999. Characterization of maize (Zea mays L.) Wee1 and its activity in developing endosperm, *Proc Natl Acad Sci U S A*, Vol. 96, pp. 4180-4185.

Takatsuka H, Ohno R, Umeda M. 2009. The Arabidopsis cyclin-dependent kinase-activating kinase CDKF;1 is a major regulator of cell proliferation and cell expansion but is dispensable for CDKA activation, *Plant J*, Vol. 59, pp. 475-487.

Tapia Jc, Bolanos-Garcia Vm, Sayed M, Allende Cc, Allende Je. 2004. Cell cycle regulatory protein p27KIP1 is a substrate and interacts with the protein kinase CK2, *J Cell Biochem*, Vol. 91, pp. 865-879.

Tomoda K, Kubota Y, Kato J. 1999. Degradation of the cyclin-dependent-kinase inhibitor p27Kip1 is instigated by Jab1, *Nature*, Vol. 398, pp. 160-165.

Umeda M, Bhalerao Rp, Schell J, Uchimiya H, Koncz C. 1998. A distinct cyclin-dependent kinase-activating kinase of Arabidopsis thaliana, *Proc Natl Acad Sci U S A*, Vol. 95, pp. 5021-5026.

Vandepoele K, Raes J, De Veylder L, Rouze P, Rombauts S, Inze D. 2002. Genome-wide analysis of core cell cycle genes in Arabidopsis, *Plant Cell*, Vol. 14, pp. 903-916.

Vandepoele K, Vlieghe K, Florquin K, Hennig L, Beemster Gt, Gruissem W, Van De Peer Y, Inze D, De Veylder L. 2005. Genome-wide identification of potential plant E2F target genes, *Plant Physiol*, Vol. 139, pp. 316-328.

Verkest A, Manes Cl, Vercruysse S, Maes S, Van Der Schueren E, Beeckman T, Genschik P, Kuiper M, Inze D, De Veylder L. 2005. The cyclin-dependent kinase inhibitor KRP2 controls the onset of the endoreduplication cycle during Arabidopsis leaf development through inhibition of mitotic CDKA;1 kinase complexes, *Plant Cell*, Vol. 17, pp. 1723-1736.

Vervoorts J, Luscher B. 2008. Post-translational regulation of the tumor suppressor p27(KIP1), *Cell Mol Life Sci*, Vol. 65, pp. 3255-3264.

Vlieghe K, Boudolf V, Beemster Gt, Maes S, Magyar Z, Atanassova A, De Almeida Engler J, De Groodt R, Inze D, De Veylder L. 2005. The DP-E2F-like gene DEL1 controls the endocycle in Arabidopsis thaliana, *Curr Biol*, Vol. 15, pp. 59-63.

Walker Jd, Oppenheimer Dg, Concienne J, Larkin Jc. 2000. SIAMESE, a gene controlling the endoreduplication cell cycle in Arabidopsis thaliana trichomes, *Development*, Vol. 127, pp. 3931-3940.

Wang H, Fowke Lc, Crosby Wl. 1997. A plant cyclin-dependent kinase inhibitor gene, *Nature*, Vol. 386, pp. 451-452.

Wang H, Qi Q, Schorr P, Cutler Aj, Crosby Wl, Fowke Lc. 1998. ICK1, a cyclin-dependent protein kinase inhibitor from Arabidopsis thaliana interacts with both Cdc2a and CycD3, and its expression is induced by abscisic acid, *Plant Journal*, Vol. 15, pp. 501-510.

Wang H, Zhou Y, Bird Da, Fowke Lc. 2008. Functions, regulation and cellular localization of plant cyclin-dependent kinase inhibitors, *Journal of Microscopy*, Vol. 231, pp. 234-246.

Wang H, Zhou Y, Gilmer S, Cleary A, John P, Whitwill S, Fowke L. 2003. Modifying plant growth and development using the CDK inhibitor ICK1, *Cell Biology International*, Vol. 27, pp. 297-299.

Wang H, Zhou Y, Gilmer S, Whitwill S, Fowke Lc. 2000. Expression of the plant cyclin-dependent kinase inhibitor ICK1 affects cell division, plant growth and morphology, *Plant Journal*, Vol. 24, pp. 613-623.

Wang H, Zhou Y, Torres-Acosta L, Fowke L. 2007. CDK Inhibitors. In D Inze (Ed.), *Cell Cycle Control and Plant Development*, Vol. 32. Oxford: Blackwell Publishing.

Wang H, Zhou Ym, Gilmer S, Cleary A, John P, Whitwell S, Fowke L. 2003. The CDK inhibitor ICK1 affects cell division, plant growth and morphogenesis, *Plant Biotechnology 2002 and Beyond*, pp. 259-260
619.

Wang W, Chen X. 2004. HUA ENHANCER3 reveals a role for a cyclin-dependent protein kinase in the specification of floral organ identity in Arabidopsis, *Development*, Vol. 131, pp. 3147-3156.

Wei N, Chamovitz Da, Deng Xw. 1994. Arabidopsis COP9 is a component of a novel signaling complex mediating light control of development, *Cell*, Vol. 78, pp. 117-124.

Wei N, Serino G, Deng Xw. 2008. The COP9 signalosome: more than a protease, *Trends Biochem Sci*, Vol. 33, pp. 592-600.

Weingartner M, Binarova P, Drykova D, Schweighofer A, David Jp, Heberle-Bors E, Doonan J, Bogre L. 2001. Dynamic recruitment of Cdc2 to specific microtubule structures during mitosis, *Plant Cell*, Vol. 13, pp. 1929-1943.

Weinl C, Marquardt S, Kuijt Sj, Nowack Mk, Jakoby Mj, Hulskamp M, Schnittger A. 2005. Novel functions of plant cyclin-dependent kinase inhibitors, ICK1/KRP1, can act non-cell-autonomously and inhibit entry into mitosis, *Plant Cell*, Vol. 17, pp. 1704-1722.

Yamaguchi M, Umeda M, Uchimiya H. 1998. A rice homolog of Cdk7/MO15 phosphorylates both cyclin-dependent protein kinases and the carboxy-terminal domain of RNA polymerase II, *Plant J*, Vol. 16, pp. 613-619.

Yang X, Menon S, Lykke-Andersen K, Tsuge T, Di X, Wang X, Rodriguez-Suarez Rj, Zhang H, Wei N. 2002. The COP9 signalosome inhibits p27(kip1) degradation and impedes G1-S phase progression via deneddylation of SCF Cul1, *Curr Biol*, Vol. 12, pp. 667-672.

Zhou Y, Niu H, Brandizzi F, Fowke Lc, Wang H. 2006. Molecular control of nuclear and subnuclear targeting of the plant CDK inhibitor ICK1 and ICK1-mediated nuclear transport of CDKA, *Plant Molecular Biology*, Vol. 62, pp. 261-278.

Zhou Y, Wang H, Gilmer S, Whitwill S, Fowke Lc. 2003. Effects of co-expressing the plant CDK inhibitor ICK1 and D-type cyclin genes on plant growth, cell size and ploidy in Arabidopsis thaliana, *Planta*, Vol. 216, pp. 604-613.

Zhou Y, Wang H, Gilmer S, Whitwill S, Keller W, Fowke Lc. 2002. Control of petal and pollen development by the plant cyclin-dependent kinase inhibitor ICK1 in transgenic Brassica plants, *Planta*, Vol. 215, pp. 248-257.

Zhou Ym, Li Gy, Brandizzi F, Fowke Lc, Wang H. 2003. The plant cyclin-dependent kinase inhibitor ICK1 has distinct functional domains for in vivo kinase inhibition, protein instability and nuclear localization, *Plant Journal*, Vol. 35, pp. 476-489.

PUBLICATIONS AND COMMUNICATIONS

Publications:

Mehdi Nafati, Nathalie Frangne, Michel Hernould, Christian Chevalier and Frédéric Gévaudant. “Functional characterization of tomato Cyclin-Dependent Kinase inhibitor SlKRP1 domains involved in protein-protein interactions”. *New Phytologist* (2010) 188:136-149

Mehdi Nafati, Catherine Cheniclet, Phuc Thi Do, Alisdair R. Fernie, Michel Hernould, Christian Chevalier, Frédéric Gévaudant. “Tomato mesocarp specific overexpression of the Cyclin-Dependent Kinase inhibitor SlKRP1 disrupts the tight proportionality between endoreduplication and cell growth”. Submitted to The Plant Journal.

Matthieu Bourdon, Nathalie Frangne, Elodie Mathieu-Rivet, **Mehdi Nafati**, Catherine Cheniclet, Jean-Pierre Renaudin and Christian Chevalier. “Endoreduplication and growth of fleshy fruits“, U. Lüttge *et al.* (eds.), *Progress in Botany* 71, Springer Verlag Berlin Heidelberg 2010.

Oral presentations:

M. Nafati, F. Gévaudant, M. Hernould, C. Chevalier. "Molecular analysis of Kip-related proteins in *Solanum lycopersicum*", SOL2008 meeting, 12-16 october 2008, Köln (Germany).

M. Nafati, F. Gévaudant, M. Hernould, C. Chevalier. "Molecular analysis of Kip-related proteins in *Solanum lycopersicum*", Colloque Projet Européen EU-SOL (workpackages 1 and 2), 3-4 april 2008, Bordeaux (France).

Posters:

M. Nafati, F. Gévaudant, M. Hernould, C. Chevalier. "Molecular analysis of Kip-related proteins in *Solanum lycopersicum*". Journée de l'Ecole Doctorale Sciences de la Vie et de la Santé, april 2008, Arcachon (France).

Résumé

L'objet de cette étude est la protéine de tomate Kip-Related Protein 1 (SlKRP1), un inhibiteur du cycle cellulaire. Chez la tomate, 4 KRPs ont été identifiées, et annotées SlKRP1 à 4. Lors du développement du fruit de tomate, *SlKRP1* et *SlKRP3* sont exprimés dans les phases de croissance du fruit, alors que *SlKRP2* et *SlKRP4* sont plus fortement exprimés dans les premiers jours du développement. La famille des Kip-Related Proteins peut être séparée en deux sous-groupes phylogénétiquement distincts identifiables par la présence de motifs protéiques spécifiques, impliqués dans la localisation cellulaire des KRPs ou les interactions protéine-protéine. Sur-exprimée au moyen d'un promoteur spécifique des cellules en expansion au sein du mésocarpe de tomate, SlKRP1 ralentit le phénomène d'endoréduplication dans le mésocarpe. Néanmoins, alors que la croissance cellulaire est proportionnelle au niveau d'endoréduplication dans les cellules durant le développement normal du fruit, il apparaît que les cellules dont le niveau d'endoréduplication a été diminué pas la sur-expression de SlKRP1 ne sont pas affectées au niveau de leur croissance. En conclusion, la protéine SlKRP1, dont nous avons caractérisé la séquence primaire, inhibe l'endoréduplication dans les cellules de mésocarpe de tomate. De plus, si l'endoréduplication est proportionnelle à la taille cellulaire, elle ne semble pas définir la taille finale des cellules.

Summary

The purpose of this study is the tomato Kip-Related Protein 1 (SlKRP1), a cell cycle inhibitor. In tomato, 4 KRPs were identified and annotated SlKRP1 to 4. During the development of tomato fruit, SlKRP1 and SlKRP3 are expressed during fruit growth phases, while SlKRP2 and SlKRP4 are highly expressed in the early days of development. The Kip-Related Proteins family can be separated into two subgroups phylogenetically distinct which are identifiable by the presence of specific protein motifs, involved in the cellular localization of KRPs and protein-protein interactions. Over-expressed using a promoter specific to growing cells of tomato mesocarp, SlKRP1 slows the phenomenon of endoreduplication in the mesocarp. However, while cell growth is proportional to the level of endoreduplication in cells during normal fruit development, it appears that cells whose level of endoreduplication was decreased due to SlKRP1 over-expression have their size unaffected. In conclusion, the protein SlKRP1, of whose primary sequence was characterized, inhibits endoreduplication in tomato mesocarp cells. Moreover, if endoreduplication is proportional to cell size, it does not seem to define the final size of the cells.